PROBABILISTIC PERFORMANCE-BASED OPTIMUM SEISMIC DESIGN OF REINFORCED CONCRETE STRUCTURES

A Thesis Submitted to
the Graduate School of
İzmir Institute of Technology
In Partial Fulfillment of the Requirement for the Degree of

DOCTOR OF PHILOSOPHY

In Civil Engineering

by
Nisar Ahmad KARIMZADA

December 2023
İZMİR

We approve the thesis of **Nisar Ahmad KARIMZADA**

Examining Committee Members:

Prof. Dr. Engin AKTAŞ
Department of Civil Engineering, İzmir Institute of Technology

Prof. Dr. İ. Serkan MISIR
Department of Civil Engineering, Dokuz Eylül Üniversitesi

Assoc. Prof. Dr. Gürsoy TURAN
Department of Civil Engineering, İzmir Institute of Technology

Assoc. Prof. Dr. Emre ERCAN
Department of Civil Engineering, Ege University

Asst. Prof. Dr. Tolga ERCAN
Department of Civil Engineering, İzmir Institute of Technology

11 December 2023

Prof. Dr. Engin AKTAŞ
Supervisor,
Department of Civil Engineering
İzmir Institute of Technology

Assoc. Prof. Dr. Sadık Can Girgin
Co-Supervisor
Department of Civil Engineering,
Dokuz Eylül University

Prof. Dr. Cemalettin DÖNMEZ
Head of the Department of
Civil Engineering

Prof. Dr. Mehtap EANES
Dean of the Graduate School

ACKNOWLEDGMENTS

Completing a PhD is an outstanding and unforgettable achievement, and it is difficult for me to believe that I have reached this milestone. I want to thank everyone who has been a part of this wonderful and amazing journey with me.

First and foremost, I would like to express my deepest gratitude and respect to my supervisor, Prof. Dr. Engin. AKTAŞ. His constant encouragement, guidance, and support have been invaluable throughout the entire journey. From the initial stages of refining my research proposal to the final submission of my thesis, his unwavering presence and wealth of wisdom have been instrumental in shaping my academic growth. I extend my heartfelt appreciation to my co-advisor, Assoc. Prof. Dr. Sadık Can GIRGIN, for his keen interest and valuable guidance, strong motivation, and constant encouragement through this work.

I would like to convey my sincere gratitude to the members of the thesis monitoring committee, Prof. Dr. İ. Serkan MISIR and Assoc. Prof. Dr. Gürsoy TURAN for their valuable comments and pinpointed recommendations to enhance this work. Their significant contributions bring the main objectives of this study to light. Additionally, I would like to thank the thesis defense committee members, Assoc. Prof. Dr. Emre ERCAN and Asst. Prof. Dr. Tolga ERCAN for contributing to my thesis with their valuable comments. I would also like to thank Dr. Amir SHIRKHANI for his help and support in understanding and applying the Endurance Time method.

I would like to express my special thanks to each member of my family, my brothers, sisters, wife, and kids, for their unlimited love and support in completing this journey, especially to my respected parents, Prof. Dr. Abdul Qayoum KARIMZADA and Humaira KARIMZADA. The meaning of my life and work is incomplete without paying my regards to them, whose blessings and continuous encouragement have shown me the path to achieve my goals. I would also like to express my deepest gratitude and heartfelt appreciation to my wife, S. KARIMZADA, for her endless love, support, and patience while I was far away from her for such a long time. I want to thank her for helping me in such a way that always gave me the strength to fight my stresses during this journey. Finally, I would like to apologize to my angel, Yusra KARIMZADA, and my prince, Mohammad Yousuf KARIMZADA, for not being next to them for a long time. This thesis is dedicated to each member of my family.

ABSTRACT

PROBABILISTIC PERFORMANCE-BASED OPTIMUM SEISMIC DESIGN OF REINFORCED CONCRETE STRUCTURES

Traditional seismic design codes have been developed and used for decades to stipulate the rules for earthquake-resistant design of structures. They are mainly based on the Force-Based Design (FBD) approach and on some linear elastic techniques. The inelastic seismic response of the structure is not directly addressed in the traditional seismic design codes. The initial aim of the current seismic design codes is public safety. In seismic codes, some information is provided regarding the damaged states of structural components, while limited information is provided regarding the damaged states of nonstructural members. In addition, no clear information is provided regarding economic losses and business interruption.

The Performance-Based Seismic Design (PBSD) approach, a reliable approach for the seismic design of structures, is capable of providing more detailed information on the performance levels of both structural and nonstructural members and content systems. Some current seismic design codes adapted concepts of the PBSD approach in a deterministic manner, considering uncertainties implicitly.

In this study, efforts have been made to develop a Probabilistic Performance-Based Optimum Seismic Design (PPBOSD) methodology for Reinforced Concrete (RC) structures, considering uncertainties explicitly to provide a more practice-oriented approach. It is a powerful seismic design tool that provides structures with economical, robust, and rational design. In addition, structures designed using this approach could satisfy the target performance levels at multi-limit states. For the optimization problem, the objective function is given in terms of minimizing the expected total cost of the structure at a specific intensity level. Pacific Earthquake Engineering Research Center's Performance-Based Earthquake Engineering (PEER PBEE) methodology is used for the performance assessment of the structure. The Endurance Time method is used in the PEER PBEE methodology framework while performing optimization. After the optimum solution is obtained, the Incremental Dynamic Analysis (IDA) method is used to verify the performance levels. The proposed methodology is applied to RC frame buildings with different numbers of stories. OpenSees software is used together with codes written in python for the design and analysis purpose.

ÖZET

BETONARME YAPILARIN OLASILIKSAL PERFORMANSA DAYALI OPTİMUM SİSMİK TASARIMI

Yapıların sismik etkilere karşı tasarımını yapabilmek için geleneksel yapı tasarım kodları uzun bir süredir kullanılmaktadır. Bu kodlar elastik lineer tekniklerle Kuvvet Esaslı Tasarım yaklaşımı izlemektedir. Geleneksel yapı tasarım kodlarında elastik ötesi davranış doğrudan hesaba katılmamaktadır. Mevcut deprem yönetmeliklerinin ilk hedefi kamu güvenliğinin sağlanmasıdır. Yapısal elemanların hasar durumları ile ilgili bilgi sunulsa bile yapısal olmayan elemanların hasar durumları hakkında çok kısıtlı bilgi sunmaktadır. Buna ek olarak ekonomik kayıplar ve işlerdeki kesintiler ile işlerin durmasının doğurduğu etkiler konusunda herhangi bir bilgi sunulmamaktadır.

Yapıların sismik etkiler karşısında tasarımı için güvenle kulllanılabilecek Performansa Dayalı Sismik Tasarım (PDST) yaklaşımı yapısal ve yapısal olmayan elemanlar ve yapı içindeki bulunan sistemlerin performans seviyeleri hakkında detaylı bilgi sunabilmektedir. Halihazırda bazı sismik tasarım kodları, PDST yaklaşımını, belirsizlikleri üstü kapalı dikkate alarak deterministik şekilde kullanıma sunmaktadır.

Bu çalışmada betonarme yapılar için belirsizlikleri açık bir şekilde hesaba katan ama pratik uygulamaya da olanak sağlayacak, Olasılıksal Performansa Dayalı Optimum Sismik Tasarım (OPDOST) esaslı bir metot geliştirilmiştir. Bu metot, ekonomik, robust ve rasyonel tasarımlar sunabilecek güçlü bir tasarım aracıdır. Ayrıca, çoklu sınır şartlarınında da, hedef performans seviyelerinin yakalanması mümkün olacaktır. Optimizasyon için amaç fonksiyonları beklenen toplam maliyet ve risk seviyelerini düşürmek ve hasar seyivesinin belirlenen hedef seviyesini geçmeme olasılığının güven seviyesini maksimize etmek şeklinde sunulmuştur. Yapıların performans seviyelerinin belirlenmesi PEER PBEE (Pacific Earthquake Engineering Research Center's Performance-Based Earthquake Engineering) yaklaşımı ile yapılmaktadır. PEER PBE analizlerinde Dayanıklılık Süresi Yöntemi (Endurance Time Method) kullanılmıştır. Optimum çözüme ulaşınca artımsal dinamik analiz (IDA) kullanılarak sonuçlar performans açısından kontrol edilmiştir. Önerilen yaklaşımın faklı kat adetlerine sahip betonarme binalara uygulaması gösterilmiştir. Tasarım ve analiz süreçlerinde OpenSees yazılımı python ile yazılmış kodlarla birlikte kullanılmıştır.

TABLE OF CONTENTS

APPENDICES

LIST OF FIGURES

Figure **Page**

Figure **Page**

Figure **Page**

Figure **Page**

Figure **Page**

LIST OF TABLES

Table **Page**

Table **Page**

LIST OF ABBREVIATIONS

ADRS	Acceleration-Displacement Response Spectra
ASCE	American Society of Civil Engineers
ATC	Applied Technology Council
CAV	Cumulative Absolute Velocity
CDF	Cumulative Distribution Function
COV	Coefficient of Variation
CP	Collapse Prevention
DDBD	Direct Displacement-Based Seismic Design
DM	Damage Measure
DV	Decision Variable
DZ	Damage Zone
EDP	Engineering Demand Parameter
ELF	Equivalent Lateral Force
ERF	Earthquake Rupture Forecast
ET	Endurance Time
ETEF	Endurance Time Excitation Function
FBD	Force-Based Design
FEMA	Federal Emergency Management Agency
GA	Genetic Algorithm
GM	Ground Motion
IDA	Incremental Dynamic Analysis
IDR	Interstory Drift Ratio
IM	Intensity Measure
IMR	Intensity Measure Relationship
IO	Immediate Occupancy
LCC	Life Cycle Cost
LCCA	Life Cycle Cost Analysis
LS	Life Safety
MADRS	Modified Acceleration-Displacement Response Spectra
MAF	Mean Annual Frequency
NTHA	Nonlinear Time History Analysis

OpenSees	Open System for Earthquake Engineering Simulation
OpenSHA	Open-Source Seismic Hazard Analysis
PBEE	Performance-Based Earthquake Engineering
PBSD	Performance-Based Seismic Design
PDaA	Probabilistic Damage Analysis
PDeA	Probabilistic Demand Analysis
PDF	Probability Density Function
PEER	Pacific Earthquake Engineering Research
PFA	Peak Floor Acceleration
PGA	Peak Ground Acceleration
PGV	Peak Ground Velocity
PLA	Probabilistic Loss Analysis
PPBOSD	Probabilistic Performance-Based Optimum Seismic Design
PSHA	Probabilistic Seismic Hazard Analysis
RC	Reinforced Concrete
RDR	Residual Drift Ratio
SDOF	Single-Degree-Of-Freedom
SEAOC	Structural Engineers Association of California
USGS	United States Geological Survey

CHAPTER 1

INTRODUCTION

Structural engineering aims to design structures to sustain various types of loads imposed by their service requirements and natural hazards. The seismic load caused by an earthquake is one of the dynamic loads that a structure may experience in its lifetime. Earthquake is a natural disaster that may cause significant damage, especially to infrastructure. The prediction of the actual behavior of the structure under earthquake action is a complex procedure. This is due to the nature of earthquakes, which are random and unpredictable events. Thus, better engineering methods and advanced tools are required to design and predict the behavior of the structure under seismic action. The structures should be designed for seismic loading not only to survive in very rare earthquakes but also to be capable of experiencing less damage in frequent earthquakes. Performance-Based Seismic Design (PBSD) approach may serve to this purpose efficiently, which is capable of predicting the performance of the structure effectively.

The design of structures is guided through codes and standards. For many years, the traditional prescriptive design approach based on linear elastic techniques has been developed to design structures against different types of loadings, especially seismic loadings. The traditional design approach has some drawbacks, one of which is that it does not directly address structural inelastic seismic responses and thus cannot effectively deal with damage loss due to structural and nonstructural failures during earthquakes. As a result, the long-term risk and benefit implications cannot be assessed using a traditional design approach. After the Northridge Earthquake in 1994, the Structural Engineers Association of California (SEAOC), for the first time, recognized the need for the development of a new performance-based methodology for seismic design and construction of buildings. After that, the appearance of the PBSD approach appeared to be the future direction of seismic design codes (Zou et al., 2007).

PBSD under continuous development, is the art of design, rehabilitation, and maintenance of new or existing structures (Foley et al., 2007a; Kaveh et al., 2014). There exist some problems and limitations in the traditional seismic design codes that are mostly based on the Force-Based Design (FBD) approach. To overcome these problems and limitations, PBSD is a good alternative (Bazeos, 2009; Foley et al., 2007a; Hamburger et al., 2004; Kaveh et al., 2014; Saadat et al., 2016). PBSD helps stakeholders and decision-makers assign sources based on more accurate data (Zhang & Alam, 2019). It makes it possible to select various performance objectives for different seismic hazard levels and then design structures accordingly to satisfy these performance objectives (Khalilian et al., 2021). In addition, it promises to produce structures with a realistic understanding of the risk of casualties, occupancy interruption, and economic loss (Karimzada & Aktaş, 2016). It has the capability to clearly and explicitly explain the performance of a structure. One of its important characteristics is that it establishes a direct link between structural performance and the design process and eliminates inherent uncertainties. It also improves the risk control and management (Zhang & Alam, 2019).

Furthermore, compared to the traditional design codes, the PBSD approach explicitly requires the performance of the structure based on its deformation under various hazard levels. This requirement causes to have a more reliable design for the structure, which not only the lives of the occupants would be safe under severe earthquakes but also would be able to have less damage in frequent earthquakes (Kaveh et al., 2014). Moreover, probabilistic models serve as the foundation for both demand and capacities in the PBSD approach (Mackie & Stojadinović, 2005). In addition, with the PBSD, owners and designers can communicate more easily and could be able to obtain performance goals without having to adhere to prescriptive procedures of the traditional codes, which are defined for the structures (Zhang & Alam, 2019).

Some modern building codes, such as ASCE 7-2022 and IBC-2020, allowed the PBSD procedure for the design of the structures as long as the reliability target provided in these codes could be satisfied by the designed structure (Padalu & Surana, 2023). The uncertainties are not modeled explicitly in these codes because they use a practical PBSD approach and prescribe deterministic seismic design using characteristic values of capacity parameters. However, uncertainties cannot be avoided in the performance assessment step of the PBSD approach; therefore, they should be modeled explicitly. Cornell & Krawinkler (2000) proposed a probabilistic performance assessment methodology for the performance evaluation of the structures considering uncertainties explicitly. The methodology is then developed by the Pacific Earthquake Engineering Research (PEER) Center, known as the PEER Performance-Based Earthquake Engineering (PBEE) methodology.

The PEER PBEE methodology includes four major steps: the Probabilistic Seismic Hazard Analysis (PSHA), the Probabilistic Demand Analysis (PDeA), the Probabilistic Damage Analysis (PDaA), and the Probabilistic Loss Analysis (PLA). The four steps are then integrated using the total probability theorem. The methodology is completely a probabilistic approach that considers uncertainties in the hazard, structural response, damage, and loss. Furthermore, the PEER PBEE methodology quantifies the performance of a structure in terms of total risk. The framework of the methodology is used to express the seismic risk by using terms that are more easily understandable to the stakeholders and engineers involved in the practice. The performance metrics in this methodology could be classified further into direct economic loss, downtime, injuries, and casualties (Shahnazaryan, 2021).

A comprehensive systematic performance assessment methodology is offered by the FEMA-P-58-1 (2018) report, which predicts the loss due to earthquakes in a quantifiable manner (Xu et al., 2019). FEMA P-58, which is often used in seismic loss estimates, includes the prediction techniques and sufficient loss data of structural and nonstructural components, which is provided as an Excel file (FEMA P-58_FragilityDatabase_v3.1.2.xls). The database contains information related to the fragility functions and consequence functions of the structural and nonstructural components. The medians and dispersions, which are in terms of different Engineering Demand Parameters (EDPs), such as Interstory Drift Ratio (IDR), Peak Floor Acceleration (PFA), and Peak Floor Velocity (PFV), of the fragility functions for different Damage States (DSs), are provided in this database (FEMA-P-58-1, 2018).

Frequent earthquakes may cause lots of damage to a structure during its lifetime, which may result in some sort of loss, such as repair cost, repair time, injuries, and fatalities. The loss due to the damage in the lifetime of the structure could be obtained through Life Cycle Cost Analysis (LCCA) procedure, an assessment tool for the performance assessment of structures (Mitropoulou et al., 2011). The cost obtained through the LCCA procedure is known as the Life Cycle Cost (LCC) of the structure, which is one of the important decision variables for the owners and stakeholders. To this end, the LCCA must be included in the design process of a structure (Mitropoulou & Lagaros, 2016). The LCC of the structure includes the initial construction cost of the structure, the costs due to damage repair cost, repair time, maintenance, injuries, and fatalities (Kaveh et al., 2014). Without the maintenance costs, the additional costs that result from the earthquakes in a structure's lifetime are obtained through PEER PBEE or FEMA-P-58-1 assessment methodology.

1.1. Research Motivation

In structural engineering, a challenging part for structural engineers is to design the structures to sustain the various types of loads, particularly the dynamic loads imposed on the structure during its lifetime (Karimzada et al., 2024). As mentioned, the design of the structures for different types of loadings is carried out using conventional code-based design methods, which are mostly based on the FBD approach. However, there are some limitations of current seismic design codes. Some of these limitations are discussed in the previous section, while some others are presented in the next chapter. One of these limitations is that they mainly concentrate on the forces, and then later, they check the buildings for displacement and drift limits (Padalu & Surana, 2023).

PBSD, which is continuously under development, is a relatively new approach for the design of new structures and the evaluation and retrofitting of existing structures, which has attracted many professionals and researchers recently (Karimzada et al., 2024). Structures can be designed using the PBSD approach with a more realistic understanding of the risk of casualties, occupancy interruption, and economic losses. Furthermore, structures designed through the PBSD approach would be able to show different performance levels for different earthquake Ground Motions (GMs), (FEMA-445, 2006).

Currently, some seismic design codes have adapted the PBSD approach. In such codes, which use a practical PBSD approach and prescribe deterministic seismic design using characteristic values of capacity parameters, uncertainties are not modeled explicitly. Instead, they are using design factors, including partial load and resistance factors, to assume that uncertainties are covered through these factors. While it has been extensively recognized that, because of the uncertainties that exist inherently in the input GM hazard and as well as in the structural properties, to be able to claim that target performance is achieved, e.g., with an acceptable value of the Mean Annual Frequency (MAF) of exceedance, the performance of the structure should be obtained in a probabilistic manner in PBSD by modeling uncertainties explicitly (Franchin et al., 2018).

Furthermore, due to the reduction of conventional energy sources and, on the other hand, the need for sustainable development around the world, it is required to optimize the production and use of construction materials and reduce their environmental impact, at the same time, the significant role of the construction sector in economic development and prosperity should be maintained (Yazdani et al., 2017).

Concrete is one of the construction materials widely used in structures around the world. It is believed that it is the second most-consumed material after water. Its annual consumption is almost one metric ton per person. Further, the production of concrete contributes to global anthropogenic carbon dioxide (CO_2) emissions significantly (i.e., more than 5%), which is one of the main reasons for climate change. These effects can be minimized by using some optimization methods for the design of structures, especially for Reinforced Concrete (RC) structures (Yazdani et al., 2017).

Currently, some studies have been conducted using PBSD optimization methods for both steel and RC structures. Some of these studies have used pushover analysis for the performance evaluation of the structures in the optimization process, e.g., (Chan & Zou, 2004; Fragiadakis et al., 2006; Ganzerli et al., 2000; Lagaros et al., 2008) while some others have used the well-known Incremental Dynamic Analysis (IDA) method (Mitropoulou et al., 2011; Mitropoulou & Lagaros, 2016; Saadat et al., 2015). Some of these studies used only the initial construction cost as an objective function for the optimization problem, such as (Lagaros & Papadrakakis, 2007), while some others used the expected total cost, which is the combination of the initial construction cost and the Life Cycle Cost (LCC) of the structure due to the occurrence of earthquakes, such as, (Mitropoulou & Lagaros, 2016; Möller et al., 2015; Saadat et al., 2016). On the other hand, some studies used the Endurance Time (ET) method instead of the IDA method for optimization purposes, such as (M. Basim et al., 2016; Khalilian et al., 2021; Mirfarhadi & Estekanchi, 2020), which reduced the computational time significantly.

1.2. Objective and Scope

This study has made efforts to develop a Probabilistic Performance-Based Optimum Seismic Design (PPBOSD) methodology for RC structures, considering uncertainties explicitly and showing efforts to assure yet to be practice-oriented. It is a powerful analytical tool to satisfy not only the requirements of the acceptable different performance levels of the structure under different hazard levels but also to satisfy economic and social losses. Meanwhile, it is possible to satisfy the target performance levels for multi-limit states. In addition, it will be possible to control the desired targeted risk level in a direct manner.

The main goal of the methodology is to minimize the expected total cost of the structure. The proposed methodology is applied to RC frame building. For the analysis and design, Open System for Earthquake Engineering Simulation (OpenSees), together with Python, has been used. In the optimization procedure, the ET time method is utilized for performance assessment once the optimal design has been obtained, then the IDA method has been used for performance evaluation purpose. It should be noted that nonlinear static pushover analysis is also used to obtain the yield drift ratio. For pushover analysis, forces are needed to be applied on top of each story. These forces were obtained through the Direct Displacement-Based Seismic Design (DDBD) approach proposed by Priestley & Kowalsky (2000).

The method is first demonstrated using a 2-Story RC building structure. The structure is assumed to be symmetric in both directions in the plan; therefore, a single 2D frame having two equal spans has been used for further analysis and design. Later on, the methodology is applied to the 3-, 6, and 9-Story commercial office buildings. They were also assumed to be symmetric in both directions in the plan, and the selected 2D frame has three equal spans. The same structures are optimized using Code-Based design and PBSD methods. For the optimization of the structures, for Code-Based design and PBSD methods, the initial cost is used as an objective function. In contrast, for the proposed methodology, the expected total cost is used as an objective function to be minimized at a specific hazard level. For Code-Based design optimization, the Equivalent Lateral Force (ELF) method is used in the optimization procedure, while for the PBSD and the PPBOSD methods, the ET method has been utilized.

After the optimum solution is obtained, in the performance assessment procedure, the IDA method has been utilized for all structures. The results are compared in terms of the initial costs, expected costs at three different Intensity Measure (IM) levels, and the expected total costs in three hazard levels. In addition, the expected performance of the structure is obtained using the well-known capacity spectrum method, for which a graphical procedure described in the FEMA-440 (2005) is adopted. The performance points were obtained for the structures designed with three different approaches, and the results were compared.

1.3. Methodology

As discussed previously, structures designed using traditional seismic design codes could not answer some problems related to the probable seismic performance of the structure, especially corresponding to business interruption or downtime, and as well could not provide enough information about the damaged state of nonstructural elements. In addition, structures designed with traditional seismic design codes could manage life safety, but extensive structural and nonstructural damages could be experienced that would not be practical to repair; thus, it causes high economic losses.

Furthermore, some of the current codes adopted the PBSD concept in a deterministic manner, managing uncertainties implicitly. However, researchers found it necessary to explicitly take into account uncertainties involved in the PBSD framework to have a satisfactory performance from the designed structures. In this research, efforts have been made to develop a more practical PPBOSD approach in which uncertainties will be considered explicitly. The general flowchart of the methodology is provided in the following figure.

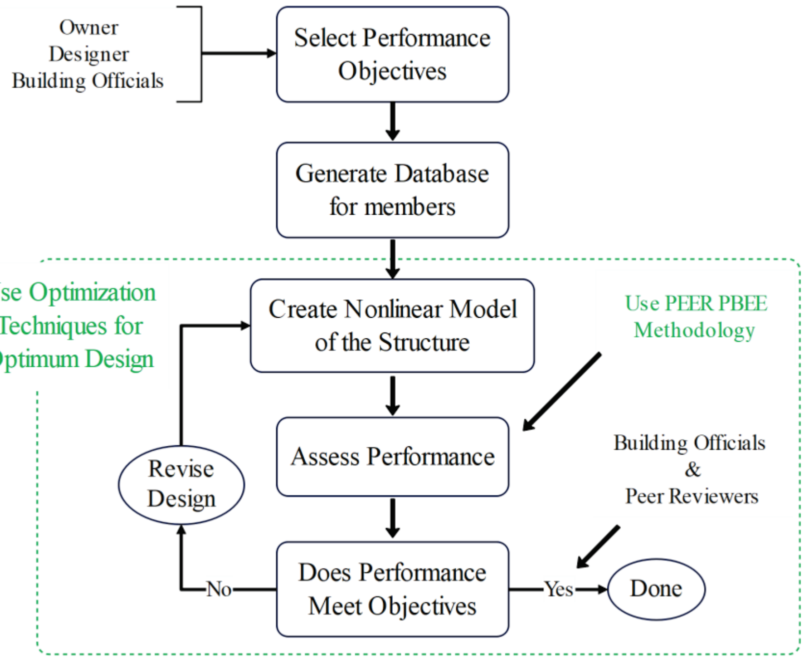

Figure 1.1. General Framework for PPBOSD

The first thing is to select performance objectives. In this study, three different performance objectives are selected in terms of performance levels corresponding to specific hazard levels. Three performance levels are the Immediate Occupancy (IO), Life Safety (LS), and Collapse Prevention (CP) levels, which correspond to the hazard levels of 50%, 10%, and 2% probability of exceedance in 50 years, with a mean return period of 72, 475 and 2475 years, respectively. After selecting performance objectives, databases are generated for the cross-sectional dimensions and reinforcement configuration for the members of the structures, which are beams and columns in this study. In the optimization procedure, the cross-sections are selected randomly from the database. The nonlinear model of the structure is built using selected members. Then, performance assessment is carried out using the PEER PBEE methodology, initially proposed by Cornell and Krawinkler (2000). The PEER PBEE methodology is provided in the following figure.

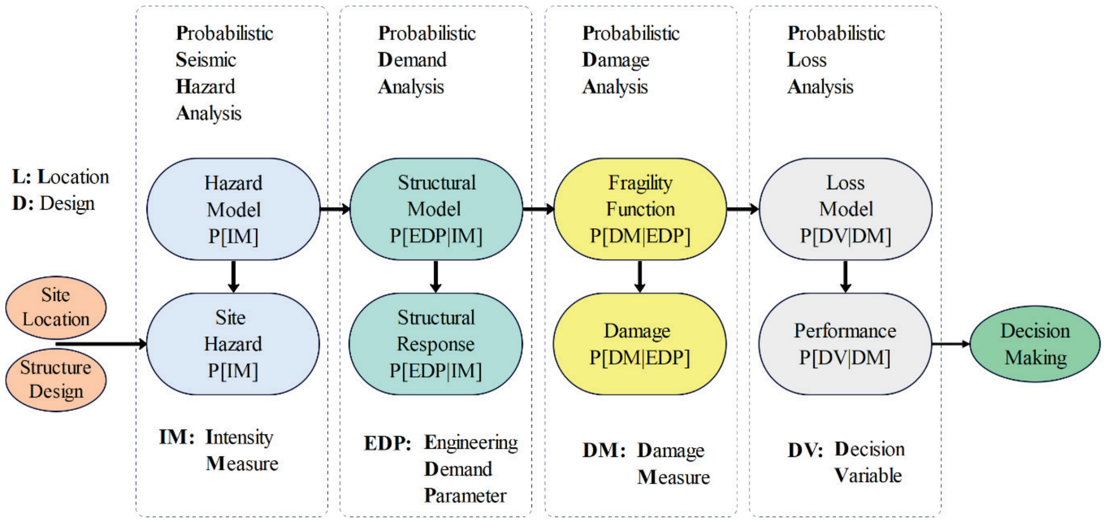

Figure 1.2. Framework of the probabilistic PEER PBEE methodology (Source: Y. Li 2014)

For optimization in the proposed methodology, the expected total cost is considered as the objective function. The minimum design requirements of ACI 318 (2019) and the performance-based criteria are used as constraints of the optimization problem. In the proposed methodology, a Genetic Algorithm (GA) is used to solve the optimization problem. Therefore, the flowchart will take the following form in this case.

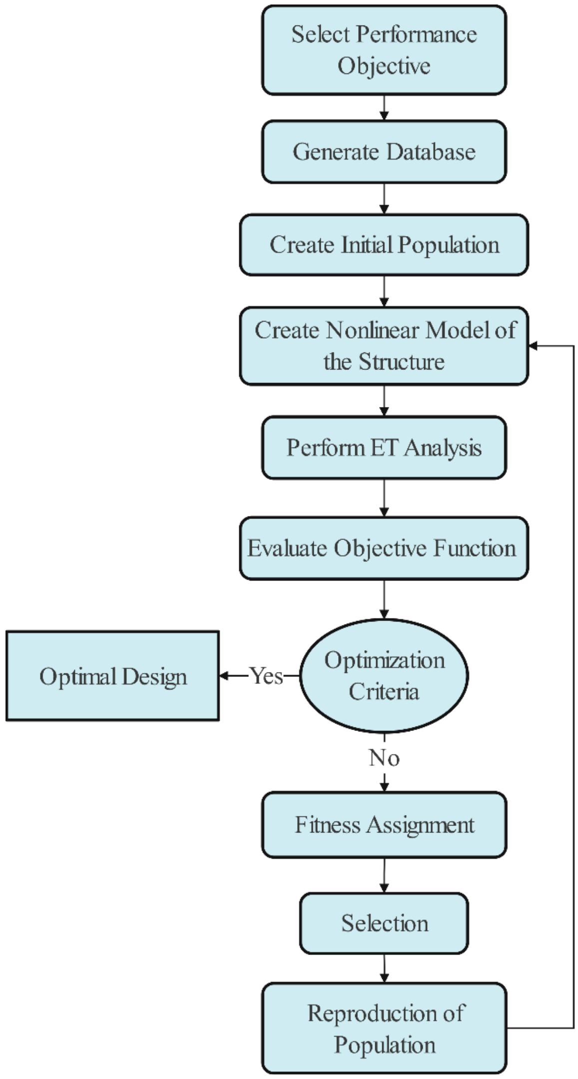

Figure 1.3. Framework of PPBOSD in GA format

The detailed PEER PBEE methodology for the loss estimation is given in the following figure, adapted from Elkady & Lignos (2020) with some modifications. The flowchart given in this figure would provide the LCC for different decision variables. First, it is required to define a range of IM values of interest. This means that, from a very low IM level, that may not cause loss to the intensity of interest that is meaningful for the decision-makers and stakeholders.

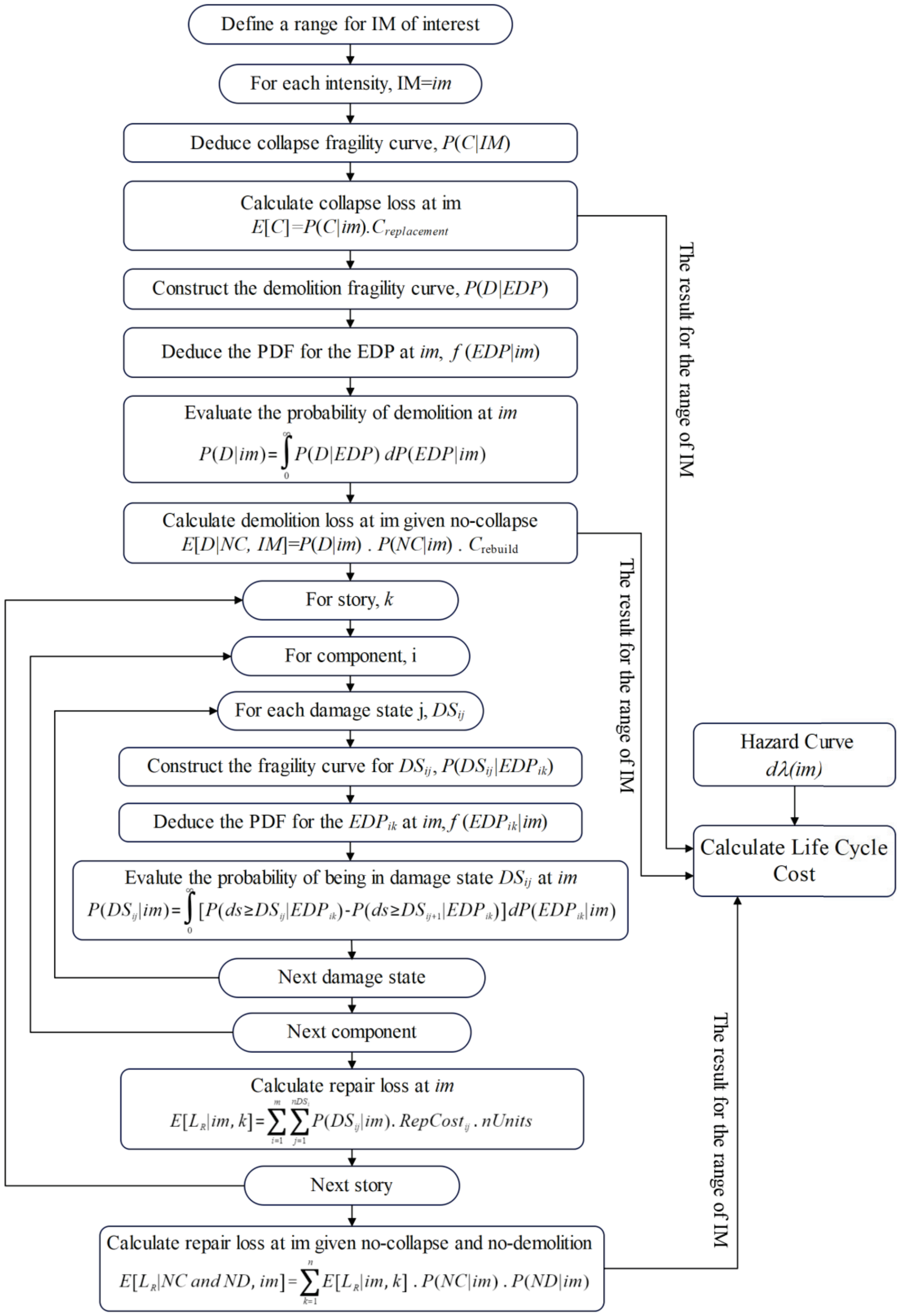

Figure 1.4. Decision variable LCCA procedure (Adapted from Elkady & Lignos, 2020)

CHAPTER 2

LITERATURE REVIEW

Seismic design codes are migrating from traditional seismic design codes to PBSD codes. Currently, some seismic design codes have adapted the prospective PBSD approach in a deterministic manner, in which uncertainties are considered implicitly. However, there exist different sources of uncertainties, for example, inherent uncertainties in hazard and demand, uncertainties in material properties, and the response of the structure, etc. Therefore, such uncertainties should be included explicitly in the framework of the PBSD process for the design of different types of structures.

This chapter first provides a short discussion of the PBSD approach. The problems with the FBD method, which most of the traditional seismic design codes are based on, are discussed, and then the state of development of the PBSD approach with some background studies is summarized.

2.1. Performance-Based Seismic Design

The PBSD is a design approach used for the seismic design of new structures and seismic performance evaluation and retrofitting of existing structures (Karimzada & Aktaş, 2016). Seismic performance, in the context of earthquake engineering, is an index that measures the degree of damage sustained by a structure during a specific earthquake (Padalu & Surana, 2023). For the last two decades, the PBSD approach has been improved significantly and is still continuously under development. It is capable of explicitly evaluating the probable performance of a structure under a given earthquake, considering the uncertainties in the potential hazard and the uncertainties in the assessment of the actual building performance. In addition, it is a reliable approach that produces a structure with a realistic understanding of the risk of casualties, occupancy interruption, and economic loss. Further, it allows the structures to show different performance levels corresponding to different hazard levels (Karimzada & Aktaş, 2016). These distinct characteristics make the PBSD methodology more suitable for use in structural design practice (Padalu & Surana, 2023).

The procedure of PBSD given in FEMA-445 (2006) is shown in Figure 2.1. The PBSD procedure is an iterative procedure, which starts by selecting performance objectives and ends with assessing the performance of the structure until the performance is met. A performance objective is the combination of a performance level and a specific seismic hazard level. Seismic hazard level obviously has inherent uncertainties, which should be considered in the design process.

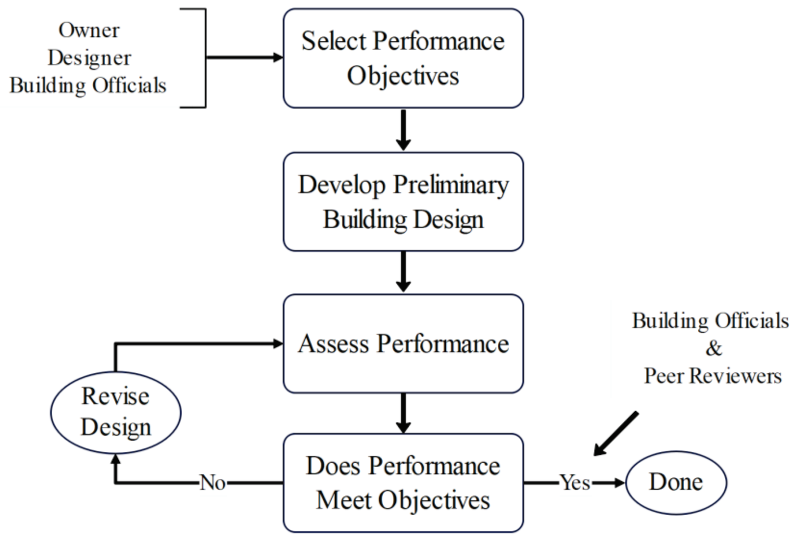

Figure 2.1. Performance-Based design flow diagram (Source: FEMA-445, 2006)

A series of simulations is required to assess the probable performance of a structure. The performance assessment process is shown in detail in Figure 2.2, which is adopted from FEMA-445 (2006). From the figure, it can be seen that it starts with the characterization of ground-shaking hazard and ends with the prediction of losses as a function of damage. In addition, from the given figure, it is clear that uncertainties exist in each step of performance assessment for both structural and nonstructural systems. Thus, for a complete performance assessment procedure, statistical relationships are required between earthquake hazards, building response, damages, and losses (FEMA-445, 2006).

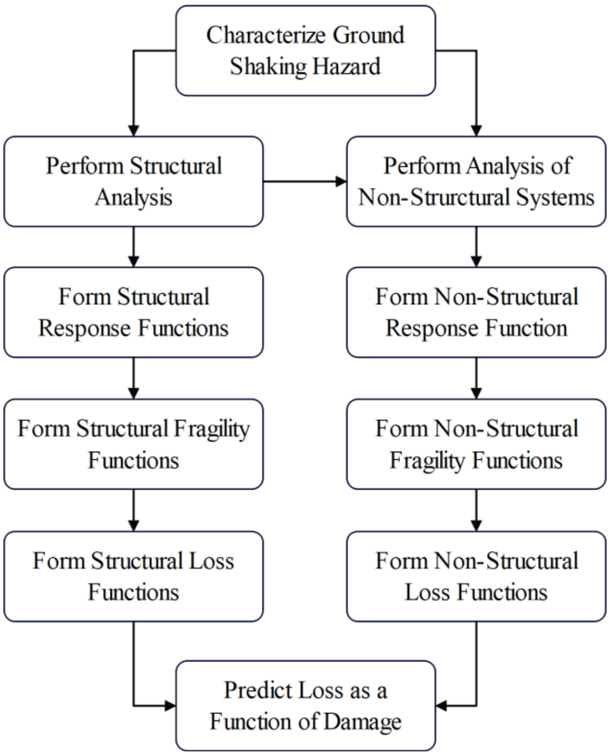

Figure 2.2. Performance assessment process (Source: FEMA-445, 2006)

Furthermore, the outcome of the performance assessment process is four different types of generalized random variables. Intensity Measure (IM) such as Peak Ground Acceleration (PGA), Peak Ground Velocity (PGV), etc., Engineering Demand Parameter (EDP) such as IDR, maximum drift, floor acceleration, etc., Damage Measure (DM), such as spalled concrete, collapse, etc. DMs are important to form fragility functions, and one of the concepts used to obtain such measures is the concept of damage indices. Fragility functions could be used to show the relationship between damage and the response of the structure. The last and final outcome is the value of the Decision Variable (DV), for example, repair cost, fatalities, downtime, etc. (Deierlein, 2004; FEMA-445, 2006; Mitrani-Reiser, 2007; Zareian & Krawinkler, 2012).

One of the main parameters in the PBSD approach is the selection of performance objectives; thus, they are discussed in more detail in the subsequent section. In addition, the performance assessment is also very important, and PEER PBEE methodology is used for this purpose in this study. Therefore, it is discussed in detail in the next chapter of this thesis.

2.2. Performance Objective

A performance objective is the specification of the expected seismic performance regarding the damage states, and it is the combination of a performance level and a specific seismic hazard level. Structural Engineering Association of California (SEAOC-Vision-2000, 1995) has provided the following performance matrix that shows the relationship between the performance level and hazard level. Each square in this matrix shows a specific performance objective, and the inclined lines, each of which is a set of performance objectives, show the design criteria. In the figure, four different performance levels are shown together with three different hazard levels. In addition, three different groups of buildings with respect to their performance are listed in this figure, namely, the basic or ordinary buildings, essential buildings, and hazardous buildings.

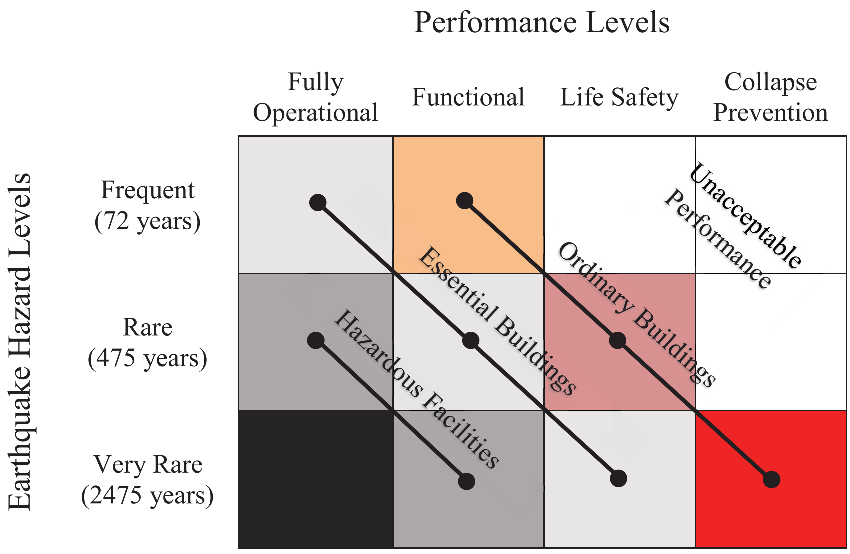

Figure 2.3. SEAOC Vision 2000 performance objectives for buildings (Source: Celik & Ellingwood, 2010)

Buildings in the hazardous facilities group are the ones that have storage for hazardous materials, such as nuclear power plants. The essential buildings group includes, e.g. hospitals, fire stations, etc. Ordinary buildings group consists of buildings such as residential buildings, office buildings, etc. To elaborate a little more, if, for instance, an office building is designed using the provided performance levels, the building should satisfy the LS performance level under rare earthquakes with a mean return period of 475 years while the same structure should satisfy the CP performance level under very rare earthquake hazard level, with a mean return period of 2475 years.

Some other guidelines and provisions, for example, FEMA-273 (1997), FEMA-356 (2000), and FEMA-389 (2004), provided the following table to present building performance objectives. An extra hazard level is also included in the table adopted from FEMA-356 (2000). Even though the building performance objectives given in the table are for evaluating the existing structures, they can also be used for the new design. From the table and figure, it can be observed that the performance levels provided by SEAOC Vision 2000 are similar to the ones given in FEMA-356.

Table 2.1. Performance objectives

<table>
<tr><th colspan="2" rowspan="2"></th><th colspan="4">Target Building Performance Levels</th></tr>
<tr><th>Operational (1-A)</th><th>Immediate Occupancy (1-B)</th><th>Life Safety (3-C)</th><th>Collapse Prevention (5-E)</th></tr>
<tr><td rowspan="4">Earthquake Hazard Levels</td><td>50% / 50 years</td><td>a</td><td>b</td><td>c</td><td>d</td></tr>
<tr><td>20% / 50 years</td><td>e</td><td>f</td><td>g</td><td>h</td></tr>
<tr><td>BSE-1
10% / 50 years</td><td>i</td><td>j</td><td>k</td><td>l</td></tr>
<tr><td>BSE-2
2% / 50 years</td><td>m</td><td>n</td><td>o</td><td>p</td></tr>
</table>

Note:

1. Each cell in the above table represents a discrete rehabilitation objective.
2. Three specific rehabilitation objectives are defined in FEMA-356.
   Basic Safety Objective = cells k+p
   Enhanced Objectives = cells k+p+any of a, e, i, b, f, j, or n
   Limited objectives = cell k alone or cell p alone.
   Limited objectives = cells c, g, d, h, l.

2.2.1. Building Performance Levels

Performance level describes a structure's post-earthquake physical damage condition, and it is a limit for allowable damage that a structure can tolerate for the specific hazard level, and beyond that, the damages are not acceptable. These damages cause loss, including monetary loss, casualties and fatalities, and loss due to downtime. A structural performance level and a nonstructural performance level are combined to form a building performance level, i.e., the performance level can be determined using the damage states of structural and nonstructural components and content systems (FEMA-356, 2000; FEMA-389, 2004).

Qualitatively, a building's performance can be defined as follows (FEMA-389, 2004):

- During and after an earthquake, the safety of occupants.
- Repair cost of the building to bring it back to it is pre-earthquake condition.
- Repair time that the building is nonfunctional or out of service.
- Significant architectural, historic, and economic impact on the community

Some guidelines, such as FEMA-273 (1997), FEMA-356 (2000), and FEMA-389 (2004), provide detailed information regarding each performance level. They are briefly discussed in the following sections.

2.2.1.1. Fully Operational Performance Level

Also called the operational performance level, the building will maintain almost its initial stiffness and strength at this performance level after an earthquake. Some minor cracks could be observed in structural and nonstructural components, such as partitions, ceilings, and facades. However, it is anticipated that other elements and systems will remain functional, e.g., mechanical, plumbing, and electrical systems, which are required for the normal operation of the building. The risk to occupants of the buildings is negligible, and the overall damage to the structure is ignorable. Generally, buildings under frequent earthquakes shall meet or exceed this performance level. Designing buildings for this performance level under rare earthquakes, except buildings with hazardous facilities, is not economically practical.

2.2.1.2. Immediate Occupancy Performance Level

This performance level is also called functional. Generally, the building is experiencing light damage; the damage state for structural elements will be the same as in the operational performance level; on the other hand, nonstructural elements will have some more damage compared to the operational performance level. The risk to occupants is very low; however, some restoration, repair, and cleanup might be required. The initial stiffness and strength of the building remain almost the same as prior to the earthquake. Some owners expect this performance level from buildings under moderate earthquake hazard levels, while some other owners expect this performance level from buildings under severe earthquake hazard levels. For this performance level, the limit for peak IDR is 1%, and the structure has negligible permanent drift.

2.2.1.3. Life Safety Performance Level

In this performance level, the building may lose its significant amount of strength and stiffness. Still, it will have some lateral strength against collapse, and the gravity load-carrying capacity of the vertical members will be functional. The building could be repaired; however, it will not be economically practical. Structural and non-structural elements will experience significant damage, falling elements will be secured, and mechanical, electrical, and architectural systems will be damaged. The peak IDR for this performance level is 2%, and the building will have some permanent drift for which a 1% permanent drift limit is recommended. Although the building has gravity load-bearing capacity, re-occupancy is unsafe until repair. In traditional seismic design codes, this performance level is the base for the design of new structures under rare earthquake hazard level, with a 475-year return period.

2.2.1.4. Collapse Prevention Performance Level

The building is severely damaged, and columns and walls can carry the gravity loads; however, the overall lateral strength of the building is lost significantly, and the building is near collapse condition. The structural elements will experience severe damage, and non-structural elements, such as infill walls and unbraced parapets, may fall, which might cause blockage of the exit of the buildings. It may not be possible to repair the structure. The peak IDR and permanent drift for this performance level is 4%, according to FEMA-356 (2000). In addition, the building is very risky for life; thus, reoccupying the building is not safe.

It should be noted that most owners and stakeholders would prefer to demolish the structure if the repair cost reaches around 50% of the replacement cost.

2.3. Problems with the FBD Method

Current practice for the design of structures against seismic forces is based on the traditional seismic design codes. These codes use the FBD and some linear techniques to achieve the desired LS performance level under design earthquake with a 10% probability of exceedance in 50 years. Further, most of these codes do not consider the inelastic behavior of the structures directly in the design process rather, they use the response modification factor to consider the inelastic behavior of the structure implicitly (Benedetti et al., 2008; Karimzada, 2015; Priestley, 2000). As a result, a structure designed using the FBD process may experience unacceptable large inelastic deformation. Besides, the design of critical structures, such as hospitals, schools, etc., is carried out considering important factors that provide the performance of the structure implicitly (Padalu & Surana, 2023). In addition, past earthquakes showed that although many structures designed using traditional seismic design codes survived the collapse, their damage states were beyond the socio-economic levels (Karimzada, 2015). They were not repairable and needed to be demolished. On the other hand, many other structures that were supposed to be operational after the earthquakes, such as hospitals, communication towers, bridges, etc., in reality, they lost their functionality, and they were not immediately operable after the earthquakes (Padalu & Surana, 2023).

Moreover, under a certain earthquake hazard level, known as design earthquake, a structure may satisfy the LS performance level, which is the main goal of most of the traditional seismic design codes (Karimzada et al., 2024). However, damages to structural and non-structural components and content systems may cause lots of loss in such a situation (Dowrick, 1985; Padalu & Surana, 2023). The loss includes the direct monetary loss due to repair cost and indirect monetary loss due to the repair time. Because of the repair time, the structure may not be functional, which could cause a delay in the manufacturing of products, for example, in an industrial structure, or there may exist rental loss, for example, for an office or residential structure. In light of these facts, multi-objective seismic design criteria must be considered in the design process for a structure (Padalu & Surana, 2023). Besides, all performance objectives cannot be controlled by a single design parameter at all performance levels (Krawinkler, 1996). Therefore, the seismic design should take into account a number of performance control criteria (Padalu & Surana, 2023).

Another deficiency of the traditional seismic design codes is that they cannot produce structures with uniform risk in the same seismic zone. To elaborate more, for example, consider two different structures located in the same seismic zones, and both are designed using the design criteria of the same traditional seismic design code. There is a possibility that one of them may show a better performance than the minimum given in these codes, while the other may show poor performance than the minimum described in these codes (FEMA-445, 2006).

PBSD is a methodology that allows for the concurrent consideration and handling of multiple performance control criteria as well as multiple performance objectives. In this approach, the desires of the stakeholders and the owners are defined in terms of single or multiple performance objectives, and the structures are designed to fulfill these performance objectives (Padalu & Surana, 2023). It is a consequences-based design procedure, i.e., it deals with the outcome of a structure rather than how it is going to be built (Karimzada et al., 2024). In addition, structures with uniform risk could be produced using the PBSD approach. The actual behavior of the structure could be more reliably anticipated by using the PBSD approach. Furthermore, since, in the PBSD, the nonlinear deformation of the members is explicitly considered, the actual strength and ductility capacity are obtained accurately (Padalu & Surana, 2023).

2.4. State of Development of the PBSD

One of the most destructive natural disasters to structures is an earthquake. Buildings were designed and constructed to withstand these phenomena for the first time in the eighteenth century. The aim of which was to avoid the overall collapse of the structure. In the early twentieth century, following the occurrence of Messina, Italy, in 1911 and Kanto, Japan, in 1923 earthquakes, standards and codes were developed that included different levels, from simple to complex, of engineering calculations. Furthermore, in the United States, the design requirements were first put in the code format following the Santa Barbara earthquake in 1925, which caused lots of damages, including monetary and casualties. The main purpose of these requirements was to prevent buildings from overall collapse or to avoid the collapse of large elements of the buildings (NEHRP, 2009).

These primary goals well-suited the prescriptive design aims of LS performance level. This performance level is still the main goal of the traditional seismic design codes, besides the improvements over the years (NEHRP, 2009). The design lateral forces due to earthquakes were taken 10% of the structure's weight, ignoring its dynamic behavior (Padalu & Surana, 2023). It has been observed through years of research and developments in conventional code provisions that critical buildings, such as hospitals, schools, emergency facilities, etc., must be able to function more efficiently than normal buildings, such as office buildings, residential buildings, etc. They should be able not only to fulfill the LS performance level but also to maintain their functionality after severe earthquakes (NEHRP, 2009).

The need for retrofitting existing buildings to comply with traditional seismic design codes was identified in 1960 after engineers and professionals found that most of these buildings did not fulfill the requirements of the codes (Ellingwood, 2008; NEHRP, 2009). The owners wanted to know the probable performance of the retrofitted buildings under future earthquakes and decide whether to retrofit and strengthen their buildings or not. Therefore, engineers in the United States involved in retrofitting existing buildings in the 1980s got interested in the PBSD, which was the beginning of the PBSD approach. This was because the engineers discovered that codes currently in place did not explicitly provide information on the probable performance of the existing building during an earthquake. Furthermore, it was difficult and not financially feasible to retrofit the existing buildings with the traditional building code requirements, which were primarily for the seismic design of new buildings. To this end, to determine the probable performance of an existing structure, engineers developed some primary assessment procedures, and for utilizing assessment, they had to rely on their own experience and judgment (Hamburger et al., 2004).

Moreover, the Applied Technology Council (ATC) published many documents in the mid-1980s to make the practice in this area in a standard form. One of these documents is the ATC-13, "*Earthquake Damage Evaluation Data for California*", which was released in 1985. This report contains statistical data for the probable repair costs of various types of buildings. ATC-14, "*Evaluating the Seismic Resistance of Existing Buildings*", was published in 1987, which includes a standard methodology for evaluating the life safety hazard of a building in an earthquake. Nevertheless, these reports do not give information on how to retrofit an existing building to obtain improved performance (Hamburger et al., 2004). To solve this issue, a series of studies were funded by the Federal Emergency Management Agency (FEMA) in 1989 (NEHRP, 2009). The main objective of these documents was the development of the PBSD for the existing buildings. FEMA 237, "*Seismic Rehabilitation of Buildings, Phase I: Issues Identification and Resolution",* was the first report of FEMA released in 1992. The effective introduction of performance goals at the outset of these studies provided a good foundation toward PBSD (FEMA-389, 2004).

ATC carried out a FEMA-funded project after the earlier studies in collaboration with the Building Seismic Safety Council (BSSC) and the American Society of Civil Engineers (ASCE). FEMA-273 (1997), "*NEHRP Guidelines for the Seismic Rehabilitation of Buildings",* FEMA-274 (1997), *NEHRP "Commentary for the Guidelines for the Seismic Rehabilitation of Buildings"*, and FEMA-276 "*Example Uses of the NEHRP Guidelines for Building Seismic Rehabilitation"* were the outcomes of this project. These documents contain comprehensive information about the PBSD concept for retrofitting and rehabilitation of existing buildings to improve their performance for future earthquakes. These documents cover various performance levels for various ground shakings (FEMA-389, 2004). They were later converted by the ASCE to FEMA-356 (2000), "*Pre-Standard and Commentary for the Seismic Rehabilitation of Buildings",* retaining all concepts developed for FEMA-273 (1997), including performance levels and explanation of the performances (FEMA-389, 2004; Padalu & Surana, 2023).

Furthermore, Vision-2000 was developed by the Structural Engineers Association of California (SEAOC) in 1995, which contains a framework for the PBSD of new buildings (FEMA-389, 2004; NEHRP, 2009). On the other hand, in about the same period, ATC-40 (1996), "*Seismic Evaluation and Rehabilitation of Concrete Buildings",* was published in 1996 by the Applied Technology Council. This report is about a comprehensive procedure, based on the PBSD concepts, for the performance assessment and retrofitting of concrete buildings (FEMA-389, 2004; NEHRP, 2009). The procedure of FEMA-273 (1997) was examined and improved by the ASCE and then published ASCE-41 in 2006 as a national standard: "*Seismic Rehabilitation of Existing Buildings"*. The first generation of the PBSD procedure is thought to have been presented by ASCE-41 because, although it is initially used for the rehabilitation of existing buildings, its performance objectives and technical data could be used for the design of new buildings (NEHRP, 2009; Sood, 2010).

In addition, FEMA-445, "*Next-Generation Performance-Based Seismic Design Guidelines: A Program Plan for New and Existing Buildings",* was also introduced in 2006 by ATC, which contains two phases. The first phase is to develop a methodology for assessing the seismic performance of buildings, and the second stage is the development of the PBSD procedure and guidelines. In FEMA-445, three main issues were considered to be developed and advanced for practical use. These include the Performance-Based Assessment, Performance-Based Design, and Performance-Based Upgrades of Existing Buildings (FEMA-445, 2006). In this regard, significant improvement has been made in the PBSD procedure for the last two decades, specifically when PBSD has adapted probabilistic approaches in its framework. To this end, a probabilistic PBSD framework has been developed in which different sources of uncertainties could be considered, and the damage level of a building and its content could be predicted easily (Padalu & Surana, 2023).

FEMA-P695, "*Quantification of Building Seismic Performance Factors"*, report was published in June 2009. This report outlines a methodology for reliably quantifying the performance of a building and its related response parameters. The response parameters are used for the purpose of seismic design. The methodology offers a rational basis for determining global seismic performance factors. These factors include the response modification factor (R), system overstrength factor (Ω_0), and deflection amplification factor (C_d). One of the principles of the methodology is utilizing the nonlinear collapse simulation on a set of archetype models to measure performance. In this regard, while evaluating the collapse performance, uncertainties are considered explicitly (FEMA-P695, 2009). In addition, as a main design criterion for the PBSD, this report uses the acceptable collapse risk (Padalu & Surana, 2023).

Furthermore, a set of FEMA-P-58 reports were published in 2018. FEMA-P-58-1, "*Seismic Performance Assessment of Buildings Volume 1-Methodolgy"*. FEMA-P-58-2, "*Seismic Performance Assessment of Buildings, Volume 2 – Implementation Guide"*. FEMA-P-58-3, "*Seismic Performance Assessment of Buildings, Volume 3 – Supporting Electronic Materials and Background Documentation"*. All of these reports are used together for the performance assessment of a building. FEMA-P-58-1 provides the probabilistic seismic performance assessment methodology. The performance of the building for a given earthquake hazard is presented in terms of probable consequences, including repair cost, repair time, injuries, and fatalities. The methodology could be applied to any type of building structure without considering the age of the building, its construction, or occupancy. However, its implementation requires a basic understanding of structural and non-structural damageability and consequences. This methodology uses the development of basic building information, fragility functions, consequence data, and response quantities as inputs (FEMA-P-58-1, 2018). As a primary design criteria, this report also uses the acceptable collapse risk (Padalu & Surana, 2023).

2.5. General Overview of Structural Optimization

Several studies have been conducted for the structural design optimization of the steel and RC structures. One of the earliest research in this regard is the work of Frangopol (1986). In this research, he proposed a computer-automated approach that could be used for the designing of steel and RC structures. Optimization is carried out for minimizing the weight of the structure, and reliability analysis is included in the optimization problem to obtain the constraints for both serviceability and ultimate performance levels of the structures.

An optimal computer-based design method for RC structures is introduced by Moharrami & Grierson (1993). The design variables are the cross-sectional dimensions of the members and the reinforcement ratio of these members. As an objective function, they minimized the cost of the concrete, steel, and formwork, while strength and stiffness were used as constraints of the optimization problem.

Ganzerli et al. (2000) proposed a framework for the optimum seismic design of RC frames, which includes the performance-based design criteria in terms of beam and column plastic rotations as constraints. The objective function used was the minimization of the structural cost. They used pushover analysis in the optimization process.

In accordance with the cost-effectiveness criterion, an optimal decision model of the target value of the performance-based structural system reliability of RC frames is formulated by (G. Li & Cheng, 2001). They showed that the better indices to express the target performance levels for a structure are the target values of the performance-based structural system reliability.

An efficient optimization method for the design of elastic and inelastic drift performance under response spectrum loading and pushover loading in RC buildings is introduced by Chan & Zou (2004). They considered two levels of earthquake loading that are related to minor and severe earthquake events. Accordingly, the optimization is carried out in two phases. In the first phase, they performed elastic design optimization to minimize the structural cost under minor earthquake loading in terms of the elastic response spectrum, and the design variables were taken as the dimensions of the members. In the second phase, the optimum member sizes were kept constant, the reinforcement ratio was considered as design variables, and the design optimization was carried out for steel reinforcement under inelastic pushover displacement response constraint.

The PBSD of steel structures was developed by Liu et al. (2005) as a multi-objective optimization problem, considering initial cost and cost due to future risk, i.e., repair cost as two competitive objective functions. They considered the peak IDR to represent the risk at two hazard levels with a 2% and 50% probability of exceedance in 50 years.

A methodology that accounts for the inelastic behavior is proposed by Fragiadakis et al. (2006) for the performance-based optimal design of steel structures. In the methodology, static pushover analysis is used inside the optimization process to predict the damage at various earthquake intensity levels. The initial cost and the life cycle cost of the structure are considered as objective functions for the optimization problem.

Using nonlinear dynamic analysis as the analytical basis, Foley et al. (2007) presented a multi-objective optimization procedure for the design of steel moment-resisting frames based on probabilistic performance-based formulations. Several formats for optimal design problems have been created using this probabilistic design methodology. In one of the formats, they used two objective functions: maximizing confidence level for achieving IO and CP performance levels, while the second objective function was the minimization of the volume of the material.

Lagaros & Papadrakakis (2007) designed a 3D RC structure following Eurocode 8 and the performance-based design approach within the context of the multi-objective optimization framework. For the objective functions of the multi-objective optimization problem, they considered the initial construction cost and the peak IDR for the hazard level with a 10% probability of exceedance in 50 years. The resulting design for the two different design approaches was compared in terms of fragility functions obtained from the corresponding Pareto front curve of each method. It was shown that the structure designed using Eurocode 8 was more vulnerable than the one designed with respect to the performance-based design approach.

Lagaros et al. (2008) proposed a Neural Network (NN) approximation of the limit-state function and combined it with either Monte Carlo Simulation (MCS) or First Order

Reliability Method (FORM) approaches for handling the uncertainties in order to determine the most effective methodology for carrying out reliability analysis in conjunction with performance-based optimum design under seismic loading. While performing reliability analysis, they used two categories of random variables. The ones that have impact on the seismic demand level and those that have impact on the structural capacity. They showed that using these two methodologies (combination of the NN approximation with MCS or FORM) together with the topology design variables and the sizing reduced the computational effort by two orders of magnitude. They applied the methodology on the steel structure and used pushover analysis for response capacity analysis.

In a research conducted by Mitropoulou et al. (2011), a methodology was proposed for the quantitative estimation of the life cycle cost and seismic risk of RC buildings. They designed a 3D RC building structure with respect to Code-Based design optimization, for which initial construction cost is considered an objective function. In addition, they designed the same structure with respect to the performance-based design optimization method, for which the total cost (initial construction cost plus life cycle cost) of the structure is used as an objective function. They showed that the structure designed with the prescriptive/Code-Based design approach is more vulnerable than the one designed with the PBSD approach. They used both IDA and pushover analysis in their study, which causes the methodology to be expensive computationally.

A framework for the optimum seismic design of steel structures based on life-cycle costs was developed by Kaveh et al. (2012), which is capable of solving the performance-based multi-objective optimization problem, and they made an effort to reduce the computational time of necessary pushover analyses during the optimization process to make the framework suitable for large-scale structures. They showed the effectiveness of the framework in terms of the computational time through solving examples. They used the ATC-13 (1985) drift limits for seven damage states.

To reduce computational time, Kaveh et al. (2014) proposed a methodology for steel structures for solving the performance-based multi-objective optimization problem, in which the initial cost and the life cycle cost of the structure are used as two conflicting objective functions, attempting to reduce the computational time. They used a simplified nonlinear structural modeling strategy and wavelet analysis to reduce analysis time. In the wavelet analysis, the number of acceleration points is reduced. The ability of the proposed framework to solve the current multi-objective optimization problem is demonstrated by the numerical application results on a 10-story steel structure. They used the ATC-13 (1985) drift limits for seven damage states.

Based on the concept of uniform deformation, Mohammadi & Sharghi (2014) developed a framework for the performance-based optimum seismic design of eccentrically braced steel frames. They showed that the frames designed using the proposed methodology have less damage than those designed using Code-Based design methods.

Saadat et al. (2015) presented a probabilistic PBSD of steel structures considering multi-objective optimization. The defined optimization problem takes into account the direct social and economic losses relevant to the seismic events. They used three performance objectives, which are the initial cost of the structures, expected annual costs related to damages due to the occurrence of earthquakes, and expected social loss. They showed that with an increase in the initial cost, the direct economic loss and the social loss decreased.

Möller et al. (2015) introduced a framework for the performance-based optimum seismic design of buildings to achieve minimum total cost and reliability levels at various performance levels. For performance evaluation of the structure and obtaining the reliability levels, they used a neural network for a set of design variables. In addition, rather than using the standard fragility method, this framework operates directly with the set of GM and structural variables. Further, the total cost in their study consists of the initial cost, repair cost in the lifetime of the structure, and associated social costs.

Saadat et al. (2016) proposed a PBSD methodology for the optimization of the steel structure. In the methodology, they considered the performance of the structural and nonstructural systems as well as seismic losses. The objective functions are the initial cost of the structure and the expected annual loss as a result of the occurrence of earthquakes. They used the fragility functions to attain the damage probabilities of the structural system and nonstructural components. They also investigated the effect of the geographical location on the loss results, considering two different locations. They showed that there is a significant difference between the calculated loss of the two locations, which is mainly due to the slope of the hazard curve and the characteristics of the seismic events.

In a study by Mitropoulou & Lagaros (2016), performance evaluation is conducted for 3D fixed and base-isolated RC structures considering the initial and life cycle costs. They first designed both of the structures using a PBSD optimization method, for which peak IDR limits at three hazard levels were used as constraints, and only the initial cost of the structure was used as the objective function of the optimization problem. They concluded that the structure with a fixed base has a lower initial cost compared to the base-isolated structure; in contrast, the total cost (initial cost plus life cycle cost) is significantly higher.

Fragiadakis & Papadrakakis (2008) introduced a fully automated Performance-Based Design (PBD) methodology for RC structures, which is based on Nonlinear Time History Analysis (NTHA). An optimization algorithm is used to replace the traditional trial-error process for a better design. Two different alternatives of the design methodology are presented. The first alternative formulations are presented in a deterministic manner to obtain the optimum design, which is denoted as Deterministic-Based Structural Optimization (DBO). In contrast, in the second alternative, Reliability-Based Optimization (RBO) formulations are suggested to obtain the desired optimum design. They applied the proposed methodology on two RC frame structures, a two-story with a single span and a six-story with two equal spans. The construction cost of the structure is used as an objective function of the optimization problem in both cases. The design variables are the cross-sectional dimensions of the elements of the frames and the longitudinal reinforcement. The shear reinforcement is not considered as a design variable.

Different limit states, from serviceability to CP limit states, are considered in the formulation of both cases. In RBO, probabilistic constraints are used in terms of MAF of exceedance of multi-limit states. Three performance levels, IO, LS, and CP, that corresponds to hazard level of 50%, 10%, and 2% probability of exceedance in 50 years, respectively, are considered as limit states. It is shown that, by adopting design criteria related to the PBD concept in a better sense, RBO approach procedure is more effective compared to the deterministic formulation for the optimum design problem. The RBO approach gives a more economical design with respect to the DBO. Further, they concluded that each of these alternatives provides structures with better performance compared to the conventional design methods. They showed that by using the proposed methodology, the construction cost of the structure could be reduced significantly while maintaining better control over the seismic performance.

Basim et al. (2016) proposed a new methodology called Value-Based Design (VBD) of structures. They used the ET method for the performance assessment purpose in the optimization procedure. The expected total cost of the structure, which consists of the initial construction cast and the expected cost due to the occurrence of earthquakes, is assumed as an objective function of the optimization problem to be minimized. For the solution of the optimization problem, the GA has been utilized. They designed a prototype steel frame using the proposed methodology. The same structure is designed by the conventional Code-Based design and PBSD approaches. The seismic performance of the frames designed through different design methods is compared in terms of the expected cost components. They showed that the initial cost of the steel frame designed with respect to the prescriptive design method is the lowest, while for the frame designed to VBD method is the highest. In contrast, the expected total cost for the frame designed through the VBD method is the lowest, and for the one designed using the prescriptive design method is the highest.

In their study, seven limit states are utilized to define the performance of the structure. The IDR limits, which are based on the ATC-13 (1985), are used to obtain the loss of the structural components, while the PFA limits, which are provided in Elenas & Meskouris (2001), are used for evaluating the loss of the contents. In addition, damage state parameters for cost calculations of the different consequences (decision variables, e.g., injury rate, death rate, etc.) are adopted from ATC-13 (1985) and FEMA-227 (1992).

Yazdani et al. (2017) proposed a probabilistic performance-based optimum seismic design methodology for RC Structures, in which the effect of soil-structure interaction is also considered. The method is the combination of the Modified Discrete Gravitational Search Algorithm (MDGSA) and metamodel, which is developed to minimize the total cost of the structure (construction cost plus repair cost). Deterministic and probabilistic constraints have been used in the optimization problem. MDGSA is the modified form of the original Gravitational Search Algorithm (GSA) proposed by Rashedi et al. (2009) and the Discrete Gravitational Search Algorithm (DGSA) proposed by Khatibinia et al. (2013). The crossover and mutation operators are used in MDGSA to enhance the exploitation and exploration of the original GSA. A metamodel also called a surrogate model, which is produced from the actual model by using a limited number of simulations on the original model. It is a simplified form of an actual model for anticipating the response of the structure.

The methodology is utilized on a 9-story, three-dimensional RC building. The cross-sectional dimension of columns and beams and the reinforcement ratio in these elements are used as design variables. The finite element model of the soil-structure system is conducted considering the effects of nonlinear soil-interaction to see its effects on the response of the structures. The same structure is designed using the original GSA, and the results are compared with the one designed by MDGSA. It was shown that compared to the original GSA, using the proposed MDGSA method, a more economical RC structure could be obtained with fewer iterations. In addition, the method is claimed to be important for long-period RC structures. Specifically, while considering soil-structure interaction effects in the design of such structures, due to the fact that some sort of soil (e.g., soft sediments) could amplify the GM intensity, which in turn causes dynamic amplification of the structures. However, damage caused by the nonstructural elements and content systems, which may signify the total cost, are not considered.

Y. Li (2014) and Li et al. (2019) introduced a Probabilistic Performance-Based Optimum Seismic Design (PPBOSD) framework with the goal of encouraging the practical application of probabilistic methods for design purposes. This framework is an enhancement of the Performance-Based Earthquake Engineering (PBEE) methodology, which was achieved by utilizing mathematical optimization to encircle the forward PBEE analysis in the design process with a decision-making layer. They used the forward PBEE expression to the traditional PBEE methodology, which is usually used for seismic performance evaluation of existing or new structures. The proposed methodology is initially explained and applied on an inelastic single-degree-of-freedom (SDOF) bridge model to check the validation of the proposed method. In this study, they used a targeted loss hazard curve as a probabilistic performance objective, which corresponds to a set of previously selected optimum design parameters (initial stiffness and yield strength). The intended PPBOSD framework is anticipated to guide the design process so that the loss hazard curve approaches the target loss hazard curve as closely as possible. In their findings, they showed that there is a little bit of difference between the target loss hazard curve and the obtained loss hazard curve through this methodology. The error between the initial stiffness of the structure corresponding to the target loss hazard curve and the one obtained through this methodology is 1%, while there is a 2.4% error in the yield strength of the two cases.

The proposed methodology is used to optimize the seismic design of the isolator for the California high-speed rail (CHSR) prototype test-bed bridge with nine spans (Y. Li, 2014; Y. Li & Conte, 2018). The usefulness and optimality of the CHSR prototype bridge were investigated (Y. Li, 2014; Y. Li & Conte, 2018). In this regard, parametric probabilistic demand analysis is conducted using high-throughput cloud computing resources for the CHSR prototype bridge in the seismic isolator parameter space. The elastic yield, initial stiffness, and postyield-to-preyield stiffness of the seismic isolator are considered as design variables of the optimization problem. In order to demonstrate the effectiveness of the suggested optimum seismic design framework with explicit consideration of the uncertainties in the seismic loading, the performance of the optimum design of the isolated bridge is compared with the performance of the isolated bridge that has been initially designed without optimization. In addition, they compared the performance of the optimally designed isolated bride with the nonisolated bridge.

The outcomes of the probabilistic seismic demand analysis for the EDP, which was utilized in the objective function, are used to compare the seismic performance of the three mentioned cases. The maximum total transverse base shear is used for the objective function, and as a constraint function for the optimization problem in the isolated bridge, the maximum transverse base moment is used. The demand hazard results showed that the isolated bridge designed with the proposed methodology fell between the isolated bridge with the initial design and the nonisolated bridge. The isolated bridge designed with the proposed methodology gives a higher seismic demand in terms of base shear force compared to the isolated bridge with the initial design. The reason behind the higher demand is that probabilistic constraints are used in the optimization problem. In addition, the probabilistic constraints were satisfied in the isolated bridge designed using the proposed methodology; however, the isolated bridge with the initial design violates the constraints. In addition, the isolated bridge designed by the proposed methodology gives a lower seismic demand compared to the nonisolated bridge.

Compared to the IB with the initial isolator design, the optimum isolator design leads to higher seismic demand for the total transverse base shear. This is due to the satisfaction of the probabilistic constraints imposed in the optimization problem, while these constraints are not satisfied by the initial isolator design.

In a study by **Khalilian et al. (2021),** an effort has been made to introduce a life cycle cost-based optimal performance objective for the performance-based design method. The proposed methodology is applied to the steel moment frame structure. In their study, they investigated the optimized total cost of the structure for the optimum hazard level that is related to the LS performance level. To clarify, first, they used the PBSD approach to optimize the structures to satisfy the LS performance level for five different seismic hazard levels, considering only the initial cost of the structure as an objective function. Later, they used the FEMA-P-58-1 (2018) assessment methodology to obtain the life cycle cost of the structure. Then, they select the design alternative with minimum life cycle cost, and its corresponding hazard level is called the optimum hazard level for the LS performance level. They showed that a 25.1% increase in initial cost corresponding to the optimum hazard level will decrease the life cycle cost by 57.7% and the expected total cost by 16%.

In addition, they also investigated the effect of the discount rate, building lifetime, and building depreciation overtime on the optimal seismic hazard level. They showed that with an increase in the discount rate, the life cycle cost of the structure decreases. In addition, the life cycle cost increases with an increase in the lifetime span.

In a research conducted by **Mirfarhadi & Estekanchi (2020)**, an optimal seismic design framework for the structures is proposed. The value of the structure, which is the ratio of the performance or function over the cost (Mukhopadhyaya, 2009), is considered as an objective function to be maximized. Each DV, including repair cost, repair time, injuries, and fatalities, is translated into the equivalent economic values and used directly in the design procedure. They considered the construction cost and the expected cost due to seismic effects on the value of the structure. The performance of the structure is evaluated using the FEMA-P58 methodology. The ET method is used for the analysis of the structure to obtain EDP at various hazard levels, specifically in the optimization procedure. The IDA method is used for assessing the performance of the structure to confirm the results of the ET method.

The method is applied to 4-story and 8-story structures, and as mentioned, the total value of each structure is considered as objective function to be maximized. They used the requirement of current codes for detailing the structural components and the limitations on the minimum stiffness and strength of these components as constraints for the optimization problem. Similar structures are also designed using conventional Code-Based design approach, and the construction cost is considered an objective function for the optimization problem. They used the Iranian National Building Code (INBC) in this case. The resulting designed structures in both cases are then assessed using ET and IDA methods. The results are compared in terms of the values and the seismic response. They showed that the value-based design approach increases the construction cost significantly compared to the conventional Code-Based design, consequently improving the performance of the structure.

In their study, since they only considered the construction cost and the expected cost due to seismic effects, they did not consider the performance objectives and ignored the prescribed design criteria. They considered the section dimensions and longitudinal rebar of beams and columns as design variables. However, the shear reinforcements are not considered as design variables. In addition, the structure's performance is presented in terms of economic values, which makes it easier for stakeholders and engineers to communicate while deciding on the design of the structure. They also claim that the method could be applied to other hazards as well.

In their study, they used the set of inx Endurance Time Excitation Functions (ETEFs). These functions are generated from 20 GM records of FEMA 440 for soil type C. The records are optimized in the nonlinear range to fit the average response spectrum of the mentioned GM records. One of the problems with these excitation functions is that the durations of the GMs are not considered directly, which is one of the important parameters that may affect the response of the structure significantly while generating these excitation functions. These excitation functions are up to 20sec with an increment of 0.1sec.

They used the FEMA P58 loss analysis procedure (following figure) for the seismic performance assessment of the structures.

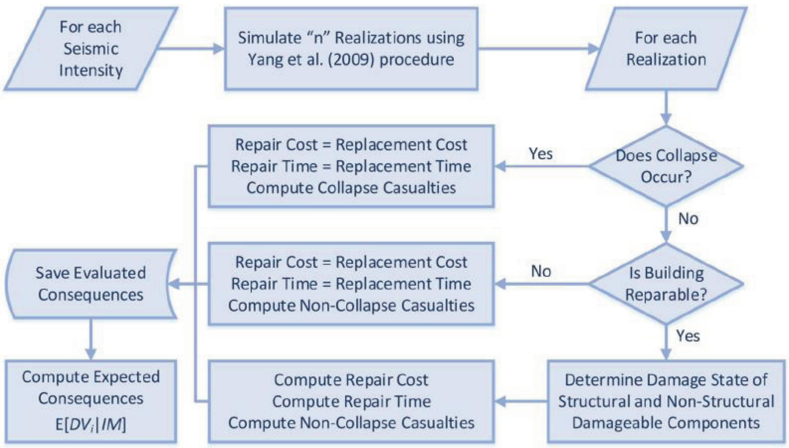

Figure 2.4. FEMA P 58 loss analysis framework (Source: Mirfarhadi & Estekanchi, 2020)

CHAPTER 3

PERFORMANCE ASSESSMENT OF THE STRUCTURES

Pacific Earthquake Engineering Research (PEER) Center has developed a probabilistic PBD assessment methodology for the performance evaluation of the structures, known as the PEER Performance-Based Earthquake Engineering (PBEE) methodology. The developed PEER PBEE methodology, originally proposed by Cornell and Krawinkler (2000), is given in Figure 3.1, adopted from Li Yong (Y. Li, 2014).

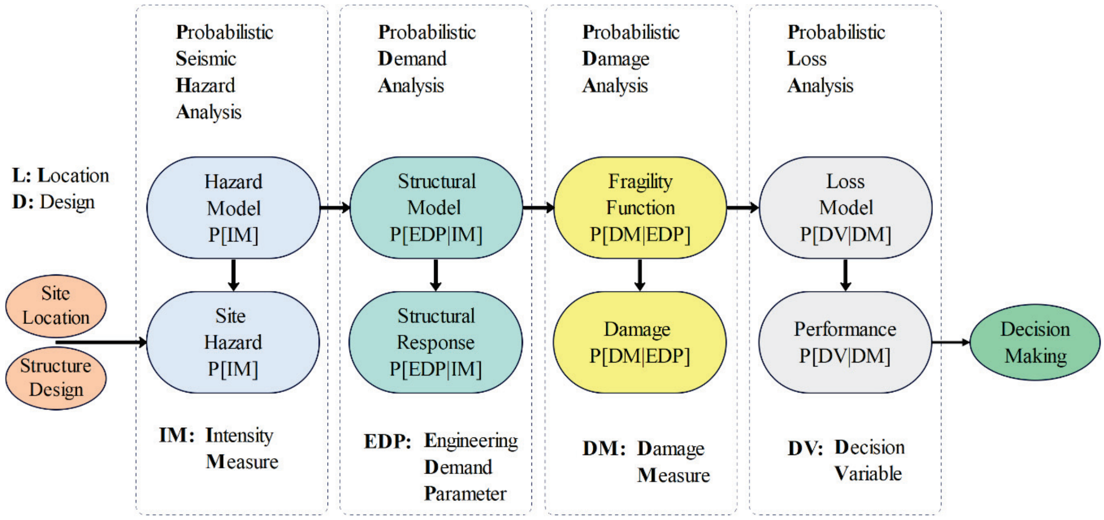

Figure 3.1. Framework of the probabilistic PEER PBEE methodology (Source: Y. Li, 2014)

The PEER PBEE methodology evaluates the risk on a structure in a quantitative format in terms of probability due to possible future earthquakes. Seismology, geotechnical engineering, structural engineering, and construction or repair cost estimation are involved in the methodology. Using the total probability theorem in the framework of the PEER PBEE methodology, it would be possible to obtain the probabilistic estimation of the performance of the structure considering uncertainties in the mathematical model of the structure, which in turn spread out the inherent uncertainties in the intensity of the earthquake that a structure would possibly face in the future (Y. Li, 2014).

From Figure 3.1, it is evident that in the PEER PBEE methodology, four probabilistic analysis procedures are included, which are probabilistic seismic hazard, probabilistic demand, damage, and loss analyses. In addition, it is evident from Figure 3.1 that uncertainties are considered explicitly in the performance assessment through the PEER PBEE procedure.

3.1. PEER PBEE Framework Equation

As mentioned earlier, the outcome of the performance assessment procedure in the framework of PBSD is four different types of variables, which are IM, EDP, DM, and DV. Thus, these variables can be combined by using the total probability theorem, which gives a mathematical model for risk that explains the outcome in a probabilistic manner. The equation, also referred to as the PEER PBEE framework equation, is provided as follows (Günay & Mosalam, 2013; J Moehle & GG Deierlein, 2004; Y. Li, 2014).

$$\lambda(DV) = \iiint G\langle DV \mid DM \rangle \, dG\langle DM \mid EDP \rangle \, dG\langle EDP \mid IM \rangle \, dG(IM) \qquad (3.1)$$

Where:

λ represents the MAF.

G represents the conditional probability.

$\lambda(\mathrm{DV})$ is the probabilistic description of DV.

$\mathrm{G}\langle \mathrm{DV}|\mathrm{DM}\rangle$ is the probability of DV on the condition that DM is given.

$\mathrm{dG}\langle \mathrm{DM}|\mathrm{EDP}\rangle$ is the derivative of the probability of DM on the condition that EDP is given.

$\mathrm{dG}\langle \mathrm{EDP}|\mathrm{IM}\rangle$ is the derivative of the probability of EDP on the condition that IM is given.

$d\lambda(\mathrm{IM})$ is the derivative of the probability of the IM.

It should be noted that, in the above equation, independent conditional probabilities are used to describe the uncertainties at each part of the equation. For example, $\mathrm{G}\langle \mathrm{DV}|\mathrm{DM}\rangle$ is the conditional probability of the DV, which is dependent only on DM, and independent of the EDP and IM. Moreover, $\mathrm{G}\langle \mathrm{DM}|\mathrm{EDP}\rangle$ is the conditional probability of DM, only dependent on EDP and independent of the IM.

3.2. Probabilistic Seismic Hazard Analysis

Probabilistic Seismic Hazard Analysis (PSHA) is the first step of the PEER PBEE methodology, which is the most accepted approach for describing earthquake hazards probabilistically (Günay & Mosalam, 2013; Y. Li, 2014). The outcome of the PSHA is the hazard curve, which is given in the IM and its MAF of exceedance (or mean annual probability of exceedance p[IM]) format. The most commonly used IM parameters are PGA, PGV, and spectral acceleration, $Sa(T_1)$, at the first mode period (Günay & Mosalam, 2013).

In the PSHA procedure, different types of uncertainties are considered and quantified, which are due to a number of parameters, such as distance from the fault, magnitude-recurrence rates, fault mechanism, condition of the site, type of soil, etc. In this study, to explain the procedure of PSHA, only uncertainties due to the site's distance from the fault and magnitude-recurrence rates are considered. Usually, engineers are searching for worst-case GM intensity while designing. In the PSHA framework, there is no need to consider the worst-case. Instead, all possible earthquake events and resulting GMs, along with their associated probabilities of occurrence, in order to find the level of GM intensity exceeded with some tolerably low rate, are covered (Baker, 2008).

The PSHA framework has five basic steps, as provided below (Baker, 2008).

1- Specify all earthquake sources that can produce damaging GMs.
2- Specify the distribution of earthquake magnitudes (the occurrence rate of the earthquake expected to occur with different magnitudes).
3- Determine the distribution of source-to-site distances associated with potential earthquakes.
4- The distribution of GM intensity should be anticipated as a function of earthquake magnitude, distance, etc.
5- Using the total probability theorem, all uncertainties due to earthquake size, location, and GM intensity, should be combined.

As mentioned, all possible causative seismic sources (i.e., number of seismic sources, N_S) in a given site location should be considered in the PSHA procedure. The total probability theorem is then used to integrate these sources. For this purpose, the following assumptions are used (Y. Li, 2014).

1. The occurrence of earthquakes due to different sources is independent of each other.
2. The magnitude and source-to-site distance are independent statistically for a given occurrence of an earthquake from an i^{th} specific source.

The following equation is used for the PSHA (Mitrani-Reiser, 2007):

$$\lambda_{IM}(im) = \sum_{i=1}^{N_S} \lambda_i P[IM \geq im \mid \text{event of interest of } i^{th} \text{ fault}]$$
$$= \sum_{i=1}^{N_S} \lambda_i \iint P[IM \geq im \mid M_i, R_i]\, p(M_i, R_i)\, dM_i\, dR_i \qquad (3.2)$$

Where:

$\lambda_{IM}(im)$ is the mean total rate of seismic events of interest given IM $\geq$ im

λ_i is the mean rate of occurrence of events of interest on the i^{th} fault.

$p(M_i, R_i)$ is the joint probability density function of the magnitude (M_i) and source-to-site distance (R_i), given that an event of interest has occurred on the i^{th} fault.

$P[IM \geq im \mid M_i, R_i]$ is the complementary cumulative distribution function of IM, conditioned on M_i and R_i for an event on the i^{th} fault, which is given by the ground-motion attenuation model.

3.2.1. Identification of Earthquake Sources

The first thing that should be done in the PSHA frame is to identify and characterize all earthquake sources that are capable of producing damaging GMs at a site. The probability distribution of potential rupture locations within the source must also be determined. Usually, each source zone is given a uniform probability distribution, which implies that earthquakes are equally likely to occur at any point within the source zone. To obtain the source-to-site distance probability distribution the source geometry is combined with the aforementioned uniform probability distribution of each source zone. Earthquake source could be a point, linear, or areal source. After all earthquake sources are identified, then the distribution of magnitudes and source-to-site distances, which are associated with earthquakes from each source, could be determined (Baker, 2008; Kramer, 1996).

3.2.2. Identification of Earthquake Magnitudes

Earthquakes with different magnitudes or sizes can occur on tectonic faults. In a research conducted by Gutenberg and Richter (1944) on the observations of earthquake magnitudes, they discovered that in a region, these earthquake sizes follow a specific distribution, which is provided in the following equation and also known as *Gutenberg-Richter recurrence law*:

$$\log \lambda_m = a - bm \tag{3.3}$$

Where:

λ_m is the mean annual rate of exceedance of magnitude larger than m.

10^a is the mean yearly number of earthquakes of magnitude greater than or equal to zero.

b is a value that describes the relative probability of large and small earthquakes.

These parameters are shown in the following figure.

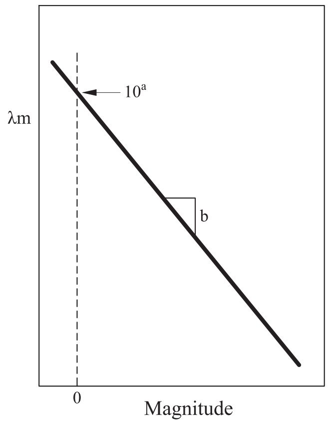

Figure 3.2. Gutenberg-Richter Recurrence Law, showing the meaning of values a and b (Source: Kramer, 1996)

Equation (3.4) could also be presented as follows:

$$\lambda_m = 10^{a-bm} = e^{\alpha-\beta m} \tag{3.4}$$

Where:

$$\alpha = 2.303a, \qquad \beta = 2.303b$$

The standard Gutenberg-Richter recurrence law includes the range of magnitude between $-\infty$ and $+\infty$. Removing very small magnitude earthquakes lower than the threshold magnitude of m_{min} , the effects of which are of little interest to engineers; the MAR of exceedance is can be found using the following equation (Kramer, 1996):

$$\lambda_m = v e^{-\beta(m-m_{\min})} \qquad m > m_{\min} \tag{3.5}$$

Where:

$$v = e^{\alpha-\beta m} \tag{3.6}$$

Considering the lower bound for the magnitude in Gutenberg-Richter recurrence law, the following equation, given in terms of Cumulative Distribution Function (CDF), could be written for the probability distribution of the magnitude.

$$F_M(m) = P[M < m \mid M > m_{\min}] = \frac{\lambda_{m_{\min}} - \lambda_m}{\lambda_{m_{\min}}} = 1 - e^{-\beta(m-m_{\min})} \tag{3.7}$$

Its corresponding Probability Density Function (PDF) is equal to:

$$f_M(m) = \frac{d}{dm} F_M(m) = \beta e^{-\beta(m-m_{\min})} \tag{3.8}$$

Equations (3.7) and (3.8) could also be written as follows, respectively:

$$F_M(m) = 1 - 10^{-b(m-m_{\min})} \qquad m > m_{\min} \tag{3.9}$$

$$f_M(m) = b\ln(10)10^{-b(m-m_{\min})} \qquad m > m_{\min} \tag{3.10}$$

It should be noted that these equations depend on the Gutenberg-Richter law without an upper limit for earthquake magnitude, which physically there is always an upper limit for an earthquake for a specific location. If an upper limit (i.e. m_{max}) could be determined, then these equations could be written as follows for $m_{min} < m < m_{max}$:

$$\lambda_m = v \frac{e^{-\beta(m-m_{\min})} - e^{-\beta(m_{\max}-m_{\min})}}{1-e^{-\beta(m_{\max}-m_{\min})}} \tag{3.11}$$

$$F_M(m) = P[M < m \mid m_{\min} < m < m_{\min}] = \frac{1-e^{-\beta(m-m_{\min})}}{1-e^{-\beta(m_{\max}-m_{\min})}} \tag{3.12}$$

$$f_M(m) = \frac{\beta e^{-\beta(m-m_{\min})}}{1-e^{-\beta(m_{\max}-m_{\min})}} \tag{3.13}$$

or

$$F_M(m) = \frac{1-10^{-b(m-m_{\min})}}{1-10^{-b(m_{\max}-m_{\min})}} \qquad \mathrm{m}_{\min} < m < m_{\max} \tag{3.14}$$

$$f_M(m) = \frac{b\ln(10)10^{-b(m-m_{\min})}}{1-10^{-b(m_{\max}-m_{\min})}} \qquad \mathrm{m}_{\min} < m < m_{\max} \tag{3.15}$$

Usually, the continuous distribution of magnitudes is converted to a discrete set of magnitudes. Presuming that they are the only possible magnitudes, their probability of occurrence could be obtained using the following equation:

$$P(M = m_j) = F_M(m_{j+1}) - F_M(m_j) \tag{3.16}$$

Where:

m_j denotes the discrete set of magnitudes, and they are ordered such that $m_j < m_{j+1}$. The probabilities calculated using the above equation between m_j and m_{j+1} are given to the magnitude m_j. This approximation will not affect the numerical values and will be valid until the discrete magnitudes are closely spaced.

3.2.3. Identification of Earthquake Distances

Modeling the distribution of the distances of the considered site from the earthquakes is also essential for predicting ground shaking. For a given earthquake source, it is commonly assumed that earthquakes will occur with equal probability at any location, i.e., earthquakes are usually assumed to be uniformly distributed within a particular source zone (Baker, 2008; Kramer, 1996).

There are different types of sources regarding their geometry that rely on the tectonic processes involved in their formation. For instance, earthquakes affiliated with volcanic activity typically come from zones close to the volcanoes that are small enough to be considered as point sources. In contrast, fault planes that are clearly defined could be treated as two-dimensional area sources on which earthquakes can take place in various locations (Kramer, 1996).

According to the relative geometry of the source and site of interest, as well as the accuracy and quality of the source information, the source zones for a seismic hazard analysis may be similar to the actual source zones, or they may differ from it. For instance, Figure 3.3a could be treated as a point source since it is relatively short, and the distance between any point along the fault length and the site is almost constant. In addition, the fault plan shown in Figure 3.3b could be modeled as a linear source because the depth of the fault is sufficiently small that variations in hypocentral depth have little impact on hypocentral distance. However, it should be noted that there would be negligible accuracy loss by such approximations.

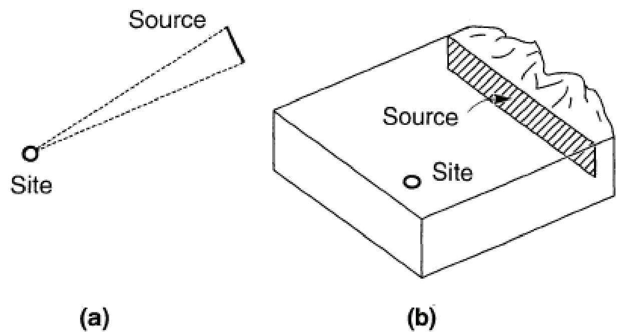

Figure 3.3. Examples of source zone geometries (a) short fault that can be modeled as a point source, (b) shallow fault that can be modeled as a linear source (Source: Kramer, 1996)

As mentioned earlier, in general, earthquakes are assumed to be uniformly distributed within a specific source; however, such distribution does not usually correspond to a uniform distribution of source-to-site distance. In addition, the spatial uncertainty must be described concerning the relevant distance parameter because of predictive relationships that express GM parameters in terms of some measure of source-to-site distance. A PDF could be used to describe the uncertainty in the source-to-site distance (Kramer, 1996). Given that the locations are uniformly distributed, it is typically easy to determine the distribution of source-to-site distances using only the source's geometry (Baker, 2008).

Point Source:

For a point source, since there is only a single value for distance (R=r), therefore:

$$\begin{aligned} P(M = r) &= 1.0 \\ P(M \neq r) &= 0.0 \end{aligned} \tag{3.17}$$

Linear Source:

For a linear source, the length of the source is divided into n_r number of segments. The distance from the center of each line segment to the site (r) should be determined. In addition, the maximum distance (r_{max}) and minimum distance (r_{min}) from site-to-source are identified. To obtain the probability distribution for the site, the histogram of the distances from the site to the source has to be obtained. For this purpose, the range between r_{max} and r_{min} should be divided into a specific number of equal intervals (N_R), and their mean values should be obtained. The length of the intervals (L_{int}) could be calculated using the following equation (Kramer, 1996).

$$L_{\text{int}} = \frac{r_{\text{max}} - r_{\text{min}}}{N_R} \tag{3.18}$$

The number of distances from site-to-source (n_{r_int}) should be counted within each interval, which will provide a histogram for the site-to-source distance and divide the number of distances within each interval (n_{r_int}) on the total number of distances (n_r) will give the probability for each interval.

$$f_R(r) = P[R = r] = \frac{r_{r\_\text{int}}}{n_r} \tag{3.19}$$

Alternatively, if earthquakes are assumed to be uniformly distributed over the length of the fault (L_f), then the PDF of (r) could be obtained using the following equation (Kramer, 1996):

$$f_R(r) = \frac{r}{L_f\sqrt{r^2 - r_{\min}^2}} \tag{3.20}$$

Area Source:

A similar numerical procedure could be utilized for an area source. For example, for a rectangular area source, the area is divided into a number of small rectangles (usually squares), and the distance from the center of each small rectangle is obtained. The rest of the calculation could be done similarly to the linear source.

3.2.4. Ground Motion Intensity

The next step is to predict the probability distribution of GM intensity as a function of earthquake magnitude, distance, etc. For this purpose, several prediction models are developed. The general form for such models are as follows (Baker, 2008):

$$\ln IM = \overline{\ln IM}(M,R,\theta) + \sigma(M,R,\theta), \varepsilon \tag{3.21}$$

Where:

$\ln IM$ is the natural logarithm of the GM intensity measure of interest (e.g. PGA, PGV, spectral acceleration at a given period, etc.)

$\overline{\ln IM}(M,R,\theta)$ *and* $\sigma(M,R,\theta)$ are the predicted mean and standard deviation, respectively, of $\ln IM$, which are the results of the GM prediction model. Both of them are the functions of the earthquake's magnitude and distance and other parameters, generally referred to as θ.

ε is a standard normal random variable that represents the observed variability in $\ln IM$, which can have both positive and negative values. It should be noted the positive values of ε result in $\ln IM$ larger than the average values, whereas negative values give $\ln IM$ smaller than the average values of $\ln IM$.

In a resource provided by John Douglas, all empirical GM prediction equations are summarized, which are developed from 1964 to 2019. These equations could estimate earthquake PGA and elastic response spectral ordinates (Douglas, 2019). Some of these

GM prediction equations are obtained for specific regions. For example, Konovalov et al. (2019) developed such an equation for Sakhalin Island, Laouami et al. (2018) for Algeria, Chousianitis et al. (2018) for Greece, Chiara et al. (2018) for Italy, etc.

For predicting $\overline{\ln IM}(M, R, \theta)$ *and* $\sigma(M, R, \theta)$, complex models have been developed; however, here, a simple model proposed by Cornell et al. (1979) for the mean of PGA $\overline{\ln PGA}$, will be used, given as follows:

$$\overline{\ln PGA} = 6.74 + 0.859M - 1.80\ln(R + 25), \qquad in\ gals = cm/\sec^2 \tag{3.22}$$

$$\overline{\ln PGA} = -0.152 + 0.859M - 1.80\ln(R + 25), \qquad in\ g \tag{3.23}$$

In this model, a constant value of 0.57 for the standard deviation of $\overline{\ln PGA}$ is considered; meanwhile, it is constant for all magnitudes and distances. Since normal distribution has been observed for the natural logarithm of PGA, knowing the mean and standard deviation, the probability of exceeding any PGA level is determined using the following equation:

$$P(PGA > x \mid m, r) = 1 - \Phi\left(\frac{\ln x - \overline{\ln PGA}}{\sigma_{\ln PGA}}\right) \tag{3.24}$$

Where:

$\Phi(\ )$ is the standard normal CDF.

It should be noted that modern prediction models could be used in equation (3.24), so the general procedure is the same when using newer models.

3.2.5. Combination of all Information

The last step in the PSHA procedure is to combine uncertainties in earthquake size, location, and GM intensity, using the total probability theorem. For a single source, the probability of exceeding IM level x for a given magnitude and distance could be computed using the following equation:

$$P(IM > x) = \int_{m_{\min}}^{m_{\max}} \int_{r_{\min}}^{r_{\max}} P(IM > x \mid m, r) f_M(m) f_R(r) \, dr \, dm \qquad (3.25)$$

Where:

$P(IM > x \mid m, r)$ the result of the GM model.

$f_M(m)$ and $f_R(r)$ are the PDFs for magnitude and distance.

Through equation (3.25), the probability of exceedance for a given occurrence of an earthquake on the source of interest can be estimated by ignoring information about how frequent earthquakes occur. A simple modification can be made to compute the rate of $IM > x$, rather than probability of $IM > x$ givne occurrence of an earthquake.

$$\lambda(IM > x) = \lambda(M > m_{\min}) \int_{m_{\min}}^{m_{\max}} \int_{r_{\min}}^{r_{\max}} P(IM > x \mid m, r) f_M(m) f_R(r) \, dr \, dm \qquad (3.26)$$

Where:

$\lambda(M > m_{min})$ is the rate of occurrence of earthquakes greater than m_{min} from the source.

To consider the effect of all possible sources on the site of interest, the following equation could be used to estimate the rate of $IM > x$, which is simply the summation of the rates of $IM > x$ from each source.

$$\lambda(IM > x) = \sum_{i=1}^{n_{sources}} \lambda(M > m_{\min}) \int_{m_{\min}}^{m_{\max}} \int_{r_{\min}}^{r_{\max}} P(IM > x \mid m, r) f_M(m) f_R(r) \, dr \, dm \qquad (3.27)$$

Where:

$n_{sources}$ is the number of sources considered, and M_i and R_i denote the magnitude and distance distribution for source i.

In practice, the estimation is carried out using the computer; thus, it would be better to discretize the continuous distribution for M and R into small portions and use summation instead of integral. In this case, equation (3.27) will take the following form:

$$\lambda\left(IM>x\right)=\sum_{i=1}^{n_{sources}}\lambda\left(M>m_{\min}\right)\sum_{j=1}^{n_M}\sum_{k=1}^{n_R}P\left(IM>x\,|\,m,r\right)P\left(M_j=m_j\right)P\left(R_k=r_k\right) \quad (3.28)$$

Where:

n_M and n_R are the number of discretized intervals for the possible range of M_i and R_i , respectively, as discussed in previous sections.

For a specific time period, the Mean Rate of Exceedance (MRE) could be obtained using the following equation adopted from Jones et al. (1991).

$$\lambda\left(IM>x\right)_N=1-\left[1-\lambda\left(IM>x\right)\right]^N \quad (3.29)$$

Where:

N is the specific time period, for example, 50 years.

An example is considered, which has three different types of sources: point source, linear source, and area source. The hazard curve for each source is obtained and combined to get the final hazard curve for that specific location. The configuration of the example is shown in the following figure, with some necessary parameters.

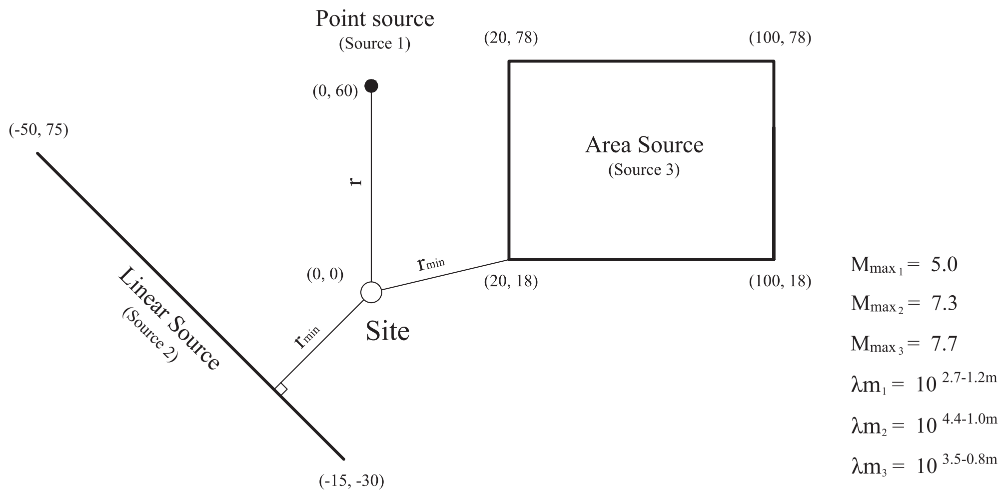

Figure 3.4. Location of the site with different earthquake sources

The hazard curves obtained through the aforementioned procedure are shown in the following figure, in which the MRE for 50 years is shown.

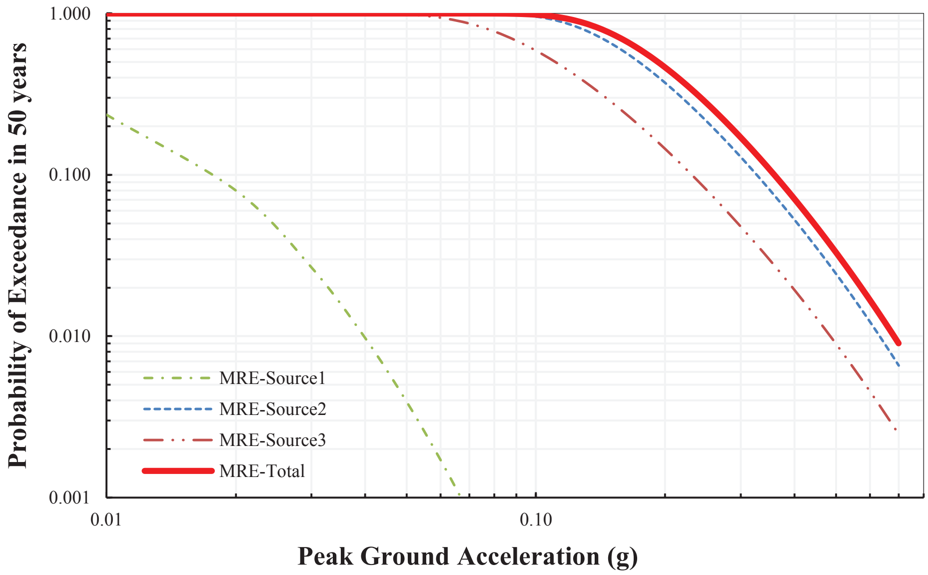

Figure 3.5. Hazard curves from different sources and their combination

3.2.6. Hazard Curves from Provided Maps

Obtaining hazard curves, especially when using modern prediction equations, is a very complicated procedure that requires strong background information in seismology. Thus, for structural engineers, it is more convenient to get such curves from already prepared hazard maps. For example, the U.S. Geological Survey(USGS) provides hazard curves for the United States of America (USA) and Alaska, and European Facilities for Earthquake Hazard and Risk (EFEHR) provides such hazard curves for specific locations around Europe and the Middle East.

The USGS website uses a tool called Unified Hazard Tool for calculating hazard curves for a specific location (i.e., for known coordinates of the site) using the different editions of the available database. The website provides the hazard curves of annual probability of exceedance in terms of PGA and Spectral Acceleration (Sa) with multiple periods ranging from 0.1 sec to 5 sec (the range of periods is for the fundamental periods of the structure).

The hazard curves, shown in Figure 3.6, are obtained for a specific location in the USA (Latitude= 37.77493, Longitude= -122.41942) from the USGS website (https://earthquake.usgs.gov/hazards/interactive/). The hazard curves related to PGA and Sa with 5 different periods are shown in the figure.

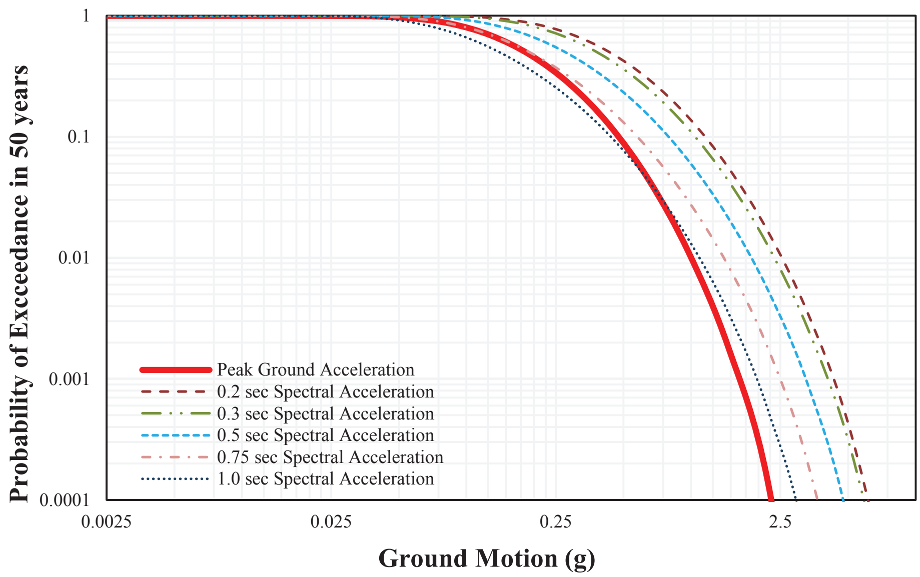

Figure 3.6. Hazard curves obtained from USGS website

3.2.7. Hazard Curves from Software

An alternative way to obtain the hazard curves is by using some available software. One such software is the Open-Source Seismic Hazard Analysis (OpenSHA). OpenSHA is an object-oriented framework that is based on a Java platform (Field et al., 2003). Using the OpenSHA, hazard curves could be obtained for different types of IM values, such as PGA and Sa. Two main types of model components are available in OpenSHA, Earthquake Rupture Forecast (ERF) and Intensity Measure Relationship (IMR). All possible earthquake ruptures and their probabilities of occurrence in a region over some time span are provided by ERF; on the other hand, IMR provides the conditional probability that a type of IM value will exceed an IM level on the condition of occurrence of a specified earthquake rupture. The hazard curves for Sa, considered as IM for different fundamental periods, are obtained using the OpenSHA software for the same location as mentioned above (Figure 3.7).

There is a little bit of difference between Figure 3.6 and Figure 3.7, and this is because the USGS website uses limited options, which are the edition of the available database, coordinates of the location of interest, site class, and type of IM. On the other hand, OpenSHA uses many other parameters in addition to these parameters. For example, there is an option available for choosing IMR, for which 28 different types of attenuation relationships are available, for example, Campbell and Borzorgnia (2014), Chiou and Youngs (2014), etc. For ERF, 25 different options are available, each of which has many other parameters to consider, for instance, rupture offset in (km). Different probability models are available, such as the San Andreas probability model, the San Gregorio probability model, etc.

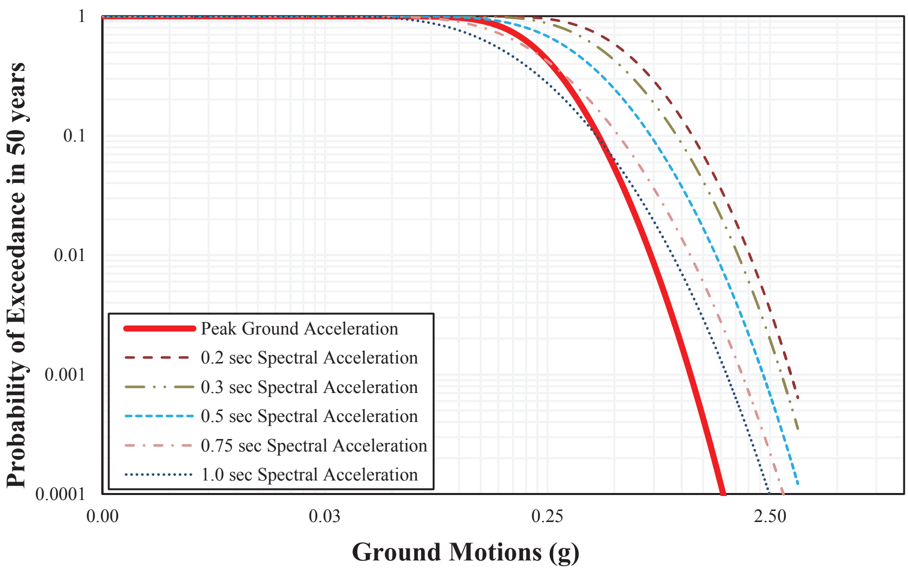

Figure 3.7. Hazard curves obtained from OpenSHA

The hazard curves obtained from OpenSHA were chosen here for two reasons. First, the hazard curves could be obtained for IM levels of interest, while the USGS website has some fixed values for IM levels. Second, the USGS provides only mean hazard curves, while using OpenSHA hazard curves for mean and different fractiles could be obtained.

3.3. Probabilistic Demand Analysis

The second step in the PEER PBEE methodology is to perform Probabilistic Demand Analysis (PDeA) or probabilistic structural analysis. Through PDeA, structural response (i.e., EDP) to future earthquakes could be predicted (Y. Li et al., 2019). A probabilistic seismic hazard curve is used as a condition in the PDeA procedure to obtain the probabilistic demand hazard curve (Mitrani-Reiser, 2007). In this step, a structure is required to be modeled and analyzed in order to obtain the probable performance of the structure under specific GM in a probabilistic manner. For the purpose of analysis, usually, NTHA is adopted for each intensity level (i.e., IM) of the earthquake hazard (Günay & Mosalam, 2013).

In performing NTHA, earthquake GM records, corresponding to the specific intensity level of earthquake hazard, are selected and scaled with respect to the design response spectrum, and the response of the structure is obtained in terms of the EDPs. Local and global parameters may be included in the EDPs. For example, element forces or deformation as the local parameters, while floor acceleration, floor displacement, and interstory drift as global parameters. In addition, axial or shear forces in a non-ductile column as element forces, and plastic rotation for ductile flexural behavior as deformations for structural elements are more suitable parameters. However, for nonstructural components and content systems, global parameters such as floor acceleration are more appropriate to be used. Further, since, in the framework of PEER PBEE, only a single value of each EDP is required; therefore, the peak values of the mentioned EDPs are used (Günay & Mosalam, 2013).

Moreover, while modeling the structure, special care should be given to the high and low levels of earthquake GMs (i.e., intensity levels). It is well known that earthquakes with low-intensity levels are more frequent, and the damages caused by such earthquakes contribute to losses. On the other hand, earthquakes with high-intensity levels are less frequent, could cause the collapse of the structure, and could be of great concern for the overall safety of the occupants (Günay & Mosalam, 2013; Mitrani-Reiser, 2007).

In an analysis carried out by Lee & Mosalam (2006) on one of the testbeds of the PEER PBEE methodology, it has been shown that local EDPs are more affected due to variation in GM compared to the uncertainties in the structural parameters (Günay & Mosalam, 2013). In addition, for each EDP, a reasonable probability distribution, such as a lognormal distribution, is assumed by calculating the distribution parameters from the data obtained from simulations with no global collapse. Structural analysis will result in several probability density functions (PDFs), which will be equal to the number of IM data points times the number of the EDPs considered in the analysis procedure (Günay & Mosalam, 2013; Y. Li, 2014).

Two different groups of approaches exist for PDeA, the conventional approach and the time-domain approach (Rai et al., 2019). The basis of the time-domain approach, which is proposed by Sehhati et al. (2010), is that, for predicting the EDP instead of correlation with IM, simplified wavelet pulses are used. This is true for the cases when earthquake GMs have pulses (Rai et al., 2019). On the other hand, the conventional PDeA is described by the convolution integral provided in equation (3.30), which gives the demand hazard curve, i.e., the mean annual probability of exceedance of a specified EDP value (edp) (J Moehle & GG Deierlein, 2004; Y. Li, 2014; Rai et al., 2019).

$$\lambda_{EDP}(edp) = \int_{IM} P\left[EDP > edp \mid IM = im\right] \left| d\lambda_{IM}(im) \right| \tag{3.30}$$

From equation (3.30), it can be concluded that the demand hazard curve could be obtained as the convolution of the probability of EDP>edp on a given condition that IM=im, i.e., P $[\mathrm{EDP} > \mathrm{edp}|\mathrm{IM} = \mathrm{im}]$, and the seismic hazard curve $\lambda_{\mathrm{IM}}(\mathrm{im})$(Y. Li et al., 2019).

To solve equation (3.30), three equivalent analytical methods exist. The first one is the numerical derivative of the hazard curve, $\lambda_{\mathrm{IM}}(\mathrm{im})$, which gives the following relation (Judd & Charney, 2014; Tothong & Cornell, 2007):

$$\lambda_{EDP}(edp) = \int_{IM} P\left[EDP > edp \mid IM = im\right] \left| \frac{d\lambda_{IM}(im)}{\mathrm{dim}} \right| \mathrm{dim} \tag{3.31}$$

The second method is to take the derivative of the fitted hazard curve. In this method, first, the hazard curve is fitted to a function, and then the derivative of the function is taken. Usually, polynomial functions are used to fit the hazard curve. The third method is to take the derivative of P $[\mathrm{EDP} > \mathrm{edp}|\mathrm{IM} = \mathrm{im}]$, for which equation (3.30) will take the following form (Judd & Charney, 2014):

assume $$P\left[EDP > edp \mid IM = im\right] = f(e)$$

$$\lambda_{EDP}(edp) = \int_0^{+\infty} \lambda_{IM}(im) f(e)\, de \tag{3.32}$$

In these equations, the most crucial part is to obtain P $[\mathrm{EDP} > \mathrm{edp}|\mathrm{IM} = \mathrm{im}]$ which requires higher computational time. This is due to the fact that for each IM data point, a number of nonlinear time history analyses should be performed. According to some standards, the minimum number of GM records is equal to 7. In contrast, some other standards recommend using 11 GM records to assess the performance of the structure while using NTHA for a single IM level.

To evaluate probabilistic structural response, i.e., $\mathrm{P}\left[\mathrm{EDP}>\mathrm{edp}|\mathrm{IM}=\mathrm{im}\right]$, different methods exist (Baker & Cornell, 2005). For example, the cloud analysis method, multiple-strip analysis method, ET analysis method, IDA method, etc. In this study, the ET analysis method is used to reduce the computational time during optimization. However, after the optimum solution is obtained, the IDA method has been adopted for detailed performance assessment purposes.

The probability of failure, i.e., $\mathrm{P}\left[\mathrm{EDP}>\mathrm{edp}|\mathrm{IM}=\mathrm{im}\right]$ is assumed to be a lognormal distribution. Thus, the logarithmic mean and standard deviation for the lognormal distribution of the peak IDR are obtained using the following equations (Andrzej S. Nowak & Collins, 2013; Ang & Tang, 2007).

$$\sigma_{\ln(X)}^{2}=\ln\left(V_X^2+1\right)=\ln\left(\left(\frac{\sigma_X}{\mu_X}\right)^2+1\right)=Var\left[\ln(X)\right] \tag{3.33}$$

$$\mu_{\ln(X)}=\ln\left(\mu_X\right)-\frac{1}{2}\sigma_{\ln(X)}^{2}=E\left[\ln\left(x\right)\right] \tag{3.34}$$

From the above equations, it is evident that first, the natural logarithm of the samples (X) is taken, and the variance ($\sigma_{\ln(X)}^2$) and expected ($\mu_{\ln(X)}$) values are then obtained from the natural logarithmic values of X, i.e., ln(X). These values are used in the above equations, which will give the mean (μ_X) and standard deviation (σ_X) of the samples. The exponential of the $\mu_{\ln(X)}$ will give the median of the sample data (Ang & Tang, 2007).

The logarithmic mean and standard deviations are used then to obtain the probability of failure, i.e., the probability of exceedance of EDP from a threshold value of edp on the condition that IM=im could be calculated using the following equation:

$$P\left[EDP>edp\,|\,IM=im\right]=1-\Phi\left(\frac{\ln EDP-\overline{\ln EDP}}{\sigma_{\ln EDP}}\right) \tag{3.35}$$

The CDF and the PDF of the peak IDR are obtained through equations (3.36) and (3.37), respectively.

$$F\left[EDP\right]=\Phi\left(\frac{\ln EDP-\overline{\ln EDP}}{\sigma_{\ln EDP}}\right) \tag{3.36}$$

$$f\left[EDP\right]=\frac{1}{EDP\sigma_{\ln EDP}}\phi\left(\frac{\ln EDP-\overline{\ln EDP}}{\sigma_{\ln EDP}}\right) \tag{3.37}$$

3.3.1. Incremental Dynamic Analysis Method

Developments in computer processing power has made it possible to use more accurate yet complex nonlinear static and dynamic analysis methods for the performance evaluation of structures. The Incremental Dynamic Analysis (IDA) method is one of these methods, and it is a powerful parametric analysis method for the evaluation of the probabilistic response of structures under seismic loads (Miano et al., 2016; Vamvatsikos & Allin Cornell, 2002). In the IDA method, a structure is subjected to a single ground acceleration record or a set of records, and a single or set of IDA curves is obtained. It should be noted that a single record IDA curve cannot capture structural behavior accurately; therefore, it is required to have a set of IDA curves. The basic steps for IDA analysis are as follows:

1- Selecting the structure and associated EDPs.
2- Generating the nonlinear model of the structure.
3- Selecting the range of IM values (e.g., 0.01g to 1g), which should capture the linear and nonlinear response of the structure sufficiently.
4- Collecting a set of N number of ground acceleration records.
5- Scaling ground acceleration records to a specific IM level.
6- Performing NTHA of the structure for scaled N number of GM records.
7- Extracting EDPs.

Steps 5 through 7 are repeated until all IM values are covered. The statistical parameters, such as the mean (μ), standard deviation (σ) of the EDPs are obtained from the extracted EDPs data, and then a lognormal distribution is assumed for $\mathrm{P}\left[\mathrm{EDP}>\mathrm{edp}|\mathrm{IM}=\mathrm{im}\right]$. It is observed that between EDP and IM values, a power form relationship exists, in which the relationship between $\ln(EDP)$ and $\ln(IM)$ is linear (Aslani & Miranda, 2005; Cornell et al., 2002; Kim et al., 2020; Mackie & Stojadinovi´, 2007).

$$EDP = a\, IM^{b} \tag{3.38}$$

or
$$\ln\left(EDP\right) = \ln\left(a\right) + b\ln\left(IM\right) \tag{3.39}$$

To use a set of GM records for the IDA method, it is first required to scale them to a specific hazard level, for which the elastic design spectrum is usually used as the target spectrum. In this study, to obtain an elastic design response spectrum, the ATC Hazard by Location website (https://hazards.atcouncil.org/) is used. For this purpose, ASCE/SEI-41-17 (2017) is chosen as a reference document, and the site class is assumed to be C. Using this website, it is possible to obtain the elastic design response spectrum at different hazard levels (IM levels). In this study, three different IM levels are chosen, which correspond to 2%, 10%, and 50% probability of exceedance in 50 years.

The location of the structure given in section 3.2.6 (Latitude= 37.77493, Longitude= -122.41942) with assumed site class C is used. Accordingly, the values for mapped spectral response acceleration parameters at a short period (S_S) and a period of 1-sec (S_1) are obtained from the ATC hazard by location website for the BSE-2N hazard level (2% probability of exceedance in 50 years). In addition, the design spectral response acceleration parameters S_{XS} and S_{X1} for a short period and a period of 1-sec are also provided. The website also provides the values for site coefficients at a short period (F_a) and a period of 1-sec (F_V). These values could also be obtained from Tables 11.4.1 and 11.4.2 of ASCE/SEI-7-16 (2017). For the hazard level BSE-1N (10% probability of exceedance in 50 years), the website provides only S_{XS} and S_{X1} values; however, F_a and F_V parameters could be taken from the aforementioned tables. The S_S and S_1 parameters for the hazard level BSE-1N are 2/3 of the S_S and S_1 parameters of the hazard level BSE-2N. For the rest of the hazard levels, it could be obtained using equation (3.63). All of these values are tabulated in Table 3.1 for the three mentioned hazard levels.

Table 3.1. Some of the parameters for different earthquake hazard levels

	Probability of exceedance in 50 years		
	2%	**10%**	**50%**
PGA	0.630	0.423	0.230
S_{XS}	1.8	1.2	0.58
S_{X1}	0.84	0.56	0.27
S_S	1.5	1.0	0.44
S_1	0.6	0.4	0.18
F_a	1.2	1.2	1.3
F_v	1.4	1.5	1.5

The elastic design response spectrum could be obtained using the following relationships provided in ASCE/SEI-41-17 (2017). Furthermore, the website also provides the long-period transition period (T_L) for the given location, and with assumed site class C, it equals 12 sec.

$$S_a(T) = \left(0.4 + \left(\frac{5}{B_1} - 2\right)\frac{T}{T_S}\right) S_{XS} \qquad (0 \le T \le T_0) \tag{3.40a}$$

$$S_a(T) = \frac{S_{XS}}{B_1} \qquad (T_0 < T \le T_S) \tag{3.40b}$$

$$S_a(T) = \frac{S_{X1}}{B_1 T} \qquad (T_S < T \le T_L) \tag{3.40c}$$

$$S_a(T) = \frac{S_{D1} T_L}{B_1 T^2} \qquad (T_L < T) \tag{3.40d}$$

Where:

T_0 and T_S are the corner periods for the design acceleration response spectrum.

B_1 could be calculated using the following equation:

$$B_1 = 4 \big/ \left[5.6 - \ln(100\beta)\right] \tag{3.41}$$

Where, β is the effective viscous damping ratio, and it is assumed 5%.

The following design response spectrum for three different earthquake hazard levels for the considered location has been obtained using the above equations.

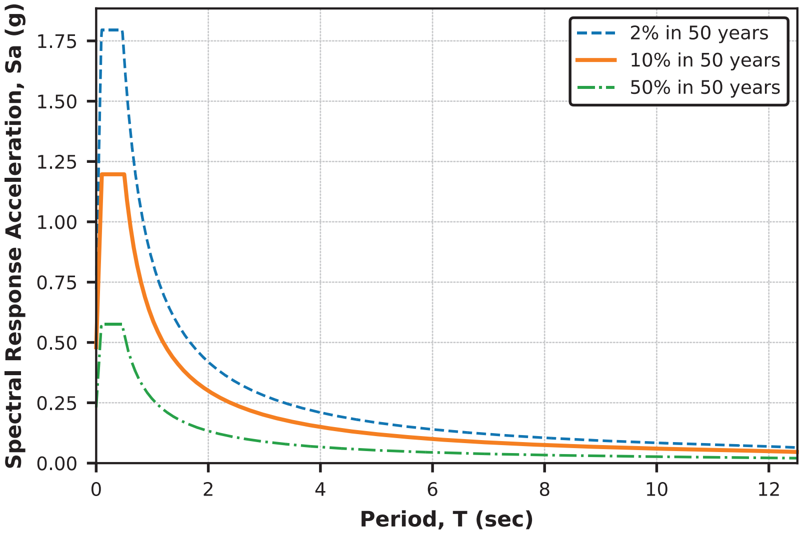

Figure 3.8. Elastic design response spectrum for different earthquake hazard levels

3.3.2. Selection and Scaling Ground Motion Records

As mentioned earlier, for each IM level, the N number of earthquake GM accelerograms should be used. These accelerograms could be artificially generated using some available software, e.g., SeismoArtif v2020 (Seismosoft, 2020), or they could be selected from the available real earthquake GM records. Once the GM records are selected, then they should be scaled to match the target response spectrum of the IM level of interest. In this study, the IDA method is used to cover the response of the structure from the elastic range to the inelastic range until collapse occurs. Therefore, the scaling procedure of FEMA-P695 (2009) is used. Two steps for scaling are recommended in FEMA-P695 (2009) for IDA analysis. The first step is normalizing the GM records, and the second step is scaling the normalized GM records to the IM level of interest.

In the first step, the selected GM records are normalized with respect to the PGV of each individual GM record. The PGV is chosen for the normalization purpose to keep the record-to-record variability (i.e., aleatory uncertainties) while eliminating some unnecessary variability resulting from the inherent variation of the GM records, such as site condition, event magnitude, source type, and the distance to the source. The Normalization factor could be calculated using the following equation (FEMA-P695, 2009):

$$NF_i = \hat{S}_{PGV_i} / PGV_i \tag{3.42}$$

In this equation, PGV_i is the geometric mean of the PGV of the two horizontal components of the ith record and $\hat{S}_{PGV_i}$ is the median of the PGV_i in the set of records. The normalized GM records are obtained by multiplying both horizontal components with the normalization factor. After the normalization, the normalized GM records are scaled to the IM level of interest such that the median of these records matches the target design response spectrum at the fundamental period of the structure only.

The FEMA-P695 (2009) far-field GM records are chosen here in this study. The records are obtained from the PEER GM database (i.e., NGA West 2 database, https://ngawest2.berkeley.edu/site). The names of the records with the normalization factors are tabulated in the following table.

Table 3.2. FEMA-P695 far-field earthquake GM records with their normalization factors

ID No	Earthquake GM records information				GMs PGA (g)	Normalization Factor	Norm. GMs PGA (g)
	RSN	Magnitude	Year	Name			
1	953	6.7	1994	Northridge	0.52	0.65	0.34
2	960	6.7	1994	Northridge	0.48	0.83	0.4
3	1602	7.1	1999	Duzce, Turkey	0.82	0.63	0.52
4	1787	7.1	1999	Hector Mine	0.34	1.09	0.37
5	169	6.5	1979	Imperial Valley	0.35	1.31	0.46
6	174	6.5	1979	Imperial Valley	0.38	1.01	0.39
7	1111	6.9	1995	Kobe, Japan	0.51	1.03	0.53
8	1116	6.9	1995	Kobe, Japan	0.24	1.1	0.26
9	1158	7.5	1999	Kocaeli Turkey	0.36	0.69	0.25
10	1148	7.5	1999	Kocaeli Turkey	0.22	1.36	0.3
11	900	7.3	1992	Landers	0.24	0.99	0.24
12	848	7.3	1992	Landers	0.42	1.15	0.48
13	752	6.9	1989	Loma Prieta	0.53	1.09	0.58
14	767	6.9	1989	Loma Prieta	0.56	0.88	0.49
15	1633	7.4	1990	Manjil, Iran	0.51	0.79	0.4
16	721	6.5	1987	Superstition Hills	0.36	0.87	0.31
17	725	6.5	1987	Superstition Hills	0.45	1.17	0.53
18	829	7	1992	Cape Mendocino	0.55	0.82	0.45
19	1244	7.6	1999	Chi-Chi, Taiwan	0.44	0.41	0.18
20	1485	7.6	1999	Chi-Chi, Taiwan	0.51	0.96	0.49
21	68	6.6	1971	San Fernando	0.21	2.1	0.44
22	125	6.6	1976	Friuli, Italy	0.35	1.44	0.5

RSN = GM record sequence number
GMs PGA = PGA of the recorded GMs.
Norm.PGA = PGA of the normalized GM records.

The target response spectrum for the IM level with a 10% probability of exceedance in 50 years against the mean and median of scaled earthquake GM accelerograms and mean plus and minus one standard deviation $(\pm\sigma)$ is shown in the following figure.

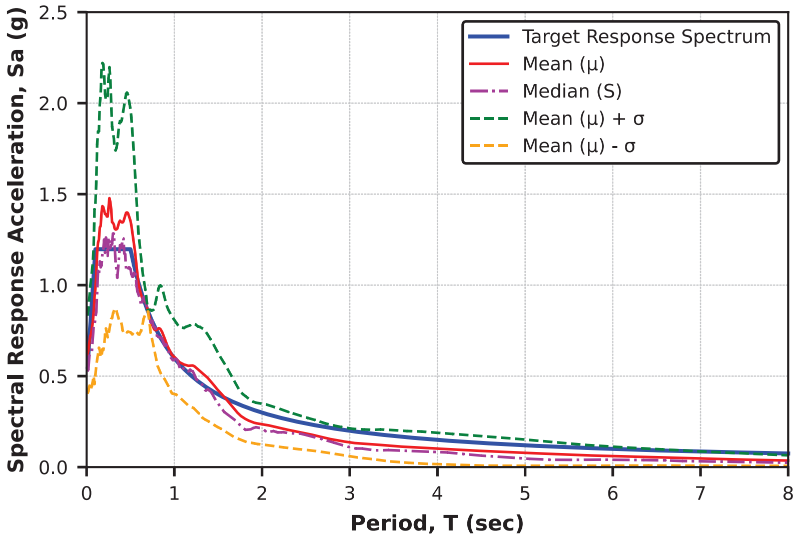

Figure 3.9. Target Response Spectrum with the mean, median, and mean $\pm\,\sigma$ of the scaled data for the IM with 10% probability in 50 years

The following figure shows the scaled response spectra of the selected data with their mean and mean $\pm\,\sigma$. It should be noted that the fundamental period is assumed to be 0.7 sec for scaling purposes of the figures.

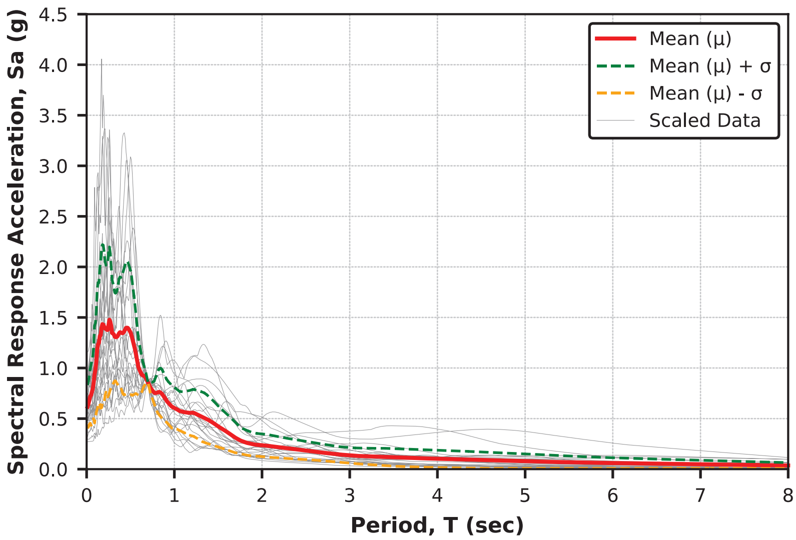

Figure 3.10. Scaled response spectra of the selected data with the mean and mean $\pm\,\sigma$ for the IM with 10% probability in 50 years

3.3.3. Nonlinear Time History Analysis

Time history analysis is one of the most powerful and reliable analysis methods for achieving the performance of a structure under design seismic intensity. Two types of time history analysis are common in literature, linear and Nonlinear Time History Analysis (NTHA). The analysis is done stepwise; the outcome is the dynamic response of the structure under time-dependent loadings (e.g., earthquake loading due to earthquake GM). OpenSees, an open-source software, is used for NTHA. Detailed information regarding modeling and analysis of the frame in OpenSees is provided in section 5.1.

For concrete, a stress-strain model developed by Mander et al. (1988), shown in Figure 3.11, is adopted. It should be noted that the tensile strength of concrete is also considered in this model. *Concrete04* type of material model is used in OpenSees for this purpose, which suits the Mander model well. In Figure 3.11, the parameters shown are:

f'_{co} is the compressive strength of unconfined concrete.

f'_{cc} is the compressive strength of confined concrete.

f'_t is the tensile strength of concrete.

ε_{cc} is the compressive strain at f'_{cc}.

ε_{cu} is ultimate concrete compressive strain.

ε_{co} is the compressive strain at f'_{co}.

ε_{sp} strain at which cover concrete is considered to have completely spalled and ceases to carry any stress.

E_c Modulus of elasticity of concrete.

E_{sec} secant modulus of elasticity of confined concrete at peak strength.

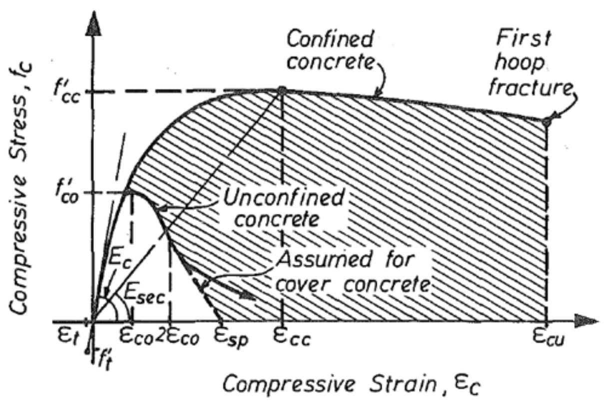

Figure 3.11. Stress-Strain model for confined and unconfined concrete (Source: Mander et al. 1988)

For the modeling frame in OpenSees, the following assumptions are made:

- Material properties for members (beams and columns) are taken homogenous.

- Material properties for concrete and steel reinforcements are defined, considering their nonlinear properties. For concrete, the *Concrete04* type of material is used, while for steel reinforcement, the *Steel02* type of material is considered.
- Columns and beams are assumed to be line elements, and it is assumed that the boundary condition of columns at the base of the first story is fully fixed.
- First, analysis due to gravity loads are considered, and then the results are imported for NTHA. Here, in the content of gravity loads, 100% of dead loads are considered, and as recommended in ASCE 7-16, 30% of the live loads in floor levels, while 100% of roof live loads are considered.
- Time history functions are defined using scaled records obtained from the PEER GM database (see section 3.3.2).

3.4. Probabilistic Damage Analysis

The third step in PEER PBEE methodology is to perform Probabilistic Damage Analysis (PDaA), in which damage due to seismic load is evaluated probabilistically. Damage Measure (DM), which quantifies the physical damage at the component or system level as a function of structural response, is the outcome of PDaA (Günay & Mosalam, 2013). The total probability theorem can be used to obtain the mean annual probability of exceedance of a specified DM value for a certain damage or limit state. The expression is provided as follows (Y. Li et al., 2019)

$$\lambda_{DM,LS_k}\left(LSt_k\right) = \int P\left[DM \geq LSt_k \mid EDP = edp\right]\left|d\lambda_{EDP}\left(edp\right)\right| \tag{3.43}$$

Where:

$\mathrm{d}\lambda_{\mathrm{EDP}}(edp)$ is the differentiation of the demand hazard curve.

$\mathrm{P}\left[\mathrm{DM} > \mathrm{LS}_k | \mathrm{EDP} = \mathrm{edp}\right]$ is the probability of exceedance of DM from a specified k$^{\text{th}}$ Limit State (LSt) on a condition that EDP is given, also known as the fragility function.

It should be noted that in the presented equation, the $\mathrm{P}\left[\mathrm{DM} > \mathrm{LS}_k | \mathrm{EDP} = \mathrm{edp}\right]$ could be related to the overall structure or to a component of the structure, such as structural, nonstructural, and content systems. However, for the loss estimation, it is related to the components of the structure. In addition, the collapse fragility function is also required in the loss analysis. Thus, not only the collapse fragility function but also the fragility functions related to the other two performance levels (IO and LS) are also developed.

3.4.1. Development of Fragility Curves

Fragility functions are statistical tools that are the basics for the vulnerability assessment of the structures. The fragility function shows the relationship between the damage state of a component or a structure and its response in a probabilistic manner. Through a fragility function, the probability that a particular type of component or structure will reach or exceed a clearly defined damage state (limit state or performance level) as a function of the structural response (i.e., as a function of EDP that represents the GM) to which it is subjected, is quantified (Günay & Mosalam, 2013; Nguyen & Lee, 2018).

To develop fragility functions, it is important to create measures of damage first. One of the concepts which can be used as measures of damage of structural elements and systems is the damage indices. Damage indices only can take values between 0 and 1, and they are dimensionless parameters. A damage index value equal to 0 means that there is no damage or negligible damage, while a damage index value equal to one corresponds to the total damage (FEMA-445, 2006).

Defining a set of discrete damage states is another way to present DMs. A damage state could be defined as exceeding a certain LSt for a specific failure mode. FEMA-356 (2000) adopted such damage states, for example, operational, IO, LS, and CP performance levels as Damage States (DS). Operational performance level has negligible DS, while CP performance level shows severe DS. In addition, Hazards United States (HAZUS-MR4, 2003) uses slight, moderate, severe, and complete DSs as measures of damage.

Another method to parameterize the damage is that the condition of each element is tracked directly, and then damages are measured on a local basis, later on, they are combined with the damages measured on the overall condition of the structure. In a moment-resisting frame, for example, checking and measuring the damages of columns and beams, their joints, beam plastic hinges, column buckling, etc. For a global system (e.g., building), measuring residual interstory drifts (e.g., 1%, 2%, etc.) in each story. The combination of the results obtained from the above measures on the system basis must be done for the entire structure (FEMA-445, 2006).

In this study, a set of discrete damage states, which are IO, LS, and CP performance levels, are used to present DM. As mentioned earlier, peak IDR of 1%, 2%, and 4% for each of these performance levels are used as LSt values. To develop fragility functions, three different methods exist. They are empirical, analytical, and expert opinion or judgment-based methods (Porter, 2020). In this study, the analytical method has been used to develop fragility functions for each performance level.

For developing the analytical fragility function, the lognormal CDF function is assumed, as given in the following equation:

$$P\left[DM \geq LS_k \mid EDP = edp\right] = \Phi\left(\frac{1}{\beta_{S_C}} \ln\left(\frac{S_C}{S_C}\right)\right) \tag{3.44}$$

Where:

$\Phi(\quad)$ is the standard normal cumulative distribution function.

$\hat{S}_c$ is the median demand.

β_{S_c} is the standard deviation of the natural logarithm of the demand, S_c.

The median demand value for a performance level corresponds to a demand value at which there is a 50% chance that the associated performance level initiates. In addition, the standard deviation is then obtained at this demand level from the response data. It should be noted that first, the natural logarithm of the demand (i.e., EDP) at IM=im is obtained, and then the dispersion is derived from the resultant natural logarithm of demand parameters (FEMA-P-58-1, 2018).

The probability of being in a damaged state is estimated using the following equations (Alabama, 2019; Deierlein, 2004):

$$P\left[DM = LS_k \mid EDP = edp\right] = \begin{cases} 1 - P\left[DM \geq LS_{k+1} \mid EDP = edp\right] & k = 0 \\ P\left[DM \geq LS_k \mid EDP = edp\right] - P\left[DM \geq LS_{k+1} \mid EDP = edp\right] & 1 \leq k < n \\ P\left[DM \geq LS_k \mid EDP = edp\right] & k = n \end{cases} \tag{3.45}$$

where n is the total number of damage states;

For example, consider the following figure, which presents the fragility functions for component C1011.001a. Details about this component are provided in section 5.3.2. The component has three damage states; therefore, there are four Damage Zones (DZs). These DZs are slight or no damage zone (DZ1), moderate damage zone (DZ2), severe or extensive damage zone (DZ3), and collapse damage zone (DZ4). The probability of zone DZ1 is one minus the probability related to the fragility curve which corresponds to the first damage state. The probability of zone DZ2 is the difference between the probabilities associated with fragility curves, which correspond to the first and second damage states. Similarly, the probability of zone DZ3 is the difference between the probabilities related to fragility curves, which correspond to the second and third damage states. Finally, the probability of DZ4 is simply the probability related to the fragility curve corresponding to the third damage state. For example, at 1.3% IDR, the probability of each zone DZ1, DZ2, DZ3, and DZ4 are 0.85%, 18.25%, 80.08%, and 0.82%, respectively.

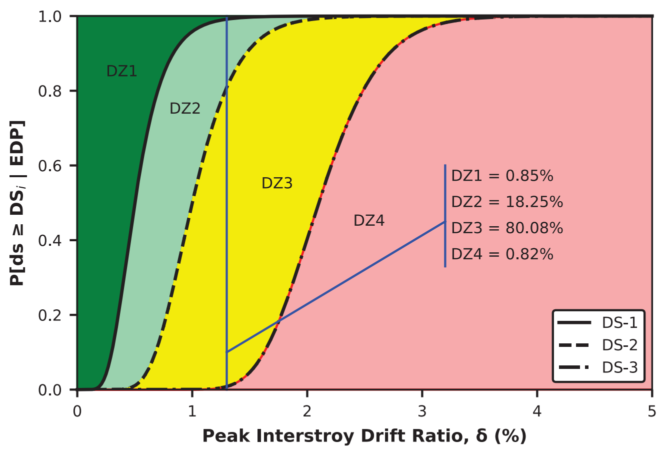

Figure 3.12. Four different damage zones for component C1011.001a

3.4.2. Fragility Curves for Residual Drift

Structures could show linear behavior up to a certain level of IM value, beyond which structure will show nonlinear behavior. If a structure experiences nonlinear behavior, there will be permanent displacement, which shows the damaged state of the structure. The permanent drift ratio (residual drift ratio) is used as a global DM parameter in literature. Residual Drift Ratio (RDR) could be obtained from peak IDR by using the following set of equations, recommended in FEMA P58-1.

$$\Delta_r = \begin{cases} 0 & for \quad \Delta \le \Delta_y \\ 0.3\left(\Delta - \Delta_y\right) & for \quad \Delta_y < \Delta < 4\Delta_y \\ \left(\Delta - 3\Delta_y\right) & for \quad \Delta \ge 4\Delta_y \end{cases} \tag{3.46}$$

In this equation, Δ is the peak IDR, and Δ_y is the peak IDR at the yield.

For obtaining the peak IDR that corresponds to yield displacement, pushover analysis is required to be implemented. For pushover analysis, forces are needed to be applied on top of each story. These forces were obtained through the Direct Displacement-Based Seismic Design approach proposed by Priestley & Kowalsky (2000).

Median demand limits for RDRs at different performance levels are provided in FEMA-356. It is negligible for the IO performance level, while for LS and CP performance levels, it is 1% and 4%, respectively. For the IO performance level in this study, 0.5% RDR is assumed, as provided in FEMA P58-1, denoted as damage state 2. The residual drift fragility function corresponding to the LS performance level is used as the repair fragility function, and the peak RDR is checked with this to see if repair is practicable. For repair fragility, the median RDR is 1%, as mentioned above, with a dispersion of 0.3, as recommended in FEMA-P-58-1 (2018).

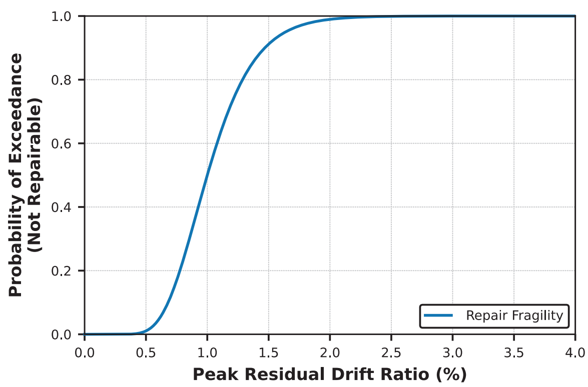

Figure 3.13. Repair fragility (Source: FEMA-P-58-1, 2018)

3.4.3. Component Fragility Curves

A performance model for a building is a set of data that is organized well. They are used to identify the building assets at risk and their exposure to seismic hazards. The data set of the performance model includes the structural components and their assemblies, nonstructural systems, nonstructural components, and content systems. The data also covers the distribution of people (occupants) within the building. For performance assessment, the vulnerable components are categorized into fragility and performance groups. Therefore, it is necessary to obtain fragility curves for components that are in the same fragility and performance groups. FEMA P58 provides a fragility database in an Excel file (FEMAP-58_FragilityDatabase_v3.1.2.xls), which contains the fragility parameters for different types of structural and nonstructural components and contents systems at multiple damage states ranging from DS_1 to DS_4. Besides, this Excel file contains data for the probability distribution of repair cost and repair time as well for the mentioned components. In addition, the database also provides the consequence functions for both repair cost and repair time.

3.5. Probabilistic Loss Analysis

The next and final step in the PEER PBEE methodology is the Probabilistic Loss Analysis (PLA). In this stage of the methodology, the conversion is made to the final DVs from damage information, which is obtained through damage analysis, i.e., through PDaA (Günay & Mosalam, 2013). In the PEER PBEE framework, DV is defined as the loss modeling measure by which the performance of a structure is defined as a continuous or discrete function with realistic decision-making potential (Petrini, 2009). In the design process, DVs could be used directly, including stakeholders, for decision making. In addition, DVs should be related to DM so that P[DV|DM] could be obtained.

The most commonly used DV is fatalities (also known as deaths), which shows the number of deaths due to the damages. Injuries could also be used as a DV, which shows the number of injuries due to the damages. The third one is the economic loss (also known as dollars), which shows monetary loss due to the repair or replacement of the damaged facility. The last commonly used DV is the repair duration (also known as downtime), which shows the nonfunctioning period of the facility during its repair.

Structural and nonstructural components are separately defined in damageable groups. For a specific value of DM, in this case, it would be possible to have different resulting values of DVs due to the distribution of the damage within the damageable group. Therefore, the total number of loss functions would be equal to the number of DMs times the number of damageable groups (Günay & Mosalam, 2013).

Furthermore, in the PLA procedure, loss functions are obtained, which show the probability of exceedance of losses from a certain value for a given damage state of the structure. Compared to the other functions, such as hazard function, response function, etc., uncertainties are more significant in the loss functions due to the high dependency on human factors (FEMA-445, 2006).

A flowchart of the PEER loss estimation methodology used in this study is given in Figure 3.14 adapted from Elkady & Lignos (2020). The collapse fragility function is used to obtain the losses due to collapse. Demolition fragility corresponds to a global damage state of the structure at which no repair is practicable, i.e., the structure should be demolished. The LS performance level is the damaged state of the structure for which repair is not practicable; therefore, the residual fragility curve related to the LS performance level could be assumed as the demolition fragility. Further, to calculate the total repair loss of the structure, repair losses should be calculated at each story, which is based on the loss curves and consequence functions of the structural and nonstructural components and content systems provided in the FEMA P-58_FragilityDatabase_v3.1.2.

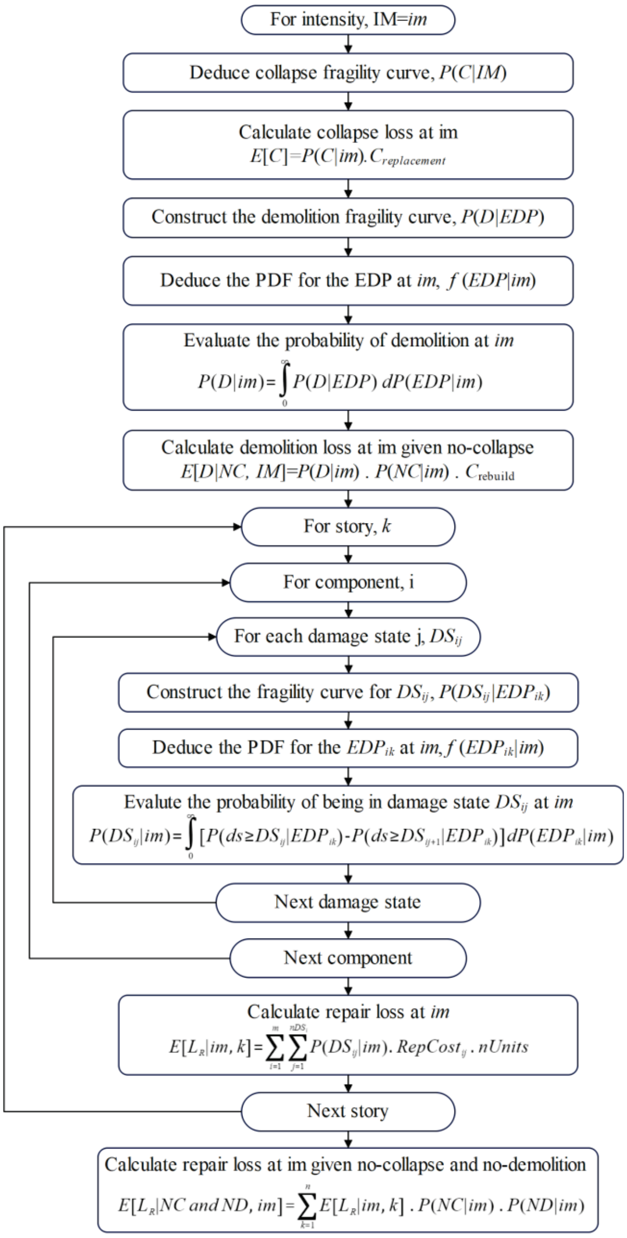

Figure 3.14. Flowchart of the PEER loss estimation methodology (Adapted from Elkady & Lignos, 2020)

3.6. Life Cycle Cost Analysis

Life Cycle Cost Analysis (LCCA) is a process that evaluates the economic performance of a newly designed structure for its entire life or the remaining life of an existing structure. The cost obtained through LCCA is called the expected total cost of the structure that includes initial construction costs, maintenance costs, and operating costs, i.e., it is the summation of the initial construction cost and the Life Cycle Cost (LCC).

In this study, the following equation, adapted from Mitropoulou & Lagaros (2016), is used to obtain the expected total cost of the structure for its entire lifetime, which is the function of the design variable (s) and the structure's lifetime (t).

$$C_{Tot}\left(t,s\right)=C_{0}\left(s\right)+C_{LCC}\left(t,s\right) \tag{3.47}$$

In this equation, C_0 is the initial construction cost of the structure, which is only the function of the design variables. C_{LCC} is the life cycle cost of the structure., which is the function of the design variables and lifetime of the structure. Since only the repair cost and cost due to repair time are considered in this study, C_{LCC} could be obtained using the following equation.

$$C_{LCC}\left(t,s\right)=C_{LCC,rep}+C_{LCC,rent}+C_{LCC,D}+C_{LCC,C} \tag{3.48}$$

In this equation, $C_{LCC,rep}$ is the repair cost in the lifetime of the structure, while $C_{LCC,rent}$ is the rental cost due to repair time in the lifetime of the structure. In addition, the failure costs, such as demolition $C_{LCC,D}$ and collapse, $C_{LCC,C}$ are also included. This study does not include other losses due to income, maintenance, injuries, and fatalities. Each portion of the equation (3.48) is the function of the design variables and lifetime, and they could be obtained using the following equation.

$$C_{LCC,DV_i}=EAL_{DV_i}\frac{1}{r}\left(1-e^{-rT}\right) \qquad DV=\{rep,\ rent,\ D,\ C\} \tag{3.49}$$

where EAL_{DV_i} is the expected annual loss of the i^{th} DV such as repair cost, rental loss, etc., r is the annual monetary discount rate, and T is the lifetime of the new structure or the remaining life of the existing structure. The expected annual loss of the i^{th} DV could be obtained using the following equation.

$$EAL_{DV_i}=\int_{im}E\left[DV_i \mid IM=im\right]d\lambda\left(im\right) \tag{3.50}$$

In this equation, $E\left[DV_i \mid IM=im\right]$ is the expected loss of the i^{th} DV at a specific IM level im, and the $d\lambda\left(im\right)$ is the annual occurrence rate of the im, which could be obtained from the hazard curve. The value of the monetary discount rate ranges from 3% to 6% (Ellingwood & Wen, 2005; Mitropoulou et al., 2011), which is assumed as 4% in this study, while the lifetime of the structure is assumed as 50 years. For the optimization problem, equation (3.47) is used as an objective function for the PPBOSD approach.

3.7. Endurance Time Method

The Endurance Time (ET) method originally introduced by Estekanchi et al. (2004) is a rather fast incremental-based dynamic time history analysis in which structures experience intensifying dynamic excitation functions. In this method, the entire performance of the structure at a continuous range of IM levels is predicted by performing a few NTHA (commonly three), which is commonly predicted by the IDA method at limited IM levels (Estekanchi et al., 2020)

The ET method has been used in several research studies recently, such as (Amouzegar & Riahi, 2015; Estekanchi et al., 2018; Hariri-Ardebili et al., 2014; Karimzada et al., 2024; Mashayekhi, Estekanchi, et al., 2019; Mashayekhi, Harati, et al., 2019; Shirkhani et al., 2020b, 2020a). The verification of the results of the ET method compared to the well-known time history analysis is presented by different studies (M. C. Basim & Estekanchi, 2015; Mashayekhi et al., 2018a, 2018b; Riahi & Estekanchi, 2010; Shirkhani et al., 2015, 2021)

3.7.1. The Concept of Endurance Time Method

To explain the concept of the ET method, a hypothetical shaking-table test can be used. The purpose of the hypothetical shaking table test is the comparison of the relative performance of the three different types of structures that are placed on the table (Figure 3.15) and subjected to intensifying artificial dynamic excitation function (Estekanchi et al., 2020).

Under the dynamic loading during the hypothetical shaking table test, the performance of the structures is monitored at each time step. The structures will show elastic behavior initially, and with the increase in the amplitude of the artificial excitation function with time, the behavior of the structures will be moved slowly from the elastic to the inelastic range and experience some damage states until collapse occurs. The results of the ET analysis method are provided in the form of ET curves. The horizontal axis of the ET curve is the ET time, and the vertical axis is the EDPs, e.g., maximum IDR. As mentioned earlier, the response of the structure at various IM levels, which is usually predicted by the IDA method, could be provided by the ET method as well. However, the main advantage of the ET method over the IDA method is that it reduces the computational time significantly (Estekanchi et al., 2009). Moreover, since the IDA method is a more precise method, the actual EDPs and final design, obtained utilizing the ET method, shall be verified by the IDA method or any other precise method, such as the cloud analysis method (Azarbakht & Dolsek, 2007; Vamvatsikos & Allin Cornell, 2002).

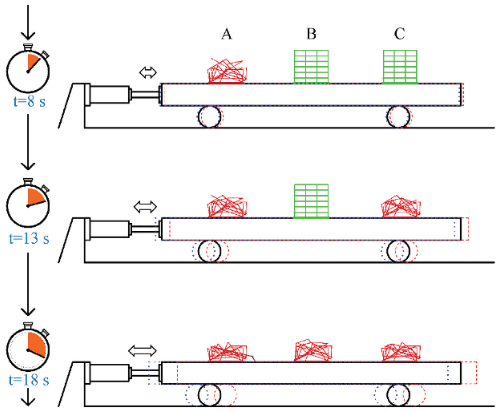

Figure 3.15. Hypothetical shaking-table test (Source: Estekanchi et al., 2020)

Conventional NTHA uses real GM accelerograms or artificially generated ones, while the ET method uses ETEFs. These functions are the main components of the ET method and directly affect the results. The ETEFs are the intensifying acceleration functions that are used for NTHA analysis. The intensity of the ETEFs increases with the increase in time, and zero to each time step corresponds to a specific seismic hazard level. They are created such that to induce suitable responses in structures compared to GMs (Mashayekhi et al., 2018a).

The ETEFs are generated from the real GM accelerograms by using simulation techniques. In this study, the ETA40l series, which is the fourth generation of ETFEs, is utilized. Since the duration of GM may significantly affect the structural response (Hancock & Bommer, 2007; Harati et al., 2019; Mashayekhi et al., 2018b, 2020), for the simulation of the ETA40lc series, the consistency of the duration of the GM is directly included in the generation process, which is not considered in the previous generation of the ETEFs. The cumulative absolute velocity (CAV) has been selected as an IM to reflect the impact of duration; to this end, the CAV is included in the generation process of the ETA40lc series of ETEFs (Mashayekhi et al., 2018a).

3.7.2. The Method of Generating ETEFs

The method of generating ETEFs is to minimize the difference between the ETEFs and GMs (in terms of the spectral values). Three different alternatives are provided for estimating the residuals, namely, absolute residuals, relative residuals, and their combination. These alternatives are objective functions, given in the following equations, which include acceleration spectra, linear displacement spectra, and CAV (Mashayekhi et al., 2018a).

$$F_{CAV-A}\left(a_g\right)=\int_{T_{\min}}^{T_{\max}}\int_{0}^{t_{\max}}\left\{\begin{array}{c}\left[S_a\left(T,t\right)-S_{aC}\left(T,t\right)\right]^2+\\ \alpha_{S_u}\left[S_u\left(T,t\right)-S_{uC}\left(T,t\right)\right]^2\\ +\alpha_{CAV}\left[CAV\left(t\right)-CAV_C\left(t\right)\right]^2\end{array}\right\}dt\,dT \tag{3.51}$$

$$F_{CAV-R}\left(a_g\right)=\int_{T_{\min}}^{T_{\max}}\int_{0}^{t_{\max}}\left\{\begin{array}{c}\left[\dfrac{S_a\left(T,t\right)-S_{aC}\left(T,t\right)}{S_{aC}\left(T,t\right)}\right]^2+\\ \left[\dfrac{S_u\left(T,t\right)-S_{uC}\left(T,t\right)}{S_{uC}\left(T,t\right)}\right]^2\\ \left[\dfrac{CAV\left(t\right)-CAV_C\left(t\right)}{CAV_C\left(t\right)}\right]^2\end{array}\right\}dt\,dT \tag{3.52}$$

$$F_{CAV-M}\left(a_g\right)=\int_{T_{\min}}^{T_{\max}}\int_{0}^{t_{\max}}\left\{\begin{array}{c}\left[\dfrac{S_a\left(T,t\right)-S_{aC}\left(T,t\right)}{S_{aC}\left(T,t\right)}\right]^2+\\ \left[\dfrac{S_u\left(T,t\right)-S_{uC}\left(T,t\right)}{S_{uC}\left(T,t\right)}\right]^2\\ \left[\dfrac{CAV\left(t\right)-CAV_C\left(t\right)}{CAV_C\left(t\right)}\right]^2\\ \left[S_a\left(T,t\right)-S_{aC}\left(T,t\right)\right]^2+\\ \alpha_{S_u}\left[S_u\left(T,t\right)-S_{uC}\left(T,t\right)\right]^2\\ +\alpha_{CAV}\left[CAV\left(t\right)-CAV_C\left(t\right)\right]^2\end{array}\right\}dt\,dT \tag{3.53}$$

where a_g is the acceleration time history of the ETEFs, which is an input to objective functions. $S_{aC}(t,T)$ is the target acceleration spectra of ETEFs, given as follows:

$$S_{aC}(t,T) = g(t) \times S_a^{\text{target}}(T) \tag{3.54}$$

where, $S_a^{target}(T)$ is GMs' target acceleration spectrum as the average acceleration response spectrum of GMs. The records of the ETA40lc series have been optimized to fit the average acceleration spectrum, average displacement spectrum, and average CAV of the first components of the FEMA-P695 (2009) far-field GM set (refer to Table 3.2). These GM records are recorded on soft rock, stiff sites, and shallow crustal sites within at least 10km site-to-source distances and with the magnitude of the events larger than 6.5. The procedure of FEMA-P695 is used for the normalization of the individual records considering their peak ground velocities. Peak ground velocity is chosen for optimization purpose because of its simplicity for removing the undesired variability between records, which are mainly due to the inherent difference in magnitude, type of the source, and the conditions of the site. Meanwhile, it is capable of keeping the inherent aleatory variability for predicting seismic response assessment.

In equation (3.54) $g(t)$, is the intensifying profile which controls the shape of increasing acceleration spectra in time. For the generation of the ETA40lc series of ETEFs, a linear function had been adopted for $g(t)$ such that (1) it must be an ascending function, (2) $g(t_{target})$ =1 (t_{target} is the time at which ETEFs match normalized GMs), and g(0)=0, as an initial condition (Mashayekhi et al., 2018a).

$S_{uC}(t,T)$ is the target linear displacement spectra of the ETEFs, which is calculated using the following equation:

$$S_{uC}(t,T) = g(t) \times S_u^{\text{target}}(T) \tag{3.55}$$

In this equation, $S_u^{target}(T)$ represents the target linear displacement spectra of the normalized GMs, that is the average displacement spectra of GMs.

$CAV_C(t)$ is the target CAV of the ETEFs, estimated using the following equation:

$$CAV_C(t) = h(t) \times CAV^{\text{target}}(T) \tag{3.56}$$

In this equation, CAV^{target} is the target CAV related to normalized GMs, which is the average CAV of the GMs, $h(t)$ is the increasing profile of CAV in time and has requirements like the ones given for $\mathrm{g}(t)$. It should be noted that $\mathrm{g}(t)$ and $h(t)$ are not the same; thus, they should be specified separately (Mashayekhi et al., 2018a).

In equation (3.53) α_{S_u} and α_{CAV} are the weight factors, which in objective function control the contribution of the residuals related to displacement spectra and CAV, respectively, and they are given in the following equations:

$$\alpha_{C_u} = \frac{\int_0^{T_{\max}} \int_0^{t_{\max}} \left[S_{aC}(T,t) \right]^2 dt\, dT}{\int_0^{T_{\max}} \int_0^{t_{\max}} \left[S_{uC}(T,t) \right]^2 dt\, dT} \tag{3.57}$$

$$\alpha_{CAV} = \frac{\int_0^{T_{\max}} \int_0^{t_{\max}} \left[S_{aC}(T,t) \right]^2 dt\, dT}{\int_0^{T_{\max}} \int_0^{t_{\max}} \left[CAV_C(T,t) \right]^2 dt\, dT} \tag{3.58}$$

In equation (3.53) $S_{\mathrm{a}}(t,T)$ is the acceleration response spectra obtained from ETEFs at time t and period of T, as follows:

$$S_a(t,T) = \max\left(\left| \ddot{u}(\tau) + a_g(\tau) \right| \right) \qquad 0 < \tau < t \tag{3.59}$$

where, a_{g} is the acceleration time history of ETEF, and $\ddot{\mathrm{u}}(\tau)$ is the relative acceleration response of an SDOF having a 5% damping ratio and natural period T under ETEFs.

In equation (3.53) $S_{\mathrm{u}}(t,T)$ is the displacement response spectra obtained from ETEFs at time t and period of T, provided in the following equation:

$$S_u(t,T) = \max\left(\left| u(\tau) \right| \right) \qquad 0 < \tau < t \tag{3.60}$$

where, $\mathrm{u}(\tau)$ is the relative displacement response of an SDOF having a 5% damping ratio and natural period T.

In equation (3.53) $CAV(t)$ is the CAV produced by ETEFs at time t, and could be calculated using the following equation;

$$CAV(t) = \int_0^t |a_g(\tau)| d\tau \tag{3.61}$$

3.7.3. Choosing Target Time

The ETEFs are used in the ET analysis method to obtain the response of the structure for a continuous range of IM levels. To obtain the response of a structure through the ET analysis method for a specific IM level, it is required to find a proper ET time known as the target time. This is a very important step in the ET analysis method, which will provide an equivalent intensity to a seismic intensity of interest. Varies approaches could be used to obtain target time. The most common ones, which are based on linear acceleration response spectra, are (1) choosing target time based on template spectra, (2) matching average spectral intensity, (3) matching minimum spectral intensity, and (4) matching scaled GMs spectra.

The first approach, choosing target time based on template spectra, is a very useful approach for the case if ETEF, used for the analysis, is produced using such template spectra. In the second approach, the average of ETEFs is obtained, and by trial and error, a target time is obtained such that the average of ETEFs matches the response spectra of interest in the neighborhood of the fundamental period of the structure. The third approach is similar to the second approach; however, the only difference is that at the range of 0.2 to 1.5 of the fundamental period, the ETEFs average spectra shall be at least above the desired design spectra.

The last approach, matching scaled GM spectra, is claimed to be likely the most appropriate approach for obtaining the target time. This approach is used when for the design basis a set of GMs is available. Initially, the set of GMs is scaled to a specific IM level as per the recommendation of the codes, such that the average response spectrum of the GMs does not fall below the design spectra at the range of 0.2T to 1.5T. Then it is used as a target spectrum for matching the ETEFs average spectra, and the target time is obtained.

In this study, the fourth generation of the ETEFs, the ETA40lc series, is used, and as mentioned that, this series of the ETEFs is obtained by using the set of FEMA-P695 far-field GM records. The target times of these excitation functions are calculated using the matching scaled GMs spectra approach. First, the GMs target acceleration spectrum is placed above the code spectrum in the range of $0.2T$ to $1.5T$, and second, the average acceleration response spectrum of ETA40lc01-03 is matched with the scaled GMs target acceleration spectrum in the same range of $0.2T$ to $1.5T$.

The target acceleration spectrum of the first components of FEMA-P695 far-field GM set together with the response spectrum of individual GM records is shown in Figure 3.16. The ETA40lc01 accelerogram and the comparison of its acceleration response spectra at different excitation times with target response spectra are shown in Figure 3.17.

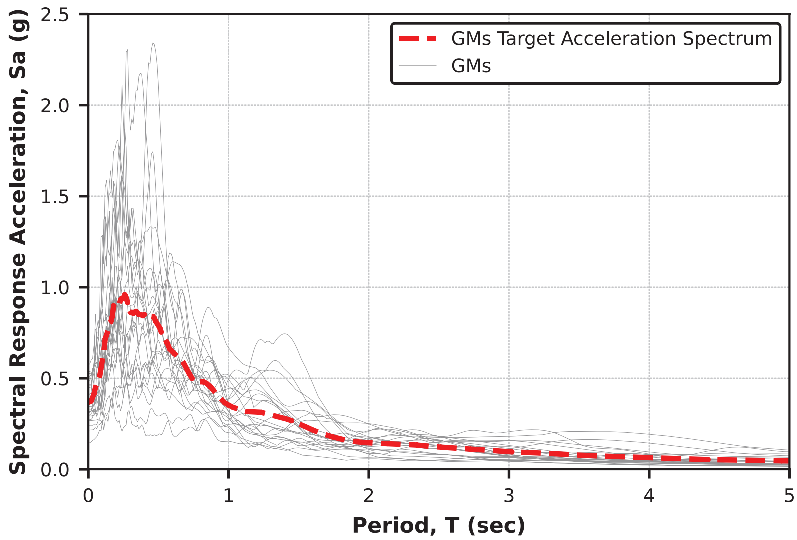

Figure 3.16. Target acceleration spectrum of first components of FEMA-P695 far-field GM set

Three excitation functions of the ETA40lc series are used in this study to reduce the effects of random scatter in the results, as recommended in research work by Estekanchi et al. (2007).

The variation of the corresponding hazard return period with the target time in ET analysis and structural period in this study is shown in Figure 3.18. A range of IM levels and a range of fundamental periods of the structure are considered for generating this figure. To obtain such figures, it is required to obtain the design response spectrum at different IM levels. For example, in the figure, the IM levels are shown in terms of the return period. The return period for any IM level could be obtained by using the following equation (ASCE/SEI-41-06, 2007):

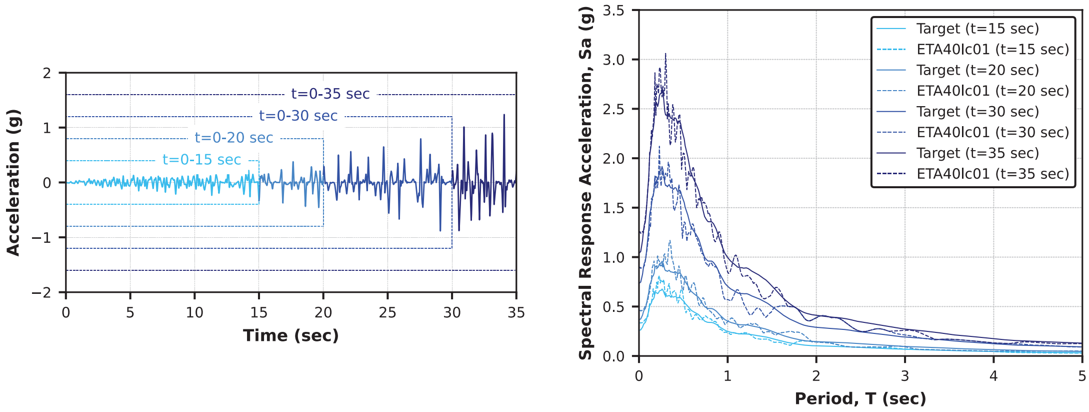

(a) ETA40lc01 accelerogram

(b) Acceleration response spectra

Figure 3.17. Target times for different IM levels

$$P_R = \frac{-Y}{\ln\left(1 - P_{EY}\right)} \tag{3.62}$$

In this equation, Y is the time duration (e.g., 50 years), and P_{EY} is the probability of exceedance in Y.

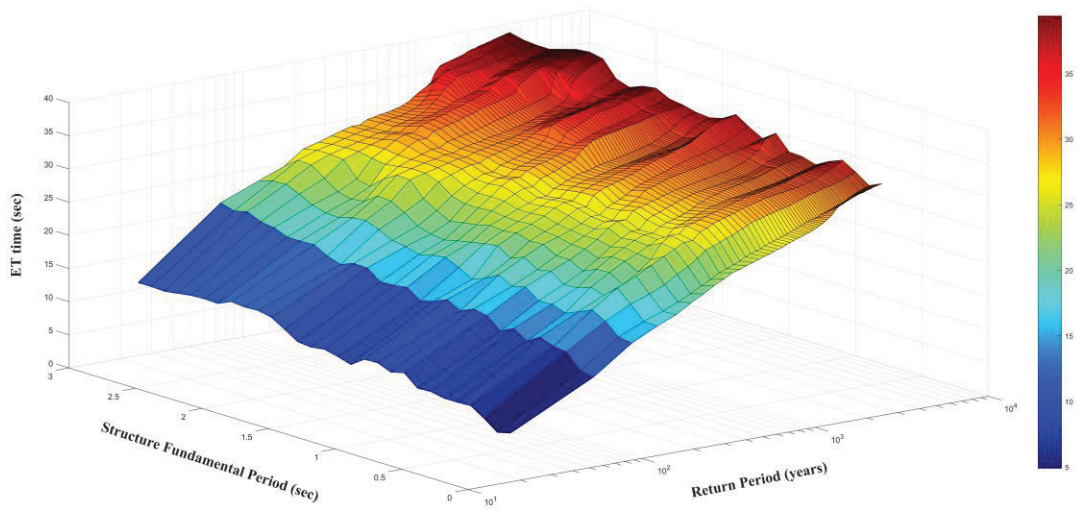

Figure 3.18. Variation of target time in ET analysis with respect to return period and fundamental period of the structure

As mentioned earlier, the codified design response spectrum is also required to obtain the target time. In fact, it is very time-consuming to obtain the design spectra for different hazard levels. To overcome this issue the following relation could be used given in ASCE/SEI-41-06 (2007) for estimating the mapped spectral acceleration parameters S_S and S_1.

$$S_i = S_{i10/50}\left(\frac{P_R}{475}\right)^n \tag{3.63}$$

where S_i is the mapped spectral acceleration (S_S or S_1) at the IM level of interest, and $S_{i10/50}$ is the mapped spectral acceleration (S_S or S_1) at the hazard level with a 10% probability of exceedance in 50 years. The exponent n is a constant number that depends on the region and the two hazard levels of 2% and 10% probability of exceedance in 50 years. For the earthquake hazard levels between 2% and 10% probability of exceedance in 50 years, and according to the selected region, n=0.29 for both S_s and S_1. However, for the possibilities greater than 10% in 50 years, n=0.44 for both S_s and S_1 (ASCE/SEI-41-06, 2007).

Figure 3.19 is extracted from Figure 3.18 for three different periods and three hazard levels to clearly see the effect of IM level and fundamental period of the structure on the target time. Figure 3.19a shows the ET time vs Return period (which corresponds to IM level) at three different fundamental periods of the structures. Similarly, Figure 3.19b shows the ET time vs fundamental period of the structure at three different hazard levels.

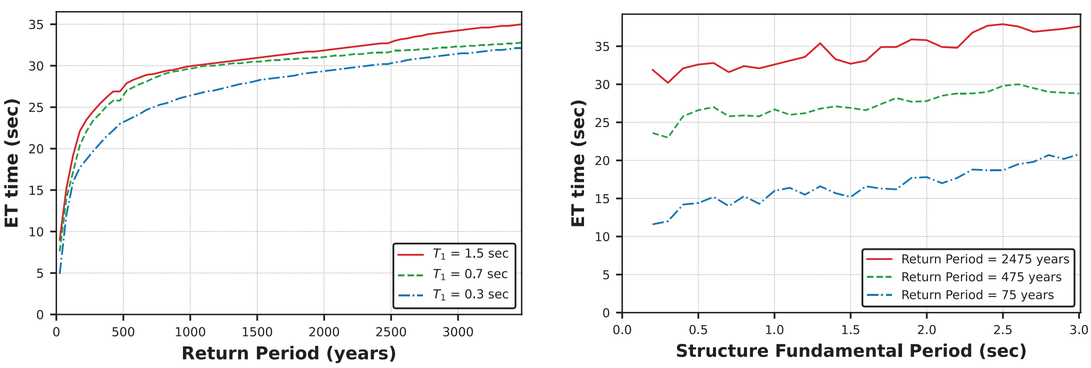

(a) ET time vs Return Period

(b) ET time vs period

Figure 3.19. Effects of return period and structure's fundamental period on ET time

From Figure 3.18 and Figure 3.19, it can be concluded that with an increase in the IM level, the ET time also increases. However, with an increase in the fundamental period of the structure, the increase in the ET time is not significant specifically for higher periods. Even in some specific hazard levels, the ET time corresponding to the lower period is larger than the ET time corresponding to the higher period.

3.7.4. Obtaining ET response curve

As mentioned earlier, the results of the ET method are shown in terms of the ET response curve. To obtain the ET response curve, for example, consider the displacement of the 2-Story structure, shown in Figure 3.20a, resulted from the NTHA analysis using the ETEFs. Figure 3.20a shows only the displacement due to the ETA40lc01 excitation function.

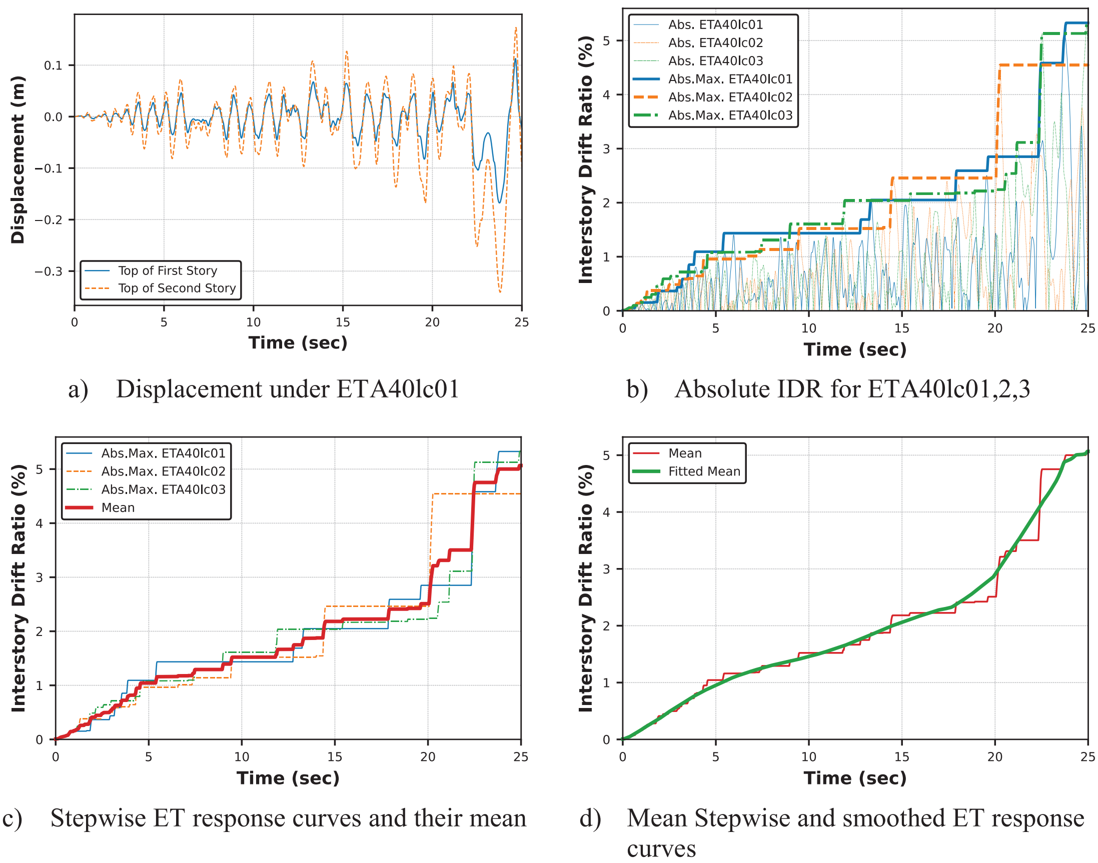

a) Displacement under ETA40lc01

b) Absolute IDR for ETA40lc01,2,3

c) Stepwise ET response curves and their mean

d) Mean Stepwise and smoothed ET response curves

Figure 3.20. The procedure of obtaining the ET response curve

Once the displacement response is achieved, then the absolute IDR at each time step is obtained (Figure 3.20b). Later, the maximum IDR from zero to each time step is attained and plotted. This step will provide a stepwise ET response curve as shown for the ETA40lc series of ETEFs in Figure 3.20b. The next step is to take the mean of the stepwise ET response curves, as shown in Figure 3.20c, and finally, making the mean smoother will give the ET response curve (Figure 3.20d).

3.8. Predicting Performance of Structure using Performance Point

The well-known capacity spectrum method could be used to determine the expected seismic performance of the structure. In this method, the capacity curve of the structure and the response spectrum (demand spectrum) are plotted in the same figure. The plot is called Acceleration-Displacement Response Spectra (ADRS), and it is in acceleration vs displacement format. The intersection of the capacity spectrum with the response spectrum is the performance point, representing the displacement demand on the structure under a given seismic hazard level. In other words, the displacement coordinate of the performance point is the demand displacement under the previously specified seismic hazard level. The structure is analyzed using nonlinear static pushover analysis method to achieve the capacity curve of the structure.

In addition to a detailed performance assessment, the expected seismic performance of the structure through the performance point is also evaluated in this study. To this end, one of the solution procedures described in FEMA-440 (2005) is implemented. Three different procedures are given in FEMA-440 (2005), which are analytical and graphical procedures for obtaining the performance points. This study adopts the graphical procedure called procedure C (MADRS locus of possible performance points). The steps for the procedure C is as follows:

1- Develop an elastic response spectrum with an initial damping ratio, usually 5%.
2- Convert the developed spectrum to the ADRS format using the following equation:

$$S_{d_i} = \frac{T_i^2}{4\pi^2} S_{a_i} g \tag{3.64}$$

In this equation, g is the gravitational acceleration. It should be noted the spectrum obtained using this equation is the initial ADRS spectrum.

3- Convert the capacity curve (base shear forces vs top displacement) to capacity spectrum (ADRS) format. For this purpose, the following relation is used.

$$S_{a_k} = \frac{V_k}{\alpha_1 W} \tag{3.65}$$

$$S_{d_k} = \frac{\Delta_{roof,k}}{\phi_{1,roof}\, PF_1} \tag{3.66}$$

Where:

PF_1 is the modal mass participation factor of the first natural mode.

α_1 is the modal mass coefficient of the first natural mode.

$\phi_{1,roof}$ is the first mode shape value of the roof level.

Δ_{roof} is the displacement of the roof.

k denotes the steps or increment of the capacity curve.

The modal mass coefficient and participation factor could be obtained using the following equations, respectively:

$$\alpha_1 = \frac{\left[\sum_{i=1}^{N} (w_i \phi_{i1})/g\right]^2}{\left[\sum_{i=1}^{N} w_i/g\right]\left[\sum_{i=1}^{N} (w_i \phi_{i1}^2)/g\right]} \tag{3.67}$$

$$PF_1 = \left[\frac{\sum_{i=1}^{N} (w_i \phi_{i1})/g}{\sum_{i=1}^{N} (w_i \phi_{i1}^2)/g}\right] \tag{3.68}$$

Where:

w_i is the mass of the ith level.

ϕ_{i1} is the mode shape value of the first natural mode at the ith level.

4- Choose a starting performance point (a_{pi}, d_{pi}). The first coordinate is spectral acceleration, and the second is spectral displacement.

5- Using the selected performance point, develop a bilinear curve representing the capacity curve. For this purpose, the equal-energy method is used, which is based on the assumption that the areas enclosed by the capacity curve below and above the bilinear curve are equal ($Area_1 \cong Area_2$).

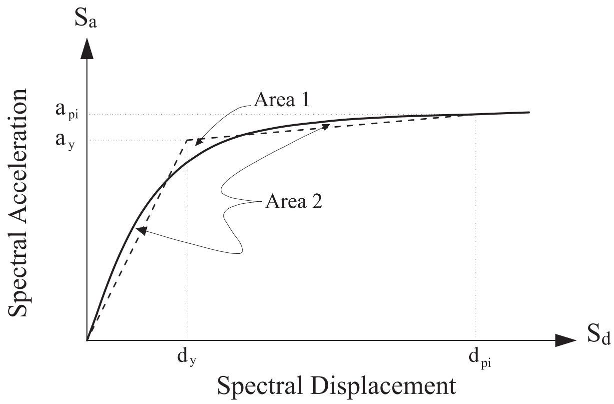

Figure 3.21. Bilinear approximation of the capacity curve

6- The post-elastic stiffness, α, and ductility, μ, for the developed bilinear representation of the capacity spectrum should be estimated using the following equations:

$$\alpha = \frac{\left(\dfrac{a_{pi} - a_y}{d_{pi} - d_y}\right)}{\left(\dfrac{a_y}{d_y}\right)} \qquad (3.69)$$

$$\mu = \frac{d_{pi}}{d_y} \qquad (3.70)$$

7- Obtain the effective damping and effective period using the following equations:

$$\beta_{eff} = 4.9(\mu - 1)^2 - 1.1(\mu - 1)^3 + \beta_0 \qquad for\ 1.0 < \mu < 4.0 \qquad (3.71a)$$

$$\beta_{eff} = 14 + 0.32(\mu - 1) + \beta_0 \qquad for\ \ 4.0 \le \mu \le 6.5 \tag{3.71b}$$

$$\beta_{eff} = 19\left[\frac{0.64(\mu-1)-1}{\left[0.64(\mu-1)\right]^2}\right]\left(\frac{T_{eff}}{T_0}\right) + \beta_0 \qquad for\ \ \mu > 6.5 \tag{3.71c}$$

$$T_{eff} = \left[0.2(\mu-1)^2 - 0.038(\mu-1)^3 + 1\right]T_0 \qquad for\ \ 1.0 < \mu < 4.0 \tag{3.72a}$$

$$T_{eff} = \left[0.28 + 0.13(\mu-1) + 1\right]T_0 \qquad for\ \ 4.0 \le \mu \le 6.5 \tag{3.72b}$$

$$T_{eff} = \left\{0.89\left[\sqrt{\frac{(\mu-1)}{1+0.05(\mu-2)}} - 1\right] + 1\right\}T_0 \qquad for\ \ \mu > 6.5 \tag{3.72c}$$

In the above equations, β_0 is the initial damping and T_0 is the initial period.

8- Adjust the initial ADRS to β_{eff}. For this purpose, the following relation is used:

$$S_\beta = \frac{(S_a)_0}{B(\beta_{eff})} \tag{3.73}$$

In this equation $B(\beta_{eff})$ is the damping coefficient, which is the function of β_{eff} and is obtained using the following equation:

$$B = \frac{4}{5.6 - \ln \beta_{eff}\,(in\,\%)} \tag{3.74}$$

9- Generate Modified Acceleration-Displacement Response Spectra (MADRS) using adjusted ADRS for β_{eff}. To obtain MADRS, the adjusted ADRS is multiplied by the modification factor (M). The modification factor could be estimated using the following equation:

$$M = \left(\frac{T_{eff}}{T_0}\right)^2\left(\frac{T_0}{T_{\sec}}\right)^2 \tag{3.75}$$

$$\left(\frac{T_0}{T_{\text{sec}}}\right)^2 = \frac{1+\alpha(\mu-1)}{\mu} \tag{3.76}$$

In these equations T_{sec} is the secant period.

10- Obtain the possible performance point from the intersection of the radial secant period (T_{sec}) with the MADRS.

11- Select a new performance point (a_{pi}, d_{pi}), and repeat the steps from 5 to 11 to obtain the family of performance points.

12- Connect the locus of performance points to create a line. The intersection of this line with the capacity spectrum provides the actual performance point.

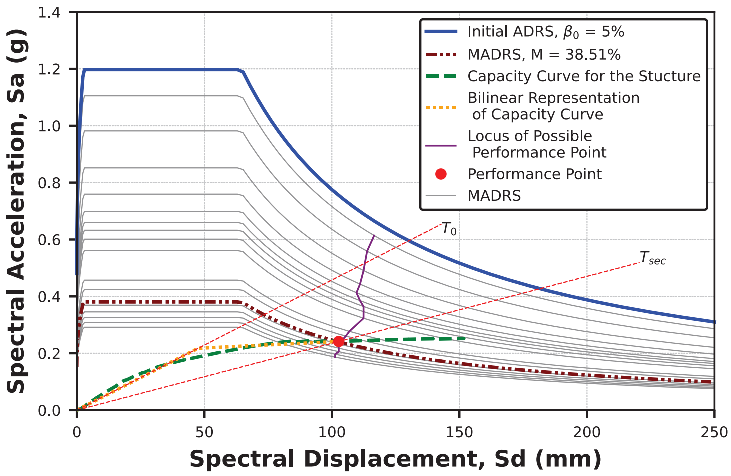

Figure 3.22. Determination of the performance point using the intersection of the capacity spectrum with MADRS (procedure C)

The figure shows the necessary parameters for a specific structure and the achieved performance point. In this figure, the final T_{sec}, the final performance point is shown. Since the method of obtaining the performance point is an iterative method, the figure also shows the MADRS achieved at each iteration.

CHAPTER 4

STRUCTURAL OPTIMIZATION

With the demand for continuous development around the world and the reduction in ordinary energy sources, the need for optimizing the production and the use of construction materials has increased significantly. During the minimization, the significant role of the construction sector in economic development and prosperity should be maintained (Yazdani et al., 2017).

Optimization is the act of making something (such as a design, system, or decision) as good as possible, i.e., it is an act, process, or methodology making something as fully perfect, functional, or effective as possible. In structural design, optimization is the search for excellent design.

Traditionally, to have a better design, structural design is carried out by trial-and-error, which is expensive computationally; in addition, it depends highly on the designer's experience. However, the final design still may not be able to achieve the desired performance, specifically for complex structures. On the other hand, optimization, also known as mathematical programming, is a systematic approach, and with the aid of computational capability, it yields the optimal design within a reasonable time frame. The obtained optimal design would be a satisfactory design regarding the desired performance.

4.1. Optimization Problem Definition

An optimization problem consists of design variables, objective function, and constraints to variables. The objective function which has to be minimized or maximized is the first and very important part of the optimization problem that should be identified. The design variables are the unknowns that affect the outcome (i.e., objective function). At the optimum outcome, the set of variables is known as the optimum solution. The general form of an optimization problem is given as follows:

$$\min_{x} f(x) \tag{4.1}$$

Subjected to:

$$g(x) \leq 0$$
$$h(x) = 0$$
$$x_l \leq x \leq x_u$$

Where $f(x)$ is the objective function, which could be a single objective function or multi-objective function. The function $g(x)$ is the inequality constraint, which could be a single scalar value or a set of values, and $h(x)$ is the equality constraint. The vector x represents the design variables, which are constrained by the lower (x_l) and upper (x_u) bounds. The design space where the optimum solution shall be searched is reduced by the lower and upper bounds. If all constraints are satisfied by a set of design variables, this set of design variables is called a feasible solution, although it may not minimize the objective function.

In addition, the process of determining the objective function, design variables, and constraint equations is called modeling of the optimization problem. Equation (4.1) is the standard form of a normalization problem. Any type of optimization problem could be converted to the standard model. For example, if the maximization of an optimization problem is required, then the objective function is multiplied by minus one (-1). Similarly, if the constraints g(x) are larger than zero, multiplying them by minus one could bring them to a standard model.

Different categories of optimization problems are presented in the literature, such as linear and nonlinear, constrained and unconstrained, discrete and continuous, single and multi-objective, etc. For example, when any of the objective or constrained functions is a nonlinear function, then the optimization problem is called a nonlinear optimization problem. In addition, if at least one variable within the set of design variables is a type of discrete variable, then the optimization problem is called a discrete optimization problem. Some more information is provided in the next section regarding these categories.

In this study, three different types of optimization problems will be solved. For the first alternative, the initial cost of the structure is chosen as the objective function to be minimized. The ELF method provided in ASCE/SEI-7-16 (2017) standard is used for the design purpose. As constraints, the requirements of ASCE/SEI 7-16, together with ACI 318 (2019), are selected.

For the second alternative, the objective function will be similar to the first alternative, while for the constraints besides the requirements of the ACI 318-19 code, the requirements of the performance-based design will also be used. For the third alternative, the constraints will be the same as for the second alternative, while the objective function will be not only the initial cost of the structure but also the expected annual cost for a specific hazard level will be included. The summation of these two costs is given the life cycle cost or expected total cost for the structure.

In addition, in this study, the cross-sectional dimensions of the members (columns and beams), the reinforcement ratios, and the configuration of closed stirrups (the diameter, the number of legs, and the spacing between the stirrups) are selected as design variables. Since the design variables are discrete, the discrete-constrained optimization problem has been solved. For this purpose, a database is first generated for square columns and a database for rectangular beams, which is briefly explained in section 4.6.

In the framework of PEER PBEE methodology, since EDPs are obtained through the IDA method, it will be computationally very expensive to use the IDA method in the optimization algorithm. Therefore, in this study, the ET method, which is a time history-based procedure for seismic performance assessment of structures under intensifying excitation functions, is utilized in the optimization algorithm.

4.2. Types of Optimization Problems

The previous section provides the general form for an optimization problem, with its main elements. Identifying the type or class of optimization problem is important since different classes of optimization problems may have different types of solution approaches and algorithms. In each objective function and constraint, at least a single design variable must be involved; otherwise, it will be meaningless and should be omitted from the optimization problem. Among the optimization problems, the particular case of continuous unconstrained linear optimization problem, which leads to an infinite solution, should not be considered. The major types of optimization problems are discussed briefly (Messac, 2015).

1. **Linear vs. Nonlinear Optimization Problems**

For the linear optimization problems, all the objective functions and both equality and inequality constraints are linear functions of the design variables. This type of optimization problem is also known as linear programming problem. On the other hand, the nonlinear optimization problem also called the nonlinear programming problem, is one if any of the objective functions or constraints are nonlinear functions of the design variables (Arora, 2017; Messac, 2015). In addition, solving nonlinear programming is much more complicated than linear programming, especially when the number of design variables is high. This study has some nonlinear constraints; therefore, nonlinear programming is dealt with (Messac, 2015).

2. **Constrained vs. Unconstrained Optimization Problems**

An optimization problem with at least one constraint is called the constraint optimization problem. On the other hand, an optimization problem without any constraint is known as an unconstrained optimization problem (Arora, 2017; Messac, 2015). For unconstrained nonlinear optimization problems, only equation 3.1 will be left, and the equality and inequality constraint equations will not be available. However, for linear optimization problems to have finite solutions, at least one of the expressions of equation (4.1) corresponding to constraints and variables must be available. In practice, optimization problems generally involve constraints, which makes the solution procedure a little bit complicated, specifically in nonlinear programming. Structural design must satisfy the codes and standards requirements, which are used as constraints in this study. To this end, the constrained optimization problem is solved (Messac, 2015).

3. **Continuous vs. Discrete Optimization Problems**

In the optimization problem, the number of design variables depends on the problem type that is considered for optimization. If only a single design variable is a discrete variable among the design variables, such an optimization problem is called a discrete optimization problem; otherwise, it is called a continuous optimization problem (Arora, 2017; Messac, 2015). There are three cases of design variables in discrete optimization problems. The first case is that the design variables could take only integer values. In the second case, the design variables are assigned only zero and one. In the third case, the design variables are defined from a prescribed set of real numbers. Considering these cases, discrete optimization problems could be divided into five categories, briefly discussed in the following paragraph (Messac, 2015).

(i) The first one is binary programming, in which the discrete variable takes only 0 and 1. (ii) The second category is known as pure integer programming problems, in which only integer design variables are involved in the optimization problem. (iii) When the design variables take the value from a set of predefined real numbers, which are not integer values, this optimization problem is called a discrete non-integer optimization problem. (iv) The other category is mixed-integer programming problems, in which some design variables have integer values while others have continuous values. (v) The last one is called the combinatorial optimization problem. In this category, the design variables take only the values from a combinatorial set of discrete values that resulted from the feasible discrete values (Messac, 2015).

In this study, the design variables are the cross-sectional dimensions of the columns and beams, the reinforcement ratios for these members, and the configuration of the confined reinforcements (diameter of the bar, spacing, and number of legs in the direction of interest). In addition, OpenSees is used for design and analysis purposes, which requires defining the members in a discrete form; thus, a discrete optimization problem is identified for the case studies.

4. Single vs. Multiobjective Optimization Problems

The single objective optimization problem is the type of optimization problem with only a single objective function to be minimized or maximized. In contrast, a multiobjective optimization problem has at least two objective functions. Usually, the objective functions are conflicting in a multiobjective optimization problem. By reducing the value of one objective function, the value for the other objective function is increasing. For example, in structural design, if someone wants to reduce the risk to life, the cost of the structure increases on the other hand. As mentioned previously that, in this study, three different design approaches, Code-Based, PBSD, and PPBOSD, are used for the design purpose. Also, it is mentioned that for the first two cases, the initial cost of the structure and for the last cast, the expected total cost of the structure is considered as an objective function. The objective functions considered in each case are the only objective functions; therefore, the single objective optimization problem has been solved in this study (Messac, 2015).

5. **Deterministic vs. Nondeterministic Optimization Problems**

In an optimization problem, sometimes randomness is involved, i.e., any optimization task that incorporates randomness, whether in the objective function or the optimization algorithm, is referred to as nondeterministic or stochastic optimization. In the objective function, randomness implies that some uncertainties exist while evaluating the solution for the objective function. The optimization algorithm for the stochastic optimization shall be chosen such that it does not get stuck in the local minima. In addition, if there are some uncertainties in the constraints or the design variables, it is still called nondeterministic optimization problems. In this study, for the first two design approaches (Code-Based and PBSD), deterministic optimization problems are solved. However, for the PPBOSD approach, since the probabilistic performance assessment is involved, the stochastic optimization problem has been solved (Messac, 2015).

6. **Simple vs. Complex Optimization Problems**

As simple as an optimization problem is, the solution is easily found. For a simple optimization problem, the following characteristics could be mentioned (Messac, 2015):

- The model of the problem is already provided.
- The design variables are all of continuous form.
- The nonlinearity is not complex, i.e., the nonlinearity is weak.
- If there are local minima, that will be sufficient as a solution.
- A small number of design variables are involved.
- The computational time is much less.
- Nondeterministic design variables are absent, i.e., they are not part of the optimization problem.

4.3. Solution Methods of Optimization Problems

The previous section briefly discusses the different types of optimization problems. Some of them may have some specific solution method, while others may be solved using different types of solution techniques or algorithms. In general, there are four different groups of solution approaches they are analytical, numerical, experimental, and graphical solution approaches (Messac, 2015).

In the analytical approach, the objective function should be available as a mathematical expression; therefore, they are also called mathematical methods. In this case, the derivative of the function at a point equal to zero could provide the optimum solution (minimum or maximum). The second derivative of the function at the mentioned point will declare that if the optimum value of the objective function is the maximum or minimum. It is a very complicated approach for the most practical optimization problems, so it is not practical to use such methods, specifically after computer technology and numerical methods have developed. The benefits of such methods are helpful for developing numerical algorithms (Messac, 2015).

The second approach is the experimental optimization approach, which is traditionally a trial-and-error approach and is an outdated approach. This approach is impractical in the modern optimization world since computational time is so high, and the cost of performing such optimization may be very high. This is because the physical model of the product should be prepared at each iteration. The other problem is that the desired solution may not be achieved, although several iterations may be performed. Moreover, it may need experience as well to work. In the first step of the experimental optimization approach, the physical model of a product should be prepared. In the second step, the prepared model's performance assessment should be utilized to obtain its performance. In the third step, checking the assessed performance of the product, if it is not the desired performance, changing design variables such that it might improve the performance of the product, and starting from the first step for the next iteration (Messac, 2015).

The third approach for solving an optimization problem is the graphical method. Using this method, the solution to the problem can be obtained using graphs. Such graphs include iterations for the object function and constraints. The graphical method shows the solution in a much better way. Graphical optimization methods have some advantages; for example, they have the capability to represent complex problems in a simple way. They are easier to understand and reproduce. Limitations of the optimization problems or their drawbacks are easily captured. Besides the advantages of the graphical methods, they also have some weaknesses. One of the main limitations of the graphical method is that it is usually applied for two variables, while sometimes it deals with three design variables and takes much time to reach a solution (Arora, 2017; Raju, 2014). They cannot be applied to the optimization problems with more than three variables. In addition, since the values of the variables are scaled on the graph, the solution of the problem is not reliable (Raju, 2014).

The last approach is the numerical optimization approach, which is widely used for the solution of optimization problems in practice. It is a modern optimization approach that can deal with small and large optimization problems and use computational capability to solve them in a reasonable time frame. It provides us the ability to deal with countless possibilities for optimization problems that are not possible to get through any manual way. Initially, design variables are selected, which may result in the worst value for the objective function, and then iterations begin with the logic defined in the optimization algorithm. The iterations continue until the stopping criteria are satisfied. In addition, due to its iterative characteristic, it has two main benefits. The first advantage is that, in this approach, the subsequent improved design is identified by the use of an algorithm. The second advantage is that since it uses computer power for iteration, even large-scale optimization problems could be solved in a suitable time frame (Messac, 2015).

Several algorithms are developed to solve numerical optimization problems. Some of them are based on direct searches, such as GA and Simplex method. While some others are gradient-based methods, e.g., the Conjugate Gradient method, Newton-Raphson Method, and Quasi-Newton method (Corriou, 2021). GAs can directly work with discrete search spaces; therefore, they are famous for solving discrete optimization problems (Messac, 2015).

The simplex method is used to solve linear programming problems. A convex polygon represents the feasible region for a standard linear problem. One of the vertices of the polygon will provide the optimal solution for the problem. Along the edges of the polygon, the solution process moves from one vertex to another. The objective function should be reduced in each iteration until the optimum value is reached (Arora, 2017; Messac, 2015). In this method, any linear problem should first be converted to the standard form by implementing specific operations. In this case, the standard form does not include the inequality constraints. In addition, there are no negative constraints for the design variables, and there must always be a bound for them (Messac, 2015). The other important thing is to form a simplex tableau, which contains the constant coefficients of the objective and constraint functions. Once the tableau is formed, the pivot column and row should be specified. After specifying the pivot column and raw, the tableau is reduced to Canonical form, and optimality is checked at the end.

The conjugate gradient method, which is first proposed for minimizing the quadratic function, $F(x)\frac{1}{2}x^T Ax - b^T x$, is an iterative method for solving unconstraint linear optimization problems (Corriou, 2021; Messac, 2015). The matrix A, also known as the Hessian matrix, $\nabla^2 f(x) = A$, should be positive definite and a symmetric matrix; this satisfies the sufficient conditions for the local minimum. In addition, the gradient of the objective function should be equal to zero to satisfy the first-order necessary conditions. For large-scale optimization problems, evaluating the Hessian matrix is costly; therefore, this method is advantageous in such situations. In this method, the conjugate directions are used to minimize the objective function iteratively; however, the convergence rate is slower (Messac, 2015).

The Newton-Raphson method also called the Newton method, is useful when the second-order derivative of a function is available. The derivative information makes it possible to provide a better search direction and define the cost surface more precisely. The quadratic convergence rate characteristic allows the method to converge faster (Arora, 2017). The problem with this method is that if the initial guess for the design variables is not good, the optimum solution cannot be obtained or may give the incorrect optimum solution (Messac, 2015). In addition, since the Hessian matrix is generated from *n(n + 1)/2* second-order derivatives (n is the number of design variables), sometimes it is very difficult to obtain the Hessian matrix, and even sometimes it may not be possible to obtain it. Furthermore, the singularity of the Hessian matrix in any iteration causes the method to encounter problems (Arora, 2017; Corriou, 2021).

The Quasi-Newton method is another gradient-based optimization algorithm usually used for solving nonlinear optimization problems. This method comes into the picture for optimization problems in which obtaining the Hessian matrix is difficult or impossible. The Hessian matrix is approximated using another matrix (must be positive definite at each iteration); the first derivative is usually considered for generating such an approximate matrix (Arora, 2017; Corriou, 2021; Messac, 2015). Thus, there is no need for the second derivative of the functions, which are complicated to obtain. Similar to the Newton method, if the initial guess for the design variables is not good, they may face convergence failure, or the solution may not be correct (Arora, 2017). The other problem with this method is that, for storing and updating the matrices, they need a high amount of memory, mainly for large-scale problems.

In this study, the discrete optimization problem is formulated for which GA has been implemented. To this end, a short discussion has been made about GAs in the following section.

4.4. Genetic Algorithms

Genetic Algorithms (GAs) are the class of evolutionary algorithms which are first conceived by Holland (1992). They are based on Darwin's theory of evolution and population-based optimization algorithms and are widely used for solving different types of optimization problems (Messac, 2015). The population of individual solutions is modified repeatedly by the GA during its entire run. Based on the specified criteria, at each iteration, the GA randomly selects individuals from the current population and uses them as parents. The parents are then used to produce the children (offsprings) for the next generation. The population evolves in the direction of an optimal solution, over successive generations (Messac, 2015).

The difference between the GAs and other normal optimization and search methods is that instead of working with the design variables themselves, GAs operate with the encoded design variables, which are usually in terms of the binary strings, i.e., zeros and ones (Cavazzuti, 2013; Goldberg, 1989). In addition, the GAs search in an entire population of each design variable points rather than a single-point search. They use the information of the objective function for the selection of the number of individuals and reproduction of the population (Goldberg, 1989). The procedure of a GA is provided in Figure 4.1.

The first step is to code the individual solutions (design variables) as a finite fixed-length string. For this purpose, usually, binary numbers, which consist of only ones and zeros, are used. The next step is to create the initial population of the individuals from the set of design variables (bounded by upper and lower values of the design variables). The size of the population presents the number of individuals in each population, which must be defined before generating a population of individuals. For each individual, the objective function is evaluated in the next step of the algorithm, and meanwhile, the provided termination criteria or optimization criteria are checked; if satisfied, the algorithm will be terminated (Messac, 2015).

In case the optimization criteria are not satisfied, the algorithm moves to the next step, called fitness assignment. For fitness assignment, different options exist; for example, in ranked-based fitness assignment, based on the objective function's value, the individuals are sorted in descending order from best to worst. In the next step, the ones with acceptable fitness (best individuals) are selected with decreasing probability as sorted (i.e., the first best individuals with higher probability, compared to the second-best individuals) for reproduction purposes (Cavazzuti, 2013; Messac, 2015).

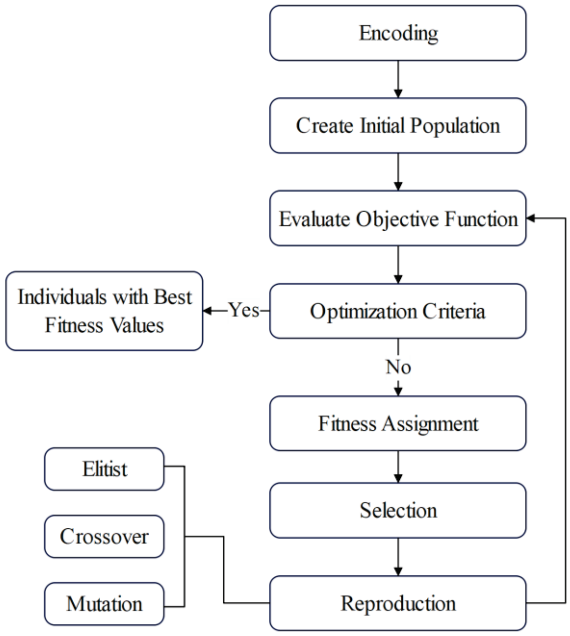

Figure 4.1. The procedure of a GA (Source: Messac, 2015)

In the process of reproduction, a new generation of individuals is generated. Here, three mechanisms have important roles, namely elitist, crossover, and mutation. Elitist guarantees the survival of the best individuals in the next generation. The crossover selects at least two parent individuals, and a portion of the encoded string related to one parent individual is swapped with the corresponding portion of the encoded string related to the other parent individual (Vijayalakshmi Pai, 2018). The importance of crossover in GAs is that, if used, the produced offspring will be different with compare to the parents. Single point, two points, or multiple points crossover operators could be used. In the mutation mechanism, a child is produced from a single parent by changing a portion of the encoding string at each individual, i.e., randomly changes zero with one or vice versa in the case of binary encoding (Vijayalakshmi Pai, 2018).

4.5. Optimization using Python Library-Pymoo

The Pymoo: Multi-Objective Optimization in Python is an open-source Python programming library developed by Blank & Deb (2020). It includes the functions already built for the different types of optimization algorithms. Different algorithms are capable of solving different types of optimization problems. In addition, in this library, each algorithm with its related function (source code of the function) is explained to utilize it for a proper optimization problem.

In the Pymoo, the general form for the multiobjective optimization problem is defined as given in the following equation (Blank & Deb, 2020), which is similar to equation (4.1).

$$\min \ f_m(x) \qquad m = 1, ..., M \tag{4.2}$$

Subjected to:

$$\begin{aligned} &g_j(x) \le 0 && j = 1, ..., J \\ &h_k(x) = 0 && k = 1, ..., K \\ &x_i^l \le x_i \le x_i^u && i = 1, ..., N \end{aligned}$$

In the equation, M is the number of objective functions, j is the number of inequality constraints, K is the number of equality constraints, and N is the number of design variables. Since, in this study, a single objective optimization type of problem is considered for each of the three design approaches, and the GA is selected as a solution method, further explanations are restricted to the GA. In the Pymoo, the first thing is to define the problem as a class function. A part of the sample code written in Python is as follows:

```
class MyProblem(ElementwiseProblem):
    def __init__(self):
        super().__init__(n_var=N,
                         n_obj=M,
                         n_constr=J,
                         xl=np.array([i=1,.., I]),
                         xu=np.array([i=1,…, I]),
                         type_var=int)
    def _evaluate(self, x, out, *args, **kwargs):
        Objective functions
```

Constraint functions

The first part of the class function, def __init__(self): super().__init(…), is to specify the number of objective functions (n_obj), constraint functions (n_constr), number of design variables (n_var) and their upper and lower bounds (xl and xu), and the type of variables (type_var). The second part of the class function, def _evaluate (…), is the evaluation part. In this part, the objective and constraint functions should be defined. The easy way is to define a function to calculate objectives and a function to estimate the constraints of the optimization problem and then call them in this part.

The second step is to define the termination criteria. The following function is termination criterion for a single objective function. If the values are not specified, then the default values are considered automatically.

```
termination = SingleObjectiveDefaultTermination (
    x_tol=1e-8,
    cv_tol=1e-6,
    f_tol=1e-6,
    nth_gen=5,
    n_last=20,
    **kwargs )
```

**kwargs is the key argument that could be entered, for example, the number of maximum generation (n_max_gen) and number of maximum evaluation (n_max_evals).

The next part is to define a solution algorithm for the optimization problem. For example, the following piece of code is the function that defines the GA with default values.

```
algorithm = GA(pop_size=100,
               sampling=get_sampling("int_random"),
               selection=get_selection('random'),
               crossover=get_crossover("int_sbx", prob=1.0, eta=3.0),
               mutation=get_mutation("int_pm", eta=3.0),
               eliminate_duplicates=True,
               )
```

The last part is to put all above information in a single function called minimize (…). This is shown in the following with the default parameters. The default definition is considered if the other parts are not specified.

```
def minimize(MyProblem,
        algorithm,
        termination=None,
        copy_algorithm=True,
        copy_termination=True,
        **kwargs):
```

To call this function, we can write the following, and if we want to save it to a variable, then the output should be named. Lets call the output variable, for example, *MyOutPut*.

```
MyOutPut = minimize(problem,
            algorithm,
            termination,
            verbose=True,
            seed=1,
            save_history=True,
            )
```

In this case, the output of the optimization problem is saved in the *MyOutPut variable*, from which the resulting parameters could be extracted. For example, if the values of the design variable, the results for the constraint and objective functions are required, they can be extracted as follows:

```
X = np.row_stack([a.pop.get("X") for a in MyOutPut.history])
G = np.row_stack([a.pop.get("G") for a in MyOutPut.history])
F = np.row_stack([a.pop.get("F") for a in MyOutPut.history])
```

4.6. Database for Cross-Sectional Configuration of the Elements

In the optimization problem, as mentioned in the previous section, design variables are the parameters that must be changed in each iteration to obtain the desired optimum solution for a problem. In OpenSees, it is required to model concrete sections in very detail, i.e., each reinforcement bar should be modeled as a fiber in its correct location, and the confined and unconfined regions should be modeled separately. Such modeling of the members of the frames (columns and beams) requires all necessary parameters needed in OpenSees to be available. Therefore, it was found necessary to generate a database for column cross-sections and a database for beam cross-sections.

For beams, rectangular cross-sections, while for columns, square cross-sections are considered. The ranges for the depth and width of the cross-section, the number of longitudinal reinforcement bars, the diameters of the longitudinal reinforcement bars, and the spacing for closed stirrups with their diameter are provided. While generating the database, ACI 318 (2019) section 18.6 and section 18.7 requirements are also applied for beams and columns, respectively. For example, minimum clear span space between two longitudinal reinforcement bars. Furthermore, the database includes the ultimate moment and shear capacity for beams, and for columns, the maximum axial capacity and shear capacity of the sections are also included. These parameters are obtained through sectional analysis.

In addition, as it will be discussed in section 5.1.3 that, for numerical modeling of concrete in OpenSees, *concrete04* type of material will be used. The parameters required for modeling this type of material are the stresses and strains of the confined and unconfined concrete. Thus, the stress and strain parameters for confined concrete are obtained through the Mander Model (Mander et al., 1988) and added to the database.

CHAPTER 5

METHODOLOGY

As mentioned in the first chapter of this thesis, this study aims to develop a PPBOSD approach, which will be capable of providing the structural design with a more rational decision to the owners and stakeholders. It is possible to quantify the risk. The probabilities could be considered in the design process explicitly. To investigate each step of the methodology, an example of a 2-Story RC structure is considered in this chapter. In this study, three performance objectives are selected: IO, LS, and CP performance levels corresponding to the 50%, 10%, and 2% probability of exceedance in 50 years, with a mean return period of 72, 475, and 2475 years hazard levels. In the next step, a database for beams and a database for columns (refer to section 4.6) were generated, which is highly dependent on the experience of the structural engineer.

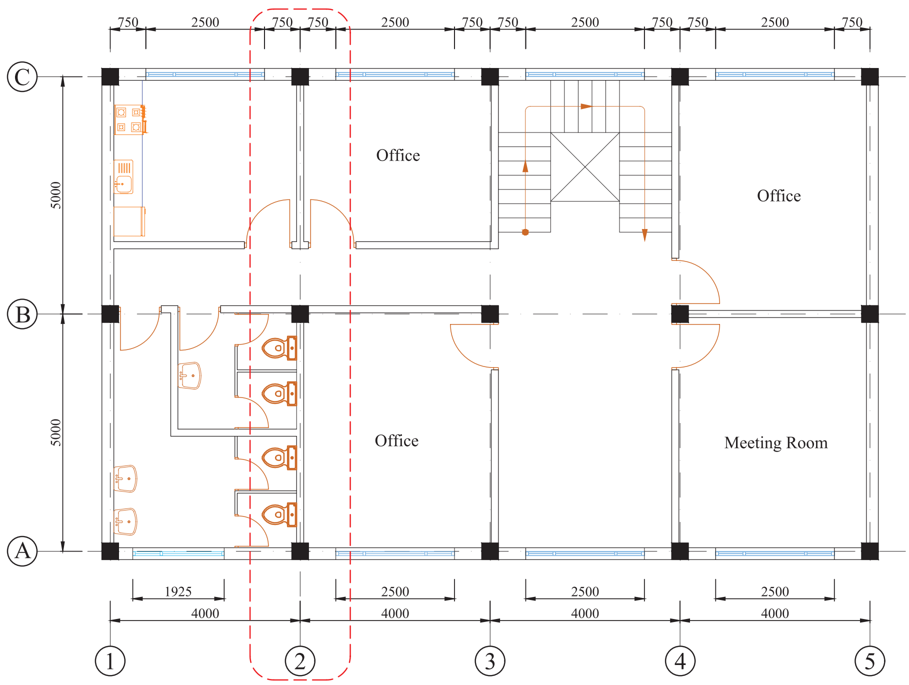

Figure 5.1. First floor plan for the 2-Story structures

In this study, an RC moment-resisting frame building is selected, and it is assumed that it is a commercial office building. The location of the structure is assumed to be in

San Francisco, USA. The building is assumed to be symmetric in both directions in the plan (see Figure 5.1). Therefore, only a 2D frame (see Figure 5.2) has been chosen for the design and assessment purposes. The resistance system of the building against horizontal earthquake forces is only these frames. The concrete used in this study is assumed to have a compressive strength of 25MPa and a modulus of elasticity of $3.1 \mathrm{x} 10^4$ MPa. Reinforcement is assumed to have yield strength of 420MPa, modulus of elasticity of $2 \mathrm{x} 10^5$ MPa, and ultimate tensile strength of 620MPa. The selected frame dimensions are shown in the following figure.

The OpenSees software has been utilized for modeling and analysis. Therefore, it is found necessary to give short information about the software and nonlinear modeling of the studied frame using numerical modeling concepts.

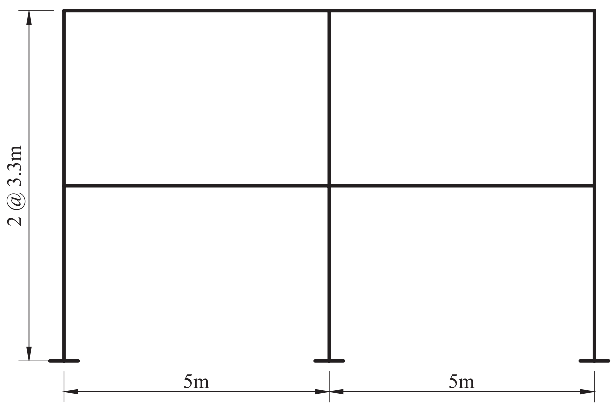

Figure 5.2. Dimensions for the selected 2D frame of 2-Story structures

5.1. Modeling of RC Frame in OpenSees

Open System for Earthquake Engineering Simulation (OpenSees) is an object-oriented, open-source software framework for simulation applications in earthquake engineering using finite element methods. It allows users to create both serial and parallel finite element computer applications for simulating the response of structural and geotechnical systems subjected to earthquakes and other hazards.

The framework of OpenSees for finite element application is given in the following figure:

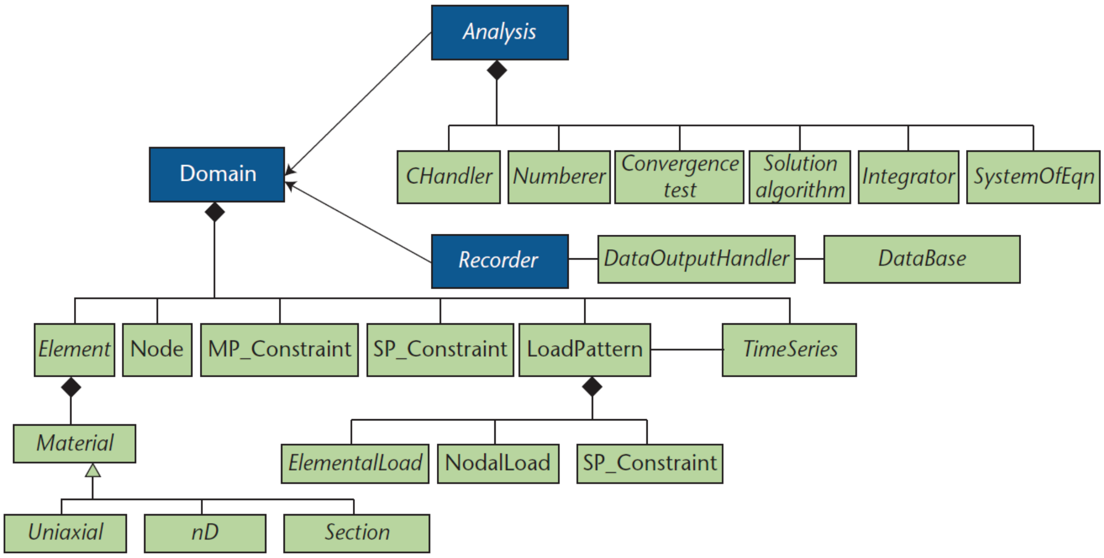

Figure 5.3. OpenSees framework for finite element application (Source: McKenna, 2011)

At first, a Model Builder is used to build the model, and then the objects are constructed in the model and added to the domain. The objects include the definition of nodes, elements, constraints, materials, etc. Second, the recorders are defined to record data from the output of the analysis. Finally, in the analysis part, the type of analysis, solution algorithm, integrator, etc., are defined.

The most important part is the numerical modeling of the elements and materials since several numerical models exist for modeling the behavior of both elements and materials. The accuracy and effectiveness of each numerical model depend on the assumption and/or simplifications (Sönmez, 2020).

5.1.1. Numerical Model for Element

For numerical modeling of elements, different methods exist, which use different types of nonlinear beam-column finite elements for performing numerical analysis. The load-deformation response of the members of a structural system is simulated using these methods. One of these methods is the finite element model, which is further divided into two parts. The first one is the distributed plasticity model, and the other one is the lumped plasticity model.

For modeling frames in this study, the distributed plasticity model is used for modeling the members of the frames, i.e., beams and columns. In this model, the plasticity is distributed over the length of the element. The distribution depends on the number of integration points used for the element. The popular distributed plasticity model, due to its accuracy, is the fiber-based element model. In this model, the cross-section of a member (element) at each integration point is divided into small fibers. Corresponding material types are assigned to each fiber. The nonlinear response at the section level is obtained by integrating the responses of fibers, and for the element as a whole, the nonlinear response is achieved by integrating the responses from the sections. The fiber-based model of an RC member is shown in Figure 5.4 with 5 integration points.

One of the advantages of the fiber-based model is that there is no need to carry out moment-curvature analysis for the section. Moreover, there is no need to consider any hysteretic rule for the section since the hysteretic behavior is directly taken from the cyclic behavior of material models. On the other hand, the disadvantage of the fiber-based model is that it ignores shear deformation; therefore, cyclic shear-flexure interaction is not considered.

In this study, the *forceBeamColumn* type of element has been used to model both beams and columns considering *FiberSection*.

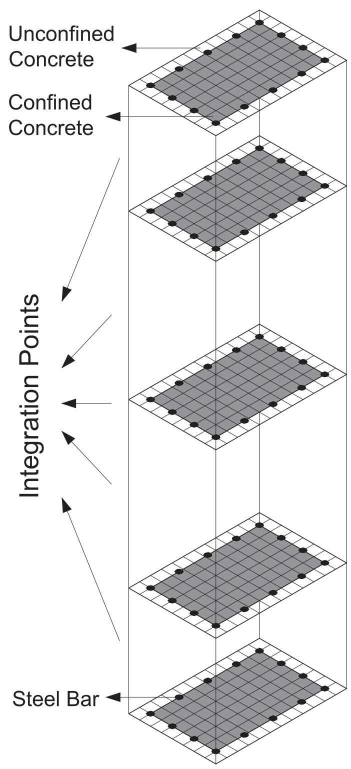

Figure 5.4. Fiber discretization of a typical confined RC member (Source: Sönmez, 2020)

5.1.2. Numerical Model for Materials

As mentioned earlier, several types of material models are available for numerical modeling of the materials in OpenSees. The models used in the analysis are expected to show the real behavior (monotonic and hysteretic) of the materials. RC members have confinement bars, in addition to longitudinal bars, to resist shear and torsional forces. To consider the effects of confinement in modeling, each section could be divided into confined and unconfined regions, and then the materials could be defined for each region separately. The capacity of unconfined concrete is considered as plain concrete, while confined concrete will have increased capacity due to confinements.

Various models exist for evaluating the stress-strain relationship of confined concrete, the most popular is the one developed by Mander et al. (1988), as shown in Figure 3.11. In this study, the *Concrete04* material type is used since it suits the Mander model pretty well compared to other types of materials provided in OpenSees. In this material type, compressive strength, its corresponding strain value, and ultimate strain are required; thus, the Mander model is used to obtain these parameters for confined concrete for all beams and columns.

Concrete04 material is based on Popovics' concrete material object (Popovics, 1973). The stiffness decreases linearly, according to the work of Karsan and Jirsa (Karsan & Jirsa, 1969). In addition, the tensile strength is decreasing exponentially. Figure 5.5a, adopted from https://opensees.berkeley.edu/ website, shows an example of the hysteretic response of the *Concrete04* material. A similar response, Figure 5.5b, has been achieved at the base of a column from a structure that has been modeled in OpenSees. The column has been modeled using a fiber-based element with 5 integration points, and the *Concrete04* material type is used to model concrete. While defining Concrete04 material in OpenSees, the compressive strength (f_c) and its corresponding strain (ε_c), ultimate strain (ε_{cu}) at crushing of concrete, tensile strength (f_{ct}) and its related strain (ε_{ct}), and the modulus of elasticity (E) values of concrete are required. The stress, denoted as β, which defines the exponential curve parameter at the ultimate tensile strain of concrete, is also required. For β, a value equal to 0.1 is recommended.

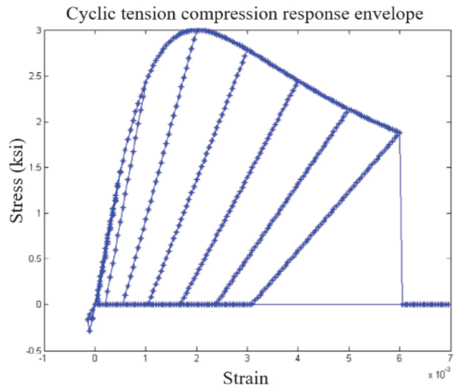

a) Example from website

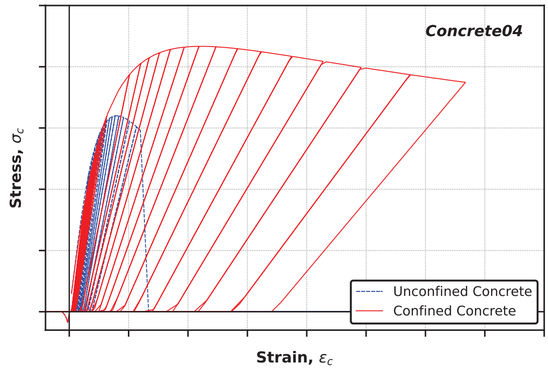

b) Example from a modeled structure

Figure 5.5. Hysteretic response of Concrete04

For steel reinforcement, the *steel02* material type has been considered. This material type uses the Giuffré-Menegotto-Pinto (Giuffrè, 1970; Menegotto & Pinto, 1973) uniaxial steel model, which considers strain hardening of the steel. Giuffré-Menegotto-Pinto is used for nonlinear modeling for RC members (Carreño et al., 2020). The parameters required for modeling reinforcement bars are yield strength (f_y), initial elastic tangent (E_0), Parameters (R_0, R_1, R_2) that control the transition from elastic to plastic branches, and strain hardening ratio (b). The recommended values for R_0 is between 10 and 20, while for R_1 and R_2 are 0.925 and 0.15, respectively. Moreover, the strain hardening ratio, which is ratio between post yield tangent and initial elastic tangent, is found from the stress-strain relation of the reinforcement bar. The response of *steel02* material used in the column modeling, mentioned in the previous paragraph, is shown in the following figure. It should be noted that the monotonic response of the material is taken from https://opensees.berkeley.edu/ website.

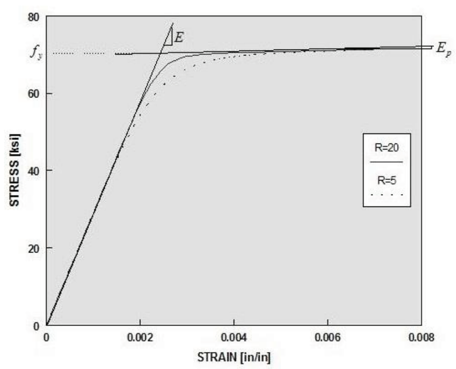

a) Monotonic

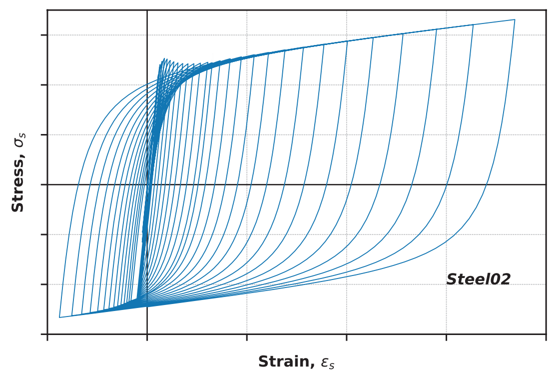

b) Hysteretic

Figure 5.6. Response of Steel02

5.1.3. Summary of Modeling in this Study

This section provides brief information on modeling the RC frame using the OpenSees framework for finite element application (Figure 5.3) in this study. For concrete, *Concrete04,* and for rebars, *Steel02* types of materials are used. For the cross-section of the members, the section type is chosen as *FiberSection*. Confined and unconfined regions of the cross-section of each member are modeled separately.

In addition, for elements, as mentioned, the *forceBeamColumn* type of element is used for columns with 5 integration points and for beams with 3 integration points. It is based on force-based formulation, in which only numerical integration error is involved. For integration, the *Lobatto* type of *beamIntegration* has been used since it is based on the Gauss-Labatto integration rule, which places the integration point at the end of elements where the response of the frame elements is more important (Neuenhofer & Filippou, 1997). Moreover, to account for the clear height of the columns and clear span of the beams, the rigid zones of the beam-column connections are modeled by using the *beam* type of *rigidlink*, which constraints the slave node with respect to the master node for both translational and rotational degrees of freedoms.

Furthermore, for beams *linear* while for columns, since second-order P-delta effects are more important, the *P-delta* type of geometric transformation is used. In both types of geometric transformations, element stiffness and resisting force are transformed from the basic system to the global coordinate system. However, P-delta effects are only considered in the *P-delta* type of geometric transformation.

For the application of loads on the frame, for gravity analysis, the loads are applied as concentrated and distributed loads considering the tributary area. Concentrated loads are applied at the top of columns, while distributed loads are applied on beams. The self-weight of the members is also applied as distributed loads for beams and columns as per unit length. For the dynamic analysis, since the masses are required, all masses are lumped at the upper nodes of the columns.

For the analysis part, the *BandGeneral* command is used for constructing a linear system of equations, which is usually used for matrix systems with the banded profile. To enforce constraint equations in the analysis, the *Transformation* method is used as the constraint handler type. In addition, for creating a map between equation numbers and degrees of freedom, an *RCM* numberer is used, which is based on the reverse Cuthill-

McKee scheme. Furthermore, for solving the nonlinear equation, the Newton-Raphson algorithm, one of the widely used algorithms, is used. As integrator type, for gravity analysis, LoadControl, for pushover analysis, DisplacementControl, and for time history analysis, the Newmark method is used.

To compare the results of the frame modeled by SAP2000 with the one modeled by OpenSees, the cross-sectional dimensions shown in Figure 5.7 are used. The frame is designed by using the DDBD approach, which is a PBSD approach. In addition, the strong column-weak beam concept has also been considered in the design of the frame. Furthermore, the LS performance level corresponding to the design earthquake level (i.e., earthquake hazard level with a 10% probability of exceedance in 50 years) has been considered for the design purpose.

The result of pushover analysis from the prepared model in OpenSees and the one obtained from SAP2000 v21 is shown in Figure 5.8. From the resulting curves, it can be observed that although the initial stiffness in the OpenSees model is higher than the SAP2000 model, the overall result matches fair enough. Some of the results are provided in the following table.

Table 5.1. Comparison of SAP2000 and OpenSees results

	SAP2000	**OpenSees**
First Mode period (sec)	0.4254	0.4133
Second Mode period (sec)	0.1464	0.1446
Base Shear Force (kN)	321.71	317.22

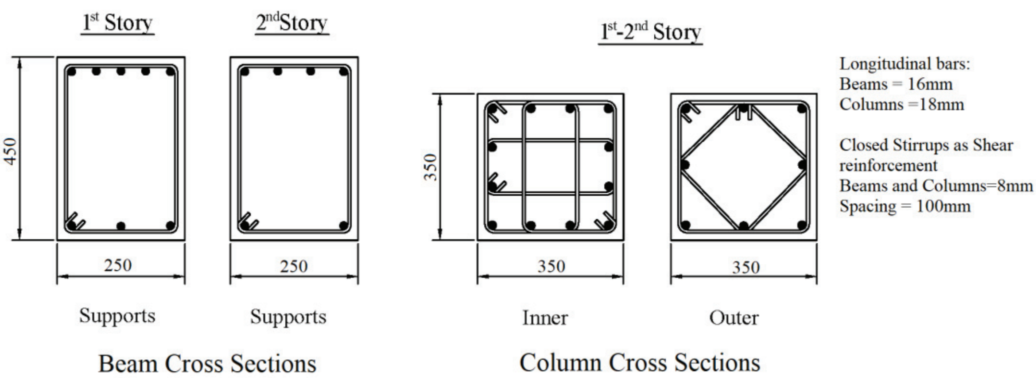

Figure 5.7. Cross-sectional dimensions of the members with reinforcement arrangement

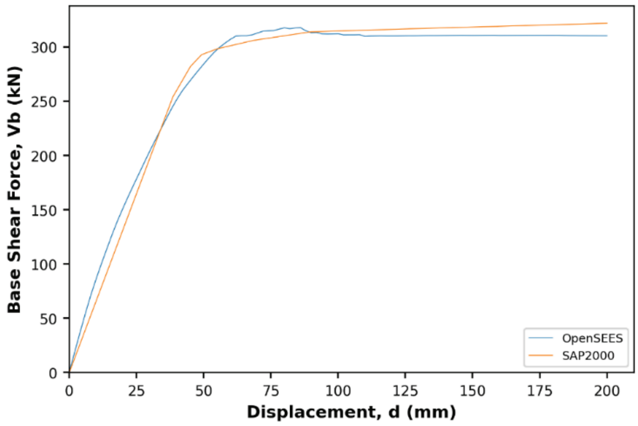

Figure 5.8. Pushover curves of the model obtained using OpenSees and SAP2000

5.2. Optimization Results

As discussed in section 4.3, the GA is used for optimization purposes. The population size was assumed to be 30, and the generation number was considered 100. The termination criteria are used only for the objective function (e.g., initial cost), and the tolerance is assumed to be 100$. As mentioned, the ET analysis method reduces the computational time significantly; thus, it was used in the optimization framework.

The initial cost of the structure is obtained in this study such that minimum cross-sectional sizes for beams and columns are considered with minimum reinforcement from the database (refer to section 4.6). The location of the structure is assumed to be in San Francisco, USA; thus, according to the ProEst website (https://proest.com/), the prices differ with respect to the number of stories. Here, for 2-Story structure, it is assumed that for a commercial office building, this cost is 3770$/m^2 for each story, and it is assumed for the minimum cross-sectional configuration according to the database. However, during the optimization process, the selected cross-sectional dimensions differ from the minimum ones. Thus, the extra amount of concrete volume and weight of reinforcement bars are estimated, and the additional cost of 250$/m^3 for concrete and 2$/Kg of reinforcement bars are used, both of which include the labor cost as well. It should be noted that the total area per floor of the structure is 160m^2.

The optimum solutions obtained through conventional code, the PBSD, and the PPBOSD approaches are given in the following figure for 2-story RC frames.

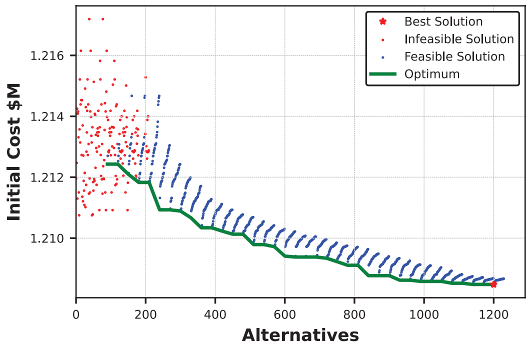

a) Code-Based

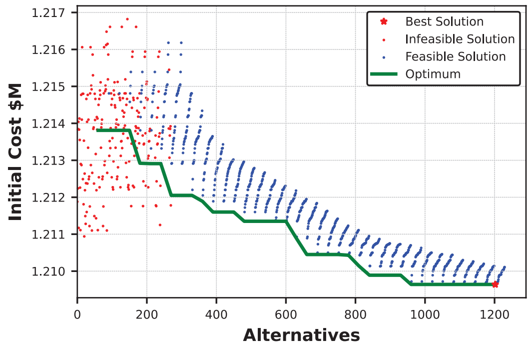

b) PBSD

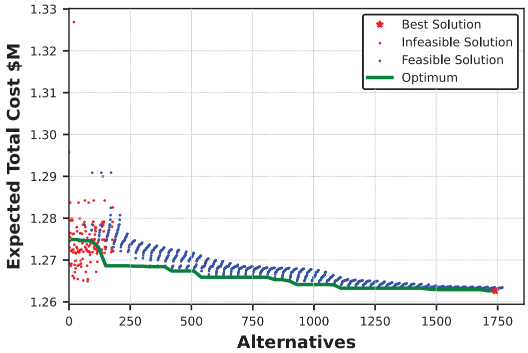

c) PPBOSD

Figure 5.9. Optimum solution for the 2-Story structures from different design approaches

The optimum initial cost value for the code-based design approach is 1.20848 $M (M denotes million), while for the PBSD approach, it equals 1.20964 $M. From the results, it could be observed that there is a very slight difference of 0.096%. On the other hand, the optimum value for the expected total cost through the PPBOSD approach is obtained as 1.26264 $M, in which the initial cost is 1.210504 $M. The difference between the initial cost of the structures designed using Code-Based design and the PPBOSD approaches is about 0.167%. As mentioned, the ET analysis method is used while evaluating LCC in the optimization process. Only the median demand could be obtained through the ET time analysis method. Therefore, the uncertainties, in terms of the logarithmic standard deviations, are obtained from the recommended values of Table 5-6 of FEMA-P-58-1 (2018). Only uncertainties related to record-to-record variabilities are considered, and in this study for the 2-Story RC structure, the logarithmic standard deviation is assumed to be 0.35. For the collapse fragility function, which is needed in the loss analysis, the recommended value of 0.6 is assumed for the logarithmic standard deviation.

The resulting cross-sectional dimensions and the configuration of reinforcement bars obtained through optimization are shown for all cases in Figure 5.10. The figure shows that the dimensions of the cross sections are the same for the first two cases; however, there are differences in reinforcement bar ratios and their configurations. While in the last case, the depth of the beams is larger.

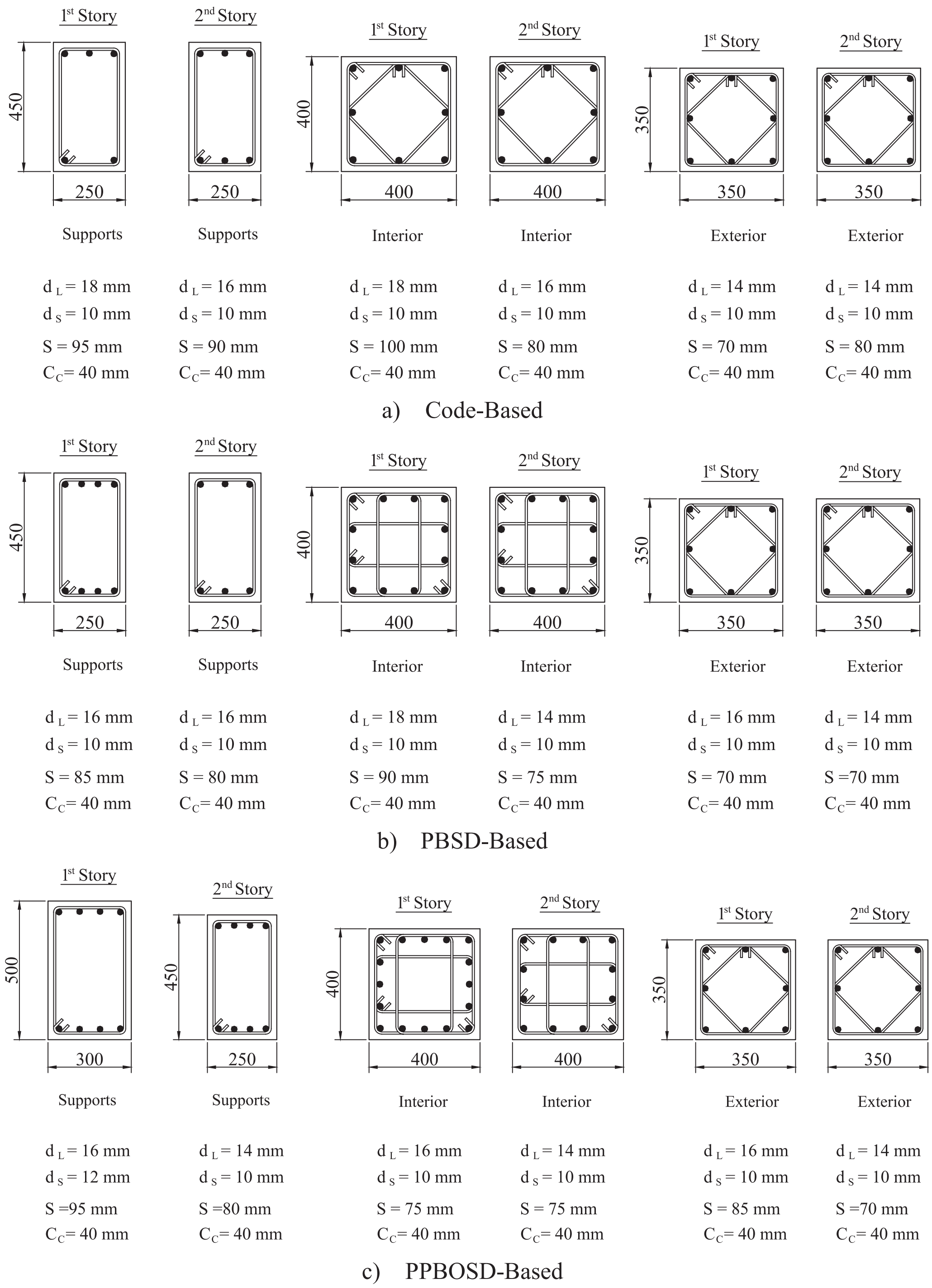

Figure 5.10. Optimum solution for the design variables of 2-Story structures

5.3. Performance Assessment Results

The performance of the structure is assessed using the PEER PBEE methodology, and the results are provided in this section. As IM value, spectral acceleration at the first natural period, $Sa(T_1)$, is used; therefore, the hazard curve related to $Sa(T_1)$, Figure 3.7, is utilized, while IDR and PFA are used as EDP. In the second step of the PEER PBEE methodology, the IDA method is implemented, for which NTHA is performed using FEMA-P695 far-field GM set. The results of each PEER PBEE methodology step are provided sequentially in the following sections.

5.3.1. Result of Probabilistic Demand Analysis

The IDA method is implemented, for which IM values are chosen in such a way as to cover the linear and nonlinear response of the structure until collapse occurs. The NTHAs are performed for each IM value, and the results are obtained for the peak IDRs.

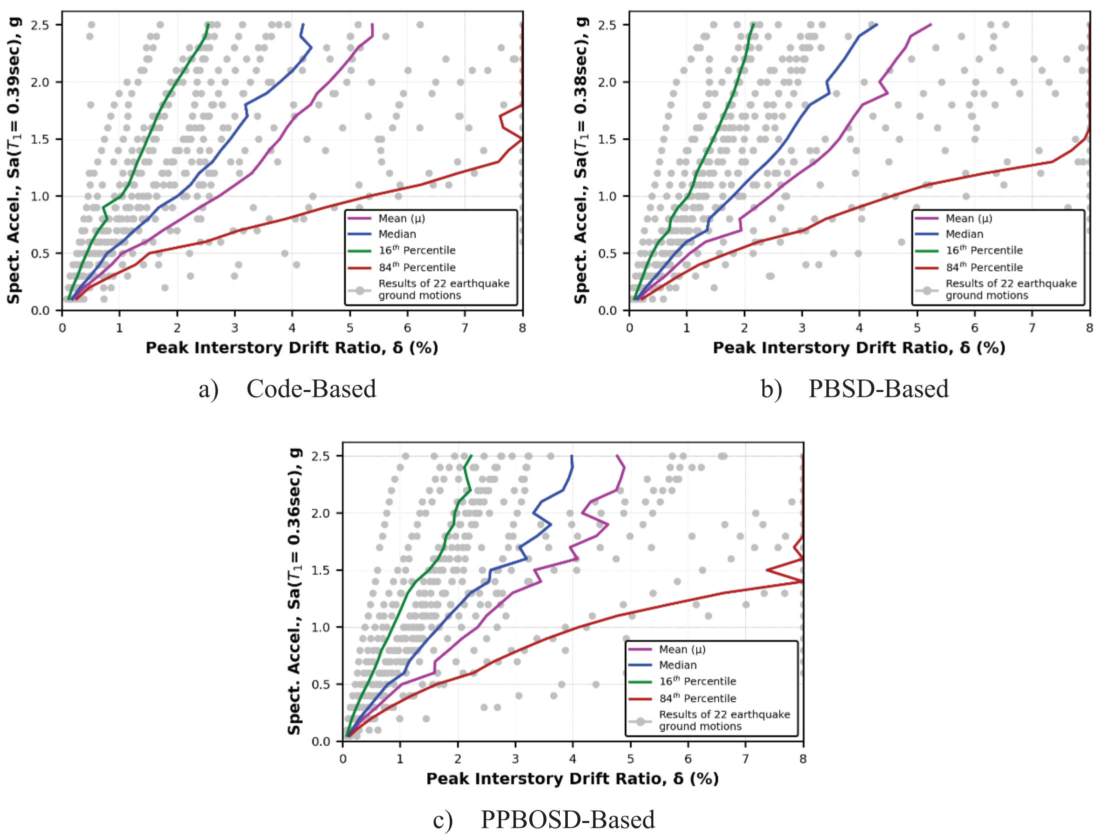

Figure 5.11. The IDA curves of 2-Story frames for the peak IDRs

For each IM level, 22-NTHA are performed, as mentioned. The Results of IDRs obtained from the IDA analysis are shown in Figure 5.11 for all three design approaches.

The results for some statistical parameters obtained using NTHA are tabulated in the following table, which corresponds to peak IDR (an EDP). For the prupose of comparison, these results are shown for three specific IM levels.

Table 5.2. Statistical parameters for IDRs of 2-Story frames at different IM levels

IM Level Sa (T_1)	**Peak Interstory Drift Ratio, IDR (%)**						
	Story #	$\mu_{ln(x)}$	μ_x	$\widehat{S}$	$\sigma_{ln(x)}$	**16th Percentile**	**84th Percentile**
Code-Based							
0.5	1	-0.1772	1.2932	0.8376	0.9320	0.3705	2.0245
	2	-0.2832	0.9940	0.7534	0.7446	0.4326	1.2082
1.0	1	0.7571	3.0638	2.1320	0.9320	0.9017	5.6588
	2	0.3928	1.9030	1.4811	0.7446	0.7912	2.5258
1.9	1	1.3110	4.6936	3.7098	0.6859	1.8385	8.0000
	2	0.9075	3.1174	2.4782	0.6774	1.3682	6.8269
PBSD-Based							
0.5	1	-0.3039	1.0158	0.7380	0.7994	0.3932	1.7195
	2	-0.3584	0.8413	0.6988	0.6091	0.3949	1.0565
1.0	1	0.5613	2.4422	1.7529	0.7994	0.9164	4.5559
	2	0.3516	1.7622	1.4213	0.6091	0.8807	2.3826
1.9	1	1.2060	4.4403	3.3402	0.7546	1.6000	8.0000
	2	0.8758	3.0161	2.4007	0.6756	1.4023	5.7162
PPBOSD-Based							
0.5	1	-0.3734	0.9546	0.6884	0.8086	0.3179	1.6318
	2	-0.3320	0.8724	0.7175	0.6253	0.4298	1.2316
1.0	1	0.5413	2.4370	1.7182	0.8086	0.8243	4.7741
	2	0.5080	2.1384	1.6620	0.6253	0.8964	3.2942
1.9	1	1.3165	4.7410	3.7301	0.6925	1.9355	8.0000
	2	1.2370	4.2950	3.4451	0.6641	1.7258	7.7188

The median, 16^{th} and 84^{th} percentile of the peak IDR and the resultant IDR from the 22 selected GM records are shown in Figure 5.12 for the same IM levels of Table 5.2. From the table and figure, it can be observed that, at the given lower, medium, and higher IM levels, all structures satisfied IO, LS, and CP performance levels except the structure designed using the Code-Based design approach, which has crossed the limit for LS performance level at the medium IM level. It should be noted that in Figure 5.12, the peak IDRs are shown for the last two IM levels for each design approach.

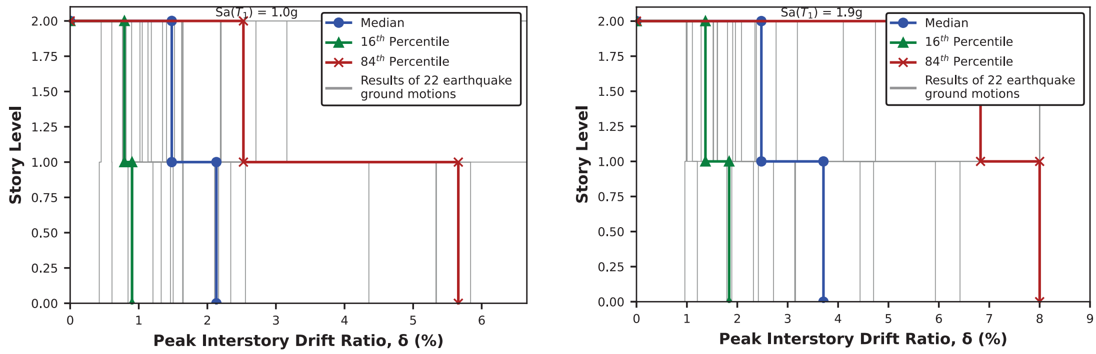

a) Code-Based

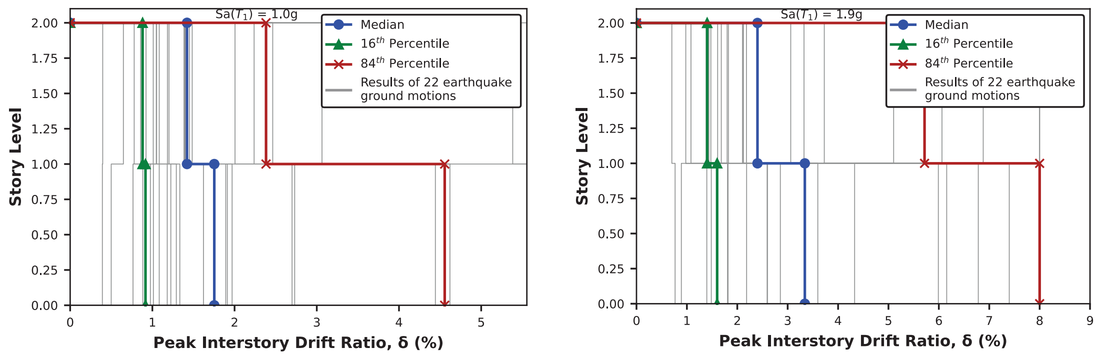

b) PBSD-Based

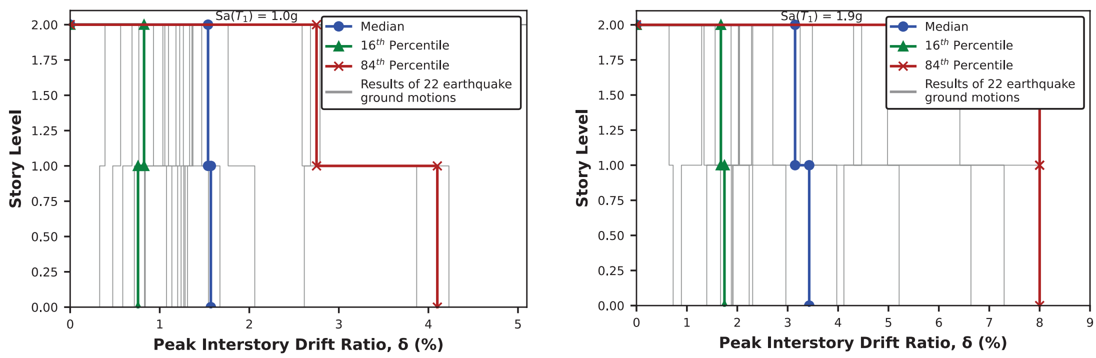

c) PPBOSD-Based

Figure 5.12. Peak IDRs for 2-Story frames corresponding to two different IM levels

From the literature, it is found that most researchers used equation (3.39), which is a linear relationship between the ln(EDP) and ln(IM) values, e.g. (Kim et al., 2020; Otsuki et al., 2019; Yakhchalian et al., 2019). Meanwhile, for fragility curves for each performance level, median demand and its related dispersion are required to be found; for this reason, it is necessary to apply the IDA method. The IDA method requires higher computation time; therefore, linear relationship between the ln(EDP) and ln(IM) is considered in this study. The results for the constants of equation (3.39) are tabulated in the following table for the 2-Story frame designed using three different design approaches. It should be noted that this table contains the constant values related to the median demand (i.e., median IDR).

Table 5.3. Constant values of equation (3.39) for the median peak IDR values of 2-Story frames

Story #	Code-Based		PBSD-Based		PPBOSD-Based	
	a	b	a	b	a	b
1	1.8875	1.0820	1.6343	1.0840	1.5942	1.0026
2	1.3319	0.9330	1.3038	0.9622	1.5018	1.0204
Maximum	1.9211	1.0712	1.7079	1.0709	1.7047	1.0075

In the above table, the maximum does not mean they are directly considered from the maximum of the two stories, i.e., they are not obtained from the maximum of, for example, the median values of the two stories. In contrast, they are obtained such that, first, the peak IDR of the two stories is obtained for each individual record at a specific IM level. Then, the mean, medians, and other statistical parameters are obtained from those maximum IDR values. After using linear relationship between ln(EDP) and ln(IM), the following statistical parameters are gained. Only the values corresponding to the maximum IDR are given in this table.

Table 5.4. IDRs of 2-Story frames corresponding to different IM levels after using linear relationship between ln(EDP) and ln(IM)

IM Level Sa (T_1)	Peak Interstory Drift Ratio, IDR (%)					
	$\mu_{ln(x)}$	μ_x	$\widehat{S}$	$\sigma_{ln(x)}$	16th Percentile	84th Percentile
Code-Based						
0.5	-0.0896	1.3572	0.9143	0.8889	0.4861	1.9155
1.0	0.6529	2.7330	1.9211	0.8396	0.9890	4.2265
1.9	1.3404	4.8225	3.8207	0.6824	1.9090	8.7954
PBSD-Based						
0.5	-0.2071	1.0708	0.8129	0.7423	0.4417	1.7607
1.0	0.5352	2.3244	1.7079	0.7851	0.9135	3.9525
1.9	1.2226	4.3854	3.3961	0.7150	1.7901	8.3576
PPBOSD-Based						
0.5	-0.1649	1.1152	0.8480	0.7402	0.4743	1.7121
1.0	0.5334	2.3898	1.7048	0.8219	0.9290	3.8237
1.9	1.1801	4.1711	3.2547	0.7044	1.7315	8.0467

The PDF and CDF for the IM levels are obtained using equations (3.36) and (3.37), respectively, and shown in the following figures only for the peak IDR.

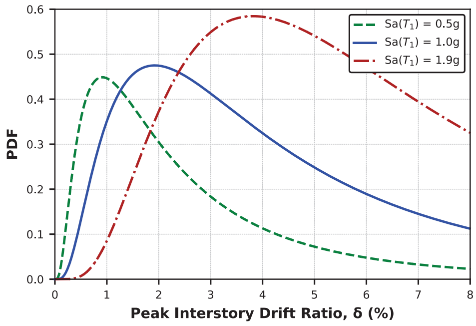

a) Code-Based

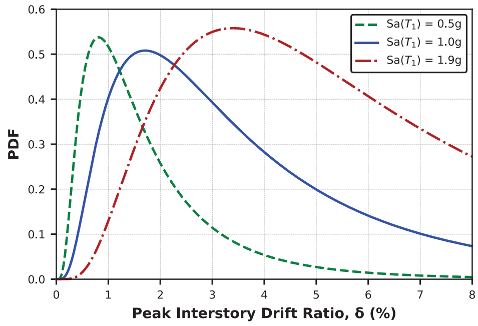

b) PBSD-Based

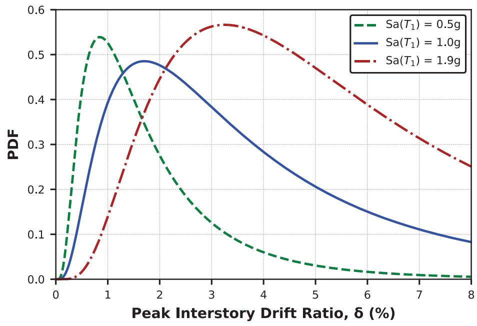

c) PPBOSD-Based

Figure 5.13. Probability density functions for peak IDRs of 2-Story frames at different IM levels

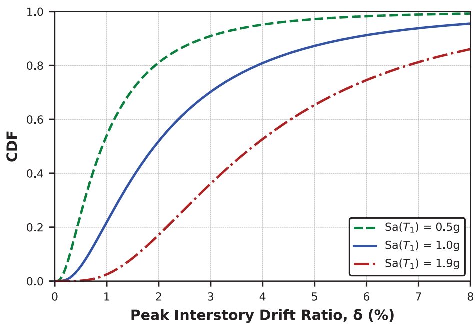

a) Code-Based

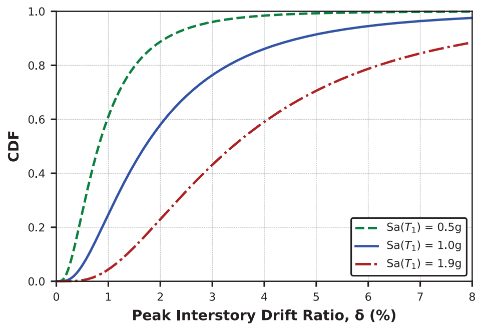

b) PBSD-Based

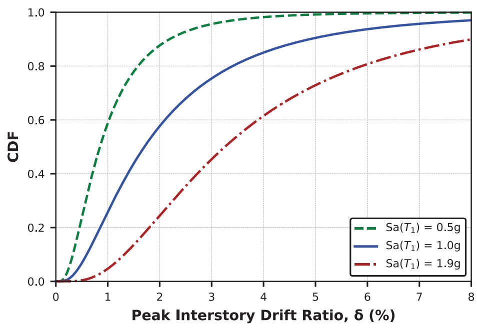

c) PPBOSD-Based

Figure 5.14. Cumulative distribution functions for peak IDRs of 2-Story frames at different IM levels

In addition, in Figure 5.15, the probability of exceedance ($P\,[EDP > edp|IM = im]$) curves together with drift limits are shown. These drift limits are 1%, 2%, and 4%, which correspond to IO, LS, and CP performance levels, respectively. The drift limits for these performance levels are adopted from FEMA-356 (2000). From the figure, it can be concluded that the worst performance is shown by the structure designed using the Code-Based design approach. However, at the high-intensity level, the structure designed by the PPBOSD approach is better, and at the lower intensity, it is very close to the ones designed by the PBSD approach.

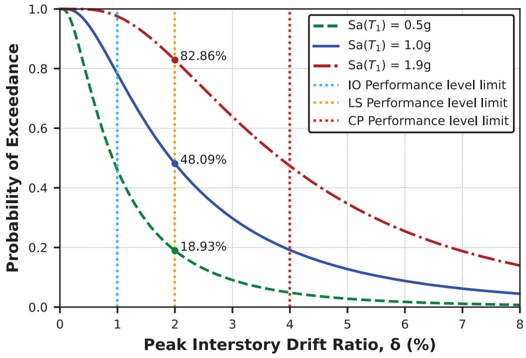

a) Code-Based

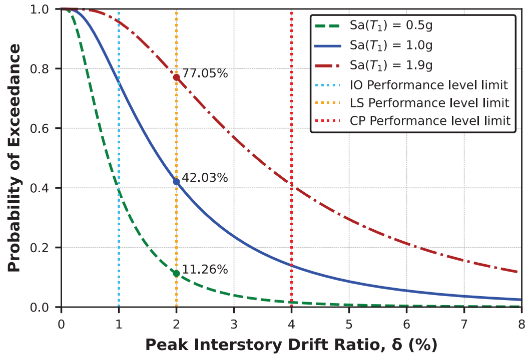

b) PBSD-Based

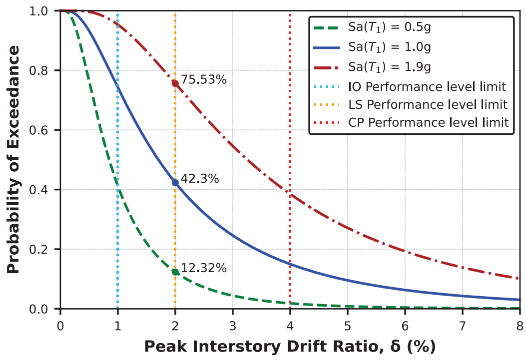

c) PPBOSD-Based

Figure 5.15. Probability of exceedance for peak IDRs of 2-Story frames at different IM levels

The hazard curves related to spectral acceleration at the first natural period, i.e., $Sa(T_1)$, are used in this study. Equation (3.30) is solved in discrete form rather than continuous form. The demand hazard curves for all cases are shown in the following figure. In the figure, the comparison of the median demand hazard curves is also shown. From the comparison, it can be concluded the structure designed using the Code-Based design approach has the worst performance; in contrast, the ones designed by the other two methods almost showed similar performance.

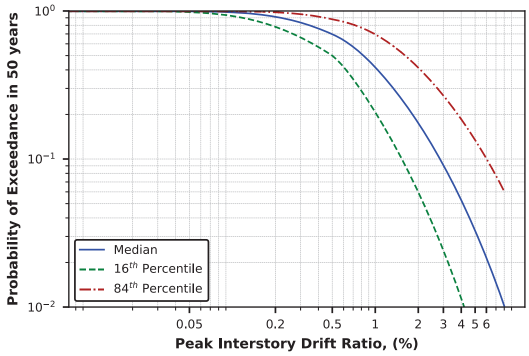

a) Code-Based

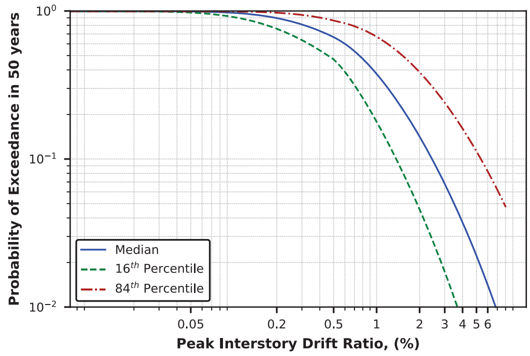

b) PBSD-Based

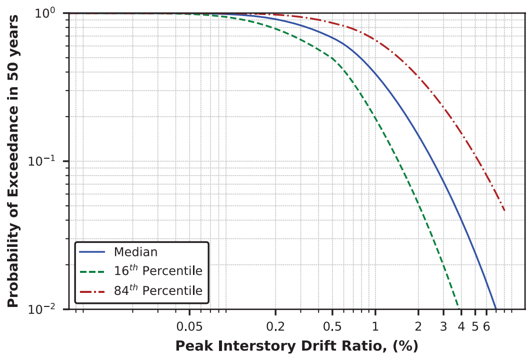

c) PPBOSD-Based

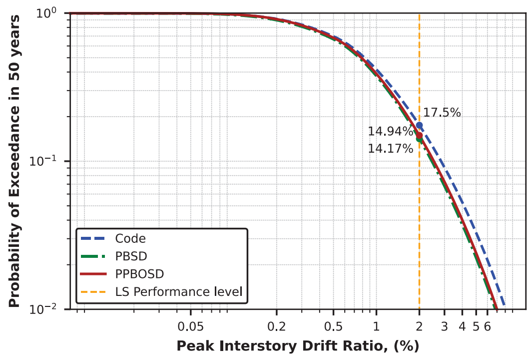

d) Comparison of median demand hazard curves

Figure 5.16. Demand hazard curves for 2-Story frames

The designed structures are also analyzed using the ET method under the ETA40lc series of ETEFs. The result of the ET analysis method is shown in terms of the so-called ET response curve. This curve could be in terms of EDP and ET time or EDP and IM values. Figure 5.17 shows the ET response curves for the 2-Story RC structure in both formats. It is a fact that each structure has its unique natural fundamental period, and as shown in Figure 3.18, with a change in the fundamental period, the ET time also changes for different IM levels. In addition, it is not appropriate to show the ET response curves of all three structures in the same figure together with the IDR limits given in ASCE/SEI-41-17 (2017) for different performance levels, which correspond to different IM levels. Therefore, they are separately shown in Figure 5.18. The figure clearly indicates that the structure designed using the Code-Based design approach does not meet the LS and CP performance levels. In contrast, the structures designed using the PBSD and the PPBOSD approaches satisfied all performance levels.

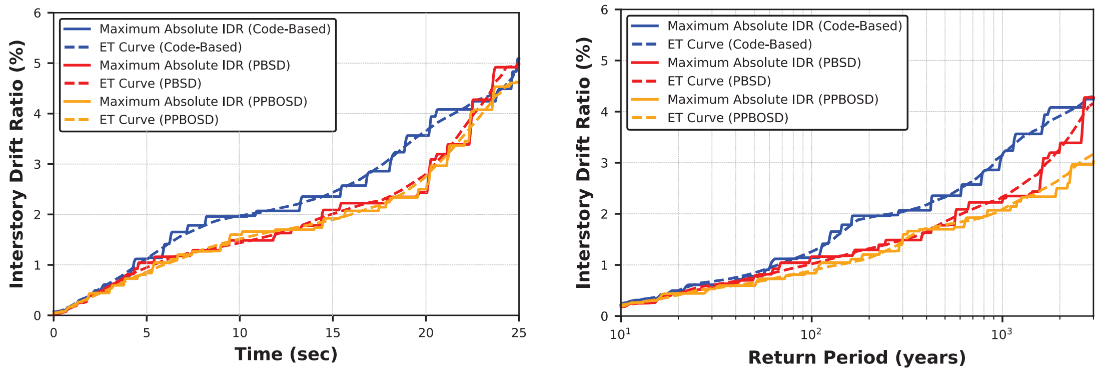

a) IDR vs ET time b) IDR vs Return Period

Figure 5.17. ET response curves of the 2-Story frames

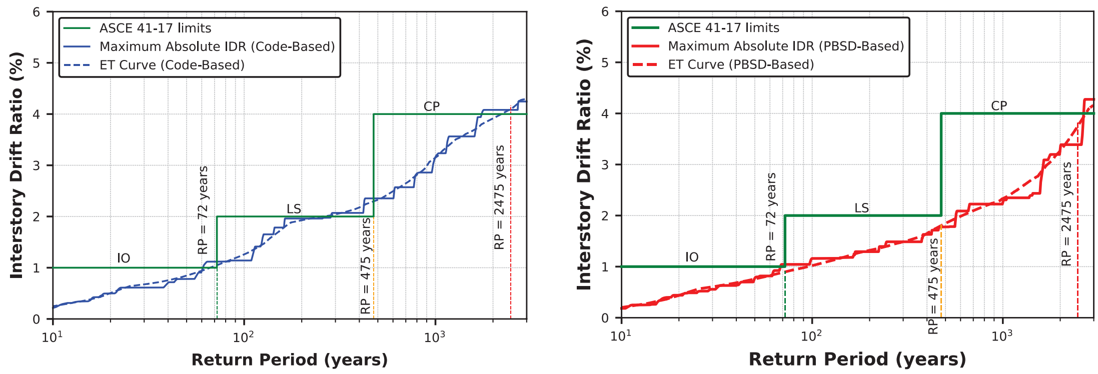

a) Code-Based b) PBSD-Based

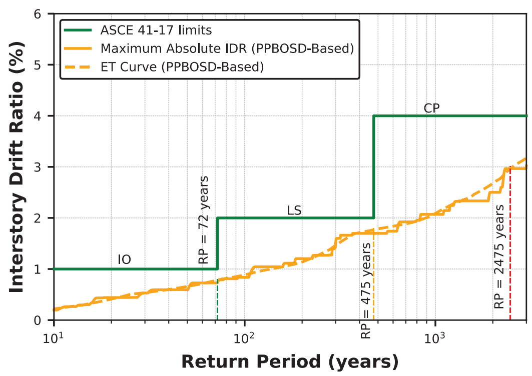

c) PPBOSD-Based

Figure 5.18. ET response curves of 2-Story frames with IDR limits for different hazard levels

5.3.2. Result of Probabilistic Damage Analysis

In section 3.4.1, it is discussed that estimation of the DM levels requires the development of fragility functions. The median demand value for a performance level corresponds to a demand value at which there is a 50% chance that the associated performance level initiates. Using this procedure, the resulting fitted fragility parameters in terms of the $Sa(T_1)$ are provided in the following table, and the related fragility functions are shown in Figure 5.19.

Table 5.5. Statistical parameters for fitted fragility curves of 2-Story frames

Performance Level	**Code-Based**		**PBSD-Based**		**PPBOSD-Based**	
	$\hat{S}$	$\sigma_{ln(x)}$	$\hat{S}$	$\sigma_{ln(x)}$	$\hat{S}$	$\sigma_{ln(x)}$
IO	0.5436	0.7602	0.6067	0.7969	0.5889	0.8080
LS	1.0383	0.7754	1.1589	0.7221	1.1718	0.7182
CP	1.9831	0.6367	2.2137	0.5866	2.3315	0.5534

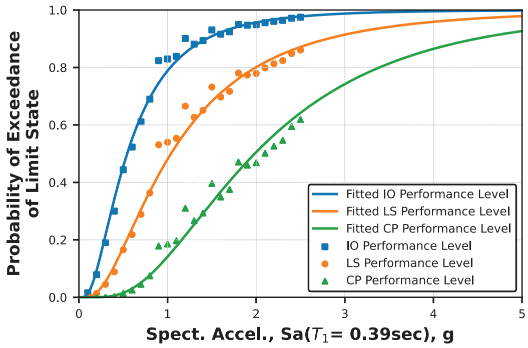

a) Code-Based

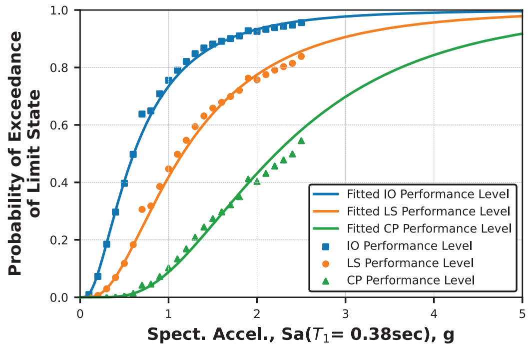

b) PBSD-Based

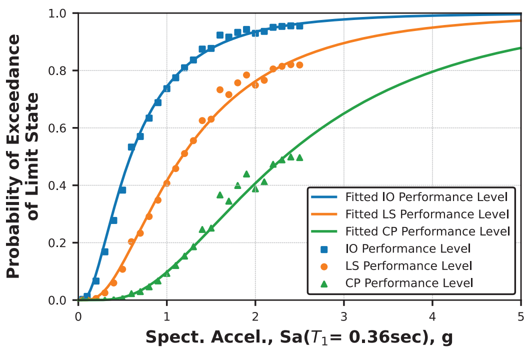

c) PPBOSD-Based

Figure 5.19. Fragility curves of 2-Story frames for different performance levels

The comparison of the fragility curves is shown in Figure 5.20. From this figure, it can be concluded that the structure designed with the conventional Code-Based design is the most vulnerable, while the one designed with the PPBOSD approach is the least vulnerable.

As shown in Figure 3.14, component fragility functions are required for loss estimation, and section 3.4.3 provides brief information regarding the FEMA-P58 fragility database. Thus, in this study, the selected components are tabulated in Table 5.6. For the structural elements, the demand parameters are IDR, while for non-structural components and content systems, the demand parameters could be IDR or PFA.

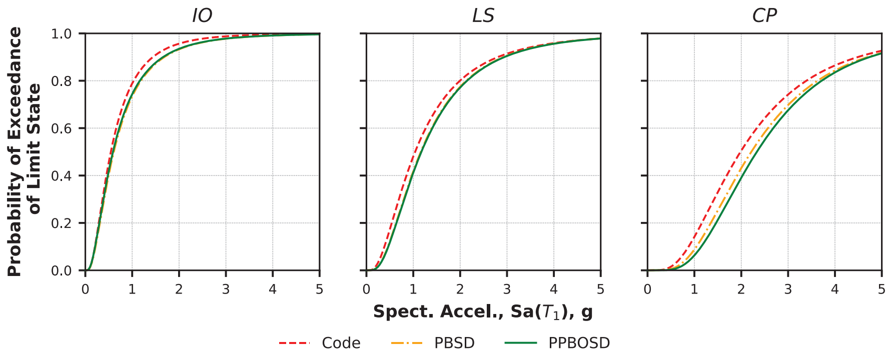

Figure 5.20. Comparison of fragility curves of 2-Story frames

Table 5.6. Selected components from FEMA P 58 database

Sheet Name	Component ID	Demand Parameter	Component Name
D3031.011a	423	PFA	Chiller - Capacity: < 100 Ton - Unanchored equipment that is not vibration isolated - Equipment fragility only.
D5012.013a	600	PFA	Motor Control Center - Capacity: all - Unanchored equipment that is not vibration isolated - Equipment.
D5012.021a	604	PFA	Low Voltage Switchgear - Capacity: 100 to <350 Amp - Unanchored equipment that is not vibration isolated- Equipment fragility only
B1041.001a	102	IDR	ACI 318 SMF , Conc Col & Bm = 24 x 24", Beam one side"
B1041.001b	103	IDR	ACI 318 SMF , Conc Col & Bm = 24 x 24", Beam both sides"
B1051.001	252	IDR	Ordinary reinforced masonry walls with partially grouted cells, shear dominated, 4 to 6"' thick, up to 12 foot tall"
B1051.011	256	IDR	Ordinary reinforced masonry walls with partially grouted cells, shear dominated, 8 to 12"' thick, up to 12 foot tall"
C1011.001a	356	IDR	Wall Partition, Type: Gypsum with metal studs, Full Height, Fixed Below, Fixed Above
C3021.001a	383	IDR	Generic Floor Covering - Flooding of floor caused by failure of pipe - Office - Dry
C3032.001a	401	IDR	Suspended Ceiling, SDC A,B,C, Area (A): A < 250, Vert support only
C3034.002	413	IDR	Independent Pendant Lighting - non seismic
D3041.011a	515	PFA	HVAC Galvanized Sheet Metal Ducting less than 6 sq. ft in cross sectional area, SDC A or B
D3041.031a	532	PFA	HVAC Drops / Diffusers in suspended ceilings - No independent safety wires, SDC C
D3041.041a	537	PFA	Variable Air Volume (VAV) box with in-line coil, SDC A or B
D2021.011a	700	PFA	Cold or Hot Potable - Small Diameter Threaded Steel - (2.5 inches in diameter or less), SDC A or B, PIPING FRAGILITY
D2022.011a	714	PFA	Heating hot Water Piping - Small Diameter Threaded Steel - (2.5 inches in diameter or less), SDC A or B, PIPING FRAGILITY
D2031.011b	728	PFA	Sanitary Waste Piping - Cast Iron w/flexible couplings, SDC A,B, BRACING FRAGILITY
B3011.012	346	PFA	Clay tile roof, tiles secured and compliant with UBC94
D1014.011	415	PFA	Traction Elevator – Applies to most California Installations 1976 or later, most western states installations
D3031.021a	451	PFA	Cooling Tower - Capacity: < 100 Ton - Unanchored equipment that is not vibration isolated - Equipment fragility only
D3052.011a	546	PFA	Air Handling Unit - Capacity: <5000 CFM - Unanchored equipment that is not vibration isolated - Equipment

Statistical parameters for the fragility functions of the selected components are provided in Table 5.7. Some of these elements have only one damage state, while some have four damage states. The fragility curves for only four of the chosen components are shown in Figure 5.21.

Table 5.7. Statistical parameters for component fragility curves

Sheet Name	DS1		DS2		DS3		DS4	
	$\hat{S}_c$	β_{S_c}	$\hat{S}_c$	β_{S_c}	$\hat{S}_c$	β_{S_c}	$\hat{S}_c$	β_{S_c}
D3031.011a	0.2	0.4	0	0	0	0	0	0
D5012.013a	0.73	0.45	0	0	0	0	0	0
D5012.021a	1.28	0.4	0	0	0	0	0	0
B1041.001a	0.02	0.4	0.0275	0.3	0.05	0.3	0.05	0.3
B1041.001b	0.02	0.4	0.0275	0.3	0.05	0.3	0.05	0.3
B1051.001	0.002	0.86	0.0033	0.77	0	0	0	0
B1051.011	0.002	0.86	0.0033	0.77	0	0	0	0
C1011.001a	0.005	0.4	0.01	0.3	0.021	0.2	0	0
C3021.001a	0.75	0.4	0	0	0	0	0	0
C3032.001a	1.17	0.25	1.58	0.25	1.82	0.25	0	0
C3034.002	1.5	0.4	0	0	0	0	0	0
D3041.011a	1.5	0.4	2.25	0.4	0	0	0	0
D3041.031a	1.3	0.4	0	0	0	0	0	0
D3041.041a	1.9	0.4	0	0	0	0	0	0
D2021.011a	1.5	0.4	2.6	0.4	0	0	0	0
D2022.011a	0.55	0.5	1.1	0.5	0	0	0	0
D2031.011b	1.2	0.5	2.4	0.5	0	0	0	0
B3011.012	1.4	0.3	1.7	0.3	0	0	0	0
D1014.011	0.39	0.45	0.39	0.45	0.39	0.45	0.39	0.45
D3031.021a	0.5	0.4	0	0	0	0	0	0
D3052.011a	0.25	0.4	0.25	0.4	0	0	0	0

The probability of being in a damage state is only shown for component C1011.001a in Figure 5.22.

After the DZs are obtained, then equation (3.43) is solved, and the probability of DM values for different limit states in 50 years is obtained for mean, median, 16th percentile, and 84th percentile. It should be noted that, in equation (3.43), the probability of being in each damage state has been used instead of directly using fragility functions because it is useful for loss analysis (Zareian & H., 2009). The values are tabulated in Table 5.8 for the 2-story frames designed using three different design approaches.

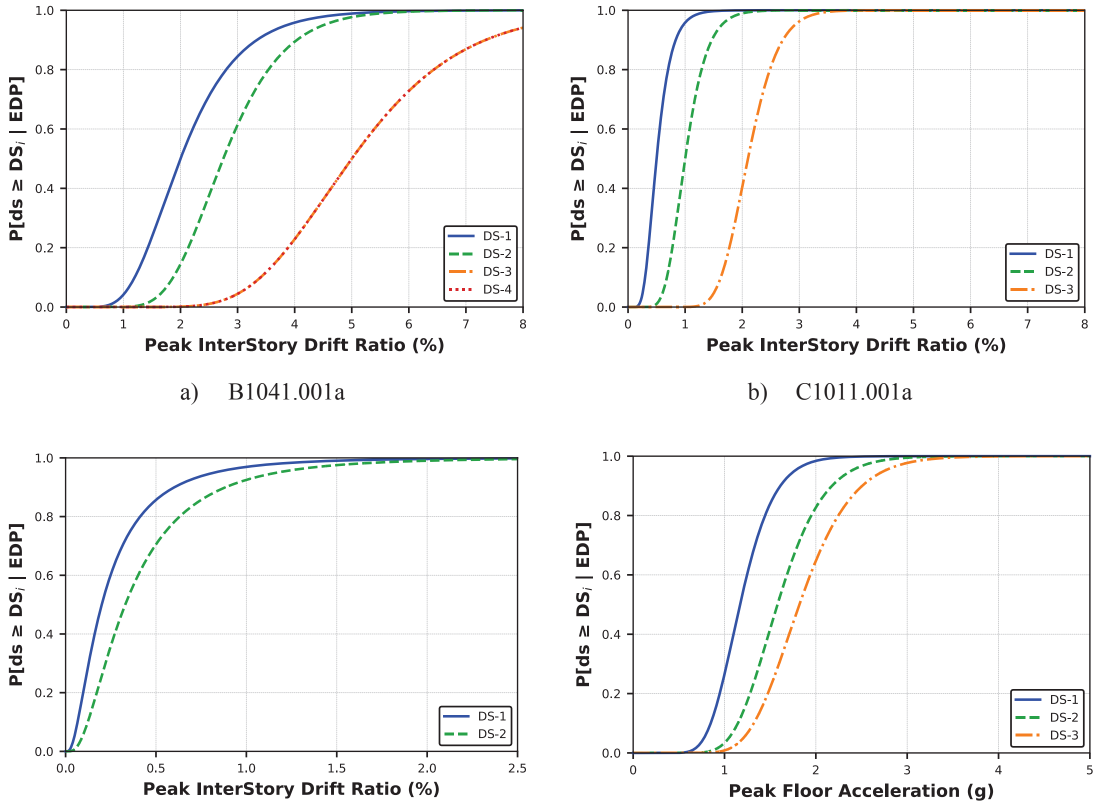

a) B1041.001a

b) C1011.001a

c) B1051.001

d) C3032.001a

Figure 5.21. Component fragility curves

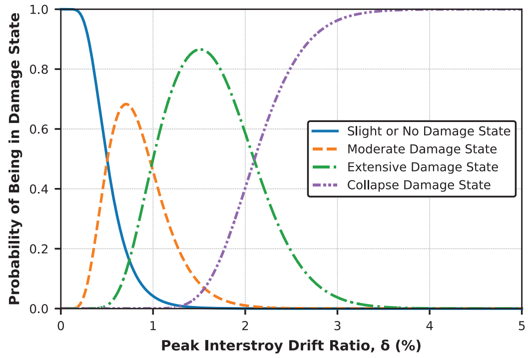

Figure 5.22. Probability of being in damage state for component C1011.001a

Table 5.8. Probability of damage measure for Component C1011.001a of 2-Story frames

Damage State	Mean Rate of Exceedance in 50 years			Return Periods (years)		
	50th Percentile	16th Percentile	84th Percentile	50th Percentile	16th Percentile	84th Percentile
Code-Based						
Slight or No	0.3133	0.5108	0.1291	134	70	362
Moderate	0.2589	0.2608	0.1795	167	166	253
Extensive	0.2551	0.1661	0.2884	170	276	147
Collapse	0.1583	0.0569	0.3384	291	854	122
PBSD-Based						
Slight or No	0.3446	0.5395	0.1455	119	65	318
Moderate	0.2665	0.2591	0.1869	162	167	242
Extensive	0.2481	0.1525	0.2924	176	303	145
Collapse	0.1303	0.0440	0.3233	359	1112	129
PPBOSD-Based						
Slight or No	0.3321	0.5196	0.1531	124	69	301
Moderate	0.2687	0.2661	0.1953	160	162	231
Extensive	0.2541	0.1630	0.2939	171	282	144
Collapse	0.1372	0.0494	0.3099	339	987	135

5.3.3. Result of Probabilistic Loss Analysis

In this section, the results obtained through PLA are provided. For this purpose, the flowchart shown in Figure 3.14 was used. To calculate expected losses due to collapse and demolition, building replacement and demolition costs are required, which are given in terms of per square meter. In this study, according to the assumed location of the structure and its occupancy type, replacement cost is assumed as 3770\$/m^{2,} and for demolition, 86\$/m^2 is assumed. The structure is assumed to have 4 bays of 4m wide each (total of 16m) out of the plan of the considered frame, and the costs are given for each story, thus:

$$A_{total} = 10x16 = 160m^2$$

$$\Rightarrow \quad C_{replace} = 3770x160x2 = 1206400\$ = 1.2064M\$$$ Replacement cost in millions \$

$$\Rightarrow \quad C_{Demolition} = 86x160x2 = 27520\$ = 0.02752M\$$$ Demolition cost in millions \$

To calculate the total repair loss of the structure, repair losses should be calculated at each story, which is based on the loss curves and consequence functions of the structural and nonstructural components and content systems provided in the FEMA P-58_FragilityDatabase_v3.1.2. Statistical parameters for repair costs and repair times of the selected components are provided in Table 5.9 and Table 5.10, respectively. These parameters are in terms of the median and Coefficient of Variation (COV).

Table 5.9. Statistical parameters for component repair cost

Sheet Name	DS1		DS2		DS3		DS4	
	$\hat{S}_c$	COV	$\hat{S}_c$	COV	$\hat{S}_c$	COV	$\hat{S}_c$	COV
D3031.011a	46200	0.1785	0	0	0	0	0	0
D5012.013a	4150	0.1826	0	0	0	0	0	0
D5012.021a	9275	0.1572	0	0	0	0	0	0
B1041.001a	21420	0.3909	32482	0.3183	39982	0.3024	32482	0.3183
B1041.001b	21420	0.3909	32482	0.3183	39982	0.3024	32482	0.3183
B1051.001	4200	0.1050	6000	0.1413	0	0	0	0
B1051.011	4350	0.1014	7633	0.1396	0	0	0	0
C1011.001a	1785	0.4814	4550	0.5559	8750	0.1959	0	0
C3021.001a	31.04	0.2850	0	0	0	0	0	0
C3032.001a	362.5	0.5508	2837.5	0.5183	5837.5	0.2026	0	0
C3034.002	495	0.6369	0	0	0	0	0	0
D3041.011a	650	0.3674	6350	0.1002	0	0	0	0
D3041.031a	3000	0.2066	0	0	0	0	0	0
D3041.041a	15000	0.2942	0	0	0	0	0	0
D2021.011a	290	0.7637	2650	0.4054	0	0	0	0
D2022.011a	290	0.7637	2650	0.4054	0	0	0	0
D2031.011b	400	0.5758	2850	0.3401	0	0	0	0
B3011.012	1025	0.4803	2000	0.3692	0	0	0	0
D1014.011	4400	0.8741	18700	0.2776	16000	0.4083	2500	0.4877
D3031.021a	23700	0.1720	0	0	0	0	0	0
D3052.011a	1000	0.1511	29200	0.1655	0	0	0	0

Table 5.10. Statistical parameters for component repair time

Sheet Name	DS1		DS2		DS3		DS4	
	$\hat{S}_c$	COV	$\hat{S}_c$	COV	$\hat{S}_c$	COV	$\hat{S}_c$	COV
D3031.011a	9.5118	0.3072	0	0	0	0	0	0
D5012.013a	1.4647	0.3096	0	0	0	0	0	0
D5012.021a	2.1824	0.2953	0	0	0	0	0	0
B1041.001a	18.9000	0.4640	28.6606	0.4048	35.2782	0.3924	28.6606	0.4048
B1041.001b	18.9000	0.4640	28.6606	0.4048	35.2782	0.3924	28.6606	0.4048
B1051.001	3.2700	0.2712	4.6800	0.2871	0	0	0	0
B1051.011	3.3900	0.2698	5.9500	0.2863	0	0	0	0
C1011.001a	1.4300	0.5424	3.5100	0.6095	6.7600	0.3176	0	0
C3021.001a	0.0288	0.3791	0	0	0	0	0	0
C3032.001a	0.3500	0.6049	2.7	0.5755	5.5750	0.3218	0	0
C3034.002	0.4950	0.6842	0	0	0	0	0	0
D3041.011a	0.7647	0.4444	2.2412	0.2693	0	0	0	0
D3041.031a	3.5290	0.3243	0	0	0	0	0	0
D3041.041a	17.6470	0.3860	0	0	0	0	0	0
D2021.011a	0.3071	0.8036	0.2806	0.4763	0	0	0	0
D2022.011a	0.3071	0.8036	0.2806	0.4763	0	0	0	0
D2031.011b	0.4235	0.6277	3.0176	0.4221	0	0	0	0
B3011.012	1.1300	0.5415	2.2100	0.4459	0	0	0	0
D1014.011	4.2059	0.9091	17.8750	0.3735	15.2941	0.4788	2.3897	0.5480
D3031.021a	5.5765	0.3034	0	0	0	0	0	0
D3052.011a	0.3529	0.2921	6.8706	0.2998	0	0	0	0

The units of measure for median values provided are different for the different types of components. For example, for component B1041.001a, the median values are given per 1 unit; for C1011.001a, it is given per 30.48m (100ft) length, while for B1051.001 and C3032.001a, they are per 9.29m^2 (100ft^2) and 23.23m2 (250ft2), respectively. The repair cost not only includes the repair cost of the component itself it also includes all the steps that are required to conduct a repair. For example, removal or protection of contents adjacent to the damaged area, protection of the surrounding area temporarily, and removal of architectural, mechanical, electrical, and plumbing systems that are necessary to remove while performing repair operations.

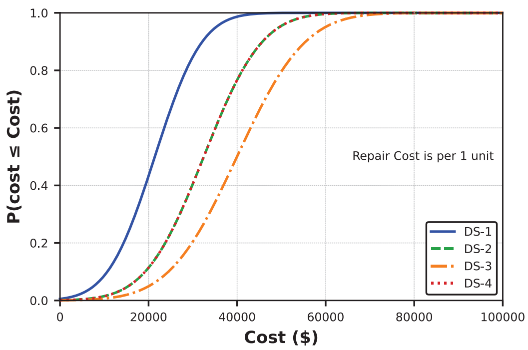

a) B1041.001a

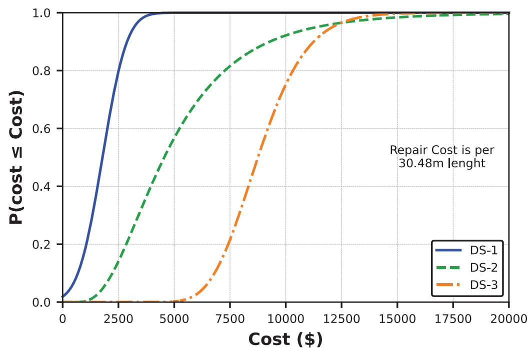

b) C1011.001a

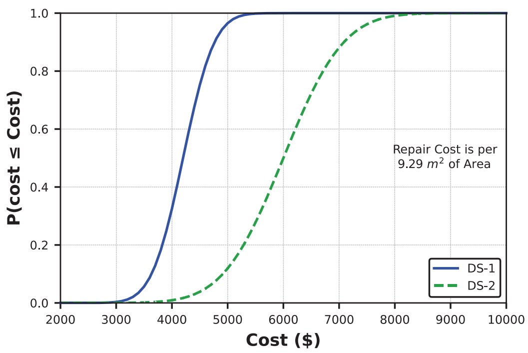

c) B1051.001

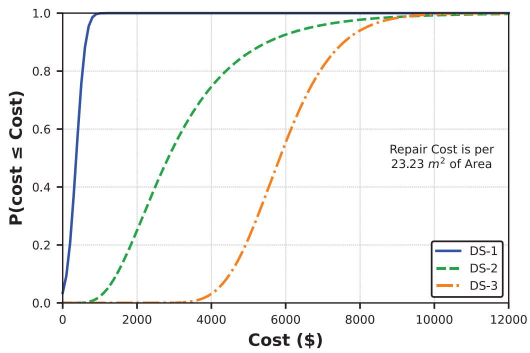

d) C3032.001a

Figure 5.23. Component repair cost curves

Table 5.11 and Table 5.12 show the consequence function of repair costs and repair times for some of the selected components.

For the repair cost consequence functions, the same units of measure are used as explained for the loss curves for different component types. For construction operations, repair cost consequence functions consider economies of scale and efficiencies. For example, contractor mobilization, demobilization, and overhead costs spread over a larger volume of work of the same type, which results in a reduction in repair costs (FEMA-P-58-1, 2018).

Table 5.11. Consequence function parameters for the repair cost

Sheet Name		B1041.001a	C1011.001a	B1051.001	C3032.001a
DS1	Lower Quantity Cutoff	5	1	2	1
	Maximum Cost Mean ($)	25704	2677.5	5040	435
	Upper Quantity Cutoff	20	10	30	10
	Minimum Cost Mean ($)	17136	1428	3360	290
DS2	Lower Quantity Cutoff	5	1	2	1
	Maximum Cost Mean ($)	38974	6825	7200	3405
	Upper Quantity Cutoff	20	10	30	10
	Minimum Cost Mean ($)	25985.6	3640	4800	2270
DS3	Lower Quantity Cutoff	5	1	-	1
	Maximum Cost Mean ($)	47978.4	10500	-	7005
	Upper Quantity Cutoff	20	10	-	10
	Minimum Cost Mean ($)	31985.6	7437.5	-	4670
DS4	Lower Quantity Cutoff	5	-	-	-
	Maximum Cost Mean ($)	38974	-	-	-
	Upper Quantity Cutoff	20	-	-	-
	Minimum Cost Mean ($)	25985.6	-	-	-

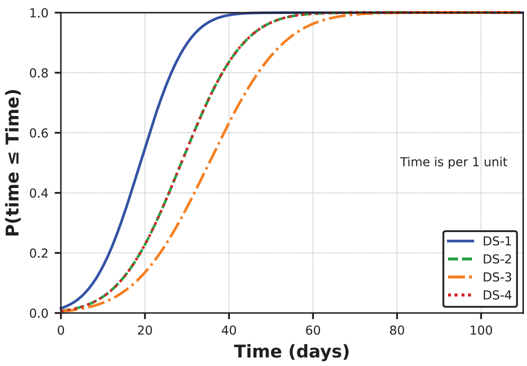

a) B1041.001a

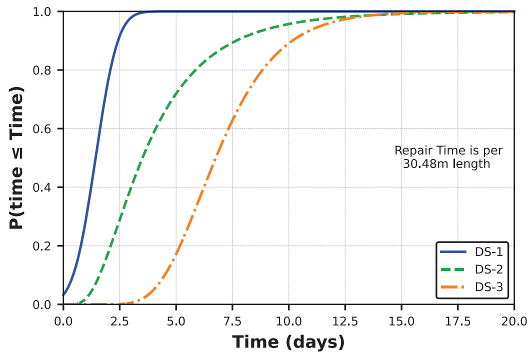

b) C1011.001a

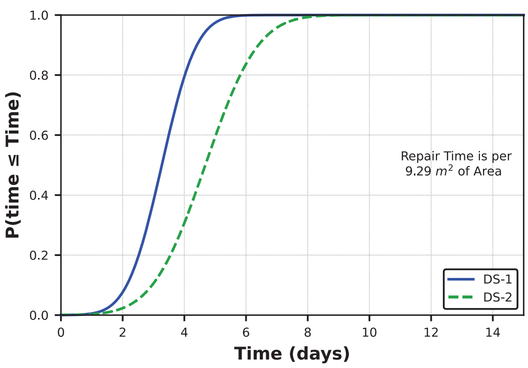

c) B1051.001

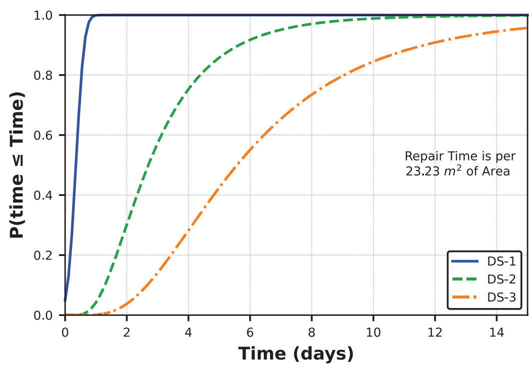

d) C3032.001a

Figure 5.24. Component repair time curves

Table 5.12. Consequence function parameters for repair time

Sheet Name		B1041.001a	C1011.001a	B1051.001	C3032.001a
DS1	Lower Quantity Cutoff	5	1	2	1
	Maximum Time (days)	22.68	2.13	3.92	0.42
	Upper Quantity Cutoff	20	10	30	10
	Minimum Time (days)	15.12	1.15	4.07	0.28
DS2	Lower Quantity Cutoff	5	1	2	1
	Maximum Time (days)	34.39	5.28	5.62	3.24
	Upper Quantity Cutoff	20	10	30	10
	Minimum Time (days)	22.93	2.8	3.75	2.16
DS3	Lower Quantity Cutoff	5	1	-	1
	Maximum Time (days)	42.33	8.12	-	6.69
	Upper Quantity Cutoff	20	10	-	10
	Minimum Time (days)	22.93	5.74	-	4.46
DS4	Lower Quantity Cutoff	5	-	-	-
	Maximum Time (days)	38974	-	-	-
	Upper Quantity Cutoff	20	-	-	-
	Minimum Time (days)	25985.6	-	-	-

Consequence functions for the repair costs of the components listed in Table 5.11, are provided in the following figure. Each point on the consequence function is the median value of the distribution of repair costs for the given quantity.

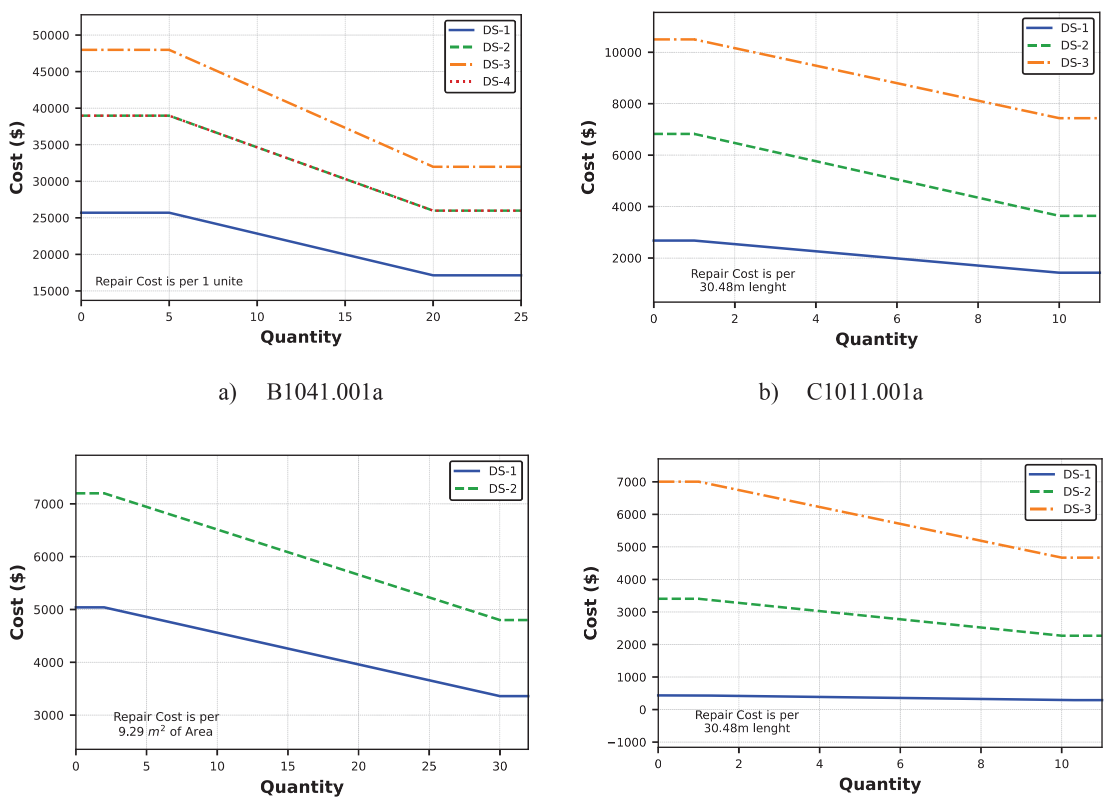

a) B1041.001a
b) C1011.001a
c) B1051.001
d) C3032.001a

Figure 5.25. Component consequence functions for the repair cost

Similarly, the consequence functions for the repair time are provided in the following figure for the components listed in Table 5.12.

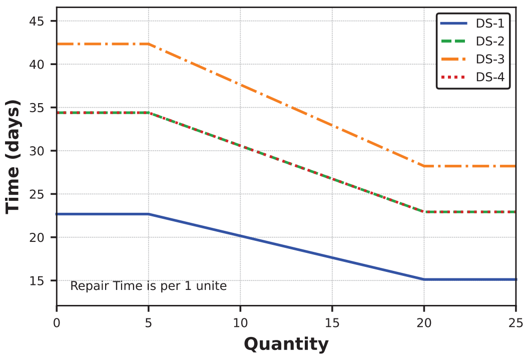

a) B1041.001a

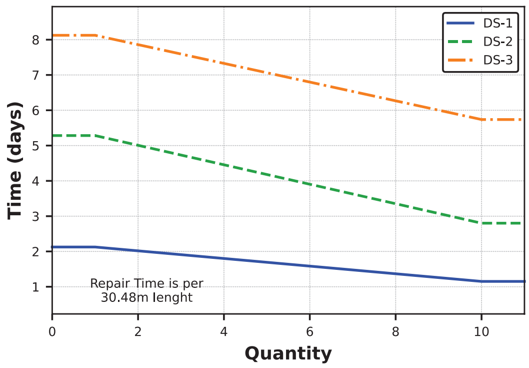

b) C1011.001a

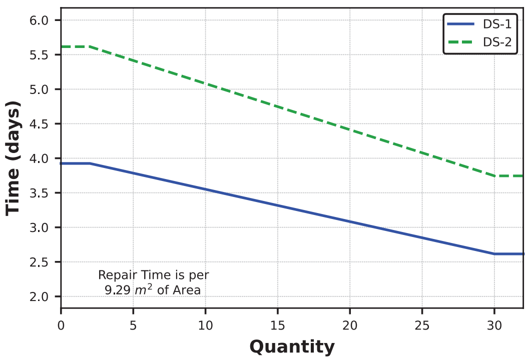

c) B1051.001

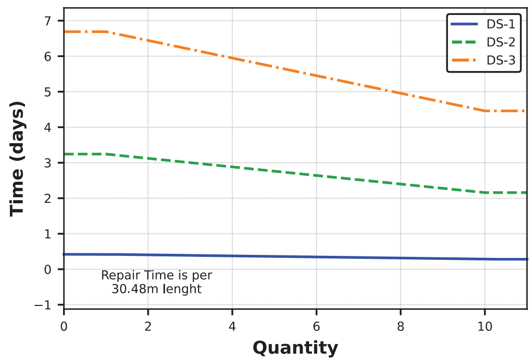

d) C3032.001a

Figure 5.26. Component consequence functions for the repair time

Note that for most of the selected components, the type of damage state is sequential at all damage state levels. However, for some of them, some damage states are sequential damage states, while some damage states are mutually exclusive damage states. The probability for the sequential damage state is equal to 1.00 for each damage state; on the other hand, for the mutually exclusive type of damage states, the total probability of the considered damage states is 1.00. For example, for component B1041.001a, the probability of DS_3 is equal to 0.8, and for DS_4 it is equal to 0.2, which gives a total of 1.00. Thus, DS_4 is the copy of DS_2 to create a mutually exclusive complement to DS_3. This could be noticed in Figure 5.23 and Figure 5.25 for the aforementioned component.

The flowchart given in Figure 3.14 is used and the loss in terms of costs at three hazard levels which correspond to the 50%, 10%, and 2% probability of exceedance in 50 years with mean return period of 72, 475, and 2475 year, are obtained. The costs are shown in Figure 5.27. Disaggregated costs for three different hazard levels of 2-Story which are disaggregated in different decision variables are shown. They are repair cost, non-functionality cost, demolition cost, collapse cost and their total. It should be noted that in non-functionality cost only the rental loss is considered. Non-functionality includes the time required for the repair, the demolition time in case the repair is not possible the structure should be demolished and replaced, and the collapse time in case of the partially or fully collapse condition of the structure that requires the replacement time for the structure. For 2-Story structure 20 days is assumed for demolition of the structure and removal of the debris. In addition, the replacement time for the structure is assumed to be 150 days. For the commercial office building in this study, at a given location 430 $/m^2$/year (40 $/ft^2$/year) of rent is assumed.

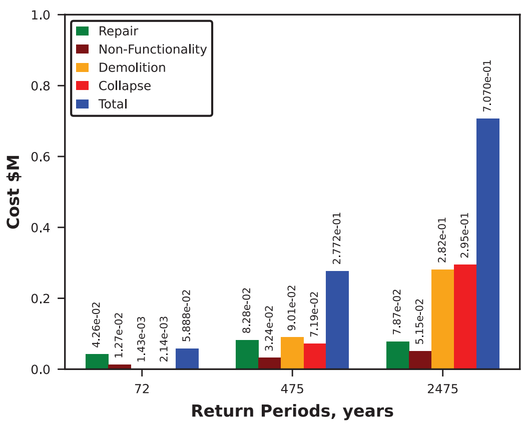

a) Code-Based

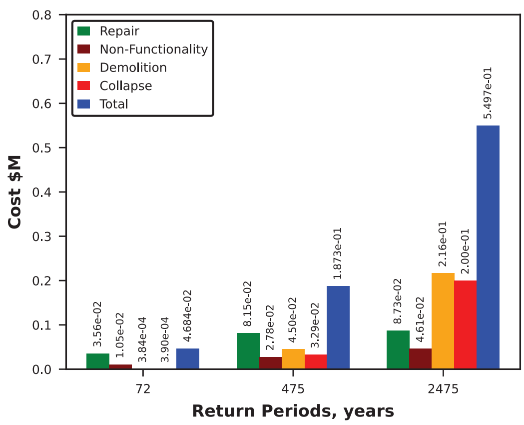

b) PBSD-Based

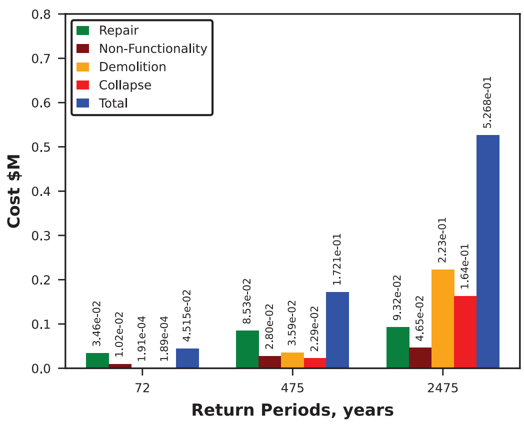

c) PPBOSD-Based

Figure 5.27. Disaggregated costs for three different hazard levels of 2-Story structures

In the above figure, the differences of costs, specifically for total cost between three design approaches could be noticed clearly at three hazard levels. It should be noted that since fundamental period for each structure is different, which give different seismic hazard curves, and as a consequence the Sa (T_1) for different hazard levels are different. To this end, to compare the results of the design approaches at the same intensity levels, the resulted costs at three intensity levels with Sa (T_1) = 0.5g, 1.5g and 3.0g are obtained, and shown in the following figure.

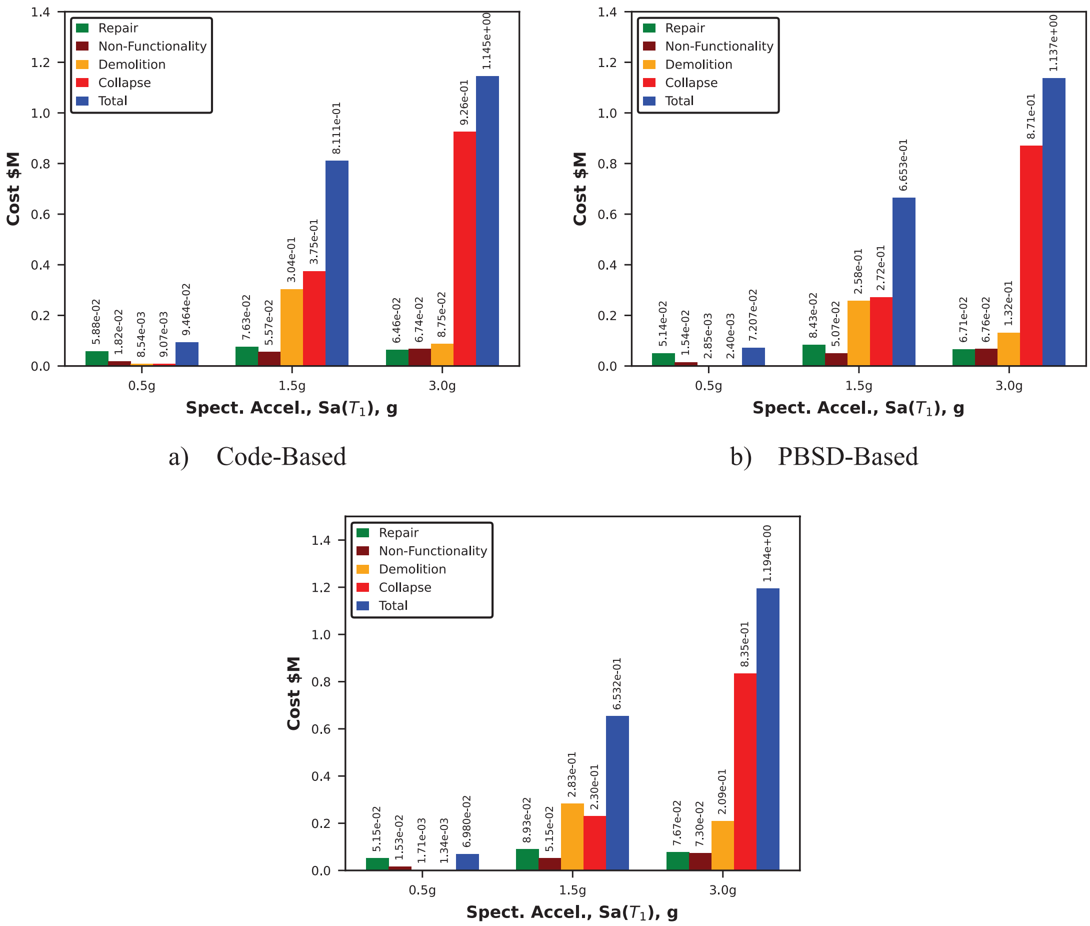

Figure 5.28. Disaggregated costs for three different IM levels of 2-Story structures

From the figure it can be concluded that at lower intensity level (0.5g and 1.5g) PPBOSD approach gives the lowest total cost, while in the higher intensity level (3.0g) the PPBOSD approach gives the highest total cost. This is because, in this IM level, without collapse cost, all other costs are higher than the ones for the other two methods, especially, the cost of demolition is much higher in this approach compared to the other two approaches. To compare the results clearly, the disaggregated costs are shown in the following figure for all three design approaches at specific intensity level (1.5g). Figure 5.29a provides the costs for all design approaches at Sa(T_1) = 1.5g, while Figure 5.29b shows the differences in percentage of the cost in terms of all components of the cost and the total cost. From Figure 5.29, it can be concluded that the PPBOSD approach gives the lowest total cost at the intermediate IM level.

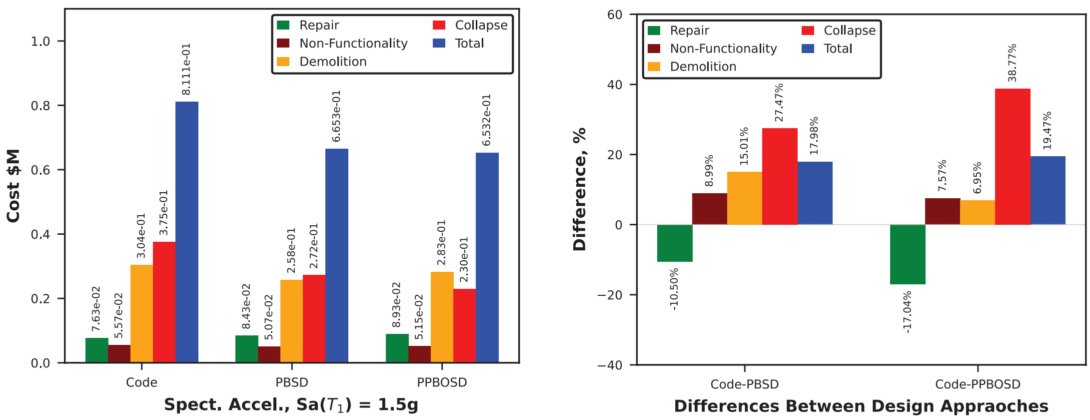

a) Costs b) Differences in percentage

Figure 5.29. Comparison of Disaggregated costs at 1.5g for 2-Story structures

5.3.4. Result of Life Cycle Cost Analysis

Brief information is provided regarding LCCA, and equation (3.47) is used to obtain the expected total cost of the structure. The resulting expected total costs are shown in Figure 5.30 with their differences. It should be noted that the hazard level with a mean return period of 72, 475, and 2475 years is considered for LCCA. In addition, Figure 5.31 shows the differences in the initial costs for the structures designed using three different design approaches.

From these figures, it could be concluded that with an increase of 0.167% in initial cost, a reduction of 1.07%, 1.70%, and 2.11% is obtained in the expected total cost of the structure for hazard levels with a mean return period of 72, 475 and 2475 years, respectively. In addition, in all three hazard levels, the expected total cost of the structure is lower for the frame designed based on the PPBOSD with compare to the structures designed using Code-Based and the PBSD approaches.

a) Expected total costs

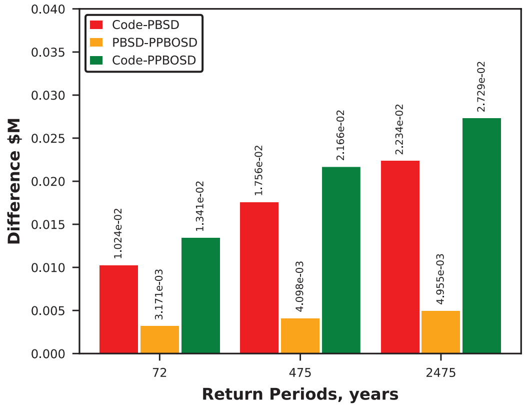

b) Differences

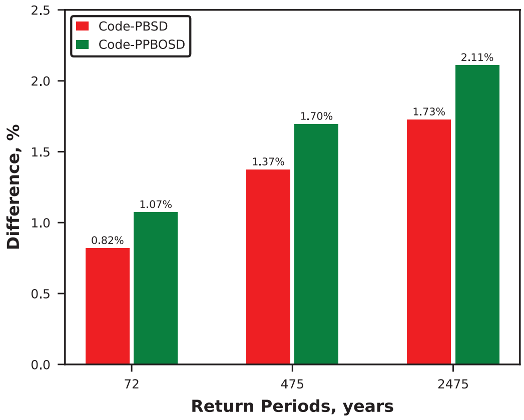

c) Differences in percentage

Figure 5.30. Expected total cost results at different hazard levels for 2-Story structures

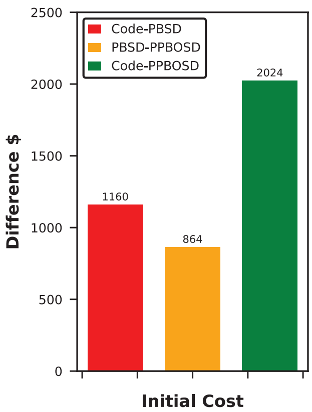

a) Difference

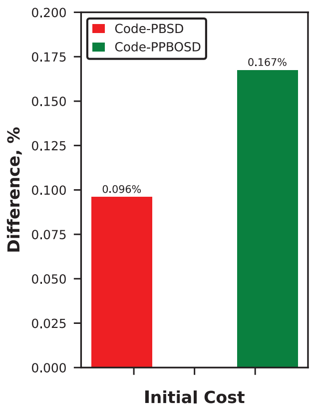

b) Differences in percentage

Figure 5.31. Differences in initial costs for the 2-Story structures

5.4. Performance of the Structure in terms of Performance Point

The Performance Point, which represents the state of maximum inelastic capacity of the structure is obtained using the procedure given in the FEMA-440 (2005). The results of the performance points are shown in the following figures for the frames designed through different approaches. Each figure includes three parts. The first one shows the capacity curve together with the acceleration response spectra that correspond to each iteration. It also includes the locus of the possible performance points. The second part consists of the capacity curve of the structure in the ADRS format together with the bilinear approximation. The third part of the figure shows the capacity curve in its normal format, together with the coordinates of the performance point.

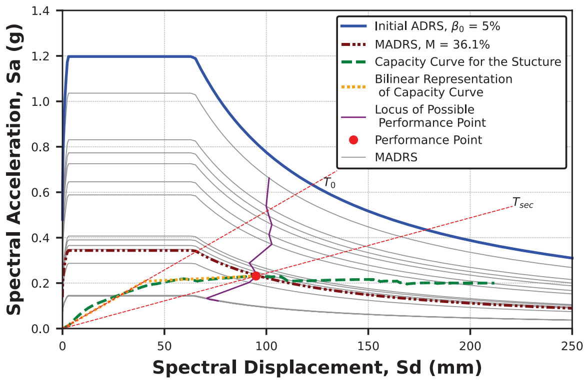

a) Schematic of the procedure C of FEMA-440

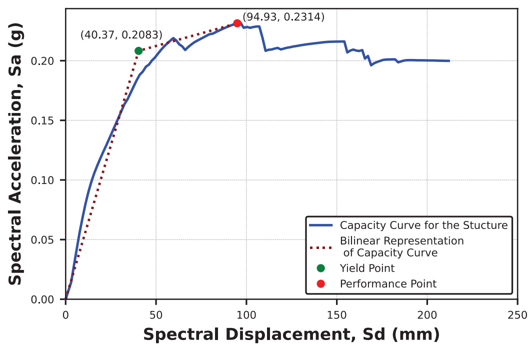

b) Capacity curve and bilinear representation in ADRS format

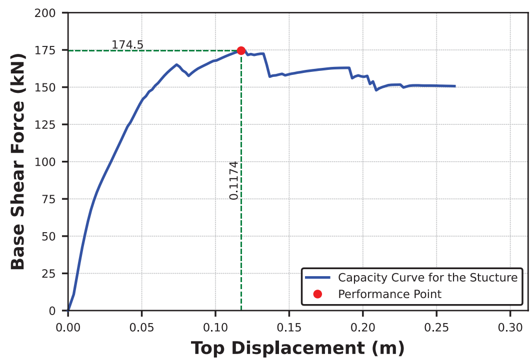

c) Capacity curve in regular format

Figure 5.32. Resulted performance point for 2-Story frame designed using Code-Based design approach

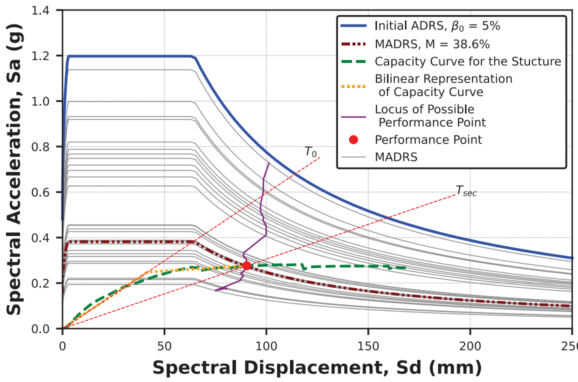

a) Schematic of the procedure C of FEMA-440

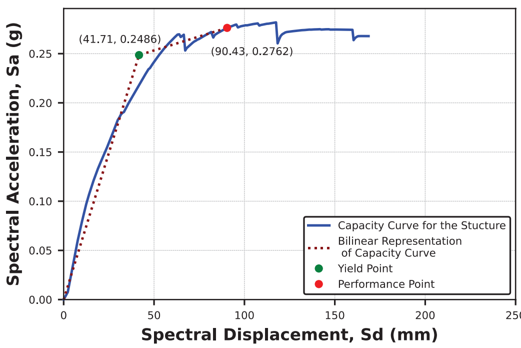

b) Capacity curve and bilinear representation in ADRS format

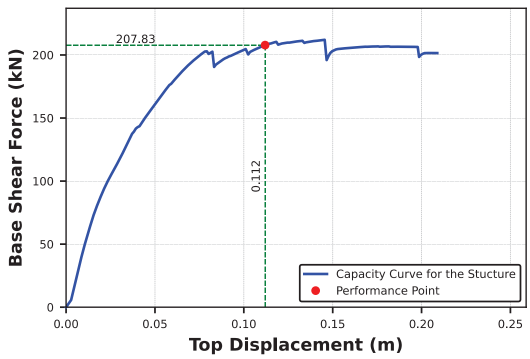

c) Capacity curve in regular format

Figure 5.33. Resulted performance point for 2-Story frame designed using PBSD approach

To compare these results, the capacity curves of the structures designed to using three different design approaches together with the performance points are shown in Figure 5.35. In the figure the LS performance limit is also shown. The displacement shown for the LS performance level is obtained for 2% peak drift ratio of the roof level with respect to the ground level i.e., the ratio of top displacement over the height of the structure.

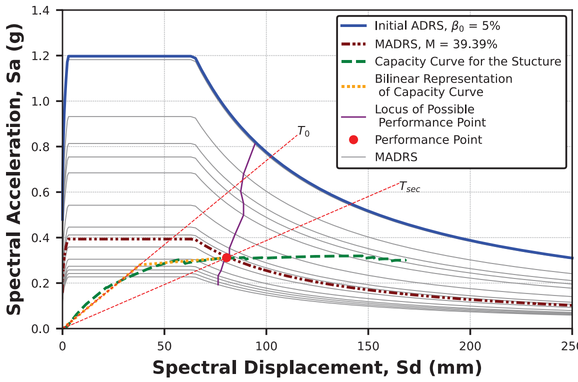

a) Schematic of the procedure C of FEMA-440

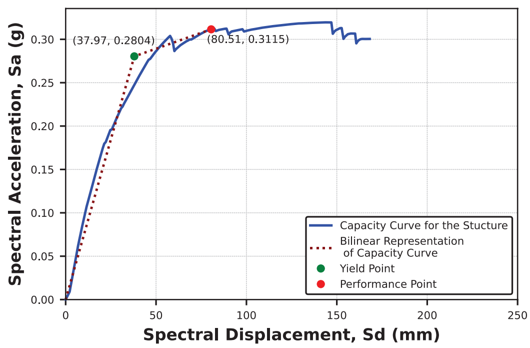

b) Capacity curve and bilinear representation in ADRS format

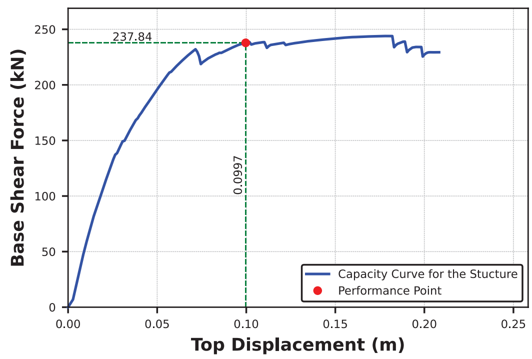

c) Capacity curve in regular format

Figure 5.34. Resulted performance point for 2-Story frame designed using PPBOSD approach

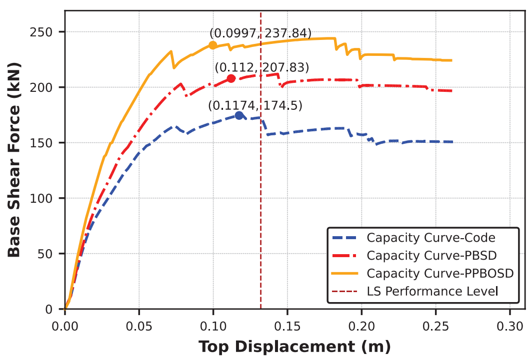

Figure 5.35. Performance points on capacity curves of the 2-Story frames

From these figures, it can be concluded that the structure designed with respect to the PPBOSD approach performs better than the structures designed using Code-Based design and the PBSD approaches. Because it gives the lower top displacement at higher base shear forces.

CHAPTER 6

CASE STUDIES

The proposed methodology is applied on structures with the same planner configurations (Figure 6.1) but different heights to check its efficiency. For this purpose, three frame structures with 3, 6, and 9 stories are chosen. It is assumed that each structure has three spans in the direction of interest with a length of 5m each, while 5 bays on the other direction with a length of 4m each. Thus, the total planner area of the structure per floor is equal to 300m^2. The selected 2D frames are shown in Figure 6.2. For the Code-Based and PBSD approaches, the initial cost is selected as the objective function, while for the PPBOSD approach, the expected total cost of the structure is used as an objective function.

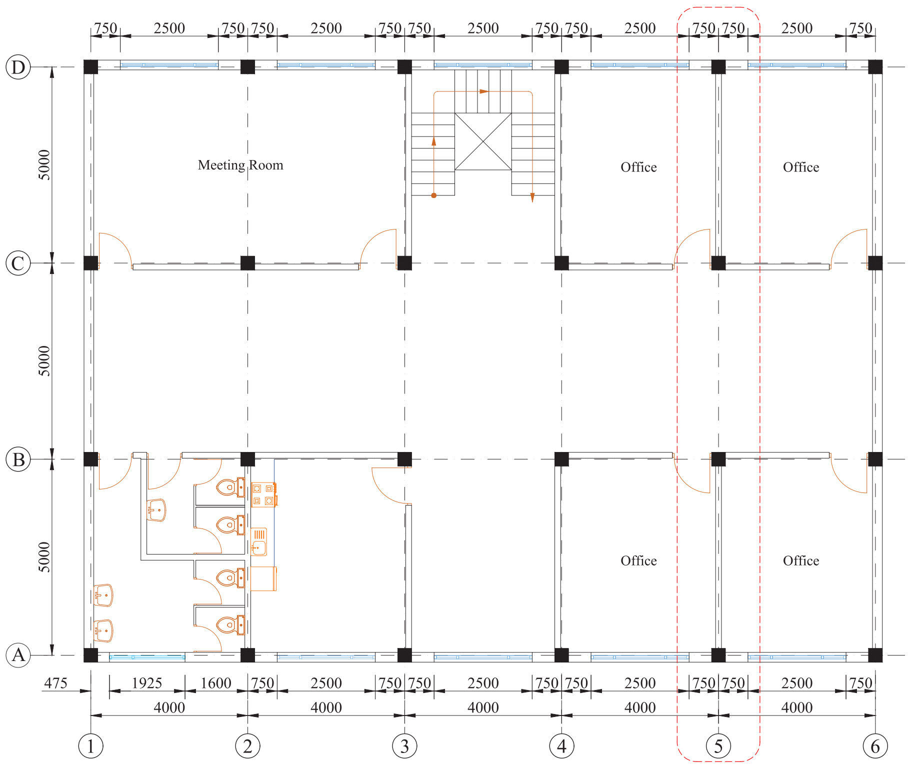

Figure 6.1. First floor plan for the 3-, 6-, and 9-Story structures

The initial cost in this study is obtained from the summation of two different costs. The first one, denoted as C_1, is the cost assumed for the structure that corresponds to the minimum cross-sectional dimensions and the least amount of reinforcement from the database, refer to section 4.6 (The first raw of the column and beam database for each type of member). The second cost, denoted as C_E, comes from extra concrete and reinforcement during optimization. This is because the cross-sectional dimensions of the member and the amount of reinforcement differ from the minimum ones during the optimization process. The additional cost is attained by assuming 250$/m^3 for concrete and 2$/Kg for reinforcement, which includes the labor and other necessary costs.

The initial cost of the structure is obtained in each case, such that minimum cross-sectional sizes for beams and columns are considered with minimum reinforcement from the database (refer to section 4.6). The location of the structure is assumed to be in San Francisco, USA; thus, according to the ProEst website (https://proest.com/), the prices differ with respect to the number of stories.

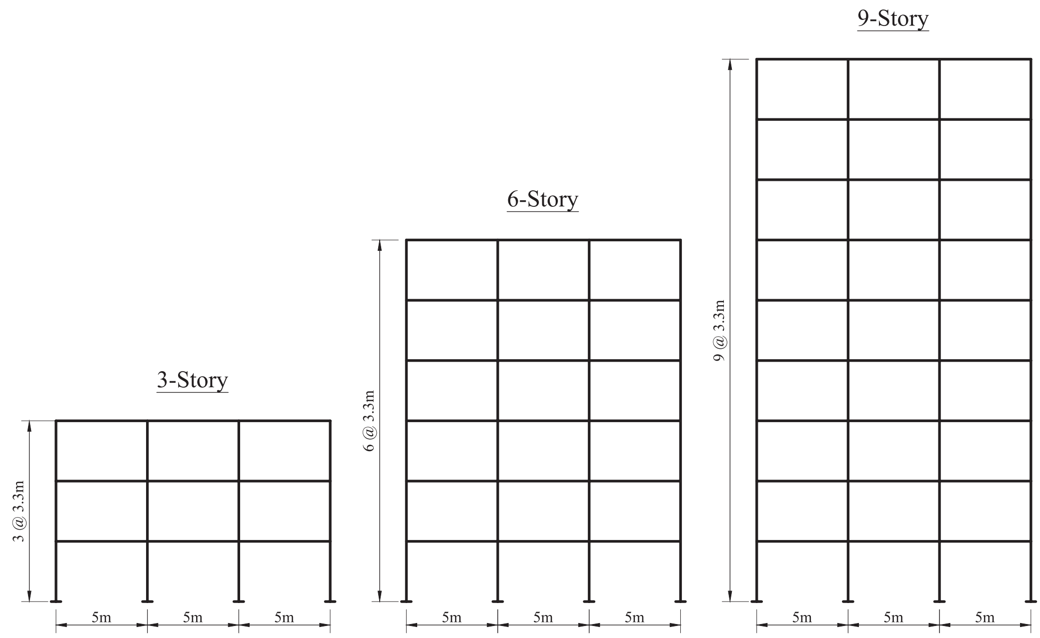

Figure 6.2. Dimensions for the selected 2D frames of 3-, 6-, and 9-Story structures

For the optimization, GA is used, the maximum population size is taken as 30, and the number of generations is considered 100. The termination criterion is used as 100$ only for the objective function. In addition, in the optimization process, the ET analysis method is utilized to reduce computational time. It should be noted that the logarithmic standard deviation for all structures (3-, 6-, and 9-Story) is assumed to be 0.4 at each IM level, and for the collapse fragility function, it is assumed to be 0.6.

6.1. Results for 3-Story Structure

6.1.1. Optimization results

As mentioned, the structure is assumed to be located in San Francisco, USA; therefore, for the Considered location of the structure, the cost of 3770$/m^2 is assumed per story according to the ProEst website (https://proest.com/). This cost includes the structural, nonstructural, content system, and all other things required for a commercial office building. The planner dimension for the structure is 15m in width and 20m in length. Therefore, $A_{total} = 300m^2$, $C_1 = 3.393\,M\$$, and $C_{Demolition} = 0.0774\,M\$$

The optimum solutions obtained through conventional code, the PBSD, and the PPBOSD approaches for the 3-Story structures are given in the following figure. The details of the cross sections are provided in Appendix A.

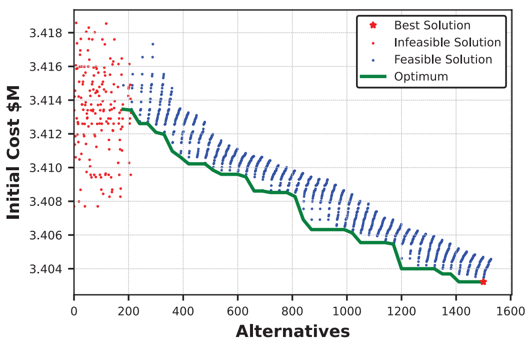

a) Code-Based

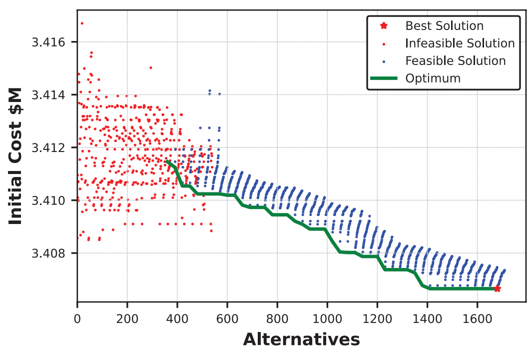

b) PBSD-Based

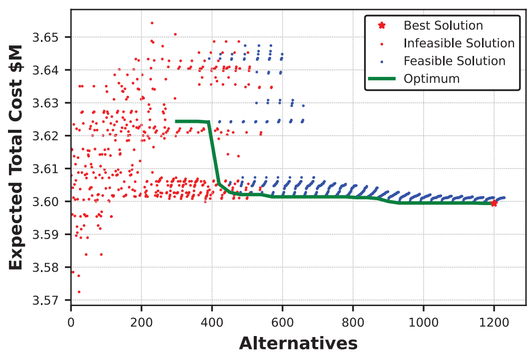

c) PPBOSD-Based

Figure 6.3. Optimum solution for 3-Story structures from different design approaches

The optimum initial cost value for the code-based design approach is 3.40322 $M, while for the PBSD approach, it is equal to 3.40665 $M. On the other hand, the optimum value for the expected total cost through PPBOSD is obtained as 3.59942 $M, in which the portion of the initial cost is 3.41290 $M. The differences between initial costs are shown in the following figure, which is only due to the differences in the amount of design variables (Beams and columns cross-sections, longitudinal and transverse reinforcement).

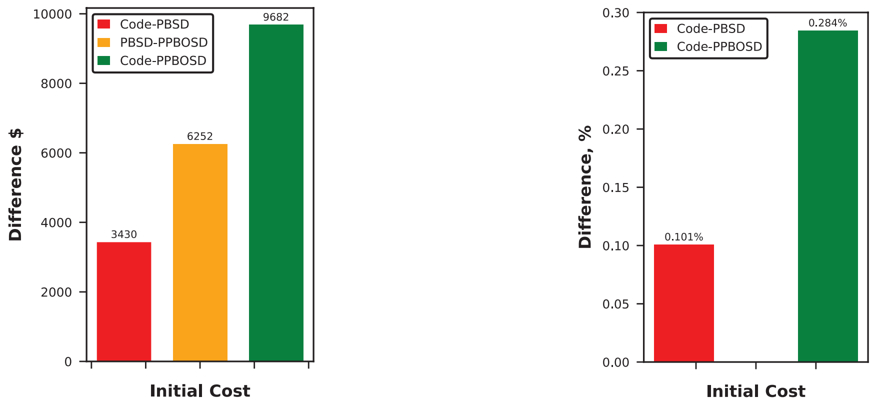

a) Difference

b) Differences in percentage

Figure 6.4. Differences in initial costs for the 3-Story structures

6.1.2. Performance Assessment Results

The performance of the structure is assessed using the PEER PBEE methodology. Results of each PEER PBEE methodology step are provided sequentially in the following sub-sections. As mentioned, the IDA method is used, for which 22 far-filed GM records given in FEMA-P695 were conducted.

6.1.2.1. Result of Probabilistic Demand Analysis

The results for some statistical parameters obtained using NTHA are tabulated in Table A.1 of Appendix A, which corresponds to peak IDR (an EDP). These results are shown for three specific IM levels selected arbitrarily. However, the median, 16^{th} and 84^{th} percentile of the peak IDR and the resultant IDR from the 22 selected GM records are shown in Figure 6.5 for the same IM levels of Table A.1 of Appendix A. From Figure 6.5 and the median values of Table A.1, it can be observed that only the structure designed using the PPBOSD approach satisfied IO, LS, and CP performance levels at the selected lower, medium, and higher IM levels, respectively. It should be noted that in Figure 6.5, the peak IDRs are shown for the medium and higher IM levels for each design approach. In addition, the constant values obtained from linear relationships between ln(EDP) and ln(IM) are tabulated in Table 6.1.

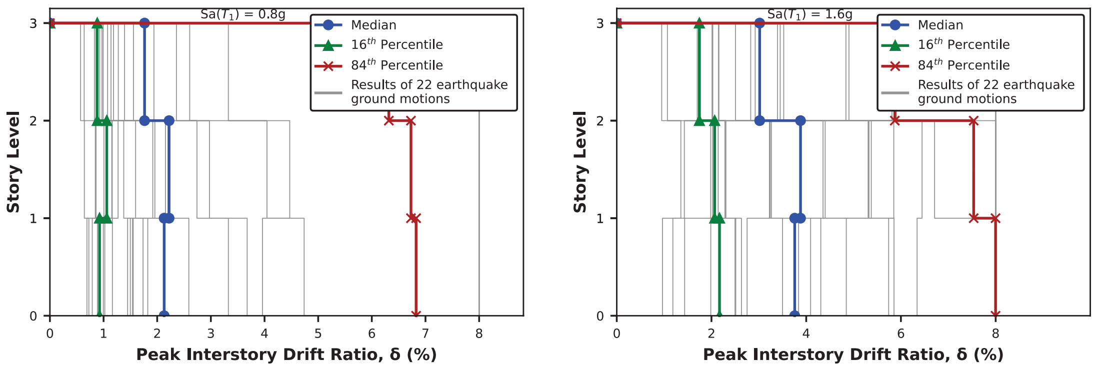

a) Code-Based

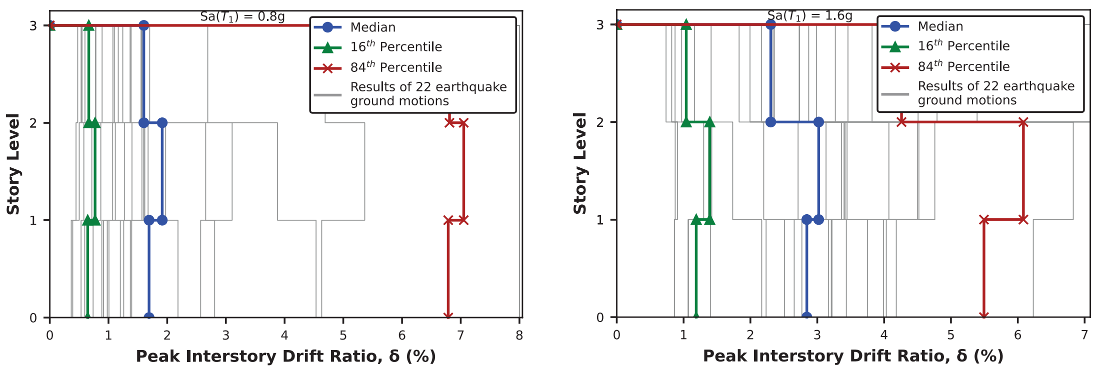

b) PBSD-Based

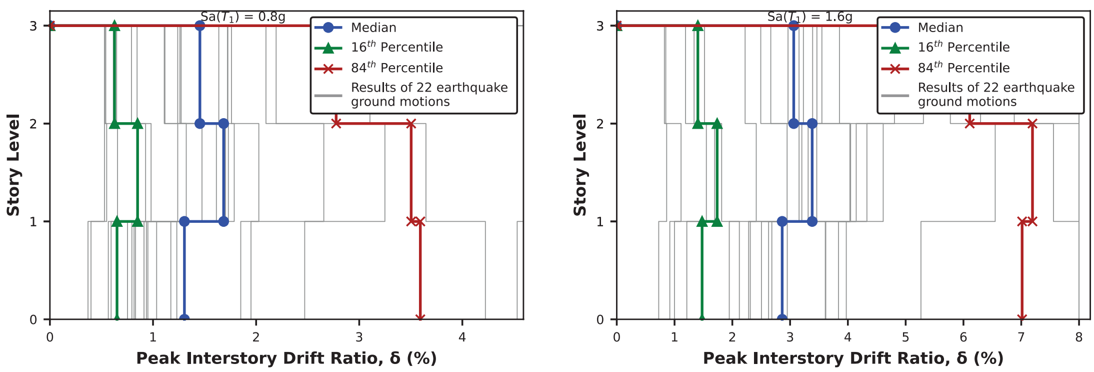

c) PPBOSD-Based

Figure 6.5. Peak IDRs for 3-Story frames corresponding to two different IM levels

Table 6.1. Constant values of equation (3.39) for the median peak IDR values of 3-Story frames

Story #	Code-Based		PBSD-Based		PPBOSD-Based	
	a	b	a	b	a	b
1	2.4105	1.0066	2.1800	1.0404	1.6104	1.0272
2	2.5428	0.9954	2.3841	1.0188	1.9823	1.0102
3	2.0684	0.9343	1.9606	0.9708	1.7729	1.0158
Maximum	2.6886	0.9997	2.4456	1.0160	2.0295	1.0123

The following statistical parameters are gained after using the linear relationship between ln(EDP) and ln(IM). Only the values corresponding to the maximum IDR are given in this table.

Table 6.2. IDRs of 3-Story frames corresponding to different IM levels after using the linear relationship between ln(EDP) and ln(IM)

IM Level Sa (T_1)	Peak Interstory Drift Ratio, IDR (%)					
	$\mu_{ln(x)}$	μ_x	$\widehat{S}$	$\sigma_{ln(x)}$	16th Percentile	84th Percentile
Code-Based						
0.4	0.0730	1.4433	1.0757	0.7667	0.5482	2.3008
0.8	0.7659	2.9053	2.1510	0.7754	1.0755	4.7437
1.6	1.4589	4.9479	4.3012	0.5293	2.1101	9.7802
PBSD-Based						
0.4	-0.0366	1.7450	0.9640	1.0894	0.4319	2.2840
0.8	0.6676	2.9125	1.9495	0.8960	0.8747	4.9871
1.6	1.3718	5.0030	3.9424	0.6903	1.7717	10.8893
PPBOSD-Based						
0.4	0.0062	1.3163	1.0062	0.7330	0.5391	1.8626
0.8	0.6012	2.3098	1.8242	0.6871	0.9532	3.5495
1.6	1.3575	4.6201	3.8866	0.5880	1.9668	8.0569

The probability of exceedance, together with the drift limits, is shown in Figure 6.6. The figure shows that the structure designed using the PPBOSD approach has the lowest exceedance probability in all selected IM levels compared to the other structures. The structure designed by the PBSD approach has a higher probability of exceedance in the lowest selected IM level compared to the one designed using the Code-Based design approach; however, it has a lower probability of exceedance in the higher IM levels.

The demand hazard curves obtained for all structures are shown in Figure 6.7, which are obtained using the discrete form of equation (3.30). In the figure, the comparison of the median demand hazard curves is also shown. From the comparison it can be observed that the structure designed using the PPBOSD approach showed better performance compared to the ones designed by Code-Based and PBSD approaches.

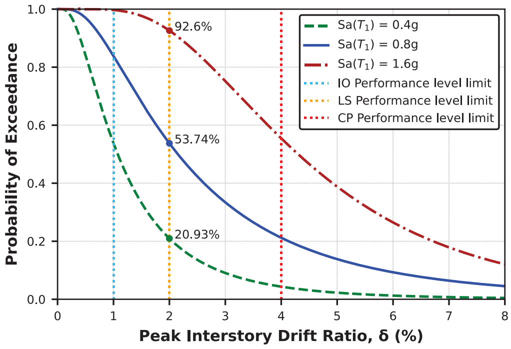

a) Code-Based

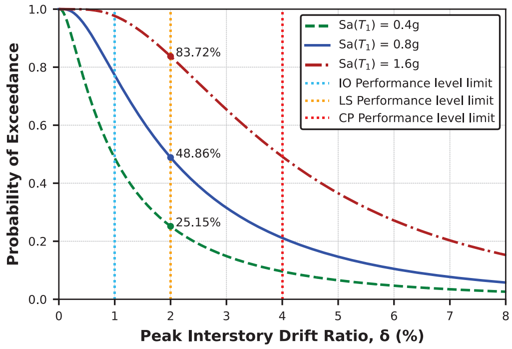

b) PBSD-Based

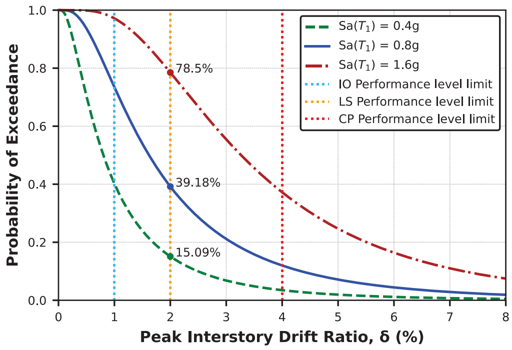

c) PPBOSD-Based

Figure 6.6. Probability of exceedance for peak IDRs of 3-Story frames at different IM levels

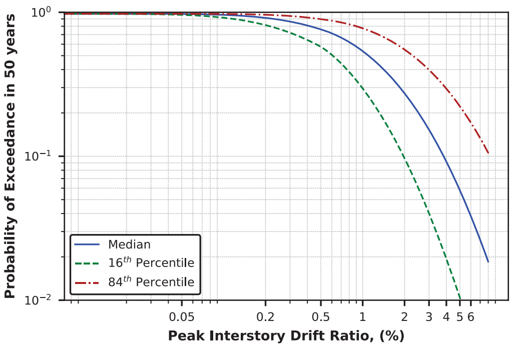

a) Code-Based

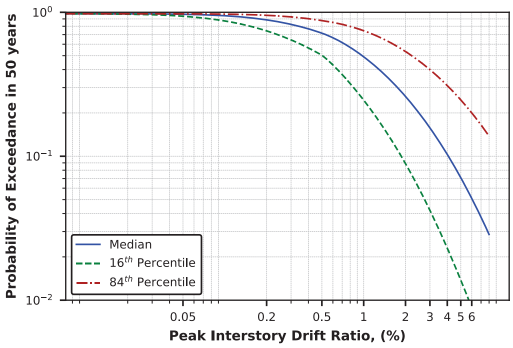

b) PBSD-Based

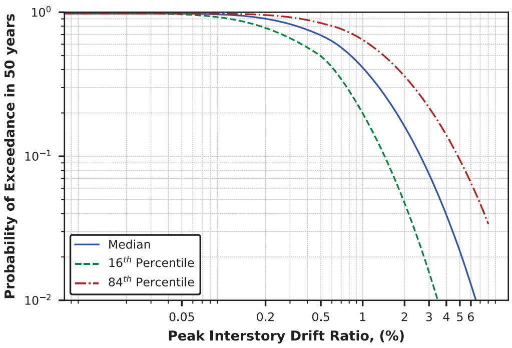

c) PPBOSD-Based

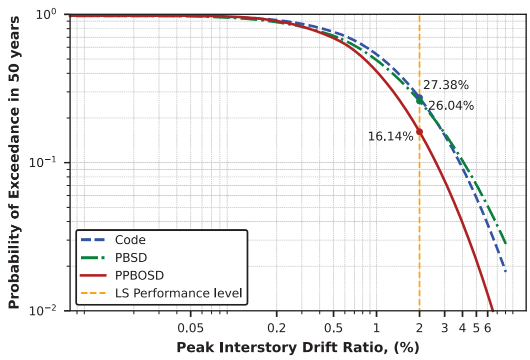

d) Comparison of median demand hazard curves

Figure 6.7. Demand hazard curves for 3-Story frames

The results of the ET method are shown in Figure 6.8 and Figure 6.9 in terms of the ET response curves in two different formats: IDR vs ET time and IDR vs return period. Figure 6.8 shows that the structure designed using the PPBOSD approach has lower IDR values than the other two structures, specifically in the higher-intensity levels.

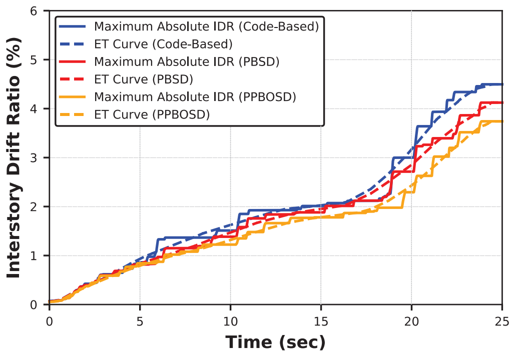

a) IDR vs ET time

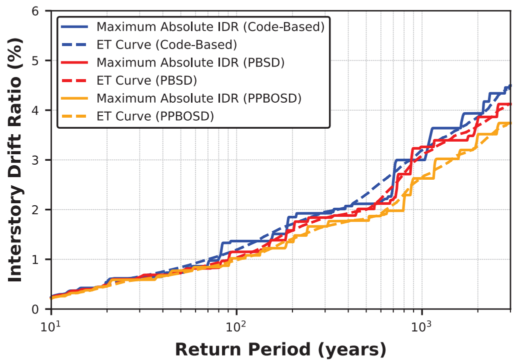

b) IDR vs Return Period

Figure 6.8. ET response curves of the 3-Story frames

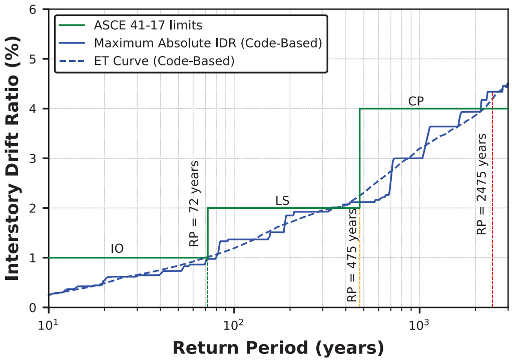

a) Code-Based

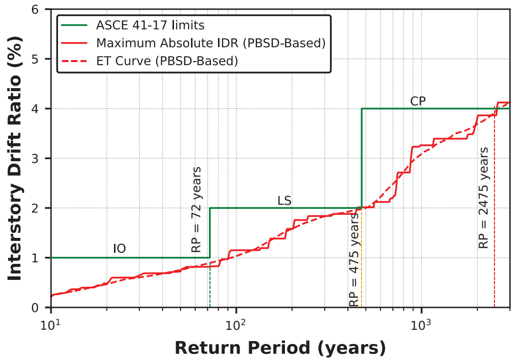

b) PBSD-Based

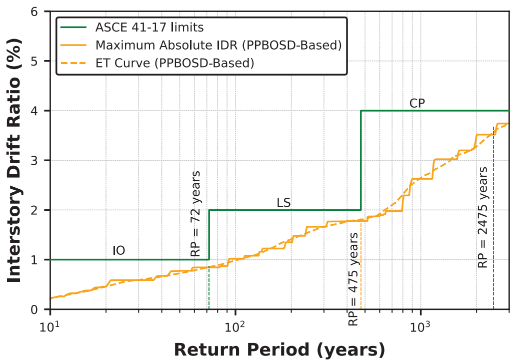

c) PPBOSD-Based

Figure 6.9. ET response curves of the 3-Story frames with IDR limits for different hazard levels

Further, Figure 6.9 indicates that the structure designed using the Code-Based design approach does not meet the LS and CP performance levels. In contrast, the structures designed using the PBSD and the PPBOSD approaches satisfied all performance levels.

6.1.2.2. Result of Probabilistic Damage Analysis

The resulting statistical parameters for the fitted fragility curves are provided in the following table, and they are shown in Figure 6.10.

Table 6.3. Statistical parameters for fitted fragility curves of 3-Story frames

Performance Level	Code-Based		PBSD-Based		PPBOSD-Based	
	$\widehat{S}_c$	β_{S_c}	$\widehat{S}_c$	β_{S_c}	$\widehat{S}_c$	β_{S_c}
IO	0.3718	0.8754	0.4147	0.8887	0.4798	0.9968
LS	0.7438	0.7718	0.8204	0.6882	0.9689	0.8123
CP	1.4879	0.5429	1.6230	0.6176	1.9568	0.6477

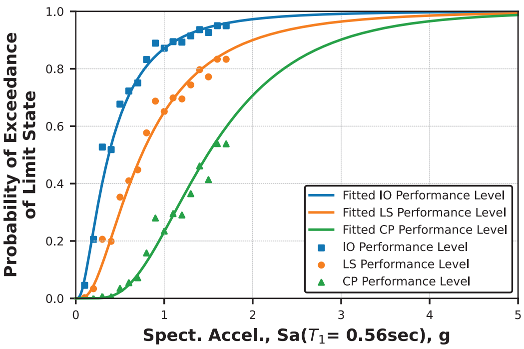

a) Code-Based

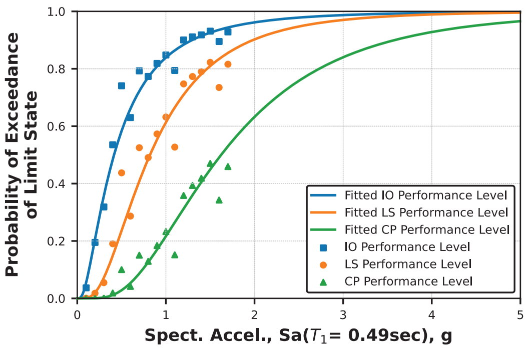

b) PBSD-Based

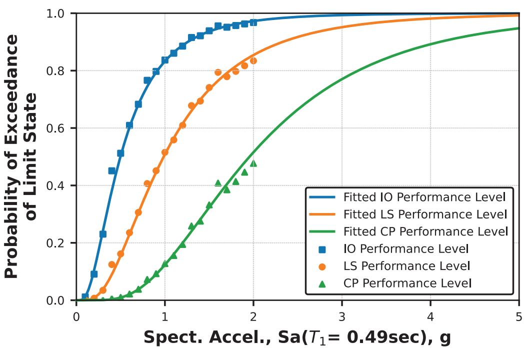

c) PPBOSD-Based

Figure 6.10. Fragility curves of 3-Story frames for different performance levels

The following figure is shown to compare the fragility curves of all three cases. The figure shows that the structure designed with the PPBOSD approach has best performance, while the one designed using conventional Code has the worst performance. For the CP performance level, at a lower intensity, approximately $Sa(T_1) = 0.6g$, they show almost the same vulnerability; after that, the one designed using the proposed methodology gives good performance.

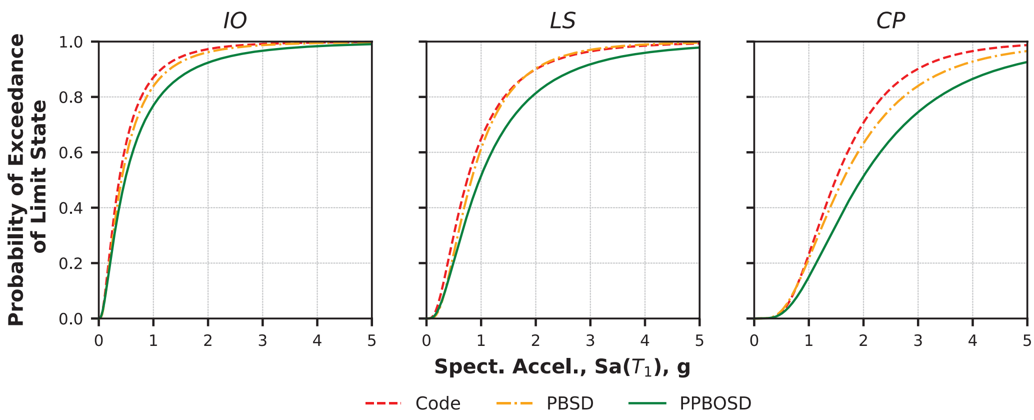

Figure 6.11. Comparison of fragility curves of 3-Story frames

6.1.2.3. Result of Probabilistic Loss Analysis

Loss analysis is carried out to obtain the loss results regarding the cost at different hazard levels and the expected total cost at three different hazard levels. Building replacement and demolition costs are required to estimate the loss due to collapse and demolition. The demolition cost is assumed to be 86$/m^2 and the replacement cost is assumed to be $ 3770$/m^2. The total area per floor level is 15m x 20m = 300 m^2. The costs obtained at three hazard levels are given in the following figure. In addition, in case the repair is not possible, the total time for the demolition and removal of the debris is taken to be 30 days, while 300 days is considered for the total replacement time.

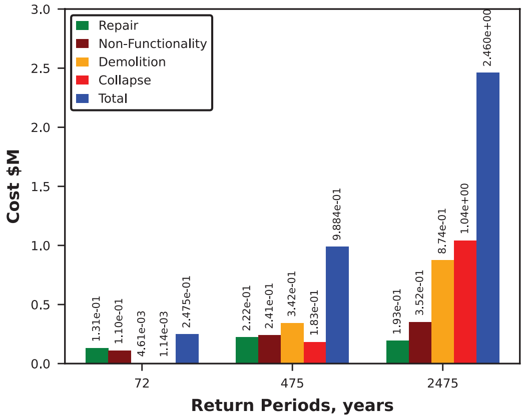

a) Code-Based

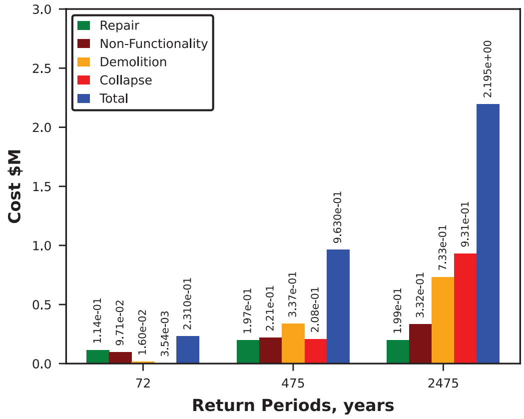

b) PBSD-Based

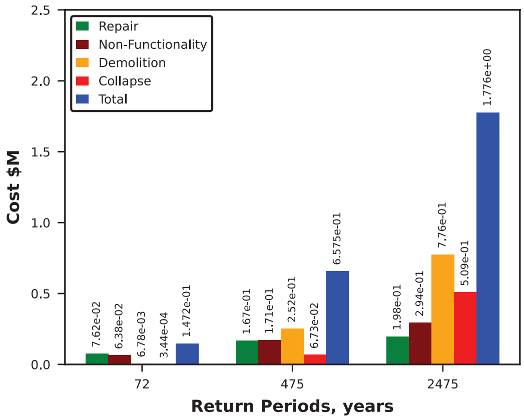

c) PPBOSD-Based

Figure 6.12. Disaggregated costs for three different hazard levels of 3-Story structures

From the figure, the differences in the costs at the three hazard levels can be noticed clearly. The structure designed with the proposed methodology has provided the lowest loss compared to other approaches.

The losses are obtained at the same IM levels for the structures designed with all three design approaches to have a better comparison and shown in Figure 6.13. From Figure 6.13, it can be concluded that the PPBOSD approach gives the lowest total cost at all intensity levels. The resulting costs for all three design approaches at $Sa(T_1) = 1.5g$ are provided in the Figure 6.14, together with the percentage difference in terms of the different decision variables.

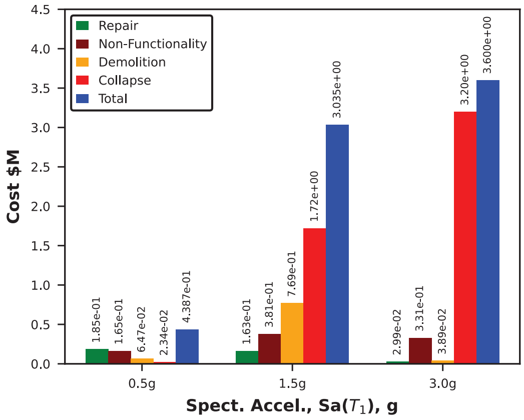

a) Code-Based

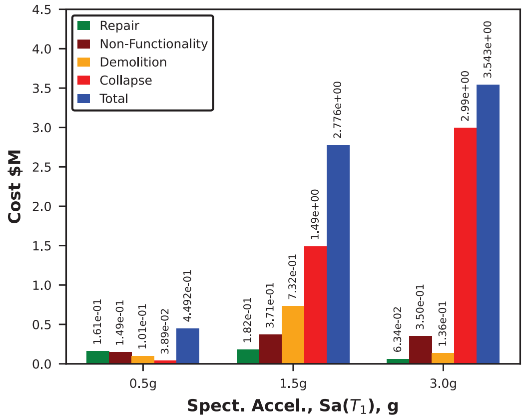

b) PBSD-Based

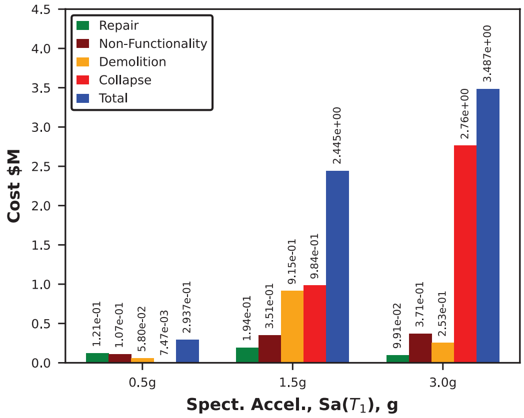

c) PPBOSD-Based

Figure 6.13. Disaggregated costs for three different IM levels of 3-Story structures

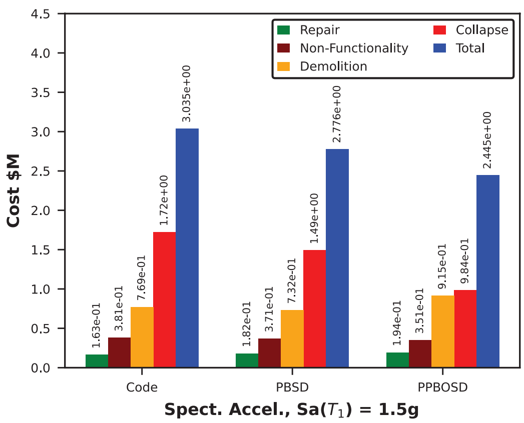

a) Costs

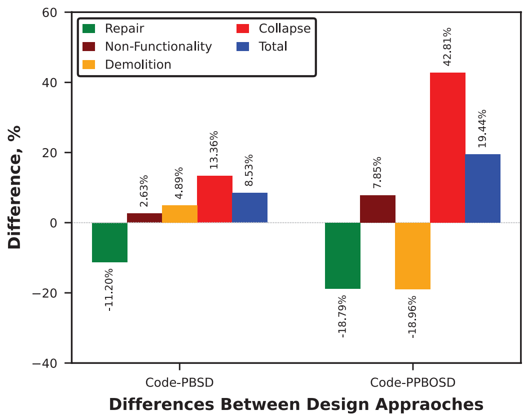

b) Differences in percentage

Figure 6.14. Comparison of Disaggregated costs at 1.5g for 3-Story structures

6.1.2.4. Result of Life Cycle Cost Analysis

The results from the LCCA are provided in the following figure for three different hazard levels. The figure also shows the difference between the expected total cost and the related percentages.

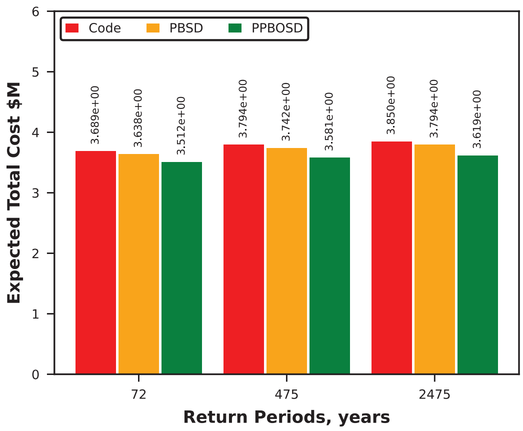

a) Expected total costs

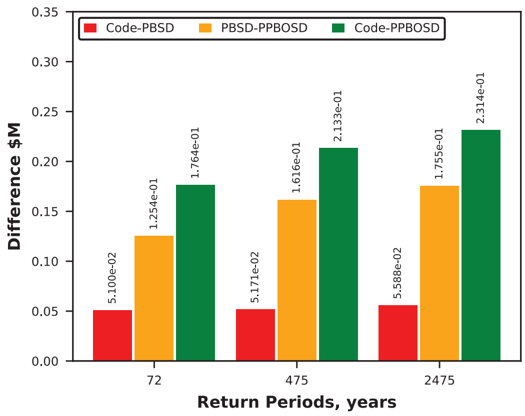

b) Differences

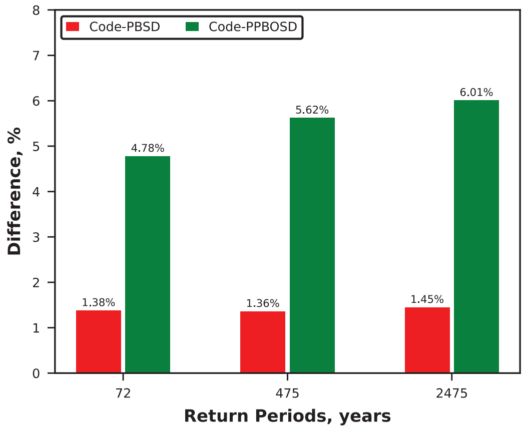

c) Differences in percentage

Figure 6.15. Expected total cost results at different hazard levels for 3-Story structures

From Figure 6.4 and Figure 6.15, it can be concluded that with an increase of 0.284% in initial cost, a reduction of 6.01% is obtained in the expected total cost of the structure. In addition, in all three hazard levels, the expected total cost of the structure is lower for the frame designed based on the PPBOSD compared to the other two approaches.

6.1.3. Performance of the Structure in terms of Performance Point

The Performance Point, which represents the state of the maximum inelastic capacity of the structure, is obtained using the procedure given in the FEMA-440 (2005). The results of the performance points are shown in Figure 6.16 for the structures designed through different design approaches. In the figure, the obtained results are compared. The figure shows that the structure designed using the PPBOSD approach has high strength compared to the structures designed using the other two methods. The figure also shows that the performance points are within the LS performance levels. The limit for the LS performance level corresponds to the roof drift ratio.

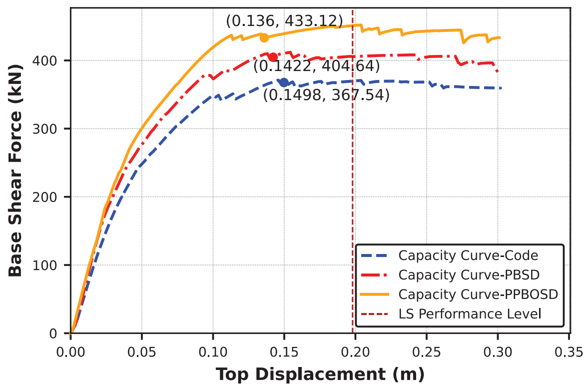

Figure 6.16. Performance points on capacity curves of 3-Story frames

6.2. Results for 6-Story Structure

6.2.1. Optimization results

For the 6-Story structure, the cost per square meter per story level is assumed to be 4100$, and 86$/m^2 per floor is assumed for demolition. In addition, the replacement time is taken as 600 days, and the demolition time is considered to be 45 days. To this end, the following costs are estimated:

$$A_{total} = 20x15 = 300m^2$$

$$\Rightarrow \quad C_1 = 4100x300x6 = 7380000\$ = 7.38M\$$$

$$\Rightarrow \quad C_{Demolition} = 86x300x6 = 154800\$ = 0.1548M\$$$

The optimum solutions for the case of the 6-Story structures, obtained through all three design approaches, are provided in the following figure. The resultant cross-sections for the members are provided in Appendix B. It should be noted that for each of the two stories same cross-sections are assigned for both columns and beams.

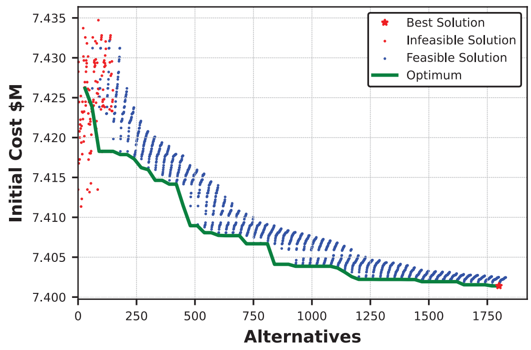

a) Code-Based

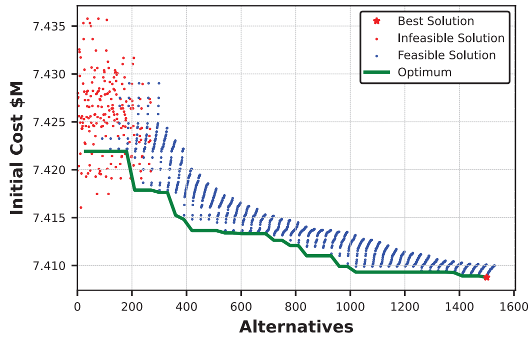

b) PBSD-Based

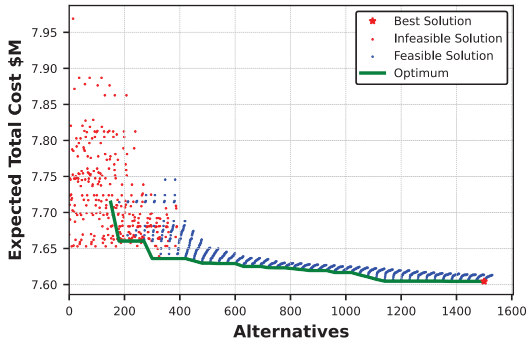

c) PPBOSD-Based

Figure 6.17. Optimum solution for 6-Story structures from different design approaches

The optimum initial cost value for the code-based design approach is 7.4014 $M, while for the PBSD approach, it is equal to 7.40876 $M. The optimum solution for the expected total cost of the structure obtained through the PPBOSD approach is 7.60445 $M, in which the portion of the initial cost is 7.4318 $M. The differences among the initial costs are shown in the following figure.

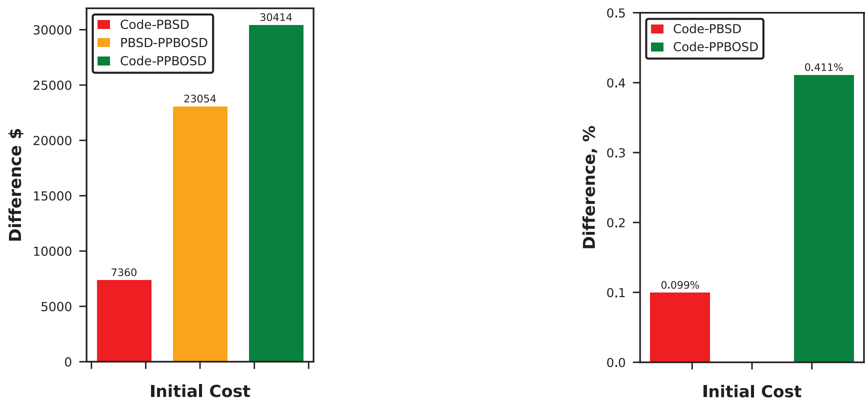

a) Difference b) Differences in percentage

Figure 6.18. Differences in initial costs for the 6-Story structures

6.2.2. Performance Assessment Results

Similar to the 3-Story structure, the IDA analysis was used for the analysis for achieving the performances of the 6-Structure. For performance evaluation of the structure, the PEER PBEE methodology is utilized.

6.2.2.1. Result of Probabilistic Demand Analysis

Three IM levels are selected with lower, medium, and higher intensities to compare the performance of the structures in terms of the median IDRs. The median, 16th and 84th percentile of the peak IDR and the resultant IDR from the 22 selected GM records are shown in Figure 6.5 for the two medium and higher IM levels. The related statistical parameters for the three selected IM levels are provided in Table B.1. From the figure, it can be observed that structures designed by the PBSD and the PPBOSD approaches satisfied LS and CP performance levels at the given medium and higher IM levels. However, the one designed by the Code-Based design approach did not satisfy the CP performance level at the higher IM level.

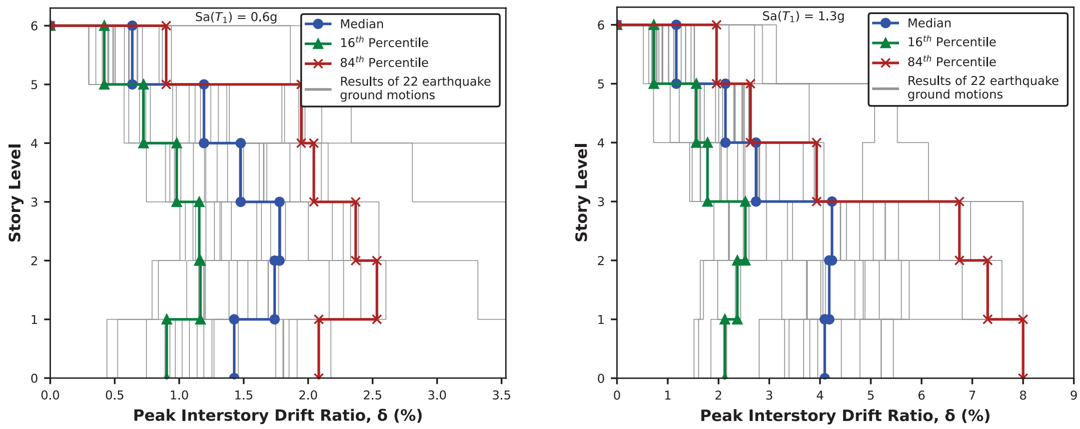

a) Code-Based

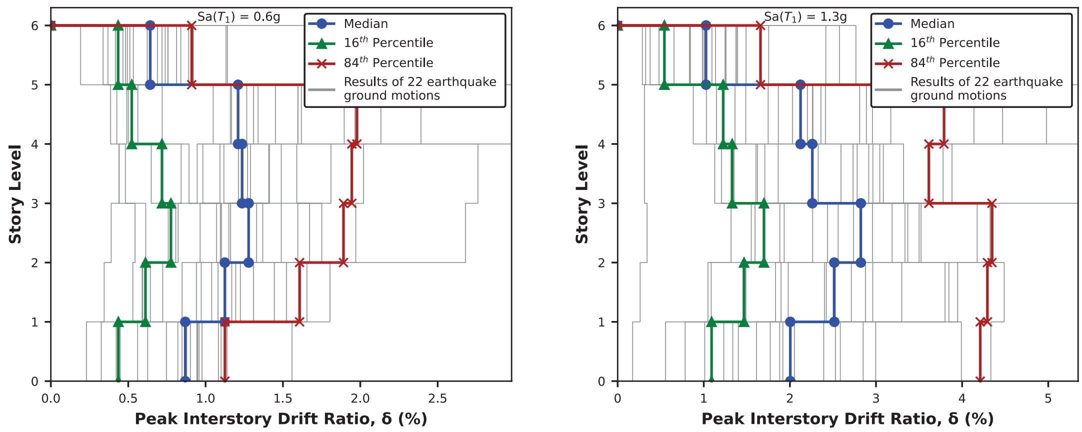

b) PBSD-Based

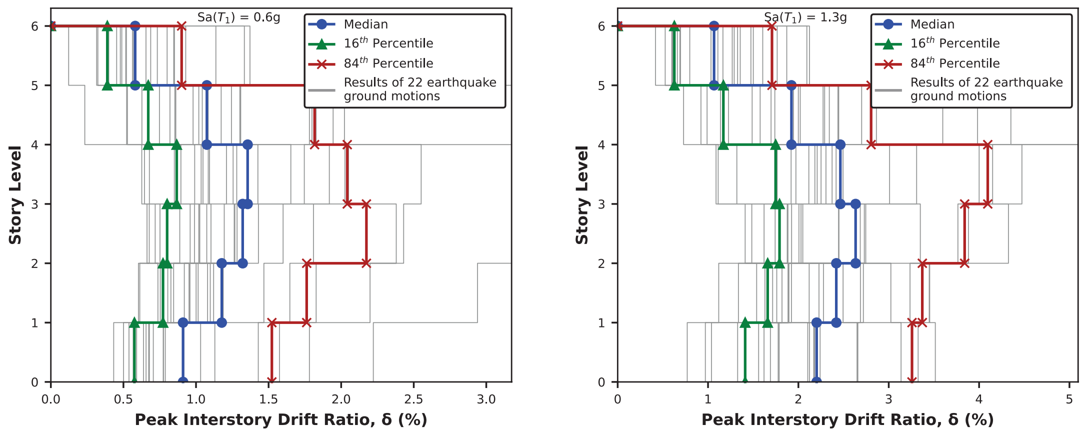

c) PPBOSD-Based

Figure 6.19. Peak IDRs for 6-Story frames corresponding to two different IM levels

The following statistical parameters are gained after using the linear relationship between ln(EDP) and ln(IM), which are just shown for the peak IDRs.

Table 6.4. IDRs of 6-Story frames corresponding to different IM levels after using the linear relationship between ln(EDP) and ln(IM)

IM Level Sa (T1)	Peak Interstory Drift Ratio, IDR (%)					
	$\mu_{ln(x)}$	μ_x	$\widehat{S}$	$\sigma_{ln(x)}$	16th Percentile	84th Percentile
Code-Based						
0.3	-0.1631	0.9677	0.8495	0.5105	0.5790	1.1928
0.6	0.6209	2.0999	1.8606	0.4920	1.2053	2.7948
1.3	1.2955	4.0757	3.6529	0.4680	2.2650	5.8151
PBSD-Based						
0.3	-0.1150	1.0268	0.8913	0.5319	0.5643	1.2857
0.6	0.6797	2.4663	1.9733	0.6678	1.1702	3.0245
1.3	1.2905	4.9046	3.6346	0.7742	2.0496	5.8370
PPBOSD-Based						
0.3	-0.0092	1.1946	0.9908	0.6115	0.6466	1.5263
0.6	0.6397	2.1324	1.8959	0.4848	1.2391	2.8997
1.3	1.3454	4.5873	3.8396	0.5965	2.5133	5.8270

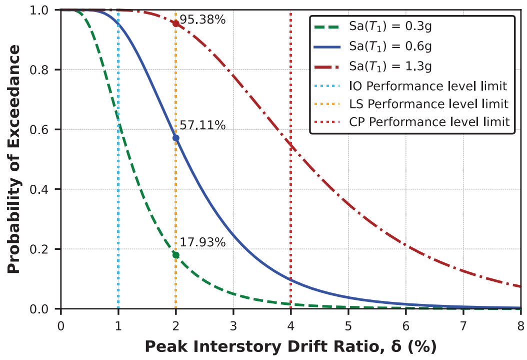

a) Code-Based

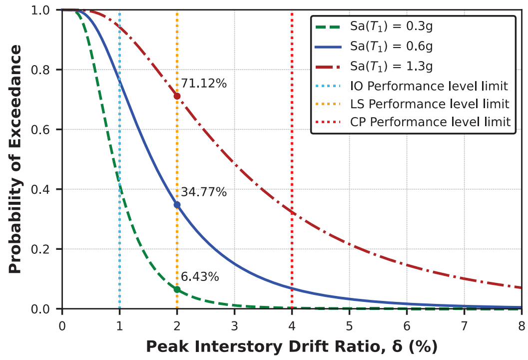

b) PBSD-Based

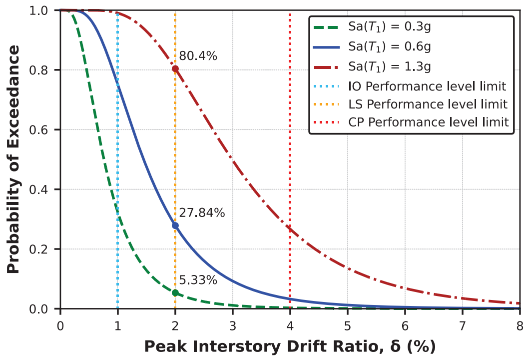

c) PPBOSD-Based

Figure 6.20. Probability of exceedance for peak IDRs of 6-Story frames at different IM levels

The probability of exceedance, together with the drift limits, are shown in Figure 6.20 at the selected three IM levels. The figure shows that the structure designed using the Code-Based design approach has the highest probability of exceedance at all selected

IM levels compared to the structures designed by the PBSD and the PPBOSD approaches. On the other hand, the structure designed by the PPBOSD approach has a lower probability of exceedance at the lower and medium IM levels, while it has a higher probability at the higher IM level compared to the structure designed using the PBSD approach. The reason is in the logarithmic standard deviation, which is higher in the case of the structure designed by the PBSD compared to the one designed by the PPBOSD approach (refer to Table 6.4).

The demand hazard curves obtained for the median, 16th, and 84th percentile are shown in the following figure. The comparison of the median demand hazard curves is also shown in the figure. From the comparison it can be observed that the structure designed using the PPBOSD approach has the lowest probability of exceedance at a specific IDR compared to the ones designed by Code-Based and PBSD approaches.

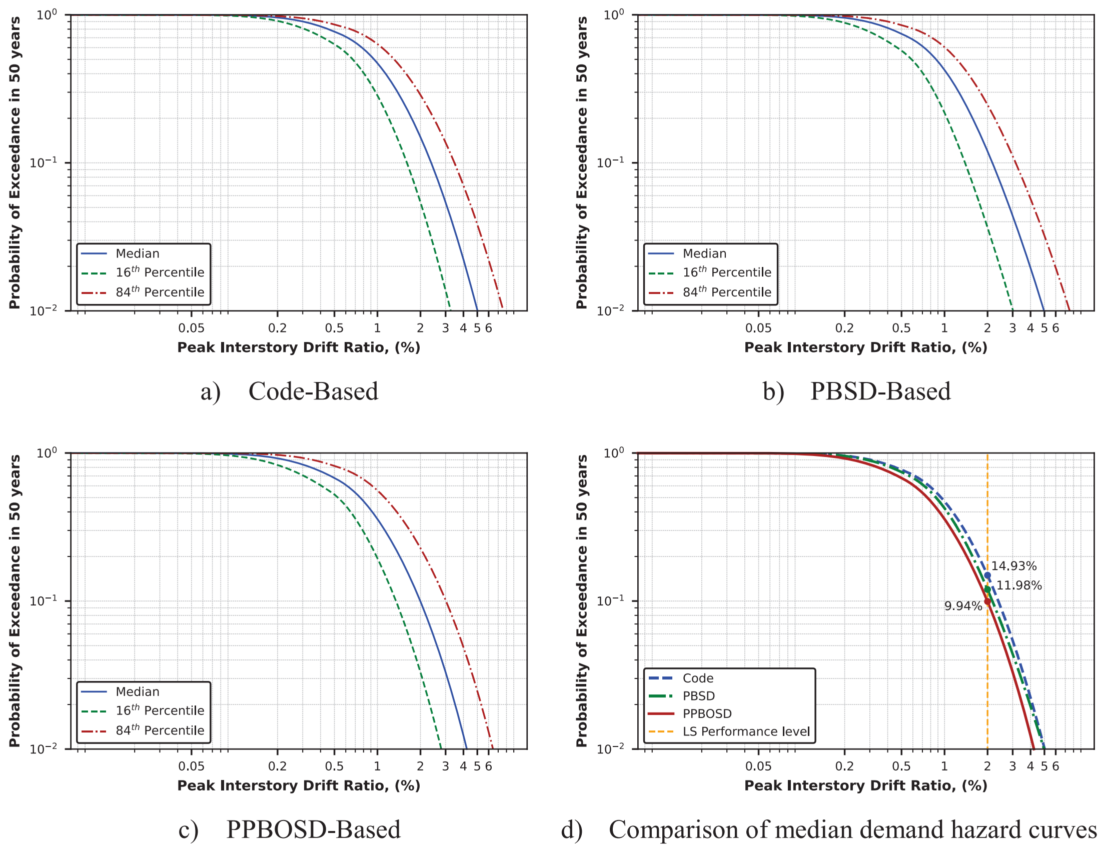

a) Code-Based

b) PBSD-Based

c) PPBOSD-Based

d) Comparison of median demand hazard curves

Figure 6.21. Demand hazard curves for 6-Story frames

The ET response curves for the 6-Story structures designed using different design approaches are shown in Figure 6.22 and Figure 6.23. The structure designed using the

PPBOSD approach performs well compared to the other two structures designed through Code-based design and the PBSD approaches, as shown in Figure 6.22.

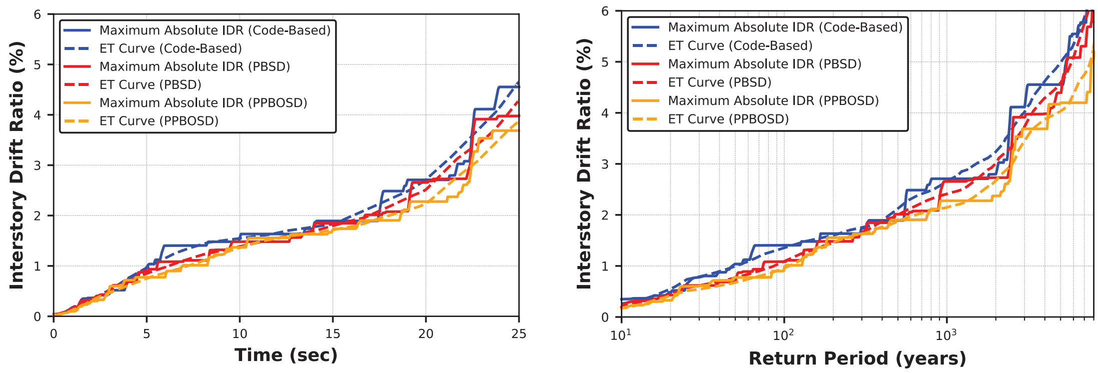

a) IDR vs ET time

b) IDR vs Return Period

Figure 6.22. ET response curves of the 6-Story frames

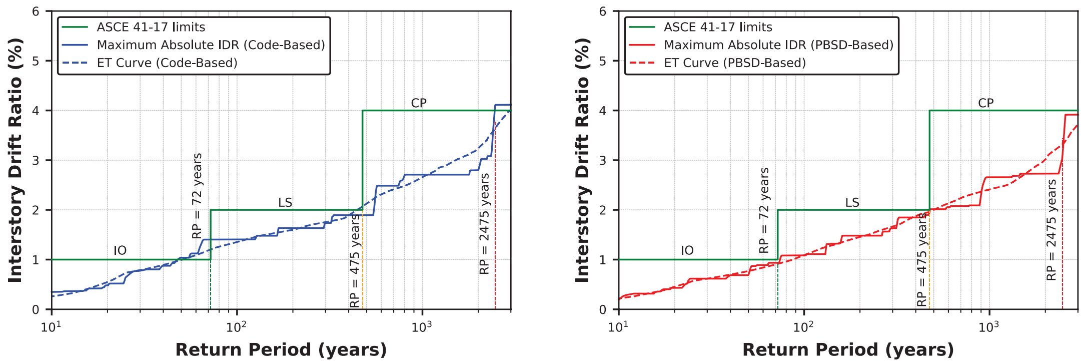

a) Code-Based

b) PBSD-Based

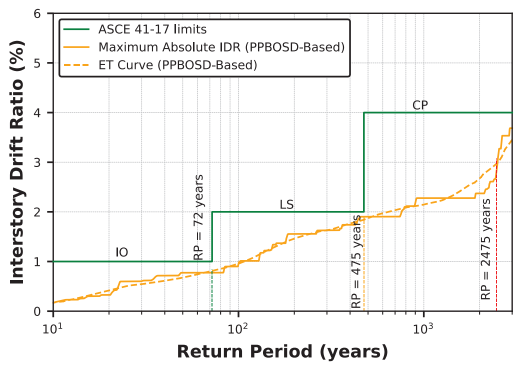

c) PPBOSD-Based

Figure 6.23. ET response curves of the 6-Story frames with IDR limits for different hazard levels

Furthermore, Figure 6.23 shows that the structure designed using the Code-based design approach does not meet the IO and LS performance levels. However, the structures designed using the PBSD and the PPBOSD approaches satisfied all performance levels.

6.2.2.2. Result of Probabilistic Damage Analysis

The fragility functions for three performance levels are obtained such that at least 50 percent of the GM records crossed the limit at each performance level. Then, they are fitted, and the results are provided in the following table and figure.

Table 6.5. Statistical parameters fitted fragility curves of 6-Story frames

Performance Level	Code-Based		PBSD-Based		PPBOSD-Based	
	$\widehat{S}_c$	β_{S_c}	$\widehat{S}_c$	β_{S_c}	$\widehat{S}_c$	β_{S_c}
IO	0.2345	0.6559	0.3458	0.6932	0.4040	0.5966
LS	0.5349	0.5722	0.8134	0.8219	0.8483	0.4805
CP	1.1327	0.4677	1.7280	0.4935	1.7764	0.5359

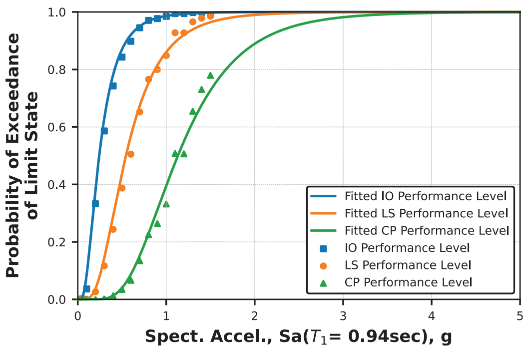

a) Code-Based

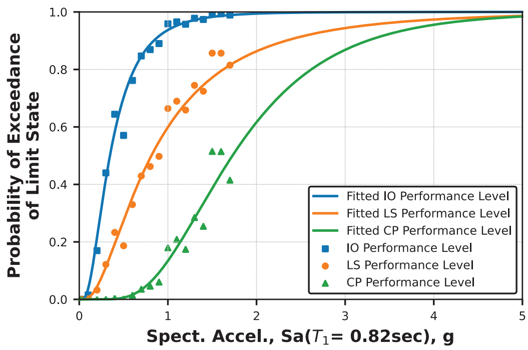

b) PBSD-Based

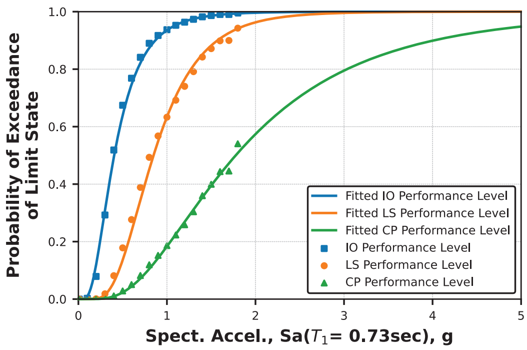

c) PPBOSD-Based

Figure 6.24. Fragility curves of 6-Story frames for different performance levels

The following figure shows that the structure designed with the conventional Code-Based design has the lowest performance. On the other hand, the ones designed through PBSD and the PPBOSD approaches are very close, except for the LS performance level. In this performance level, at lower intensities, the structure designed with the PPBOSD approach shows a lower probability of failure, while in higher intensities, it shows a high probability of failure compared to the structure designed through the PBSD approach, which is mainly due to the dispersion (refer to Table 6.5)

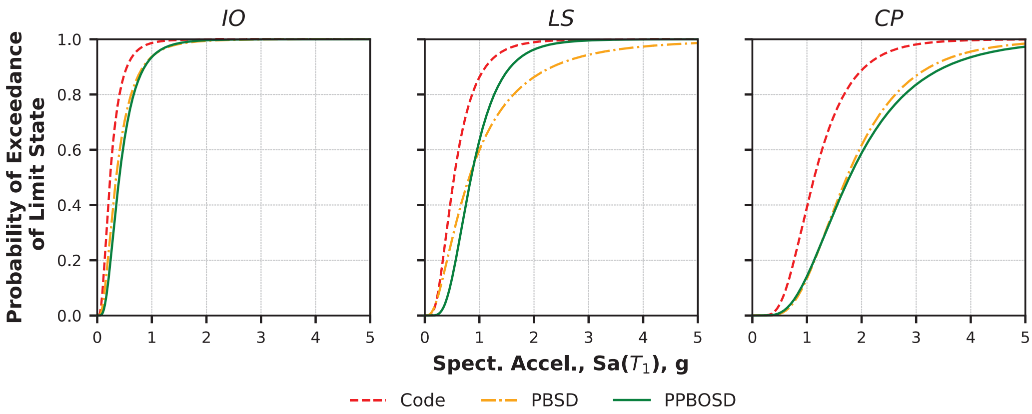

Figure 6.25. Comparison of fragility curves of 6-Story frames

From the above figure, it can be observed that the structure designed with the Code-Based design approach is the most vulnerable structure to seismic action. On the other hand, the structures designed using the PBSD and the PPBOSD approaches show almost similar vulnerability in IO and CP performance levels. However, they show different performance in the LS performance level. In the lower intensities, approximately up to Sa(T1) = 0.9g, the structure designed through the PBSD approach is vulnerable, while after that, the structure designed with the PPBOSD approach is more vulnerable. Since their medians are very close, the only reason for such an issue is due to the dispersion.

6.2.2.3. Result of Probabilistic Loss Analysis

The losses due to seismic action have been obtained at three different hazard levels with a mean return period of 72, 475, and 2475 years. As mentioned earlier, the replacement cost of the structure is estimated as 7.38 M$ and 0.1548 M$ for demolition cost of the 6-Story Structures. The estimated costs due to earthquakes are shown in the following figure.

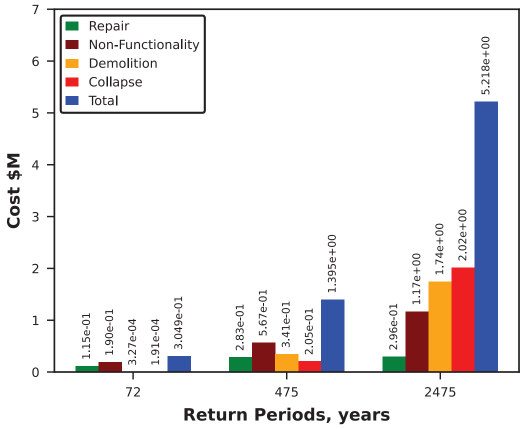

a) Code-Based

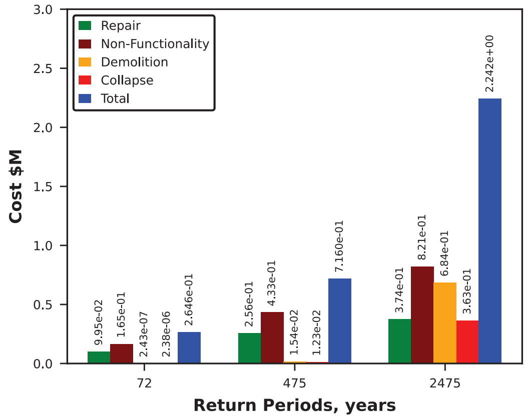

b) PBSD-Based

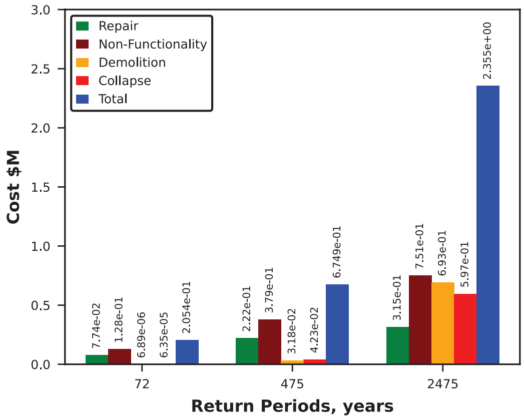

c) PPBOSD-Based

Figure 6.26. Disaggregated costs for three different hazard levels of 6-Story structures

In the above figure, the cost of the structure designed using the Code-Based design approach is the highest among the used approaches. On the other hand, as expected from the fragility functions, the PPBOSD approach gives lower cost at lower intensities, while in high intensities, the PBSD approach provides lower cost. A similar conclusion could be made regarding Figure 6.27, which compares the cost results at the same hazard levels for all structures.

Figure 6.28 shows the comparison of the losses in terms of cost at $Sa(T_1)$ =1.5g and the differences between these three approaches in percentage. At this intensity level, the PPBOSD approach has the lowest total loss.

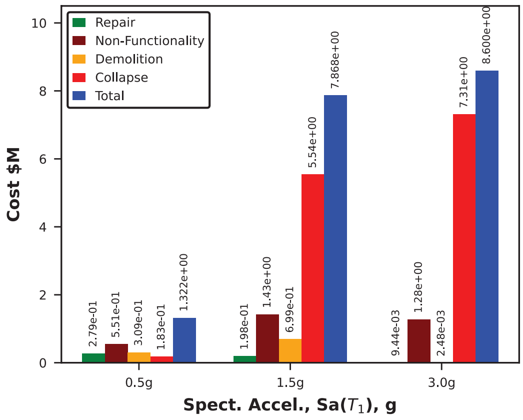

a) Code-Based

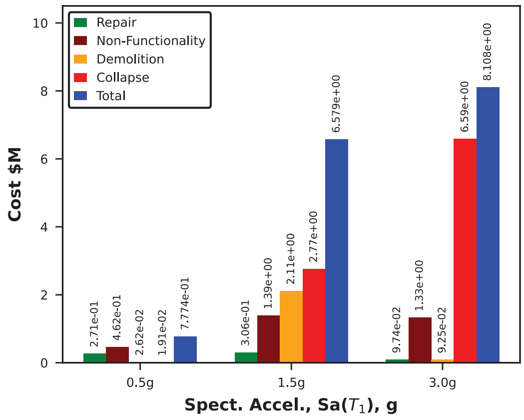

b) PBSD-Based

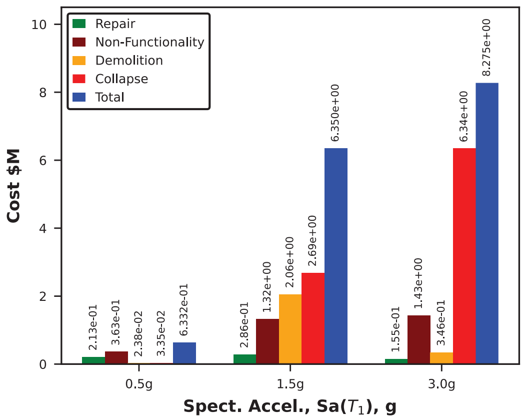

c) PPBOSD-Based

Figure 6.27. Disaggregated costs for three different IM levels of 6-Story structures

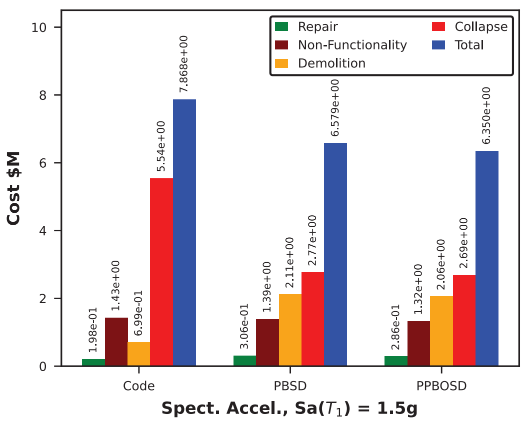

a) Costs

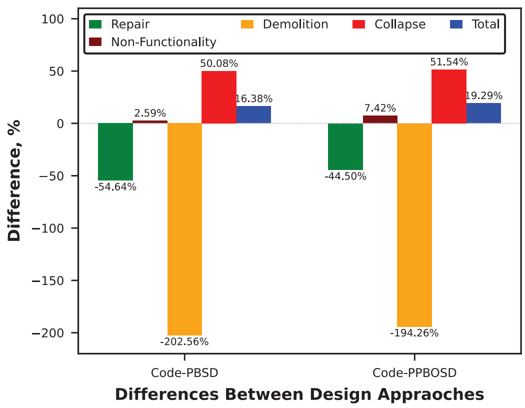

b) Differences in percentage

Figure 6.28. Comparison of Disaggregated costs at 1.5g for 6-Story structure

6.2.2.4. Result of Life Cycle Cost Analysis

The following figure shows the result of the LCCA at three different hazard levels. The figure shows the differences between the expected total cost of the structures designed using three different design approaches and the percentage difference.

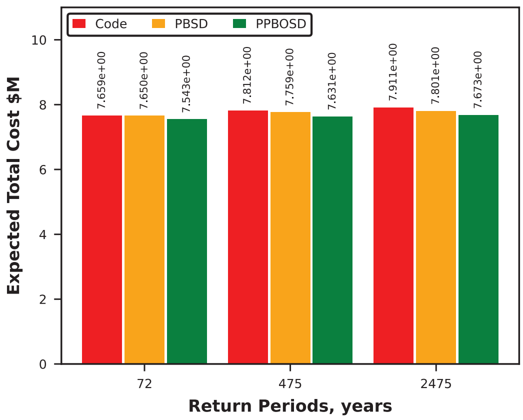

a) Expected total costs

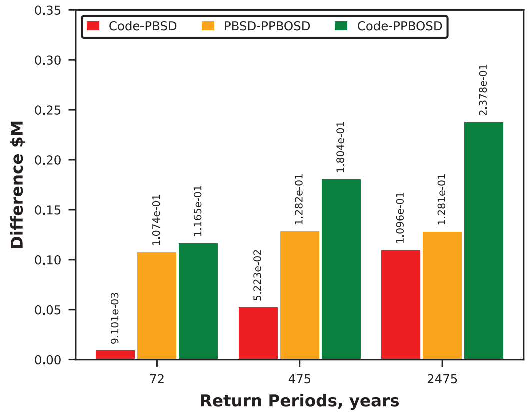

b) Differences

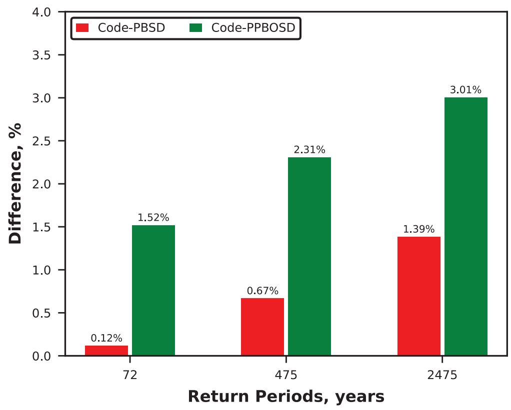

c) Differences in percentage

Figure 6.29. Expected total cost results at different hazard levels for 6-Story structures

From the above and Figure 6.18, it can be observed that with an increase of 0.411% in initial cost, a reduction of 3.01% is obtained in the expected total cost of the structure. In addition, in all three hazard levels, the LCC of the structure is lower for the frame designed based on the PPBOSD compared to the other two approaches.

6.2.3. Performance of the Structure in terms of Performance Point

The predicted performance of the structure in terms of the performance point is shown for all cases in Figure 6.30. The figure compares the resulting capacity curves of the structures and the performance points that are obtained for each case. In the figure, the limit for the LS performance level is also shown, and it is evident that the performance points are within the LS performance level. The figure also shows that the structure designed through the PPBOSD approach shows better performance regarding the capacity curve.

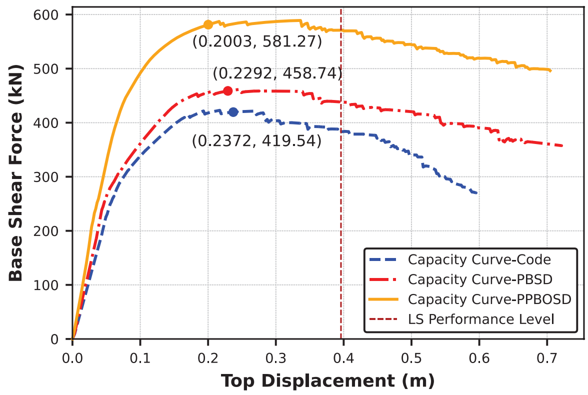

Figure 6.30. Performance points on capacity curves of the 6-Story frames

6.3. Results for 9-Story Structure

6.3.1. Optimization results

For the 9-Story structure, the cost per square meter per story level is assumed to be 5000\$, and 86\$/m^2 per floor is assumed for demolition. In addition, the replacement time is taken as 800 days, and the demolition time is considered to be 50 days. The following values are estimated, considering the assumed costs.

$$A_{total} = 20x15 = 300m^2$$

$$\Rightarrow \quad C_1 = 5000x300x9 = 13500000\$ = 13.5M\$$$

$$\Rightarrow \quad C_{Demolition} = 86x300x9 = 232200\$ = 0.2322M\$$$

The resulting optimum losses for structures designed using different design approaches are shown in the following figure for 9-Story structures. The corresponding cross-sections for each structure are provided in Appendix C. It should be noted that for each of the three stories same cross-sections are assigned both for columns and beams.

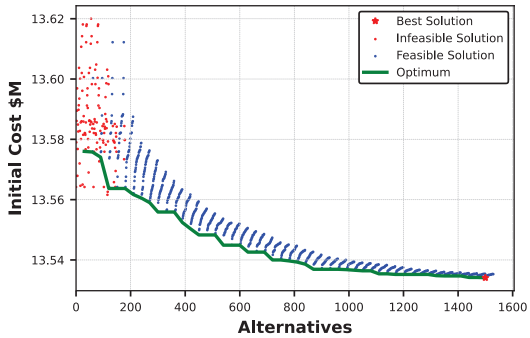

a) Code-Based

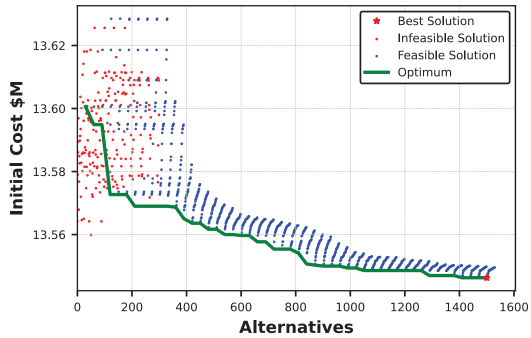

b) PBSD-Based

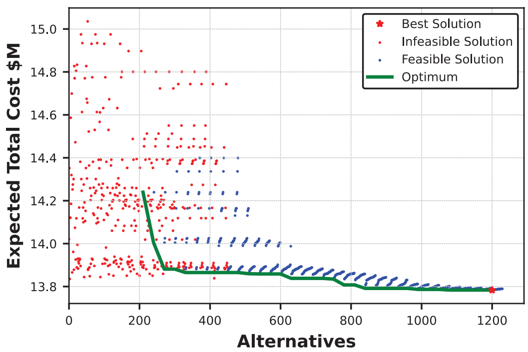

c) PPBOSD-Based

Figure 6.31. Optimum solution for 9-Story structures from different design approaches

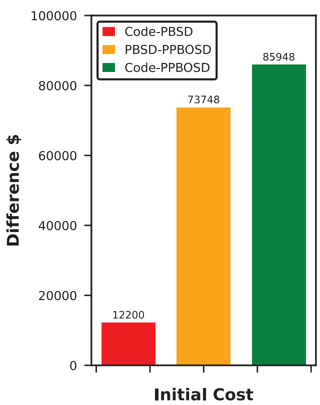

a) Difference

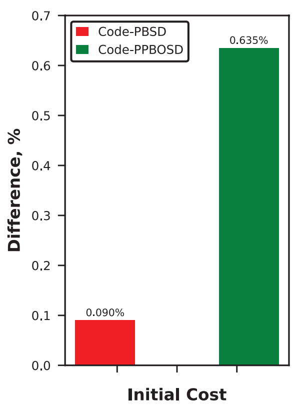

b) Differences in percentage

Figure 6.32. Differences in initial costs for the 6-story structure

The optimum initial cost value for the Code-Based design approach is 13.5341 \$M, while for the PBSD approach, it equals 13.5463 \$M. The optimum solution for the expected total cost of the structure attained using the PPBOSD approach is 13.78359 \$M, in which the portion of the initial cost is 13.62005 \$M. The differences among the initial costs are shown in the above figure.

6.3.2. Performance Assessment Results

After the optimum design has been obtained, the IDA method is utilized in the PEER PBEE methodology procedure to predict the performance of the structure.

6.3.2.1. Result of Probabilistic Demand Analysis

Similar to the other cases, three IM levels are selected with lower, medium, and higher intensities to compare the performance of the structures in terms of the median IDRs. The median, 16th and 84th percentile of the peak IDR and the resultant IDR from the 22 selected GM records are shown in Figure 6.33 for the two different IM levels. From the figure, it can be observed that all frames satisfied all performance levels at the selected IM levels.

The following statistical parameters are gained after using the linear relationship between ln(EDP) and ln(IM), which are just shown for the peak IDRs.

Table 6.6. IDRs of 9-Story frames corresponding to different IM levels after using the linear relationship between ln(EDP) and ln(IM)

IM Level Sa (T_1)	Peak Interstory Drift Ratio, IDR (%)					
	$\mu_{ln(x)}$	μ_x	$\widehat{S}$	$\sigma_{ln(x)}$	16th Percentile	84th Percentile
Code-Based						
0.3	-0.1691	1.0997	0.8444	0.7268	0.5221	1.3260
0.5	0.6451	2.3804	1.9062	0.6665	1.1254	3.1482
1.0	1.3457	4.4968	3.8410	0.5615	2.1793	6.6253
PBSD-Based						
0.3	0.0367	1.1854	1.0374	0.5164	0.6609	1.7006
0.5	0.6741	2.2325	1.9623	0.5079	1.2223	3.3504
1.0	1.3851	5.2712	3.9954	0.7445	2.4272	7.1386
PPBOSD-Based						
0.3	-0.2127	0.9187	0.8084	0.5058	0.5661	1.1354
0.5	0.4307	1.7678	1.5384	0.5273	1.0738	2.2386
1.0	1.3411	4.2190	3.8233	0.4438	2.6566	5.8503

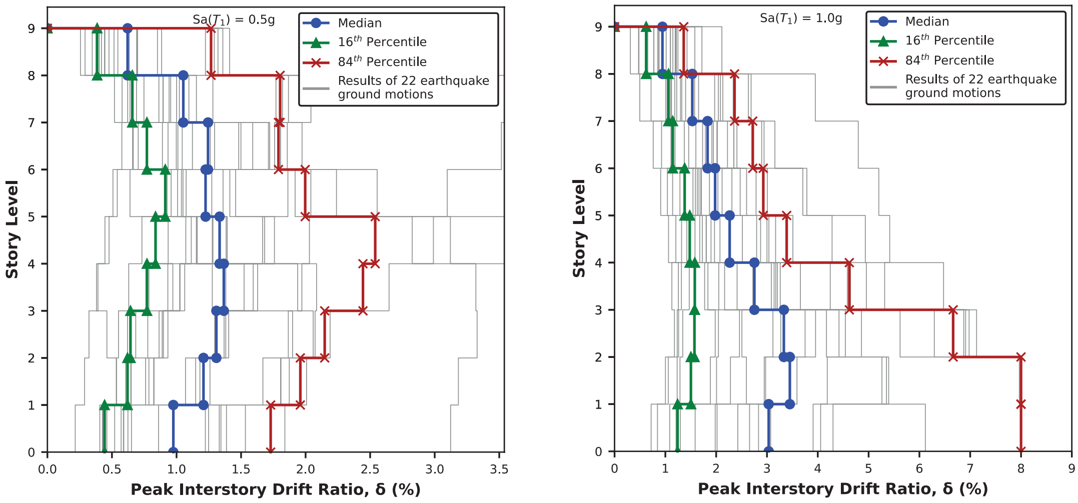

a) Code-Based

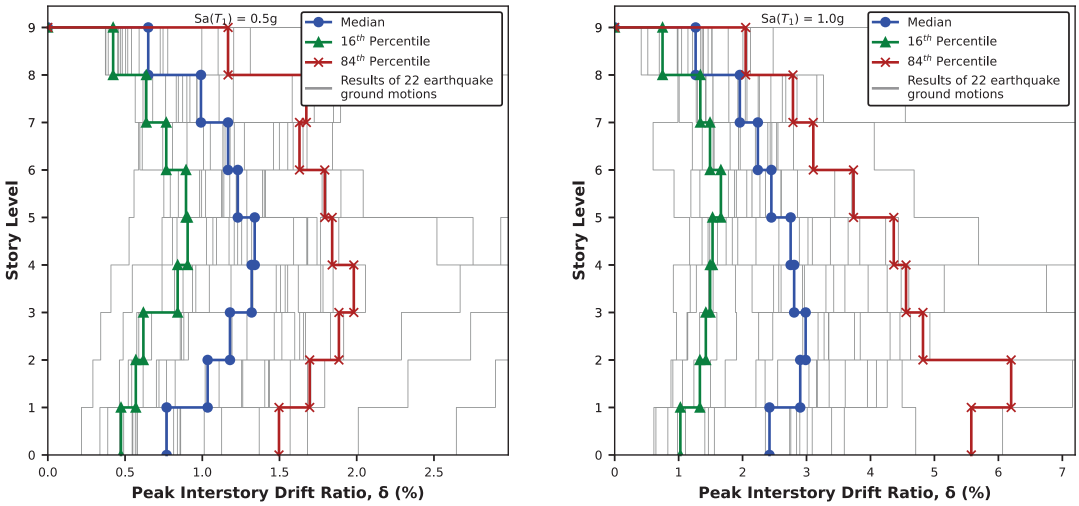

b) PBSD-Based

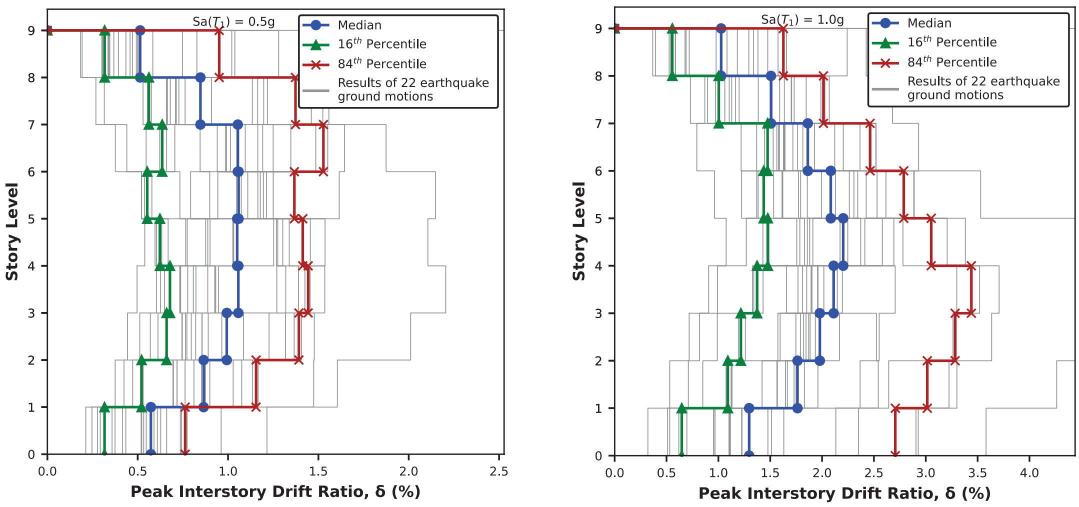

c) PPBOSD-Based

Figure 6.33. Peak IDRs for 9-Story frames corresponding to two different IM levels

The probability of exceedance, together with the drift limits, are shown in Figure 6.34 at three selected IM levels. The figure shows that the structure designed with respect to the PPBOSD approach has the lowest probability of exceedance in all IM levels compared to the ones designed using the Code-Based design and the PBSD approaches. In contrast, the structure designed by the Code-Based design approach has the highest probability of exceedance at all IM levels.

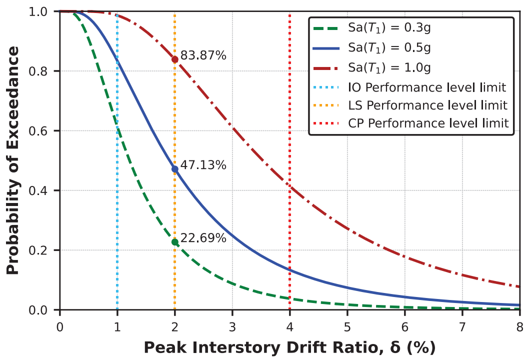

a) Code-Based

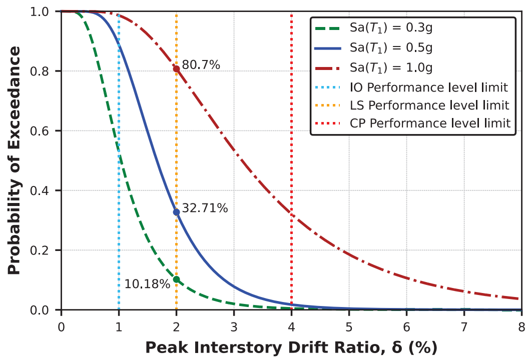

b) PBSD-Based

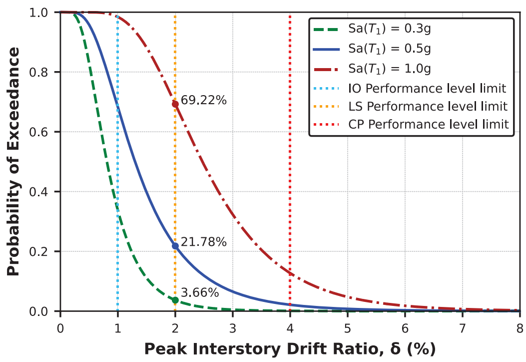

c) PPBOSD-Based

Figure 6.34. Probability of exceedance for peak IDRs of 9-Story frames at different IM levels

The demand hazard analysis results are shown in the following figures for all frames, designed through three different design approaches. The comparison of the median demand hazard curves is also shown in the figure. From the comparison it can be noticed that the structure designed using the PPBOSD approach has shown better performance compared to the ones designed by Code-Based and PBSD approaches.

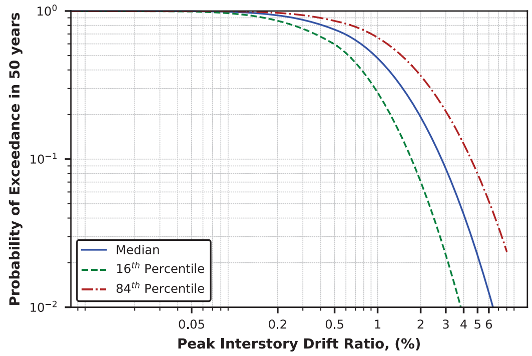

a) Code-Based

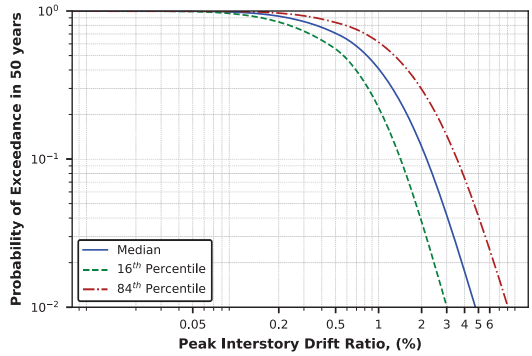

b) PBSD-Based

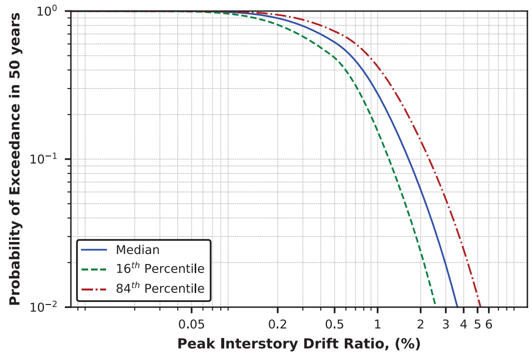

c) PPBOSD-Based

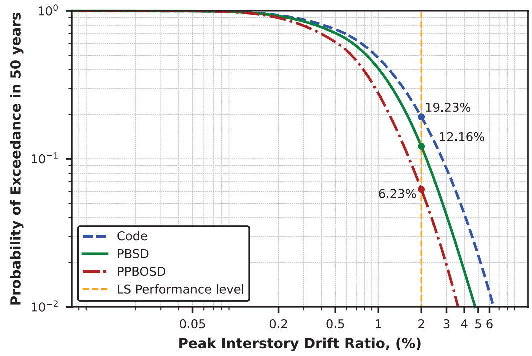

d) Comparison of median demand hazard curves

Figure 6.35. Demand hazard curves for 9-Story frames

The ET response curves for the 9-Story structures designed using different design approaches are shown in Figure 6.36 and Figure 6.37. In the lower intensities, all of the structures almost show the same performance, while in the higher intensities, the one designed with the PPBOSD approach provides better performance compared to others.

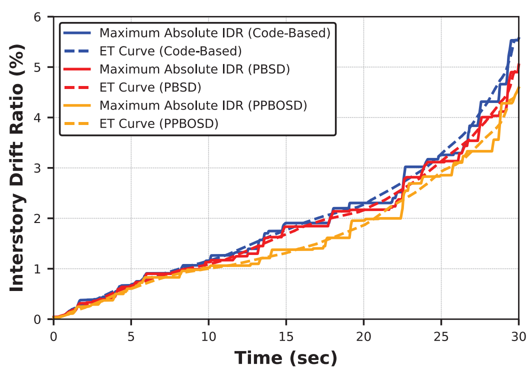

a) IDR vs ET time

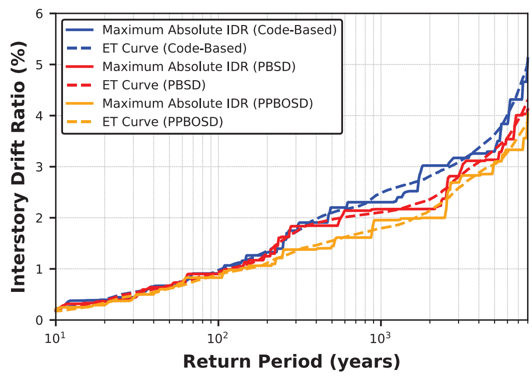

b) IDR vs Return Period

Figure 6.36. ET response curves of the 9-Story frames

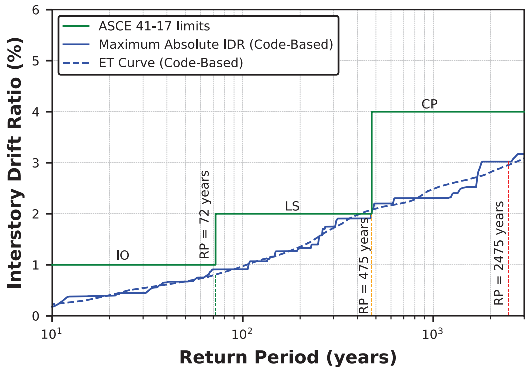

a) Code-Based

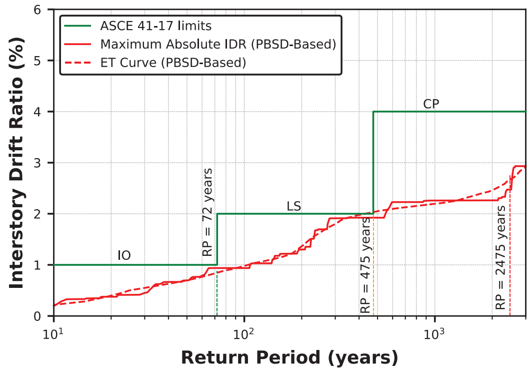

b) PBSD-Based

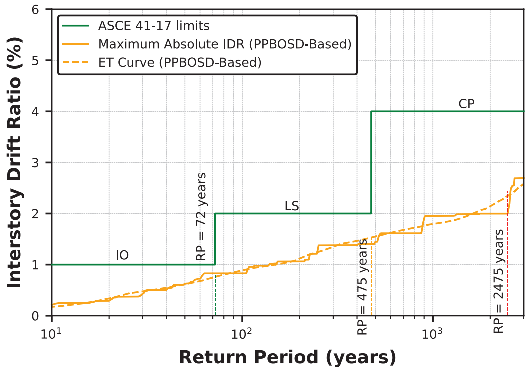

c) PPBOSD-Based

Figure 6.37. ET response curves of the 9-Story frames with IDR limits for different hazard levels

Figure 6.37 shows that the structure designed using the Code-based design approach violates only the IO performance level. However, the structures designed using the PBSD and the PPBOSD approaches satisfied all performance levels.

6.3.2.2. Result of Probabilistic Damage Analysis

The fragility functions for three performance levels are obtained such that at least 50 percent of the GM records crossed the limit at each performance level. Then, they are fitted, and the results are provided in Table 6.7 and Figure 6.38.

Figure 6.39 compares the fragility functions of the structure at different performance levels. From the figure, it is evident that the structure designed with the PPBOSD approach is the least vulnerable, while the one designed using conventional Code is the most vulnerable structure in terms of performance.

Table 6.7. Statistical parameters for fitted fragility curves of 9-Story frames

Performance Level	Code-Based		PBSD-Based		PPBOSD-Based	
	$\widehat{S}_c$	β_{S_c}	$\widehat{S}_c$	β_{S_c}	$\widehat{S}_c$	β_{S_c}
IO	0.2419	0.6974	0.2883	0.6352	0.3772	0.5890
LS	0.5278	0.6509	0.6125	0.5464	0.7952	0.4457
CP	1.1505	0.6305	1.3030	0.5795	1.6243	0.4338

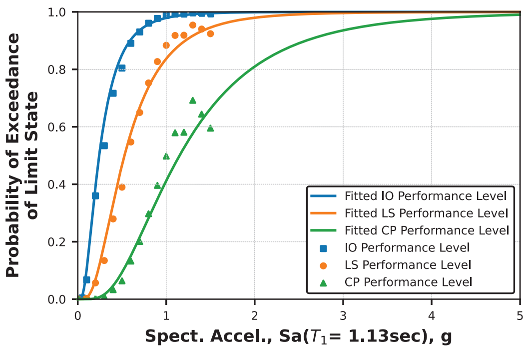

a) Code-Based

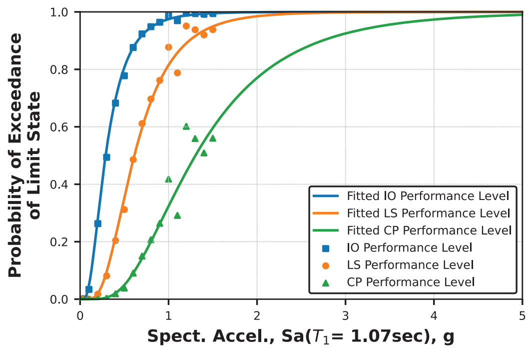

b) PBSD-Based

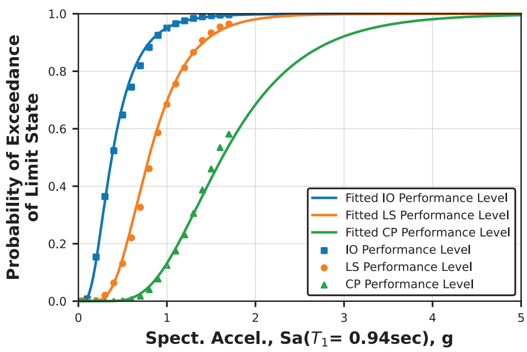

c) PPBOSD-Based

Figure 6.38. Fragility curves of 9-Story frames for different performance levels

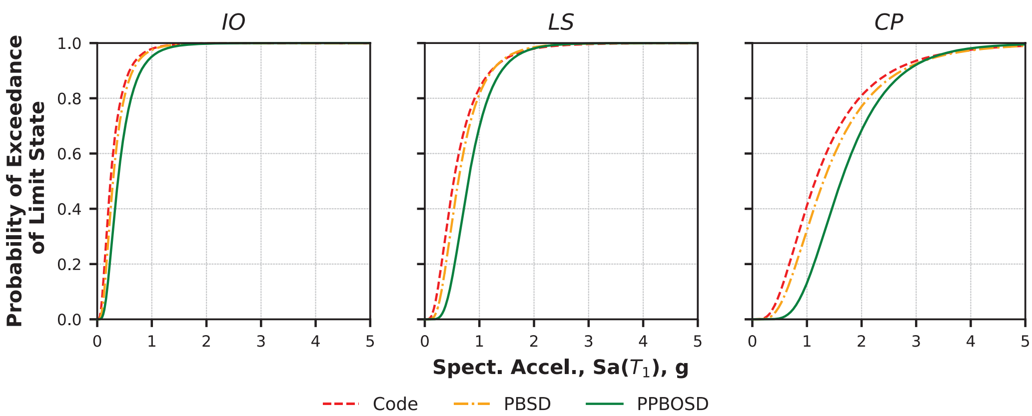

Figure 6.39. Comparison of fragility curves of 9-Story frames

6.3.2.3. Result of Probabilistic Loss Analysis

In this section, the results of the loss analysis that are obtained at different hazard levels are provided. The following figure shows the losses obtained at three hazard levels with a mean return period of 72, 475, and 2475 years. From this figure, it can be concluded the structure designed using the PPBOSD approach has the lowest loss at each hazard level compared to the structures designed using the other two design approaches.

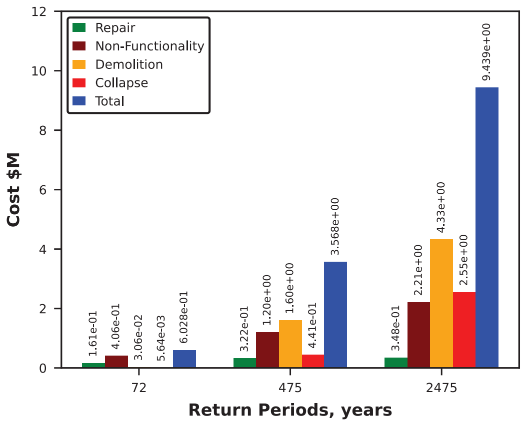

a) Code-Based

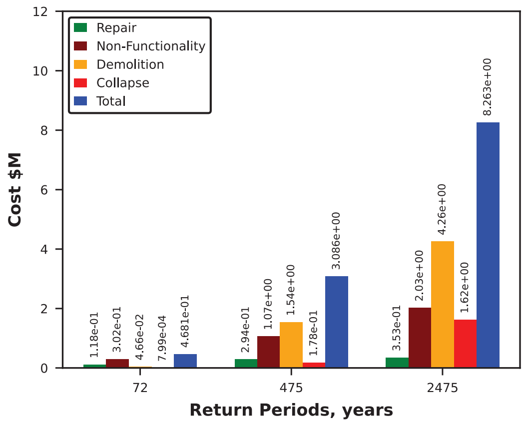

b) PBSD-Based

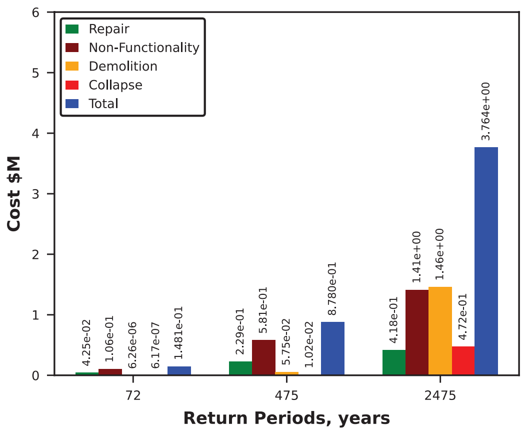

c) PPBOSD-Based

Figure 6.40. Disaggregated costs for three different hazard levels of 9-Story structures

To compare the results of the design approaches at the same IM levels, the resulting costs at three IM levels with Sa (T_1) = 0.5g, 1.5g, and 3.0g are shown for all structures in the following figure.

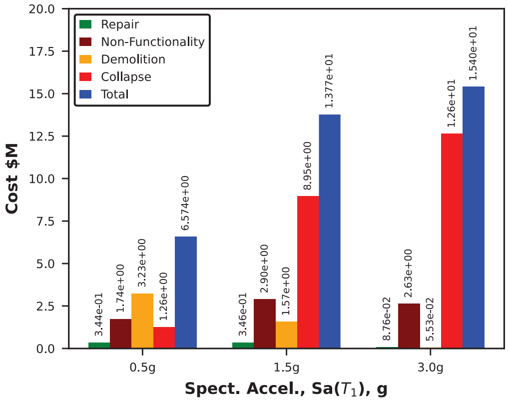

a) Code-Based

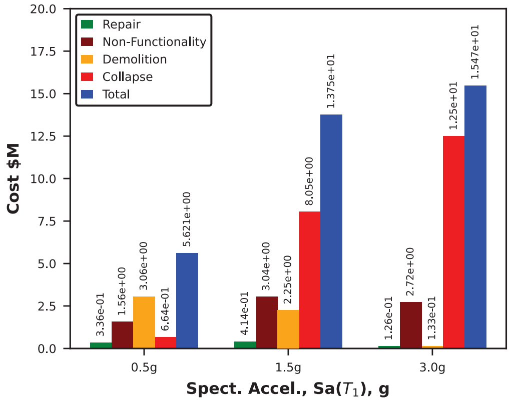

b) PBSD-Based

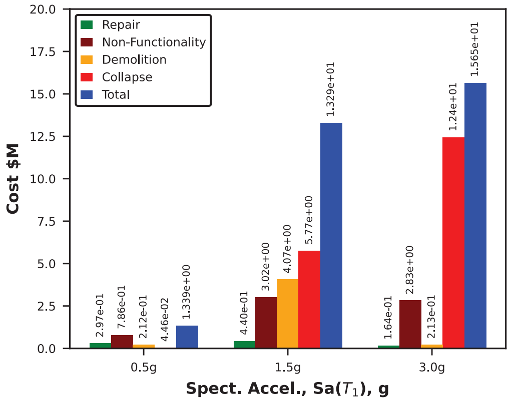

c) PPBOSD-Based

Figure 6.41. Disaggregated costs for three different IM levels of 9-Story structures

From the figure, it can be concluded that the PPBOSD approach gives the lowest total cost at all IM levels. In the following figure, the costs for all structures are shown in the same figure at $Sa(T_1)$ =1.5g, with their percentage differences.

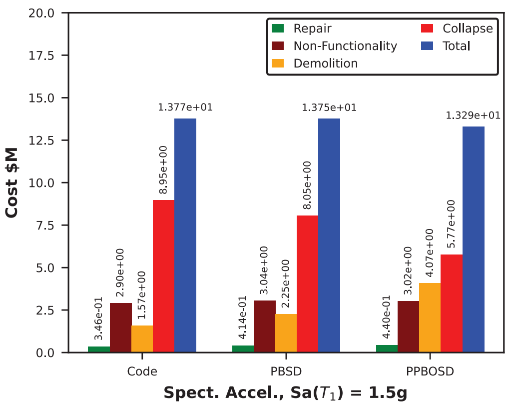

a) Costs

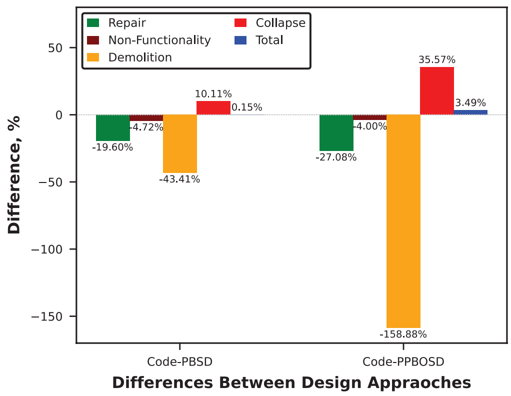

b) Differences in percentage

Figure 6.42. Comparison of Disaggregated costs at 1.5g for 9-Story structures

6.3.2.4. Result of Life Cycle Cost Analysis

The following figure shows the result of the LCCA at three different hazard levels. The figure shows the differences between the expected total cost of the structures designed using three different design approaches and the percentage difference.

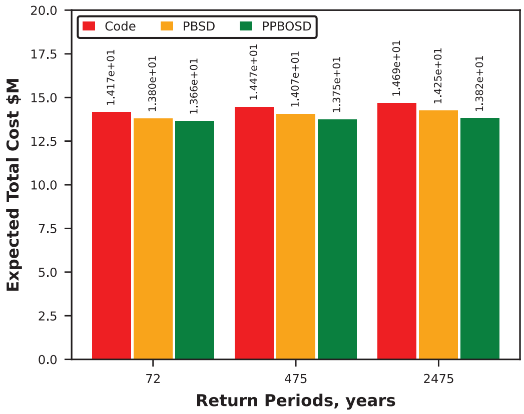

a) Expected total costs

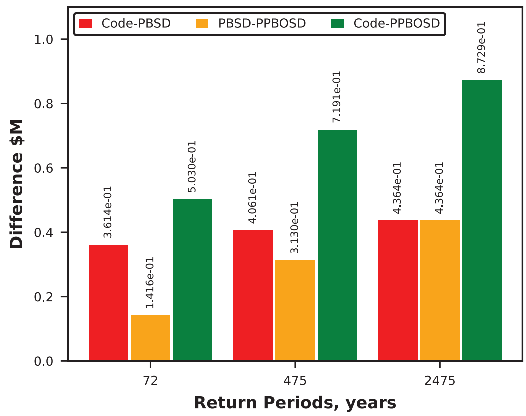

b) Differences

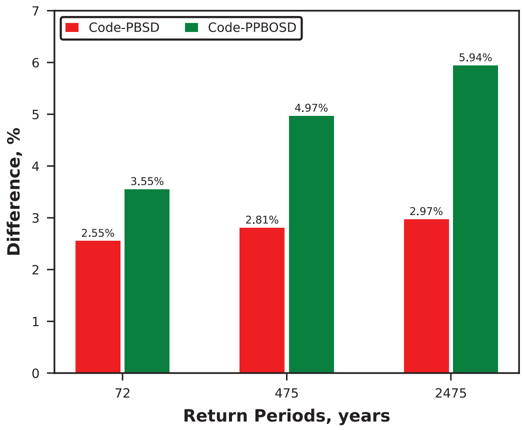

c) Differences in percentage

Figure 6.43. Expected total cost results at different hazard levels for 9-Story structures

From the above figure and Figure 6.32, it can be concluded that with an increase of 0.635% in initial cost, a reduction of 5.94% is obtained in the expected total cost. Further, in all three hazard levels, the expected total cost is lower for the structure designed with the PPBOSD than the ones designed with the other two approaches.

6.3.3. Performance of the Structure in terms of Performance Point

The predicted performance of the structure in terms of capacity curves and the performance points is shown for all cases in the following figure. The figure indicates that the structure designed using the PPBOSD is better in performance compared to other structures designed using the Code-Based and the PBSD approaches.

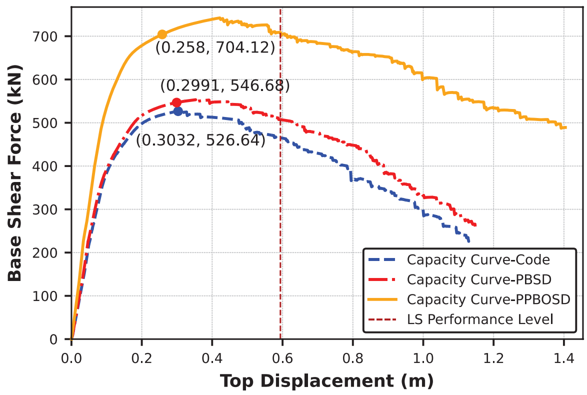

Figure 6.44. Performance points on the capacity curves of 9-Story frames

CHAPTER 7

CONCLUSIONS

Performance-Based Seismic Design (PBSD) is a new paradigm for seismic design of new structures and performance evaluation and retrofitting of the existing structures. It promises to design structures to satisfy not only the requirement of current seismic design codes but also to design structures that are very complicated to design or cannot be designed with more confidence using current practice. It provides structures that could satisfy different performance levels under various hazard levels. It can predict the risk in a quantifiable manner in terms of risk of casualties, occupancy interruption, and economic losses, which is more meaningful to the owners and stakeholders.

A Probabilistic Performance-Based Optimum Seismic Design (PPBOSD) method has been proposed in this study for designing RC structures. The methodology is first developed using a simple 2-Story RC structure and later applied to RC structures with different heights to check the effectiveness of the method. For application, 3-, 6-, and 9-Story RC structures are selected, consisting of special moment frames, which are the only lateral resisting systems. The same structures are designed using conventional Code-Based design and the PBSD approaches.

To solve the optimization problem, the GA has been conducted. For the cases of Code-Based design and the PBSD, the initial construction cost has been used as an objective function for the optimization problem. On the other hand, for the proposed methodology, the expected total cost is considered as an objective function. Code requirements are used as constraints for Code-Based design optimization. While for the PBSD and the PPBOSD approaches, in addition to the code requirements, the criteria of the PBSD is also considered as constraint, such as IDR limits for specific hazard levels. In the optimization process for the PBSD and PPBOSD approaches, the ET method is used because it reduces the computational time significantly. Once the optimum design has been obtained, then the IDA method is used while evaluating the performance of the structure. For the performance evaluation, the PEER PBEE methodology has been implemented.

The overall results showed that the structures designed using the PPBOSD approach performed well compared to the others. The performances of the structures are compared in different aspects. For example, their performances are compared in terms of median demand hazard curves, fragility functions, costs at different IM levels, expected total costs at different hazard levels, etc. The comparison of median demand hazard curves showed that in all cases, the structures designed with the PPBOSD approach presented better performance except for the 2-Story structure, which showed almost similar performance to the one designed using the PBSD approach.

In addition, fragility functions showed that the structures designed using the Code-Based design approach are more vulnerable than those designed using the PBSD and the PPBOSD approaches. For 2-Story, the fragility functions of the structures, designed with respect to the PBSD and PPBOSD, are almost the same for IO and LS performance levels. In addition, 6-Story structures designed based on the PBSD and the PPBOSD approaches showed almost the same vulnerability for CP performance level at lower intensities, while in higher intensities, the vulnerabilities are different. Further, for IO performance level the structure designed using the PBSD approach is a little bit more vulnerable compared to the one designed by the PPBOSD approach. Furthermore, for LS performance levels at lower intensities, approximately at $Sa(T_1)$ =0.9g, the structure designed using the PBSD is more vulnerable, while after that intensity, the structure designed using the PPBOSD approach is more vulnerable. For 3-Story and 9-Story structures, in all cases, the structures designed by the PPBOSD approach showed better performance than those designed with the other two design approaches.

The following table shows the $Sa(T_1)$ values for different hazard levels obtained from the hazard curves corresponding to each structure. The hazard curves shown in Figure 3.7 are for some limited periods; however, the available hazard curves are up to 7.5 sec. The hazard curve for a structure is obtained using interpolation for the fundamental period of the structure. In the following table, the values of $Sa(T_1)$ in some cases are the same, which is due to the fact that for those cases, the fundamental periods of the structures are close to each other. The other reason is that when the probability of the hazard level of interest falls between two probabilities of the interpolated hazard curve, the closest value is considered from the interpolated hazard curve. From this table and the tables related to fragility functions in each case, it can be concluded that all structures satisfied all performance levels for corresponding hazard levels.

Table 7.1. $Sa(T_1)$ values for different hazard levels corresponding to different structures

Structure	Hazard Level (MRP)	$Sa(T_1)$		
		Code	**PBSD**	**PPBOSD**
2-Story	**72**	0.42	0.42	0.42
	475	0.89	0.89	0.89
	2475	1.44	1.44	1.44
3-Story	**72**	0.28	0.35	0.35
	475	0.64	0.78	0.78
	2475	1.19	1.27	1.27
6-Story	**72**	0.21	0.22	0.28
	475	0.51	0.52	0.64
	2475	0.88	0.90	1.08
9-Story	**72**	0.14	0.14	0.19
	475	0.36	0.36	0.47
	2475	0.66	0.66	0.83

MRP = Mean Return Period

Moreover, the costs of the structures were also compared at three hazard levels given in Table 7.1 and three IM levels with $Sa(T_1)$ = 0.5g, 1.5g, and 3.0g. The results showed that in most cases, the structure designed with the PPBOSD approach gave the lowest total cost compared to the ones designed through conventional code and the PBSD approach. Further, the expected total costs at three hazard levels were also obtained for each case, and the results were compared. The comparison showed that the lowest expected total costs were attained for the structures designed using the PPBOSD.

In addition, the performances of the structures were compared in terms of the capacity curves and the performance points as well. The capacity curves showed that the structures designed through the PPBOSD approach have the highest strength and are capable of dissipating much energy compared to the structures designed by the Code-Based design and the PBSD approaches. In addition, the performance points on the capacity curves showed that the structures designed using the PPBOSD approach have the lowest displacements while they have the highest base shear forces.

The methodology could be extended for the dual wall frame structures and also for the structures considering soil interaction effects. The soil interaction effects could be considered for frame only structures and dual wall frame structures. In addition, maintenance costs, injuries, and fatalities could also be included in the methodology. Furthermore, the methodology could be applied to high-rise buildings to check the effectiveness of the methodology.

REFERENCES

ACI 318-19. (2019). Building Code Requirements for Structural Concrete (ACI 318-19). In *American Concrete Institute*. https://doi.org/10.14359/51716937

Alabama, H. (2019). *Life-cycle considerations in risk-informed decisions for energy-efficiency building design under various hazard exposures and climate conditions*. Alabama.

Amouzegar, H., & Riahi, H. T. (2015). Seismic assessment of concrete frames by endurance time method. *Proceedings of the Institution of Civil Engineers: Structures and Buildings*, *168*(8), 578–592. https://doi.org/10.1680/stbu1400042

Andrzej S. Nowak, & Collins, K. R. (2013). *Reliability of Structures* (2nd ed.). CRC Press, Taylor & Francis Group.

Ang, A. H.-S., & Tang, W. H. (2007). *Probability Concepts in Engineering Emphasis on Applications in Civil & Environmental Engineering* (2nd ed.). John Wiley & Sons. Inc.

Arora, J. singh. (2017). Introduction to Optimum Design. In *Introduction to Optimum Design* (4th ed.).

ASCE/SEI-41-06. (2007). Seismic Rehabilitation of Existing Buildings. In *ASCE Standard*.

ASCE/SEI-41-17. (2017). Seismic Evaluation and Retrofit of Existing Buildings. In *ASCE Standard*. https://doi.org/10.1061/9780784414859

Aslani, H., & Miranda, E. (2005). Probability-based seismic response analysis. *Engineering Structures*, *27*(8), 1151–1163. https://doi.org/10.1016/j.engstruct.2005.02.015

ATC-13. (1985). *Earthquake damage evaluation data for California*. Applied Technology Council, Redwood City, CA.

ATC-40. (1996). Seismic Evaluation and Retrofit of Existing Concrete Buildings. In *Applied Technology Council* (Vol. 1). Vol. 1. Applied Technology Council, Redwood City, California. Report No. SSC 96-01. November 1996.

Azarbakht, A., & Dolsek, M. (2007). Prediction of the median IDA curve by employing a limited number of ground motion records. *EARTHQUAKE ENGINEERING & STRUCTURAL DYNAMICS*, *36*(15), 2401–2421. https://doi.org/DOI: 10.1002/eqe.740 Prediction

Baker, J. W. (2008). An introduction to Probabilistic Seismic Hazard Analysis (PSHA). *Baker Research Group*, 1–72.

Baker, J. W., & Cornell, C. A. (2005). *Vector-Valued Ground Motion Intensity Measures for Probabilistic Seismic Demand Analysis* (Issue September).

Basim, M. C., & Estekanchi, H. E. (2015). Application of endurance time method in performance-based optimum design of structures. *Structural Safety*, *56*, 52–67. https://doi.org/10.1016/j.strusafe.2015.05.005

Basim, M., Estekanchi, H. E., & Vafai, A. (2016). A methodology for value based seismic design of structures by the endurance time method. *Scientia Iranica*, *23*(6), 2514–2527. https://doi.org/10.24200/sci.2016.2310

Bazeos, N. (2009). Comparison of three seismic design methods for plane steel frames. *Soil Dynamics and Earthquake Engineering*, *29*(3), 553–562. https://doi.org/10.1016/j.soildyn.2008.06.005

Benedetti, a, Landi, L., & Malavolta, D. (2008). on the Design and Evaluation of Seismic Response of Rc Buildings According To Direct Displacement-Based Design Approach. *The 14th World Conference on Earthquake Engineering*.

Carreño, R., Lotfizadeh, K. H., Conte, J. P., & Restrepo, J. I. (2020). Material Model Parameters for the Giuffrè-Menegotto-Pinto Uniaxial Steel Stress-Strain Model. *Journal of Structural Engineering*, *146*(2), 04019205. https://doi.org/10.1061/(ASCE)st.1943-541x.0002505

Cavazzuti, M. (2013). Optimization Methods: From Theory to Design. In *Springer-Verlag Berlin Heidelberg*. https://doi.org/10.1007/978-3-642-31187-1

Chan, C. M., & Zou, X. K. (2004). Elastic and inelastic drift performance optimization for reinforced concrete buildings under earthquake loads. *Earthquake Engineering and Structural Dynamics*, *33*(8), 929–950. https://doi.org/10.1002/eqe.385

Chiara, F., Giovanni, L., Maria, D. A., Rodolfo, P., Lucia, L., & Francesca, P. (2018). Ground motion model for reference rock sites in Italy. *Soil Dynamics and*

Earthquake Engineering, *110*(August 2017), 276–283. https://doi.org/10.1016/j.soildyn.2018.01.024

Chousianitis, K., Del Gaudio, V., Pierri, P., & Tselentis, G. A. (2018). Regional ground-motion prediction equations for amplitude-, frequency response-, and duration-based parameters for Greece. *Earthquake Engineering and Structural Dynamics*, *47*(11), 2252–2274. https://doi.org/10.1002/eqe.3067

Cornell, C. A., Banon, H., & Shakal, A. F. (1979). Seismic motion and response prediction alternatives. *Earthquake Engineering & Structural Dynamics*, *7*(4), 295–315. https://doi.org/10.1002/eqe.4290070402

Cornell, C. A., Jalayer, F., Hamburger, R. O., & Foutch, D. A. (2002). Probabilistic Basis for 2000 SAC Federal Emergency Management Agency Steel Moment Frame Guidelines. *Journal of Structural Engineering*, *128*(4), 526–533. https://doi.org/10.1061/(ASCE)0733-9445(2002)128:4(526)

Cornell, C. A., & Krawinkler, H. (2000). Progress and Challenges in Seismic Performance Assessment. *PEER Center News*, *3*(2), 1–4.

Corriou, J.-P. (2021). *Numerical Methods and Optimization, Theory and Practice for Engineers*. Springer Nature Switzerland AG. https://doi.org/10.1007/978-3-030-89366-8

Deierlein, G. G. (2004). Overview of a comprehensive framework for earthquake performance assessment. *Performance-Based Seismic Design Concepts and Implementation Proceedings of an International Workshop, June 28*, 15–26.

Douglas, J. (2019). Ground Motion Prediction Equations. In *SED Report SED/ENSI/R/01/20140911*.

Dowrick, D. J. (1985). Preliminary Field Observations of the Chilean Earthquake of 3 March 1985. *Bulletin of the New Zealand National Society for Earthquake Engineering*, *18*(2), 119–127. https://doi.org/10.5459/bnzsee.18.2.119-127

Elenas, A., & Meskouris, K. (2001). Correlation study between seismic acceleration parameters and damage indices of structures. *Engineering Structures*, *23*(6), 698–704. https://doi.org/10.1016/S0141-0296(00)00074-2

Elkady, A., & Lignos, D. G. (2020). EaRL—Software for Earthquake Risk, Loss and Lifecycle Analysis. *SoftwareX*, *12*. https://doi.org/10.1016/j.softx.2020.100607

Ellingwood, B. R. (2008). Structural reliability and performance-based engineering. *Proceedings of the Institution of Civil Engineers: Structures and Buildings*, *161*(4), 199–207. https://doi.org/10.1680/stbu.2008.161.4.199

Ellingwood, B. R., & Wen, Y. K. (2005). Risk-benefit-based design decisions for low-probability/high consequence earthquake events in Mid-America. *Progress in Structural Engineering and Materials*, *7*(2), 56–70. https://doi.org/10.1002/pse.191

Estekanchi, H. E., Harati, M., & Mashayekhi, M. R. (2018). An investigation on the interaction of moment-resisting frames and shear walls in RC dual systems using endurance time method. *Structural Design of Tall and Special Buildings*, *27*(12), 1–16. https://doi.org/10.1002/tal.1489

Estekanchi, H. E., Mashayekhi, M., Vafai, H., Ahmadi, G., Mirfarhadi, S. A., & Harati, M. (2020). A state-of-knowledge review on the endurance time method. *Structures*, *27*, 2288–2299. https://doi.org/10.1016/j.istruc.2020.07.062

Estekanchi, H. E., Vafai, A., & Riahi, H. T. (2009). Endurance Time Method: From ideation to Application. *US-Iran Seismic Workshop*, 205–218.

Estekanchi, H. E., Valamanesh, V., & Vafai, A. (2007). Application of Endurance Time method in linear seismic analysis. *Engineering Structures*, *29*(10), 2551–2562. https://doi.org/10.1016/j.engstruct.2007.01.009

FEMA-227. (1992). *A Benefit-Cost Model for the Seismic Rehabilitation of Buildings*. Federal Emergency Management Agency, Building Seismic Safety Council Washington DC.

FEMA-273. (1997). *NEHRP Guidelines for the Seismic Rehabilitation of Buildings*. Federal Emergency Management Agency: Washington, DC, USA. October 1997.

FEMA-274. (1997). NEHRP Commentary on the Guidelines for the Seismic Rehabilitation of Buildings. *Federal Emergency Management Agency, Washington, DC, Developed by the Applied Technology Council*, *October*.

FEMA-356. (2000). Prestandard and Commentary for the Seismic Rehabilitation of Buildings. In *Report FEMA-356, Washington, DC*. American Society of Civil Engineers.

FEMA-389. (2004). *Risk Management Series, Primer for Design Professionals: Communicating with Owners and Managers of New Buildings on Earthquake Risk*. Federal Emergency Management Agency: Washington, DC, USA. January 2004.

FEMA-440. (2005). *Improvement of nonlinear static seismic analysis procedures.* Federal Emergency Management Agency.

FEMA-445. (2006). *Next-Generation Performance-Based Seismic Design Guidelines: Program Plan for New and Existing Buildings*. Prepared for Federal Emergency Management Agency: Washington, DC, USA by Applied Technology Council, August 2006.

FEMA-P-58-1. (2018). Seismic performance assessment of buildings: Volume 1 – Methodology. In *Buildings*.

FEMA-P-58-2. (2018). *Seismic Performance Assessment of Buildings: Volume 2 – Implementation Guide*. https://doi.org/10.3390/buildings11100440

FEMA-P695. (2009). Quantification of building seismic performance factors. In *Fema P695*. Federal Emergency Management Agency.

Field, E. H., Jordan, T. H., & Cornell, C. A. (2003). OpenSHA: A developing community-modeling environment for seismic hazard analysis. *Seismological Research Letters*, *74*(4), 406–419. https://doi.org/10.1785/gssrl.74.4.406

Foley, C. M., Pezeshk, S., & Alimoradi, A. (2007a). Probabilistic Performance-Based Optimal Design of Steel Moment-Resisting Frames . I : Formulation. *Journal of Soft Computing in Civil Engineering*, *133*(6), 757–766. https://doi.org/10.1061/(ASCE)0733-9445(2007)133:6(757)

Foley, C. M., Pezeshk, S., & Alimoradi, A. (2007b). Probabilistic Performance-Based Optimal Design of Steel Moment-Resisting Frames . I : Formulation. *Journal of Structural Engineering*, *133*(6), 757–766. https://doi.org/10.1061/(ASCE)0733-9445(2007)133:6(757)

Fragiadakis, M., Lagaros, N. D., & Papadrakakis, M. (2006). Performance-based multiobjective optimum design of steel structures considering life-cycle cost. *Structural and Multidisciplinary Optimization*, *32*(1), 1–11. https://doi.org/10.1007/s00158-006-0009-y

Fragiadakis, M., & Papadrakakis, M. (2008). Performance-based optimum seismic design of reinforced concrete structures. *Earthquake Engineering and Structural Dynamics*, *37*(6), 825–844. https://doi.org/10.1002/eqe.786 Performance-based

Franchin, P., Petrini, F., & Mollaioli, F. (2018). Improved risk-targeted performance-based seismic design of reinforced concrete frame structures. *Earthquake Engineering and Structural Dynamics*, *47*(1), 49–67. https://doi.org/10.1002/eqe.2936

Frangopol, D. M. (1986). Computer-automated design of structural systems under reliability-based performance constraints. *Engineering Computations*, *3*(2), 109–115. https://doi.org/10.1108/eb023648

Ganzerli, S., Pantelides, C. P., & Reaveley, L. D. (2000). Performance-based design using structural optimization. *Earthquake Engineering and Structural Dynamics*, *29*(11), 1677–1690. https://doi.org/10.1002/1096-9845(200011)29:11<1677::AID-EQE986>3.0.CO;2-N

Giuffrè, A. (1970). II comportamento del cemento armato per sollecitazioni cicliche di forte intensità. *Giornale Del Genio Civile*.

Goldberg, D. E. (1989). *Genetic algorithms in search, optimization, and machine learning*. Addison-Wesley Publishing Company, Inc.

Günay, S., & Mosalam, K. M. (2013). PEER performance-based earthquake engineering methodology, revisited. *Journal of Earthquake Engineering*, *17*(6), 829–858. https://doi.org/10.1080/13632469.2013.787377

Gutenberg, B., & Richter, F. (1944). Frequency of earthquakes in California. *Bulletin of the Seismological Society of America*, *25*(1), 1935. https://doi.org/10.1785/BSSA0340040185

Hamburger, R., Rojahn, C., Moehle, J., Bachman, R., Comartin, C., & Whittaker, A. (2004). The ATC-58 Project: Development of Next-Generation Performance-Based Earthquake Engineering Design Criteria for Buildings. *13th World Conference on Earthquake Engineering*, August 1-6.

Hancock, J., & Bommer, J. J. (2007). Using spectral matched records to explore the influence of strong-motion duration on inelastic structural response. *Soil Dynamics and Earthquake Engineering*, *27*(4), 291–299. https://doi.org/10.1016/j.soildyn.2006.09.004

Harati, M., Mashayekhi, M., Ashoori Barmchi, M., & Estekanchi, H. (2019). Influence of Ground Motion Duration on the Structural Response at Multiple Seismic Intensity Levels. *Numerical Methods in Civil Engineering*, *3*(4), 10–23. https://doi.org/10.29252/nmce.3.4.10

Hariri-Ardebili, M. A., Sattar, S., & Estekanchi, H. E. (2014). Performance-based seismic assessment of steel frames using endurance time analysis. *Engineering Structures*, *69*, 216–234. https://doi.org/10.1016/j.engstruct.2014.03.019

HAZUS-MR4. (2003). *Multi-hazard Loss Estimation Methodology*.

Holland, J. H. (1992). *Adaptation in natural and artificial systems: an introductory analysis with applications to biology, control, and artificial intelligence*. MIT Press.

J Moehle, & GG Deierlein. (2004). A framework methodology for performance-based earthquake engineering. *13Th World Conference on Earthquake Engineering*, *August 1-6*. https://www.researchgate.net/publication/228706335

Jones, S. J., McKenna, R. F., Tillotson, J., & Jordaan, I. J. (1991). Ice-Structure Interaction: IUTAM/IAHR Symposium St. John’s, Newfoundland Canada 1989. In *Springer Science & Business Media*. https://doi.org/10.1007/978-3-642-84100-2

Judd, J. P., & Charney, F. A. (2014). Earthquake risk analysis of structures. *Proceedings of the International Conference on Structural Dynamic , EURODYN*, *2014-Janua*(July), 2929–2938.

Karimzada, N. A. (2015). *Performance-Based Seismic Design of Reinforced Concrete Frame Buildings: A Direct Displacement-Based Approach* [İzmir Institute of Technology]. http://openaccess.iyte.edu.tr/handle/11147/4333

Karimzada, N. A., & Aktaş, E. (2016). Performance-Based Seismic Design of Reinforced Concrete Frame Buildings: A Direct Displacement-Based Approach. *12 International Congress on Advances in Civil Engineering*, *21-23 September*, *Boğaziçi University*, *Istabul*, *Turkiye*.

Karimzada, N. A., Shirkhani, A., & Aktaş, E. (2024). Application of Endurance Time Method in Seismic Assessment of RC Frames Designed by Direct Displacement-Based Procedure. *Turkish Journal of Civil Engineering*, *35*(2). https://doi.org/10.18400/tjce.1239730

Karsan, I. D., & Jirsa, J. O. (1969). Behavior of concrete under compressive loadings. *Journal of the Structural Division*, *95*(12), 2543–2564.

Kaveh, A., Kalateh-Ahani, M., & Fahimi-Farzam, M. (2014). Life-cycle cost optimization of steel moment-frame structures: Performance-based seismic design approach. *Earthquake and Structures*, *7*(3), 271–294. https://doi.org/10.12989/eas.2014.7.3.271

Kaveh, A., Laknejadi, K., & Alinejad, B. (2012). Performance-based multi-objective optimization of large steel structures. *Acta Mechanica*, *223*(2), 355–369. https://doi.org/10.1007/s00707-011-0564-1

Khalilian, M., Shakib, H., & Basim, M. C. (2021). On the optimal performance-based seismic design objective for steel moment resisting frames based on life cycle cost. *Journal of Building Engineering*, *44*. https://doi.org/10.1016/j.jobe.2021.103091

Khatibinia, M., Salajegheh, E., Salajegheh, J., & Fadaee, M. J. (2013). Reliability-based design optimization of reinforced concrete structures including soil-structure interaction using a discrete gravitational search algorithm and a proposed metamodel. *Engineering Optimization*, *45*(10), 1147–1165. https://doi.org/10.1080/0305215X.2012.725051

Kim, S., Moon, T., & Kim, S. J. (2020). Effect of Uncertainties in Material and Structural Detailing on the Seismic Vulnerability of RC Frames Considering Construction Quality Defects. *Applied Sciences (Switzerland)*, *10*(24). https://doi.org/10.3390/app10248832

Konovalov, A. V., Manaychev, K. A., Stepnov, A. A., & Gavrilov, A. V. (2019). Regional Ground Motion Prediction Equation for Sakhalin Island. *Seismic Instruments*, *55*(1), 70–77. https://doi.org/10.3103/s0747923919010080

Kramer, S. L. (1996). *Geotechnical Earthquake Engineering*. Prentice-Hall.

Krawinkler, H. (1996). A few basic concepts for performance based seismic design. *Eleventh World Conference on Earthquake Engineering*.

Lagaros, N. D., Garavelas, A. T., & Papadrakakis, M. (2008). Innovative seismic design optimization with reliability constraints. *Computer Methods in Applied Mechanics and Engineering*, *198*(1), 28–41. https://doi.org/10.1016/j.cma.2007.12.025

Lagaros, N. D., & Papadrakakis, M. (2007). Seismic design of RC structures: A critical assessment in the framework of multi-objective optimization. *Pacific Conference on Earthquake Engineering*, *36*(12), 1623–1639. https://doi.org/10.1002/eqe.707

Laouami, N., Slimani, A., & Larbes, S. (2018). Ground motion prediction equations for Algeria and surrounding region using site classification based H/V spectral ratio. *Bulletin of Earthquake Engineering*, *16*(7), 2653–2684. https://doi.org/10.1007/s10518-018-0310-3

Lee, T., & Mosalam, K. M. (2006). Probabilistic Seismic Evaluation of Reinforced Concrete Structural Components and Systems. In *Pacific Earthquake Engineering Research Center*. University of California.

Li, G., & Cheng, G. (2001). Optimal decision for the target value of performance-based structural system reliability. *Structural and Multidisciplinary Optimization*, *22*(4), 261–267. https://doi.org/10.1007/s00158-001-0147-1

Li, Y. (2014). *Probabilistic performance-based optimum seismic design of seismic isolation for california high-speed rail prototype bridge*. University of California, San Diego.

Li, Y., & Conte, J. P. (2018). Probabilistic performance-based optimum design of seismic isolation for a California high-speed rail prototype bridge. *Earthquake Engineering and Structural Dynamics*, *47*(2), 497–514. https://doi.org/10.1002/eqe.2976

Li, Y., Conte, J. P., & Gill, P. E. (2019). Probabilistic performance-based optimum seismic design framework: Illustration and validation. *CMES - Computer Modeling in Engineering and Sciences*, *120*(3), 517–543. https://doi.org/10.32604/cmes.2019.06269

Liu, M., Burns, S. A., & Wen, Y. K. (2005). Multiobjective optimization for performance-based seismic design of steel moment frame structures. *Earthquake Engineering and Structural Dynamics*, *34*(3), 289–306. https://doi.org/10.1002/eqe.426

Mackie, K. R., & Stojadinovi´, B. (2007). Performance-based seismic bridge design for damage and loss limit states. *EARTHQUAKE ENGINEERING & STRUCTURAL DYNAMICS*, *36*(13), 1953–1971. https://doi.org/10.1002/eqe.699

Mackie, K. R., & Stojadinović, B. (2005). *Fragility Basis for California Highway Overpass Bridge Seismic Decision Making*. PEER Repor No. 2005/02, Department of Civil and Environmental Engineering University of California, Berkeley, Pacific Earthquake Engineering Research Center.

Mander, J. B., Priestley, M. J. N., & Park, R. (1988). Observed Stress-Strain Behavior of Confined Concrete. *Journal of Structural Engineering*, *114*(8), 1827–1849. https://doi.org/10.1061/(ASCE)0733-9445(1988)114:8(1827)

Mashayekhi, M., Estekanchi, H. E., Vafai, A., & Mirfarhadi, S. A. (2018a). Simulation of Cumulative Absolute Velocity Consistent Endurance Time Excitations. *Journal of Earthquake Engineering*, *25*(5), 892–917. https://doi.org/10.1080/13632469.2018.1540371

Mashayekhi, M., Estekanchi, H. E., & Vafai, H. (2019). Simulation of Endurance Time Excitations via Wavelet Transform. *Iranian Journal of Science and Technology - Transactions of Civil Engineering*, *43*(3), 429–443. https://doi.org/10.1007/s40996-018-0208-y

Mashayekhi, M., Estekanchi, H. E., Vafai, H., & Mirfarhadi, S. A. (2018b). Development of hysteretic energy compatible endurance time excitations and its application. *Engineering Structures*, *177*(April), 753–769. https://doi.org/10.1016/j.engstruct.2018.09.089

Mashayekhi, M., Harati, M., Darzi, A., & Estekanchi, H. E. (2020). Incorporation of strong motion duration in incremental-based seismic assessments. *Engineering Structures*, *223*(July), 111144. https://doi.org/10.1016/j.engstruct.2020.111144

Mashayekhi, M., Harati, M., & Estekanchi, H. E. (2019). Development of an alternative PSO-based algorithm for simulation of endurance time excitation functions. *Engineering Reports*, *1*(3), 1–15. https://doi.org/10.1002/eng2.12048

McKenna, F. (2011). OpenSees: A framework for earthquake engineering simulation. *Computing in Science and Engineering*, *13*(4), 58–66. https://doi.org/10.1109/MCSE.2011.66

Menegotto, M., & Pinto, P. E. (1973). Method of Analysis for Cyclically Loaded R. C. Plane Frames Including Changes in Geometry and Non-Elastic Behavior of Elements under Combined Normal Force and Bending. *Proceedings of IABSE Symposium on Resistance and Ultimate Deformability of Structures Acted on by Well Defined Loads*, 15–22.

Messac, A. (2015). *Optimization in Practice with MATLAB®: For Engineering Students and Professionals*. Cambridge University Press.

Miano, A., Jalayer, F., & Prota, A. (2016). Cloud to IDA: A very efficient solution for performing incremental dynamic analysis. *Lecture Notes in Civil Engineering*, *10*(April 2017), 355–368. https://doi.org/10.1007/978-3-319-78936-1_26

Mirfarhadi, S. A., & Estekanchi, H. E. (2020). Value based seismic design of structures using performance assessment by the endurance time method. *Structure and Infrastructure Engineering*, *16*(10), 1397–1415. https://doi.org/10.1080/15732479.2020.1712436

Mitrani-Reiser, J. (2007). *An ounce of prevention: probabilistic loss estimation for performance-based earthquake engineering*. California Institute of Technology.

Mitropoulou, C. C., & Lagaros, N. D. (2016). Life-cycle cost model and design optimization of base-isolated building structures. *Frontiers in Built Environment*, *2*(November), 1–15. https://doi.org/10.3389/fbuil.2016.00027

Mitropoulou, C. C., Lagaros, N. D., & Papadrakakis, M. (2011). Life-cycle cost assessment of optimally designed reinforced concrete buildings under seismic actions. *Reliability Engineering and System Safety*, *96*(10), 1311–1331. https://doi.org/10.1016/j.ress.2011.04.002

Mohammadi, R. K., & Sharghi, A. H. (2014). On the optimum performance-based design of eccentrically braced frames. *Steel and Composite Structures*, *16*(4), 357–374. https://doi.org/10.12989/scs.2014.16.4.357

Moharrami, H., & Grierson, D. E. (1993). Computer-Automated Design of Reinforced Concrete Frameworks. *Journal of Structural Engineering*, *119*(7), 2036–2058. https://doi.org/10.1061/(ASCE)0733-9445(1993)119:7(2036)

Möller, O., Foschi, R. O., Ascheri, J. P., Rubinstein, M., & Grossman, S. (2015). Optimization for performance-based design under seismic demands, including social costs. *Earthquake Engineering and Engineering Vibration*, *14*(2), 315–328. https://doi.org/10.1007/s11803-015-0025-2

Mukhopadhyaya, A. K. (2009). *Value Engineering Mastermind: From Concept to Value Engineering Certification*. SAGE Publications India.

NEHRP. (2009). *Research Required to Support Full Implementation of Performance-Based Seismic Design*. Prepared for The National Institute of Standards and Technology Building and Fire Research Laboratory Gaithersburg, Maryland 20899-8600 by The Building Seismic Safety Council of The National Institute of Building Sciences Washington, DC 20005. NIST GCR 09.

Neuenhofer, A., & Filippou, F. C. (1997). Evaluation of Nonlinear Frame Finite-Element Models. *Journal of Structural Engineering*, *123*(7), 958–966. https://doi.org/10.1061/(ASCE)0733-9445(1997)123:7(958)

Nguyen, D. D., & Lee, T. H. (2018). Seismic fragility curves of bridge piers accounting for ground motions in Korea. *IOP Conference Series: Earth and Environmental Science*, *143*(1). https://doi.org/10.1088/1755-1315/143/1/012029

Padalu, P. K. V. R., & Surana, M. (2023). An Overview of Performance-Based Seismic Design Framework for Reinforced Concrete Frame Buildings. *Iranian Journal of Science and Technology - Transactions of Civil Engineering*. https://doi.org/10.1007/s40996-023-01217-4

Petrini, F. (2009). *A probabilistic approach to Performance-Based Wind Engineering (PBWE)* (Issue March). Università degli Studi di Roma.

Popovics, S. (1973). A Numerical Approach to the Complete Stress-Strain Curve of Concrete. *Cement and Concrete Research*, *3*(5), 583–599. https://doi.org/10.1016/0008-8846(73)90096-3

Porter, K. (2020). *A Beginner's Guide to Fragility, Vulnerability, and Risk*.

Priestley, M. J. N. (2000). Performance based seismic design. *Bulletin of the New Zealand Society for Earthquake Engineering*, *33*(3), 325–346. https://doi.org/10.5459/bnzsee.33.3.325-346

Priestley, M. J. N., & Kowalsky, M. J. (2000). Direct Displacement-Based Seismic Design of Concrete Buildings. *Bulletin of the New Zealand Society for Earthquake Engineering*, *33*(4), 421–444. https://doi.org/10.5459/bnzsee.33.4.421-444

Rai, M., ElGawady, M. A., & Rodriguez-Marek, A. (2019). Probabilistic seismic demand analysis of a bridge with unbonded, post-tensioned, concrete-filled, fiber-reinforced polymer tube columns. *Fibers*, *7*(3), 1–23. https://doi.org/10.3390/FIB7030023

Raju, N. V. S. (2014). *Optimization Methods for Engineers*. PHI Learning Private Limited.

Rashedi, E., Nezamabadi-pour, H., & Saryazdi, S. (2009). GSA: A Gravitational Search Algorithm. *Information Sciences*, *179*(13), 2232–2248. https://doi.org/10.1016/j.ins.2009.03.004

Riahi, H. T., & Estekanchi, H. E. (2010). Seismic assessment of steel frames with the endurance time method. *Journal of Constructional Steel Research*, *66*(6), 780–792. https://doi.org/10.1016/j.jcsr.2009.12.001

Saadat, S., Camp, C. V., & Pezeshk, S. (2016). Probabilistic Seismic Loss Analysis for Design of Steel Structures - Optimizing for Multiple- Ojective Functions. *Earthquake Spectra*. https://doi.org/10.1193/080513EQS223M

Saadat, S., Camp, C. V., Pezeshk, S., & Foley, C. M. (2015). Probabilistic performance based design multi-objective optimization for steel structures. *Structures Congress 2015 - Proceedings of the 2015 Structures Congress*, *April*, 1401–1410. https://doi.org/10.1061/9780784479117.120

SEAOC-Vision-2000. (1995). *Performance-based seismic engineering of buildings*. Sacramento, CA: Structural Engineers Association of California.

Sehhati, R., Rodriguez-Marek, A., Cofer, W. F., & Elgawady, M. (2010). Response of multi-story structures to near-fault ground motions and equivalent pulses. *9th US National and 10th Canadian Conference on Earthquake Engineering 2010*, *25-29 June*.

Seismosoft. (2020). *Seismosoft [2020] "SeismoMatch 2020 – A computer program for spectrum matching of earthquake records," available from https://seismosoft.com/."*. 2020.

Shahnazaryan, D. (2021). *Integrated Performance-Based Seismic Design : Traversing Affordances for Practical Implementation*. Scuola Universitaria.

Shirkhani, A., Farahmand Azar, B., & Charkhtab Basim, M. (2020a). Evaluation of efficiency index of friction energy dissipation devices using endurance time method. *Numerical Methods in Civil Engineering*, *5*(2), 12–20. https://doi.org/10.52547/nmce.5.2.12

Shirkhani, A., Farahmand Azar, B., & Charkhtab Basim, M. (2020b). Optimum slip load of T-shaped friction dampers in steel frames by endurance time method. *Proceedings of the Institution of Civil Engineers: Structures and Buildings*, *173*(10), 746–760. https://doi.org/10.1680/jstbu.18.00169

Shirkhani, A., Farahmand Azar, B., & Charkhtab Basim, M. (2021). Seismic loss assessment of steel structures equipped with rotational friction dampers subjected to intensifying dynamic excitations. *Engineering Structures*, *238*(February), 112233. https://doi.org/10.1016/j.engstruct.2021.112233

Shirkhani, A., Mualla, I. H., Shabakhty, N., & Mousavi, S. R. (2015). Behavior of steel frames with rotational friction dampers by endurance time method. *Journal of Constructional Steel Research*, *107*, 211–222. https://doi.org/10.1016/j.jcsr.2015.01.016

Sönmez, E. (2020). *Manipulation of Structural Design Parameters to Mitigate the Concentration of Interstory Drift Ratios*. Izmir Institute of Technology.

Sood, S. (2010). *Performance-Based Seismic Design of Buildings*. Master's Thesis. Thesis of structural engineering. Department of Civil Engineering.Thapar University: Patiala, Punjab, India. July 2010. p. 140.

Tothong, P., & Cornell, C. A. (2007). *Probabilistic seismic demand analysis using advanced ground motion intensity measures, Attenuation Relationships, and Near-Fault Effects*. https://doi.org/10.1002/eqe.696

Vamvatsikos, D., & Allin Cornell, C. (2002). Incremental dynamic analysis. *Earthquake Engineering and Structural Dynamics*, *31*(3), 491–514. https://doi.org/10.1002/eqe.141

Vijayalakshmi Pai, G. A. (2018). *Metaheuristics for Portfolio Optimization: An Introduction using MATLAB* (Vol. 11). ISTE Ltd and John Wiley & Sons, Inc. https://doi.org/10.1002/9781119482840

Xu, Z., Zhang, H., Lu, X., Xu, Y., Zhang, Z., & Li, Y. (2019). A prediction method of building seismic loss based on BIM and FEMA P-58. *Automation in Construction*, *102*(January), 245–257. https://doi.org/10.1016/j.autcon.2019.02.017

Yazdani, H., Khatibinia, M., Gharehbaghi, S., & Hatami, K. (2017). Probabilistic Performance-Based Optimum Seismic Design of RC Structures Considering Soil–Structure Interaction Effects. *ASCE-ASME Journal of Risk and Uncertainty in Engineering Systems, Part A: Civil Engineering*, *3*(2), 1–12. https://doi.org/10.1061/ajrua6.0000880

Zareian, F., & H., K. (2009). *Simplified Performance Based Earthquake Engineering* (Issue 169).

Zareian, F., & Krawinkler, H. (2012). Conceptual performance-based seismic design using building-level and story-level decision support system. *Earthquake Engineering & Structural Dynamics*, *41*(11), 1439–1453. https://doi.org/10.1002/eqe.2218

Zhang, Q., & Alam, M. S. (2019). Performance-based seismic design of bridges: a global perspective and critical review of past, present and future directions. *Structure and Infrastructure Engineering*, *15*(4), 539–554. https://doi.org/10.1080/15732479.2018.1558269

Zou, X. K., Chan, C. M., Li, G., & Wang, Q. (2007). Multiobjective Optimization for Performance-Based Design of Reinforced Concrete Frames. *Journal of Structural Engineering*, *133*(10), 1462–1474. https://doi.org/10.1061/(ASCE)0733-9445(2007)133:10(1462)

APPENDIX A

SOME RESULTS FOR 3-STORY STRUCTURES

This section includes some of the results that are obtained for 3-Story structure.

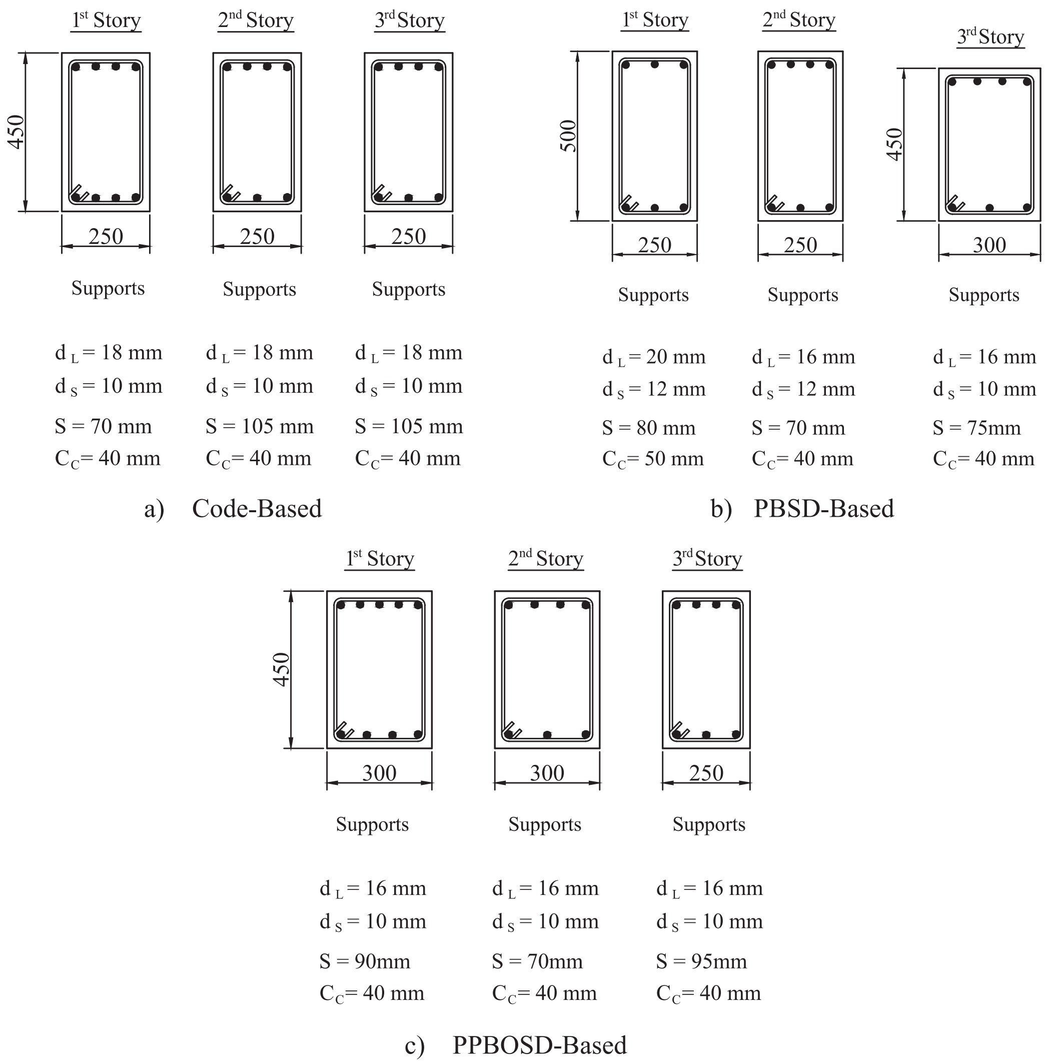

Figure A.1. Optimum solution for the beams of 3-Story frames

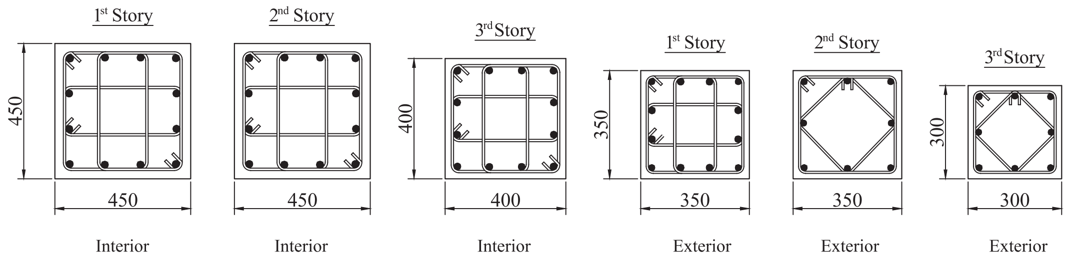

d_L = 20 mm	d_L =18 mm	d_L = 16 mm	d_L = 16 mm	d_L = 16 mm	d_L = 16 mm
d_S = 10 mm	d_S = 10 mm	d_S = 10 mm	d_S = 10 mm	d_S = 10 mm	d_S = 10 mm
S = 80 mm	S =105 mm	S = 90 mm	S = 80 mm	S = 85 mm	S = 85 mm
C_C= 50 mm	C_C= 40 mm	C_C= 40 mm	C_C= 40 mm	C_C= 40 mm	C_C= 40 mm

a) Code-Based

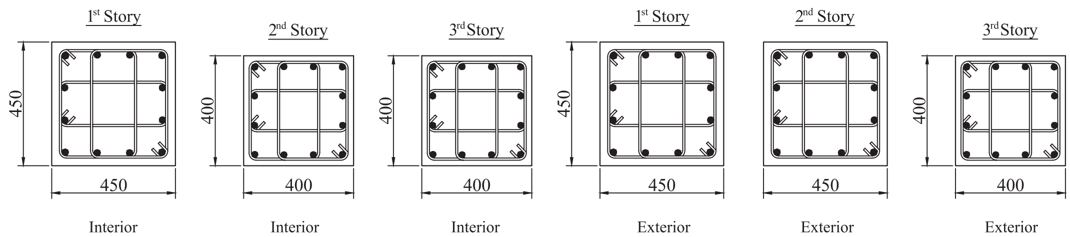

d_L = 16 mm	d_L =16 mm	d_L = 16 mm	d_L = 16 mm	d_L = 16 mm	d_L = 14 mm
d_S = 10 mm	d_S = 10 mm	d_S = 10 mm	d_S = 10 mm	d_S = 10 mm	d_S = 10 mm
S = 95 mm	S =85 mm	S = 95 mm	S = 95 mm	S = 95 mm	S = 80 mm
C_C= 40 mm	C_C= 40 mm	C_C= 40 mm	C_C= 40 mm	C_C= 40 mm	C_C= 40 mm

b) PBSD-Based

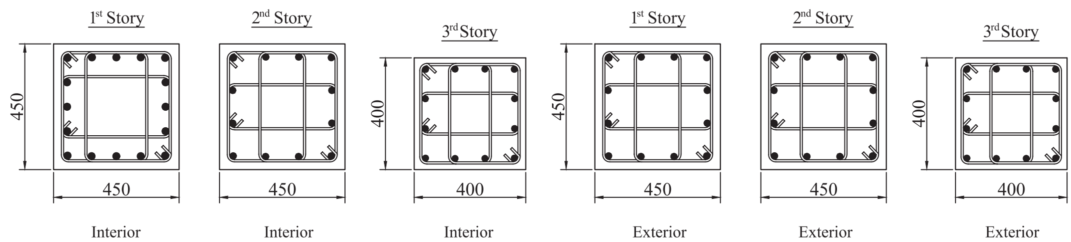

d_L = 18 mm	d_L =18 mm	d_L = 18 mm	d_L = 18 mm	d_L = 16 mm	d_L = 16 mm
d_S = 10 mm	d_S = 10 mm	d_S = 10 mm	d_S = 10 mm	d_S = 10 mm	d_S = 10 mm
S = 80 mm	S =105 mm	S = 100 mm	S = 95 mm	S = 70 mm	S = 75 mm
C_C= 40 mm	C_C= 40 mm	C_C= 40 mm	C_C= 40 mm	C_C= 40 mm	C_C= 40 mm

c) PPBOSD-Based

Figure A.2. Optimum solution for the columns of 3-Story frames

Table A.1. Statistical parameters for IDRs of 3-Story frames at different IM levels

IM Level Sa (T_1)	Peak Interstory Drift Ratio (%)						
	Story #	$\mu_{ln(x)}$	μ_x	$\widehat{S}$	$\sigma_{ln(x)}$	16th Percentile	84th Percentile
Code-Based							
0.4	1	-0.1319	1.2083	0.8765	0.8013	0.4534	1.4373
	2	-0.0227	1.3301	0.9776	0.7848	0.5078	1.3552
	3	-0.0227	1.3301	0.9776	0.7848	0.5078	1.3552
0.8	1	0.7558	2.9787	2.1294	0.8013	0.9256	6.8258
	2	0.7981	2.9902	2.2212	0.7848	1.0597	6.7293
	3	0.7981	2.9902	2.2212	0.7848	1.0597	6.7293
1.6	1	1.3238	4.5756	3.7575	0.6277	2.1699	7.9977
	2	1.3558	4.5632	3.8798	0.5697	2.0672	7.5359
	3	1.3558	4.5632	3.8798	0.5697	2.0672	7.5359
PBSD-Based							
0.4	1	-0.1106	1.7789	0.8953	1.1719	0.3557	5.8391
	2	0.0496	1.8983	1.0509	1.0875	0.4232	5.7586
	3	0.0496	1.8983	1.0509	1.0875	0.4232	5.7586
0.8	1	0.5255	2.7507	1.6912	1.1719	0.6461	6.7875
	2	0.6500	2.8851	1.9155	1.0875	0.7712	7.0513
	3	0.6500	2.8851	1.9155	1.0875	0.7712	7.0513
1.6	1	1.0451	3.5510	2.8437	0.6665	1.1893	5.4938
	2	1.1056	3.7478	3.0211	0.6566	1.3920	6.0842
	3	1.1056	3.7478	3.0211	0.6566	1.3920	6.0842
PPBOSD-Based							
0.4	1	-0.3716	1.0791	0.6896	0.9463	0.3829	1.3653
	2	-0.1190	1.3161	0.8878	0.8873	0.4431	1.5278
	3	-0.1190	1.3161	0.8878	0.8873	0.4431	1.5278
0.8	1	0.2660	1.8723	1.3047	0.9463	0.6510	3.5928
	2	0.5218	2.2502	1.6851	0.8873	0.8503	3.5040
	3	0.5218	2.2502	1.6851	0.8873	0.8503	3.5040
1.6	1	1.0520	3.6171	2.8634	0.6836	1.4773	7.0152
	2	1.2186	4.0829	3.3824	0.6135	1.7374	7.1949
	3	1.2186	4.0829	3.3824	0.6135	1.7374	7.1949

Table A.2. Probability of damage measure for Component C1011.001a of 3-Story frames

Damage State	Mean Rate of Exceedance in 50 years			Return Periods (years)		
	50th Percentile	16th Percentile	84th Percentile	50th Percentile	16th Percentile	84th Percentile
Code-Based						
Slight or No	0.2297	0.4162	0.0901	192	93	530
Moderate	0.2123	0.2550	0.1217	210	170	386
Extensive	0.2737	0.2130	0.2332	157	209	189
Collapse	0.2435	0.0910	0.4269	180	524	90
PBSD-Based						
Slight or No	0.2739	0.4886	0.1105	157	75	427
Moderate	0.2111	0.2320	0.1286	211	190	364
Extensive	0.2423	0.1714	0.2202	181	266	201
Collapse	0.2219	0.0817	0.3805	200	587	105
PPBOSD-Based						
Slight or No	0.3029	0.4982	0.1509	139	73	306
Moderate	0.2585	0.2658	0.1921	168	162	235
Extensive	0.2639	0.1698	0.2918	164	269	145
Collapse	0.1499	0.0462	0.3113	308	1058	135

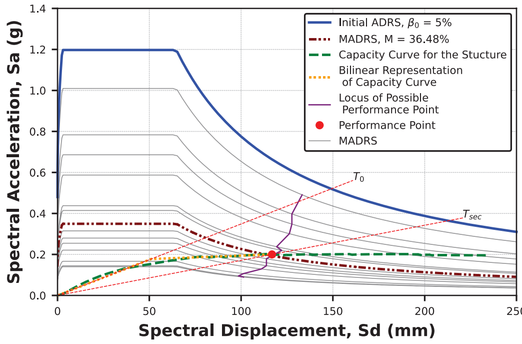

a) Schematic of the procedure C of FEMA-440

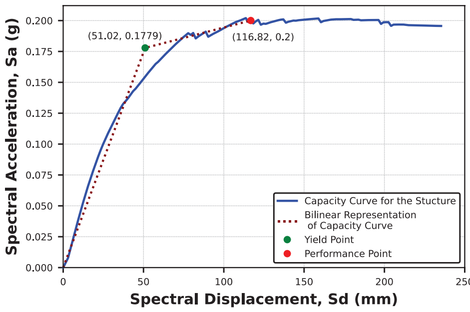

b) Capacity curve and bilinear representation in ADRS format

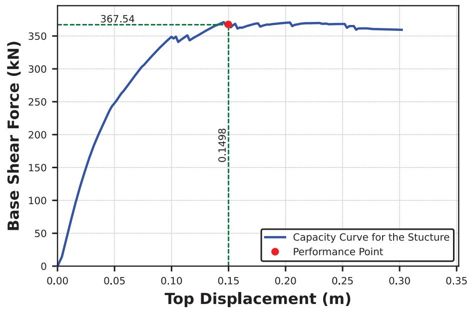

c) Capacity curve in regular format

Figure A.3. Resulted performance point for 3-Story frame designed using Code-Based design approach

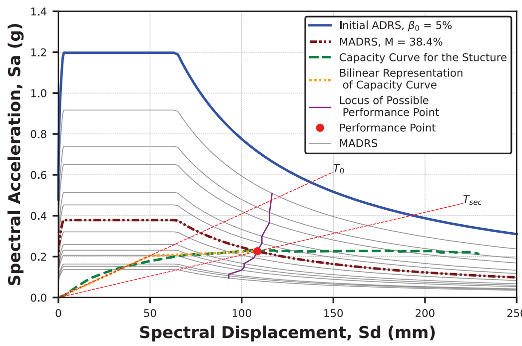

a) Schematic of the procedure C of FEMA-440

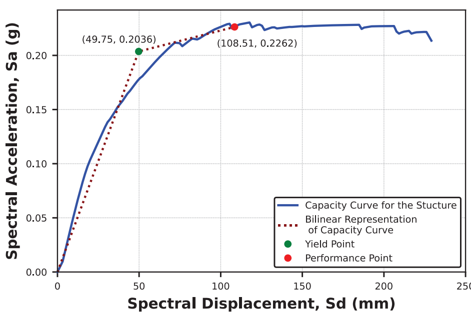

b) Capacity curve and bilinear representation in ADRS format

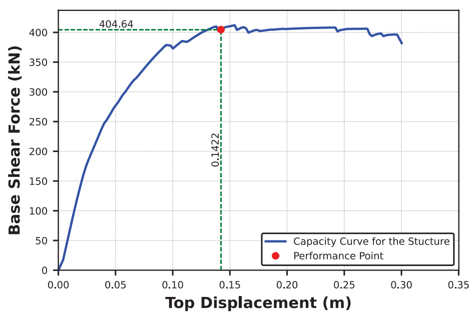

c) Capacity curve in regular format

Figure A.4. Resulted performance point for 3-Story frame designed using PBSD approach

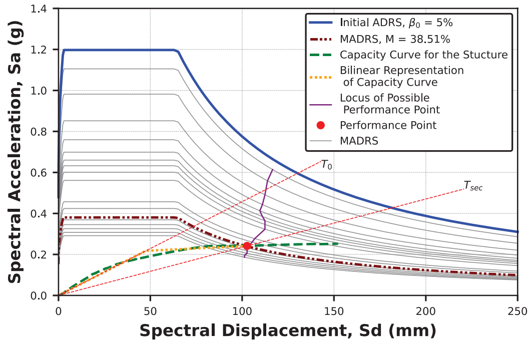

a) Schematic of the procedure C of FEMA-440

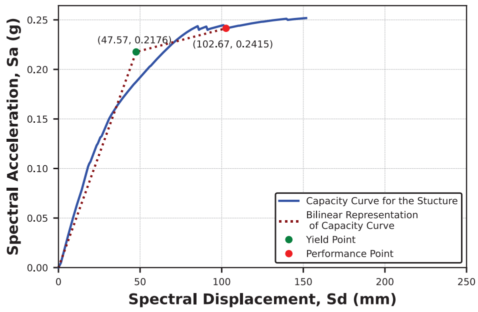

b) Capacity curve and bilinear representation in ADRS format

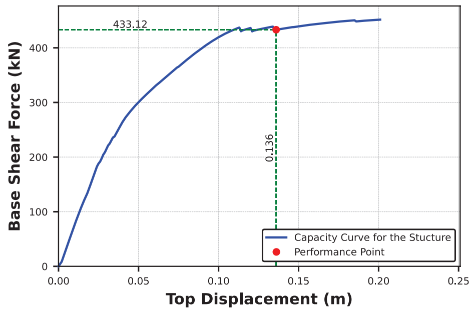

c) Capacity curve in regular format

Figure A.5. Resulted performance point for 3-Story frame designed using PPBOSD approach

APPENDIX B

SOME RESULTS FOR 6-STORY STRUCTURES

This section includes some of the results that are obtained for 6-Story structure.

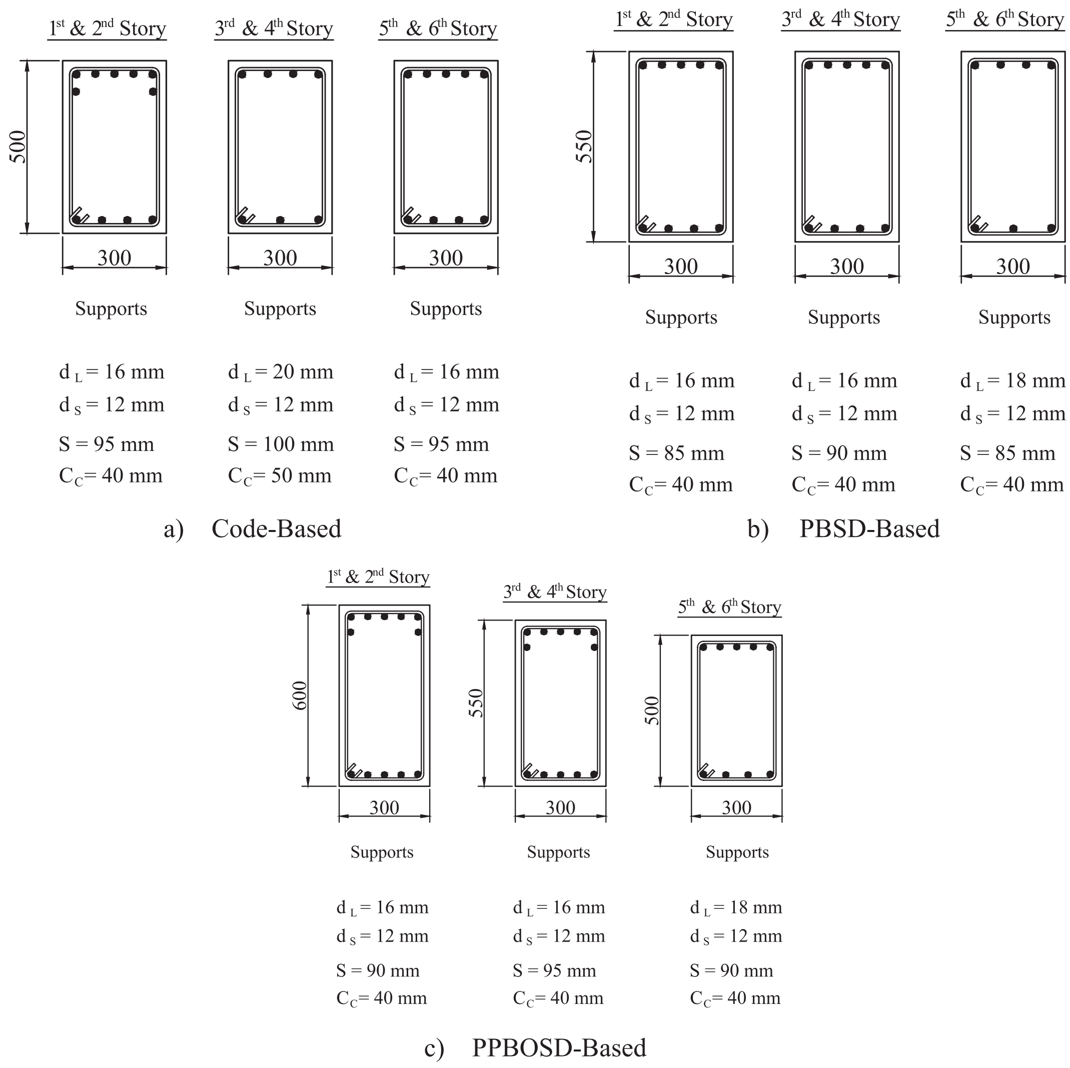

Figure B.1. Optimum solution for the beams of 6-Story frames

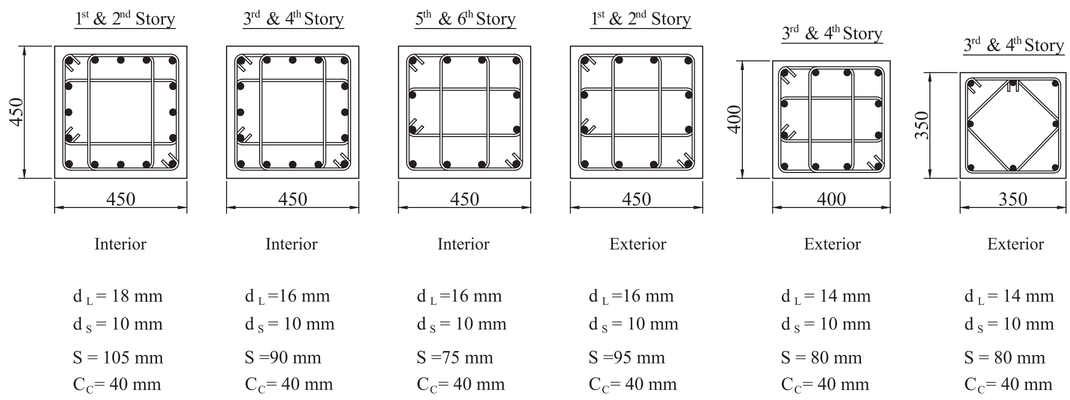

a) Code-Based

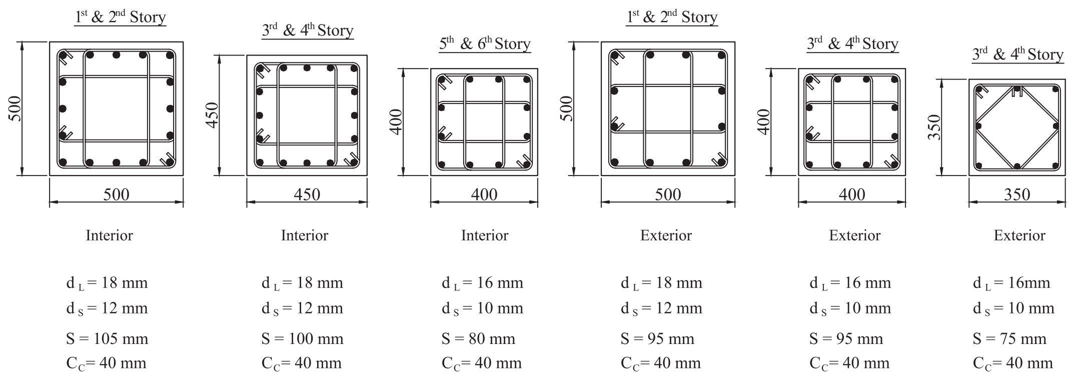

b) PBSD-Based

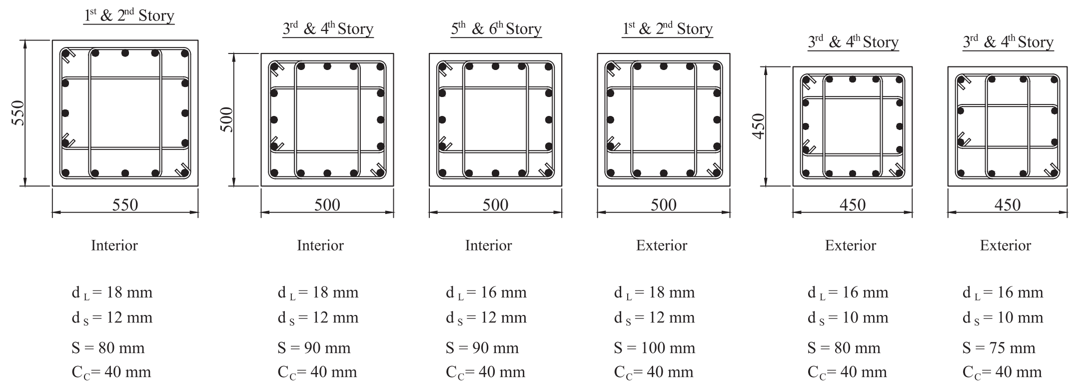

c) PPBOSD-Based

Figure B.2. Optimum solution for the columns of 6-Story frames

Table B.1. Statistical parameters for IDRs of 6-Story frames at different IM levels

IM Level Sa (T_1)	Peak Interstory Drift Ratio (%)						
	Story #	$\mu_{ln(x)}$	μ_x	$\hat{S}$	$\sigma_{ln(x)}$	16th Percentile	84th Percentile
Code-Based							
0.3	1	-0.3230	0.8882	0.7240	0.6394	0.4834	0.9707
	2	-0.0812	1.0826	0.9220	0.5666	0.5892	1.1823
	3	0.0127	1.1948	1.0128	0.5749	0.6138	1.3060
	4	-0.0422	1.0486	0.9587	0.4233	0.6390	1.1802
	5	-0.2444	0.8738	0.7832	0.4680	0.5226	1.1715
	6	-0.8681	0.4654	0.4197	0.4545	0.2551	0.7295
0.6	1	0.3554	1.7542	1.4268	0.6394	0.9037	2.0824
	2	0.5540	1.9917	1.7403	0.5666	1.1651	2.5335
	3	0.5755	1.9836	1.7781	0.5749	1.1560	2.3689
	4	0.3900	1.5943	1.4770	0.4233	0.9808	2.0442
	5	0.1758	1.3047	1.1922	0.4680	0.7236	1.9466
	6	-0.4521	0.7184	0.6363	0.4545	0.4190	0.8994
1.3	1	1.4091	4.7445	4.0924	0.5438	2.1255	8.0000
	2	1.4308	4.6967	4.1820	0.4818	2.3707	7.3022
	3	1.4436	4.6479	4.2359	0.4309	2.5288	6.7465
	4	1.0074	2.9463	2.7385	0.3824	1.7841	3.9342
	5	0.7594	2.3664	2.1369	0.4517	1.5626	2.6293
	6	0.1555	1.3195	1.1682	0.4935	0.7257	1.9613
PBSD-Based							
0.3	1	-0.6564	0.6259	0.5187	0.6128	0.3154	0.8095
	2	-0.3795	0.8028	0.6842	0.5655	0.4047	0.9606
	3	-0.2325	0.9331	0.7925	0.5714	0.4584	1.1109
	4	-0.2107	0.9491	0.8100	0.5630	0.4717	1.0665
	5	-0.3161	0.8519	0.7290	0.5584	0.4436	1.0761
	6	-0.8604	0.4633	0.4230	0.4268	0.3017	0.5755
0.6	1	-0.1408	1.1417	0.8686	0.6128	0.4365	1.1248
	2	0.1173	1.3906	1.1244	0.5655	0.6115	1.6076
	3	0.2455	1.5706	1.2783	0.5714	0.7760	1.8915
	4	0.2118	1.5120	1.2359	0.5630	0.7183	1.9453
	5	0.1905	1.4848	1.2099	0.5584	0.5229	1.9778
	6	-0.4429	0.7222	0.6422	0.4268	0.4349	0.9102
1.8	1	0.6955	2.9387	2.0047	0.8746	1.0906	4.2099
	2	0.9227	3.3386	2.5160	0.7522	1.4676	4.2937
	3	1.0380	3.5489	2.8235	0.6763	1.6988	4.3467
	4	0.8156	2.8144	2.2604	0.6621	1.3298	3.6136
	5	0.7531	2.6479	2.1236	0.6643	1.2253	3.7896
	6	0.0255	1.2350	1.0258	0.6092	0.5428	1.6589
PPBOSD-Based							
0.3	1	-0.7331	0.5923	0.4804	0.6472	0.2562	0.8922
	2	-0.5037	0.7382	0.6043	0.6327	0.3481	1.1133
	3	-0.3954	0.8056	0.6734	0.5986	0.3674	1.2109
	4	-0.4167	0.7573	0.6592	0.5266	0.3773	1.1858
	5	-0.6539	0.5719	0.5200	0.4363	0.3484	0.8363
	6	-1.1479	0.3410	0.3173	0.3793	0.2258	0.5180
0.6	1	-0.0934	1.0949	0.9108	0.6472	0.5759	1.5226
	2	0.1633	1.3871	1.1774	0.6327	0.7727	1.7626
	3	0.2789	1.5695	1.3217	0.5986	0.8010	2.1742
	4	0.3044	1.5609	1.3558	0.5266	0.8672	2.0421
	5	0.0722	1.2730	1.0749	0.4363	0.6710	1.8172
	6	-0.5431	0.6687	0.5809	0.3793	0.3892	0.9012
1.8	1	0.7894	2.6356	2.2022	0.5995	1.4112	3.2574
	2	0.8837	2.7636	2.4199	0.5154	1.6604	3.3718
	3	0.9683	2.9666	2.6334	0.4882	1.7911	3.8403
	4	0.9021	2.7571	2.4647	0.4735	1.7485	4.0959
	5	0.6541	2.1358	1.9234	0.4578	1.1698	2.8049
	6	0.0648	1.1894	1.0670	0.4662	0.6275	1.7080

Table B.2. Probability of damage measure for Component C1011.001a of 6-Story frames

Damage State	Mean Rate of Exceedance in 50 years			Return Periods (years)		
	50th Percentile	16th Percentile	84th Percentile	50th Percentile	16th Percentile	84th Percentile
Code-Based						
Slight or No	0.2461	0.3815	0.1536	178	105	300
Moderate	0.2812	0.3159	0.2206	152	132	201
Extensive	0.3275	0.2469	0.3500	127	177	117
Collapse	0.1423	0.0542	0.2660	326	898	162
PBSD-Based						
Slight or No	0.2719	0.4394	0.1641	158	87	279
Moderate	0.2979	0.3179	0.2391	142	131	183
Extensive	0.3118	0.2039	0.3591	134	220	113
Collapse	0.1148	0.0369	0.2279	411	1330	194
PPBOSD-Based						
Slight or No	0.3359	0.4889	0.1968	123	75	229
Moderate	0.2947	0.2943	0.2482	144	144	176
Extensive	0.2719	0.1821	0.3362	158	249	123
Collapse	0.0959	0.0334	0.2136	497	1471	209

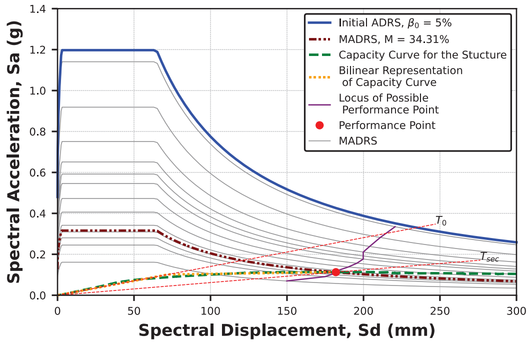

a) Schematic of the procedure C of FEMA-440

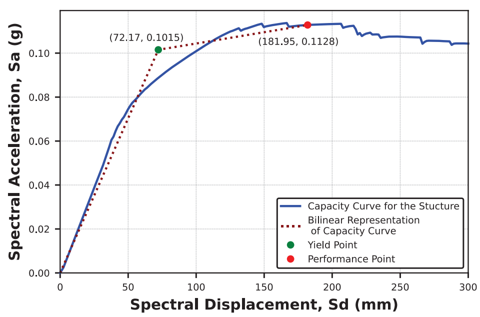

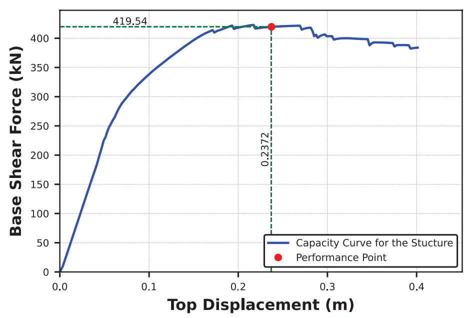

b) Capacity curve and bilinear representation in ADRS format

c) Capacity curve in regular format

Figure B.3. Resulted performance point for 6-Story frame designed using Code-Based design approach

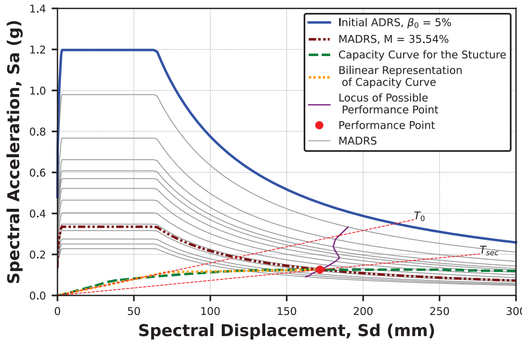

a) Schematic of the procedure C of FEMA-440

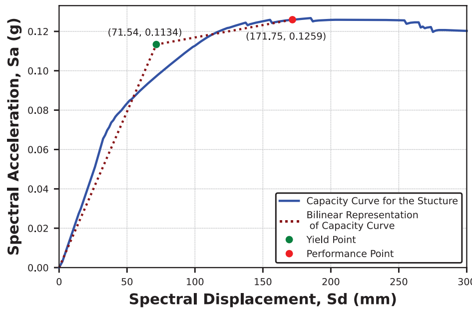

b) Capacity curve and bilinear representation in ADRS format

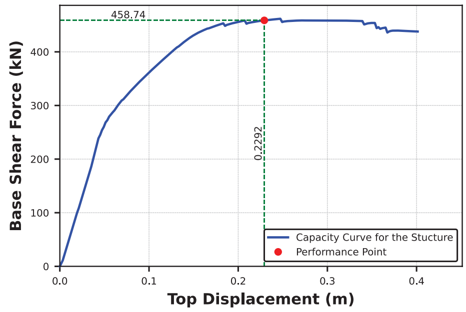

c) Capacity curve in regular format

Figure B.4. Resulted performance point for 6-Story frame designed using PBSD approach

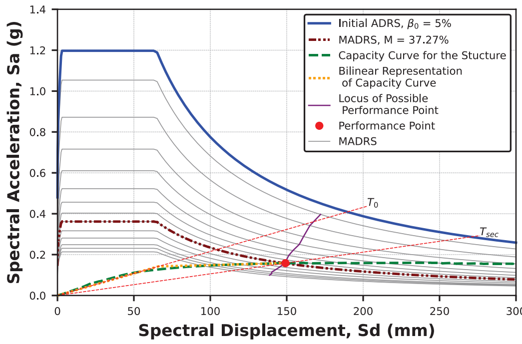

a) Schematic of the procedure C of FEMA-440

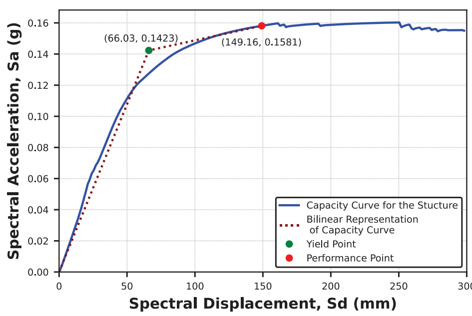

b) Capacity curve and bilinear representation in ADRS format

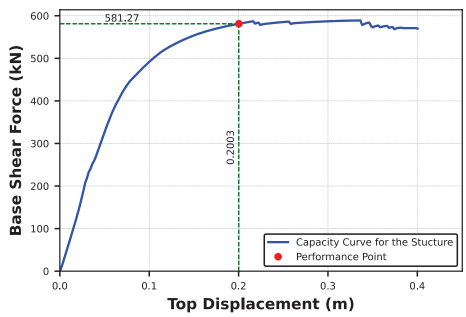

c) Capacity curve in regular format

Figure B.5. Resulted performance point for 6-Story frame designed using PPBOSD approach

APPENDIX C

SOME RESULTS FOR 9-STORY STRUCTRUES

This section includes some of the results that are obtained for 9-Story structure.

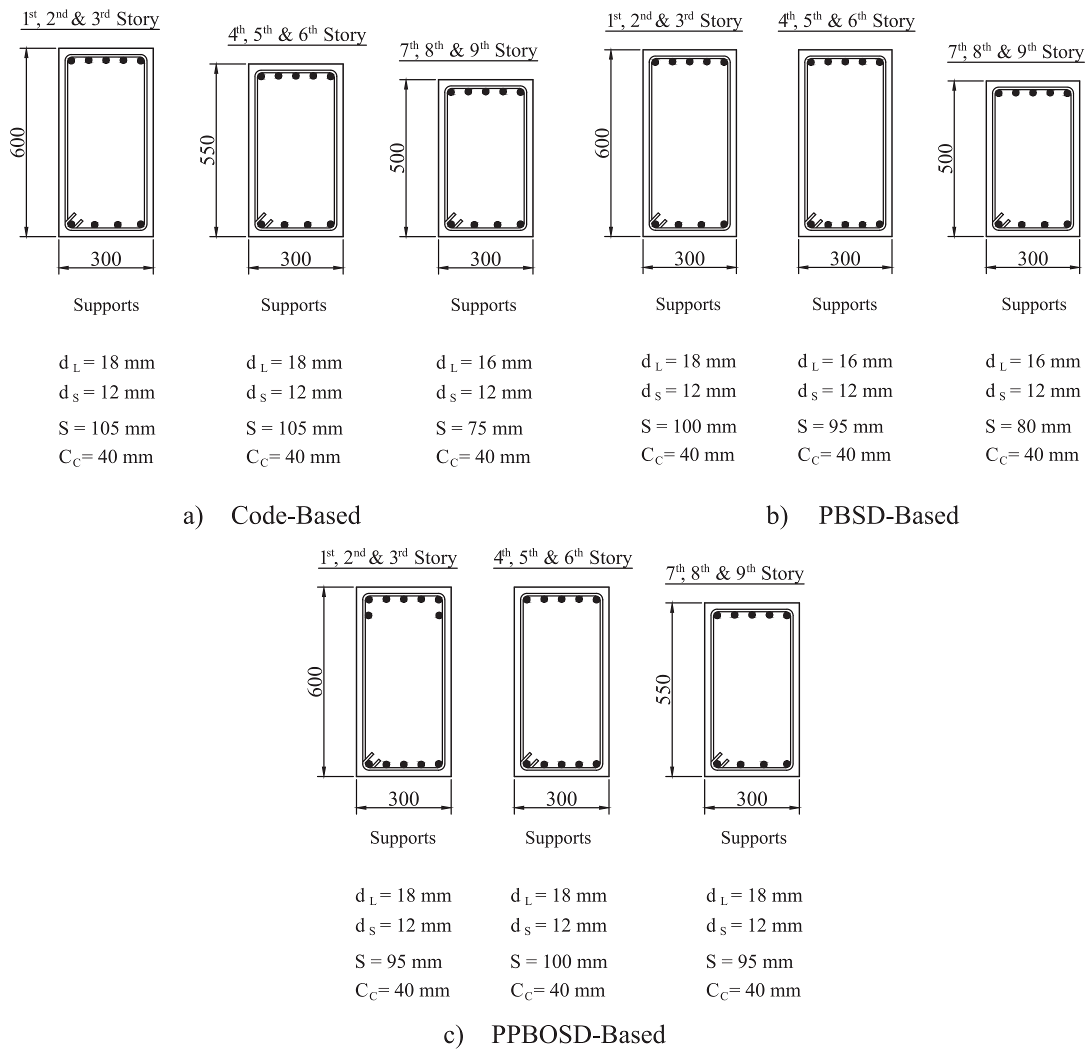

Figure C.1. Optimum solution for the beams of 9-Story frames

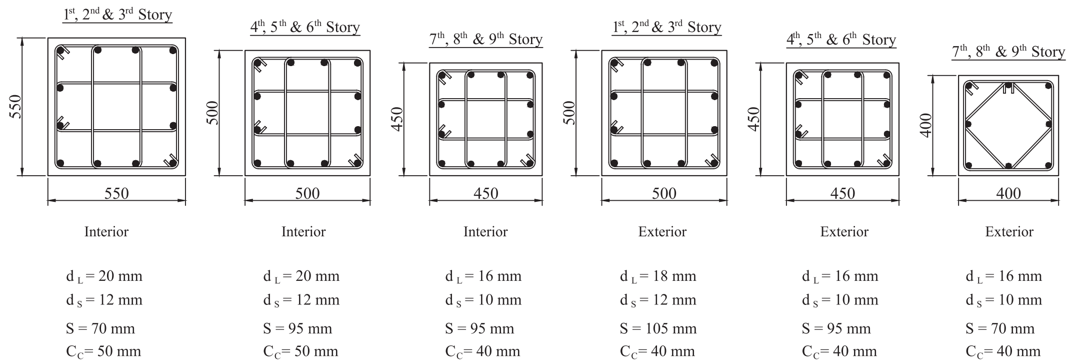

a) Code-Based

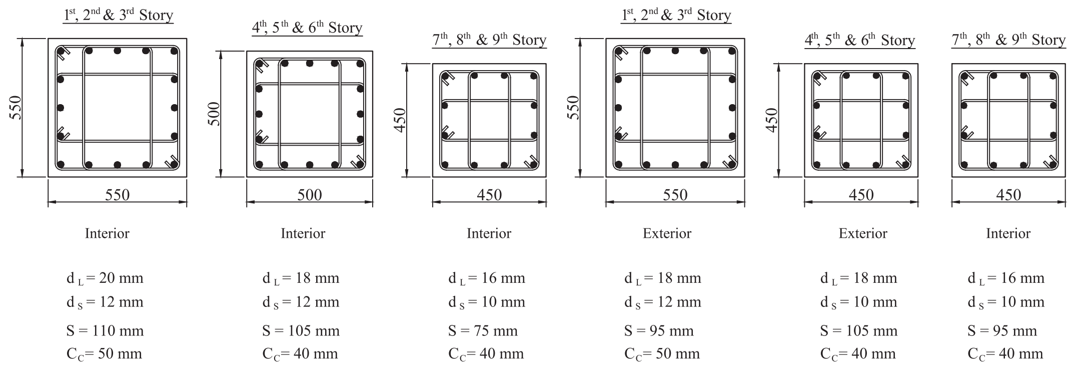

b) PBSD-Based

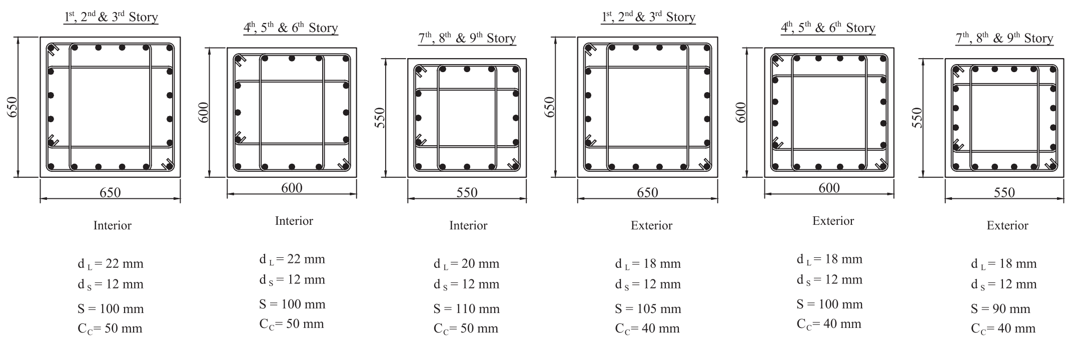

c) PPBOSD-Based

Figure C.2. Optimum solution for the columns of 9-Story frames

Table C.1. Statistical parameters for IDRs of 9-Story frames at different IM levels

IM Level Sa (T_1)	Peak Interstory Drift Ratio (%)						
	Story #	$\mu_{ln(x)}$	μ_x	$\widehat{S}$	$\sigma_{ln(x)}$	16th Percentile	84th Percentile
Code-Based							
0.3	1	-0.6781	0.7231	0.5076	0.8413	0.2594	0.6779
	2	-0.3473	0.9655	0.7066	0.7902	0.3813	1.2175
	3	-0.2376	1.0731	0.7885	0.7850	0.4499	1.4801
	4	-0.1805	1.0266	0.8349	0.6431	0.4872	1.6100
	5	-0.1637	1.0488	0.8490	0.6501	0.4685	1.5537
	6	-0.2663	0.9386	0.7662	0.6370	0.4319	1.3250
	7	-0.1580	0.9886	0.8539	0.5414	0.4935	1.3204
	8	-0.2524	0.8648	0.7770	0.4627	0.4951	1.1371
	9	-0.6728	0.5861	0.5103	0.5265	0.2958	0.7864
0.5	1	-0.0250	1.4607	0.9753	0.8413	0.4431	1.7293
	2	0.1898	1.6737	1.2090	0.7902	0.6207	1.9591
	3	0.2692	1.7822	1.3089	0.7850	0.6436	2.1479
	4	0.3122	1.7509	1.3664	0.6431	0.7712	2.4444
	5	0.2880	1.5592	1.3337	0.6501	0.8376	2.5391
	6	0.2031	1.3647	1.2252	0.6370	0.9130	1.9968
	7	0.2185	1.3652	1.2442	0.5414	0.7707	1.7897
	8	0.0511	1.1733	1.0525	0.4627	0.6579	1.8027
	9	-0.4762	0.7079	0.6211	0.5265	0.3856	1.2678
1.0	1	1.1099	4.1304	3.0342	0.7854	1.2410	8.0000
	2	1.2383	4.4056	3.4496	0.6995	1.5034	8.0000
	3	1.2036	3.9778	3.3320	0.5952	1.5726	6.6643
	4	1.0125	3.1036	2.7526	0.4900	1.5791	4.6206
	5	0.8179	2.4976	2.2657	0.4415	1.4802	3.3878
	6	0.6827	2.1649	1.9792	0.4236	1.3796	2.9271
	7	0.6047	2.0044	1.8306	0.4259	1.1459	2.7206
	8	0.4256	1.7062	1.5305	0.4662	1.0612	2.3621
	9	-0.0590	1.0418	0.9427	0.4471	0.6224	1.3621
PBSD-Based							
0.3	1	-0.8511	0.5269	0.4269	0.6487	0.2490	0.6997
	2	-0.4593	0.7576	0.6318	0.6027	0.3847	1.1060
	3	-0.3286	0.8600	0.7200	0.5962	0.4267	1.2981
	4	-0.2315	0.9161	0.7934	0.5364	0.4870	1.3647
	5	-0.2530	0.8724	0.7765	0.4826	0.5067	1.3242
	6	-0.3461	0.7889	0.7075	0.4667	0.4523	1.0564
	7	-0.2254	0.8905	0.7982	0.4678	0.5110	1.1610
	8	-0.2687	0.8440	0.7644	0.4453	0.4775	1.1735
	9	-0.7250	0.5259	0.4843	0.4058	0.3318	0.6600
0.5	1	-0.2625	0.9191	0.7691	0.6487	0.4739	1.4967
	2	0.0342	1.2102	1.0348	0.6027	0.5697	1.6954
	3	0.1650	1.3836	1.1794	0.5962	0.6187	1.8846
	4	0.2773	1.5007	1.3196	0.5364	0.8404	1.9811
	5	0.2922	1.4614	1.3394	0.4826	0.9052	1.8410
	6	0.2071	1.3155	1.2301	0.4667	0.8946	1.7930
	7	0.1542	1.2663	1.1667	0.4678	0.7667	1.6294
	8	-0.0086	1.0872	0.9915	0.4453	0.6374	1.6736
	9	-0.4305	0.7280	0.6502	0.4058	0.4230	1.1670
1.0	1	0.8840	3.2509	2.4206	0.7680	1.0274	5.5767
	2	1.0652	3.6325	2.9014	0.6704	1.3324	6.1999
	3	1.0941	3.5922	2.9864	0.6077	1.4256	4.8206
	4	1.0319	3.2741	2.8063	0.5553	1.4926	4.5562
	5	1.0121	3.1760	2.7513	0.5358	1.5302	4.3644
	6	0.8963	2.8187	2.4504	0.5292	1.6608	3.7343
	7	0.8060	2.6162	2.2390	0.5581	1.4913	3.1063
	8	0.6716	2.1053	1.9573	0.3818	1.3394	2.7879
	9	0.2356	1.4539	1.2657	0.5266	0.7488	2.0480

(Cont. on next page)

Table C.1. (Cont.)

IM Level Sa (T_1)	Peak Interstory Drift Ratio (%)						
	Story #	$\mu_{ln(x)}$	μ_x	$\hat{S}$	$\sigma_{ln(x)}$	16th Percentile	84th Percentile
PPBOSD-Based							
0.3	1	-0.9865	0.4421	0.3729	0.5837	0.2592	0.4748
	2	-0.6401	0.6022	0.5272	0.5155	0.3684	0.6507
	3	-0.5145	0.6809	0.5978	0.5102	0.3983	0.7568
	4	-0.4246	0.7502	0.6541	0.5237	0.4178	0.8896
	5	-0.3531	0.7953	0.7025	0.4981	0.4490	0.9344
	6	-0.2993	0.8401	0.7413	0.5001	0.4648	0.9634
	7	-0.3315	0.8129	0.7178	0.4988	0.5140	1.0337
	8	-0.5719	0.6408	0.5644	0.5036	0.4008	0.8233
	9	-1.0792	0.3790	0.3399	0.4666	0.2191	0.5502
0.5	1	-0.5567	0.7411	0.5731	0.5837	0.3164	0.7626
	2	-0.1451	1.0414	0.8650	0.5155	0.5213	1.1551
	3	-0.0070	1.1759	0.9931	0.5102	0.6600	1.3923
	4	0.0554	1.2419	1.0570	0.5237	0.6784	1.4437
	5	0.0494	1.2363	1.0506	0.4981	0.6230	1.4133
	6	0.0568	1.2573	1.0585	0.5001	0.5525	1.3673
	7	0.0525	1.2643	1.0540	0.4988	0.6356	1.5278
	8	-0.1657	1.0181	0.8473	0.5036	0.5618	1.3734
	9	-0.6665	0.6413	0.5135	0.4666	0.3170	0.9510
1.0	1	0.2600	1.6749	1.2970	0.7151	0.6469	2.7063
	2	0.5671	2.1026	1.7631	0.5935	1.0916	3.0147
	3	0.6822	2.3001	1.9783	0.5490	1.2172	3.2827
	4	0.7474	2.3865	2.1115	0.4949	1.3735	3.4400
	5	0.7902	2.4247	2.2039	0.4370	1.4766	3.0528
	6	0.7343	2.2799	2.0841	0.4239	1.4372	2.7876
	7	0.6219	2.0337	1.8625	0.4194	1.4748	2.4630
	8	0.4105	1.6838	1.5076	0.4702	1.0041	2.0133
	9	0.0264	1.2622	1.0268	0.6426	0.5559	1.6271

Table C.2. Probability of damage measure for Component C1011.001a of 9-Story frames

Damage State	Mean Rate of Exceedance in 50 years			Return Periods (years)		
	50th Percentile	16th Percentile	84th Percentile	50th Percentile	16th Percentile	84th Percentile
Code-Based						
Slight or No	0.2649	0.4184	0.1536	163	93	300
Moderate	0.2527	0.2851	0.1907	172	149	237
Extensive	0.2972	0.2262	0.3044	142	195	138
Collapse	0.1795	0.0685	0.3261	253	705	127
PBSD-Based						
Slight or No	0.3070	0.4594	0.1759	137	82	259
Moderate	0.2798	0.2980	0.2144	153	142	208
Extensive	0.2942	0.2026	0.3265	144	221	127
Collapse	0.1157	0.0382	0.2716	407	1283	158
PPBOSD-Based						
Slight or No	0.3980	0.5284	0.2851	99	67	149
Moderate	0.3074	0.2917	0.2868	137	145	148
Extensive	0.2325	0.1550	0.2980	189	297	142
Collapse	0.0612	0.0241	0.1276	793	2046	367

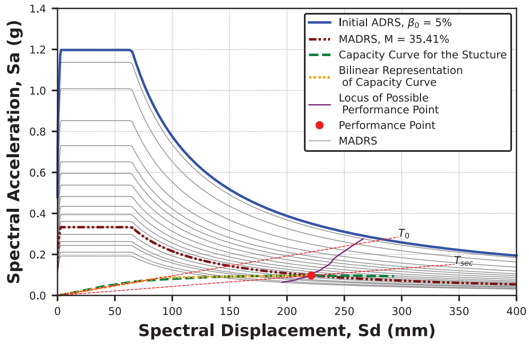

a) Schematic of the procedure C of FEMA-440

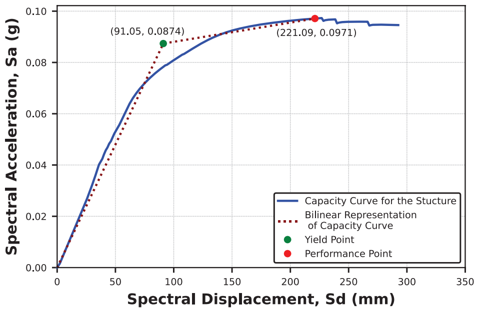

b) Capacity curve and bilinear representation in ADRS format

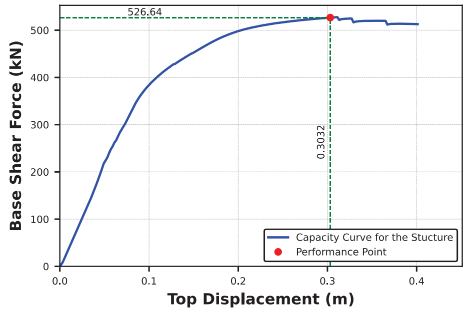

c) Capacity curve in regular format

Figure C.3. Resulted performance point for 9-Story frame designed using Code-Based design approach

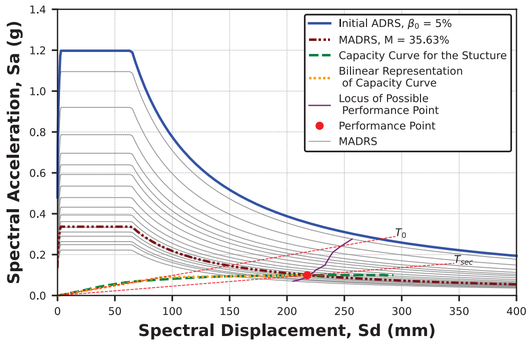

a) Schematic of the procedure C of FEMA-440

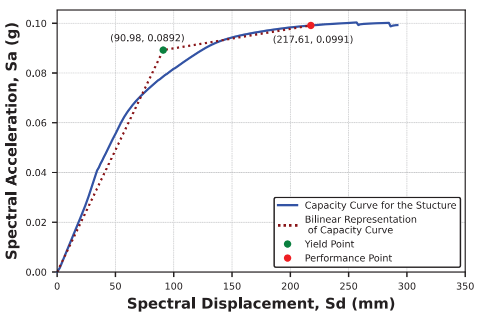

b) Capacity curve and bilinear representation in ADRS format

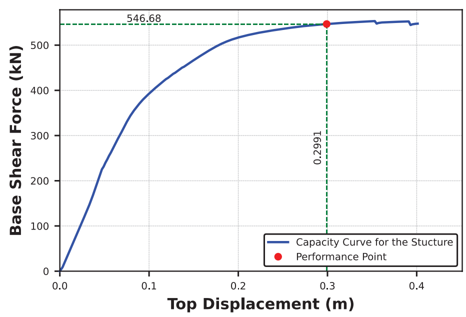

c) Capacity curve in regular format

Figure C.4. Resulted performance point for 9-Story frame designed using PBSD approach

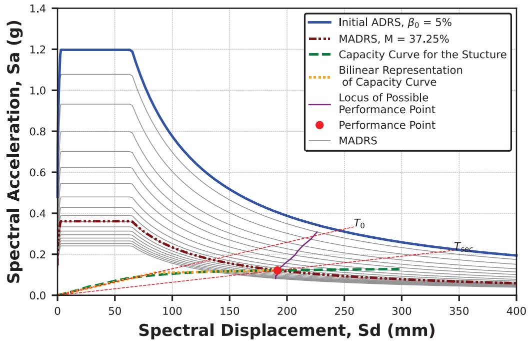

a) Schematic of the procedure C of FEMA-440

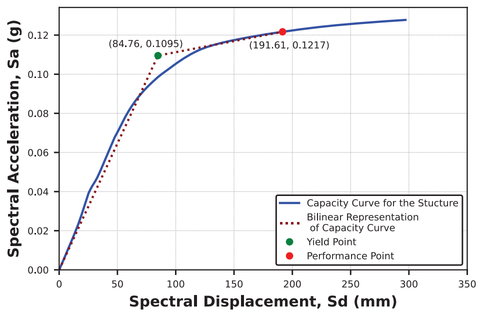

b) Capacity curve and bilinear representation in ADRS format

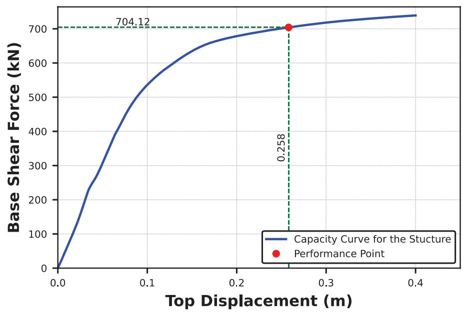

c) Capacity curve in regular format

Figure C.5. Resulted performance point for 9-Story frame designed using PPBOSD approach

VITA

Nisar Ahmad KARIMZADA

EDUCATION

Ph.D. in Civil Engineering Department
İzmir Institute of Technology, İzmir, Turkiye **2023**

M.Sc. in Civil Engineering Department
İzmir Institute of Technology, İzmir, Turkiye **2015**

B.Sc. in Civil and Industrial Engineering Department
Kabul Polytechnic University, Kabul, Afghanistan **2009**

EMPLOYMENT

Lecturer
Kabul Polytechnic University, Kabul, Afghanistan **2009-Present**

Office Engineer (*Part time*)
Ashlar Builder Construction Company (ABCC), Afghanistan **2015-2020**

Office Engineer
Morco Polo Hendukush Construction Company (MHCC), Afghanistan **2011-2012**

Quantity Surveyor and Proposal Writer
Aria Istanbul Groups (AIG), Afghanistan **2010-2011**

Construction Manager
Waykerat Construction, Rehabilitation and Organization, Afghanistan **2009-2010**

PUBLICATIONS

Journal:

Karimzada, N. A., Shirkhani, A., & Aktaş, E. (2024). Application of Endurance Time Method in Seismic Assessment of RC Frames Designed by Direct Displacement-Based Procedure. Turkish Journal of Civil Engineering, 35(2). https://doi.org /10.18400/tjce.1239730

Conference:

Karimzada, N. A., & Aktaş, E. (2016). Performance-Based Seismic Design of Reinforced Concrete Frame Buildings: A Direct Displacement-Based Approach. 12 International Congress on Advances in Civil Engineering, 21-23 September, Boğaziçi University, Istabul, Turkiye.

Erdem, T. K., Şahin, F. G., **Karimzada, N. A.**, Yıldırım, T., & Türkyener, C. (2018). Mechanical Properties of Single and Hybrid Fiber Reinforced Concretes Containing Fly Ash and Blast Furnace Slag. 13th International Congress on Advances in Civil Engineering, 12-14 September, Radisson-Blu/Çeşme, İzmir,Turkiye.